THE UNIVERSITY OF ALBERTA

EVALUATION OF THE SOIL PROPERTIES OF THE DEVON TEST FILL

by

BARBARA A. HOFMANN

A THESIS

SUBMITTED TO THE FACULTY OF GRADUATE STUDIES AND RESEARCH

IN PARTIAL FULFILMENT OF THE REQUIREMENTS FOR THE DEGREE

OF MASTERS OF SCIENCE

DEPARTMENT OF CIVIL ENGINEERING

EDMONTON, ALBERTA

SPRING, 1989

THE UNIVERSITY OF ALBERTA

RELEASE FORM

NAME OF AUTHOR BARBARA A. HOFMANN

TITLE OF THESIS EVALUATION OF THE SOIL PROPERTIES OF THE DEVON TEST FILL

DEGREE FOR WHICH THESIS WAS PRESENTED MASTERS OF SCIENCE

YEAR THIS DEGREE GRANTED SPRING, 1989

(SIGNED) B. A. Hofmann

PERMANENT ADDRESS:

#306, 727 - 1 ST. AVENUE N.W.

CALGARY, AB.

T2N 0A2

DATED SPRING 1989

THE UNIVERSITY OF ALBERTA

FACULTY OF GRADUATE STUDIES AND RESEARCH

The undersigned certify that they have read, and recommend to the Faculty of Graduate Studies and Research, for acceptance, a thesis entitled EVALUATION OF THE SOIL PROPERTIES OF THE DEVON TEST FILL submitted by BARBARA A. HOFMANN in partial fulfilment of the requirements for the degree of MASTERS OF SCIENCE in CIVIL ENGINEERING.

.....

Supervisor

.....

.....

.....

Date February 10, 1989

ABSTRACT

In an effort to assess the performance and feasibility of geogrid reinforcement of cohesive soils, a large geogrid reinforced test embankment is being constructed at Devon, Alberta. The embankment is composed of weak soil, which will deform substantially, so that the soil/geogrid stress transfers which take place can be monitored. Three quadrants of the test fill are reinforced with different types of geogrid and one quadrant is unreinforced to serve as a control slope.

The primary objective of this research is to analyze the shear strength and stress-strain properties of the fill soil being used to construct the embankment and of the underlying foundation soil. The shear strength and stress-strain properties of the fill and foundation soils are established through various laboratory shear strength and consolidation tests.

The selection of the embankment geometry and the compaction specifications required to construct an embankment which would deform significantly without geogrid reinforcement are discussed. The shear strength parameters established during the laboratory testing program are used to determine the short and long term factors of safety against a shear failure of the unreinforced slope of the test fill using limit equilibrium analyses. The laboratory stress-strain behaviour is modelled to predict the long term deformations of the unreinforced slope of the embankment

using a finite element analysis.

ACKNOWLEDGEMENTS

I would like to thank Dr. J.D. Scott for his advice and guidance throughout this research. I would also like to thank Dr. D.C. Sego and Professor E.A. Richards for the assistance they provided during the project.

Appreciation is expressed to Alberta Transportation and Utilities and to the Civil Engineering Department at the University of Alberta for providing the financial support for the construction of the test embankment and the associated research.

I am grateful to my parents, Mara and Bernhart Hofmann, for their love and encouragement. Special thanks are given to Peter Gaffran for his love and continued assistance.

Table of Contents

List of Tables

Table | Page

List of Figures

LIST OF SYMBOLS

A_c	activity
A_f	pore pressure parameter at failure
B	pore pressure parameter
BH	borehole
c'	effective stress cohesion intercept
CD	consolidated drained triaxial test
CU	consolidated undrained triaxial test
e_o	initial void ratio
e_f	final void ratio
C_c	compression index
C_r	recompression index
C_v	coefficient of consolidation
C_ϵ	secondary compression index
E	Young's modulus
E_i	initial tangent modulus
ϵ_f	strain at failure
ϵ_1	major principal strain
γ	bulk unit weight
H	length of drainage path
H_o	initial thickness of compressive soil layer
I_p	plasticity index
k	permeability
K	principal effective stress ratio
K_o	coefficient of lateral earth pressure at rest
K_b	bulk modulus
K_f	lateral stress ratio at failure

K_u	unloading-reloading modulus
m	bulk modulus exponent
M_v	coefficient of volume change
n	modulus exponent
ν	Poisson's ratio
ϕ'	effective stress friction angle determined from UU or CU triaxial tests
ϕ'_d	effective stress friction angle determined from CD triaxial tests
q_u	unconfined compression tests
R_f	failure ratio
r_u	pore pressure ratio
ρ_d	dry density
S_i, S_r	degree of saturation
σ_c	total stress cell pressure
σ_c'	effective stress cell pressure
σ_{vo}'	in situ effective vertical overburden stress
$\Delta\sigma_v$	increase in total vertical overburden stress
σ_1	major principal stress
σ_3	minor principal stress
$(\sigma_1-\sigma_3)_f$	deviator stress at failure
$(\sigma_3'/\sigma_1')_f$	principal stress ratio at failure
TP	test pit
t_{90}	time to complete 90% of primary consolidation
t_{100}	time to complete 100% of primary consolidation
T_v	time factor

UU	unconsolidated undrained triaxial test
u_f	pore pressure at failure
Δu	change in pore pressure
V_o	initial volume
ΔV	change in volume
w_n	natural water content
w_f	final water content
w_L	liquid limit
w_o	initial water content
w_{opt}	optimum water content
w_P	plastic limit

1. INTRODUCTION

1.1 General

Without the use of soil reinforcement, construction of embankment fills, earth dams or retaining walls may not be feasible due to poor soil conditions or limited right of way. Within the last 15 years high-strength polymeric materials have been used to reinforce soil in the form of plastic grids called geogrids. Layers of geogrid may be incorporated into an embankment during construction. As the fill height is increased, the slope will deform. Loads are then transferred from the soil to the stiffer geogrids in order to maintain strain compatibility and the overall factor of safety of the slope is increased.

Although there has been sufficient evidence to show that geogrids improve the stability of a slope, little is known about the mechanics by which geogrids act to reinforce a mass of soil. Consequently, reinforced slope design has been based on approximate limit equilibrium methods. Chalaturnyk (1988) presents a review of current design methodology. To date, field experience with geogrid reinforced embankments has been limited to cohesionless soil. Hence, little information is available on the behaviour of cohesive fill soils reinforced with geogrid.

In an effort to assess the performance and feasibility of geogrid reinforcement of cohesive soils, Alberta Transportation and Utilities and the University of Alberta

have undertaken a geogrid reinforcement research project. The project involves the construction of a low strength cohesive soil test fill that incorporates three different types of geogrid as well as an unreinforced control section. Alberta Transportation and Utilities requested that the Department of Civil Engineering at the University of Alberta design the test fill. This includes the selection of the soil used to construct the fill, the embankment geometery and the geogrid and instrumentation layout.

This thesis is concerned with analyzing both the fill soil with which the embankment is being constructed and the underlying foundation soil. The stress-strain properties of the fill and foundation soils established through various laboratory shear strength and consolidation tests will be presented. The selection of the embankment geometry and the appropriate fill soil will be discussed. The short term and long term factors of safety of the unreinforced control slope will then be assessed based on limit equilibrium analyses and the long term deformations of the slope will be predicted using a finite element analysis.

1.2 Statement of the Problem

In order to monitor the soil/geogrid stress transfers which takes place in the embankment, the fill must be built such that it will deform substantially. Moreover, the embankment slopes must be of homogeneous shear strength to allow for comparison between each of the geogrid reinforced

slopes and the unreinforced slope. It is, therefore, necessary to fully define the stress-strain properties of the various fill soils available to construct the embankment. It is also necessary to assess the stress-strain properties of the foundation soil such that stability and deformational analyses of the unreinforced, control slope can be conducted.

1.3 Objective of the Research

The objectives of this research are as follows:

1. To ensure that the soil and compaction specifications selected for construction of the test fill were appropriate based on the criteria that the soil deform significantly, thereby stressing the geogrids.
2. To predict the short-term and long-term factors of safety against a shear failure in the unreinforced slope of the test fill using limit equilibrium analyses with the soil parameters established during laboratory testing.
3. To predict the deformation of the unreinforced slope of the test fill using a finite element analysis with the soil parameters measured in this study.

1.4 Scope

In order to define the properties of the foundation and fill soils an extensive set of tests have been conducted. The soils tested include laboratory and field compacted fill

soil specimens and block sample and Shelby tube foundation soil specimens. Each of the soils were first characterized in terms of their Atterberg limits and grain size distributions. Unconfined compression tests, unconsolidated undrained and consolidated undrained triaxial tests with pore pressure measurements and consolidated drained triaxial tests were conducted on the fill soil specimens. Oedometer tests and consolidated undrained triaxial tests with pore pressure measurements were conducted on the foundation soil specimens.

The parameters obtained from the laboratory tests which are most representative of the field conditions were then applied to the stability and deformational analyses of an unreinforced slope, 12 m in height with 1:1 side slopes. Bishop's Modified Method of Slices (Bishop, 1955) was used to determine the short and long term factors of safety against shear failure of the unreinforced slope of the test fill. A finite element program called SAGE (Stress Analysis in Geotechnical Engineering), developed at the University of Alberta (Chan, 1988), was used to predict the long term deformations which would occur in the control slope. The analysis uses hyperbolic and elastic-perfectly plastic models to represent the stress-strain curves established for the fill and foundation soils through the laboratory testing.

1.5 Outline of the Thesis

CHAPTER 2 - A review is made of the factors which are known to affect the strength and deformation behaviour of compacted clay, similar to that which is being used to construct the test fill. The variation of soil shear strength with compacted structure, water content, and dry density is examined. The correlation between the shear strength and deformation behaviour under laboratory and field conditions is also discussed.

CHAPTER 3 - A general description of the site where the geogrid reinforced embankment is being constructed is presented. The history of the surficial geology in the Devon area is reviewed in order to assess the stress history of the test fill foundation soil. This will lead to a better understanding of how the foundation soil may deform in response to the weight of the test fill. The information obtained from a drilling and sampling program conducted at the site is presented, including the locations from which the various fill and foundation soil samples were removed. The Atterberg limits and grain size distributions established for each of the soils is presented and discussed.

CHAPTER 4 - Compaction specifications are established for the embankment fill soil based on unconfined compression test results. Detailed information on the stress-strain and

pore pressure behaviour of silt, clay and sandy clay fill soils are then presented in the form of unconsolidated undrained and consolidated undrained triaxial tests with pore pressure measurements and consolidated drained triaxial tests. A comparison is made of the differences in behaviour exhibited by the three types of fill soil specimens. The stress-strain curves to be modelled for the finite element analyses are selected.

CHAPTER 5 - One-dimensional consolidation test results are presented for several block sample specimens and Shelby tube specimens of foundation soil. The preconsolidation stress, permeability and settlement of the foundation soil is then assessed. The stress-strain and pore pressure behaviour of the foundation soil specimens are determined based on consolidated undrained triaxial tests with pore pressure measurements. Comments are made about modelling the stress-strain behaviour of the foundation soil for the finite element analysis.

CHAPTER 6 - The fill and foundation soil parameters to be used for the stability analyses are selected. Bishop's Modified Method of Slices is used to determine both the long and short term factors of safety of the unreinforced slope of the test fill. Pore pressures are considered in the short term analysis. The stress-strain models of the fill and foundation soils required for the finite element analysis

are presented. The results obtained from the analysis are then presented in the form of the distribution of horizontal strains acting in the slope at elevations of 1, 3 and 5 m. These are the elevations at which geogrids have been installed in the slopes adjacent to the control section. This information may be compared to the horizontal strains measured along the geogrids in later studies.

CHAPTER 7 - The conclusions drawn from the research are presented and recommendations for further studies are made.

2. REVIEW OF THE STRENGTH AND DEFORMATION OF COMPACTED SOILS

2.1 Introduction

It is necessary to ensure that the test fill will deform significantly in order to load the geogrids to their working stress level. This requires that compaction specifications be developed which will result in a soft embankment that deforms substantially under its own weight. It is therefore necessary to establish the factors which affect the strength and deformational behaviour of compacted clays.

In this chapter published triaxial test data obtained for compacted clays will be reviewed in which the authors assess:

1. The variation of soil shear strength with compacted structure, water content and dry density.
2. The correlation between shear strength and deformation behaviour under laboratory and field conditions.

A summary of the Atterberg limits, grain size distribution and compaction characteristics of the clay soils assessed by each of the authors is given in Table 2.1. The conclusions drawn will be compared with the stress-strain properties established in this study for several types of compacted clay soils under various test conditions in later chapters.

2.2 Variation of Shear Strength and Stress-Strain Behaviour with Compacted Structure, Water Content and Dry Density

2.2.1 Influence of Compacted Structure

Lambe (1958a) has shown that the structure of a compacted soil is governed by the as compacted water content. Soil which is compacted dry of the optimum water content will develop a flocculated structure, while soil compacted wet of optimum will develop a dispersed structure. The structure of a compacted clayey soil in turn, influences the strength and deformational behaviour of the soil. Lambe (1958b) has presented a discussion of the effects of compacted structure on the permeability, compressibility and shear strength of cohesive soil. A summary of his findings are given in Table 2.2. Lambe states that a soil compacted dry of optimum has a higher stress-strain modulus than a soil compacted wet of optimum. Therefore, since a fill which deforms under low stress levels is required for this project, the fill soil used to construct the test embankment should be compacted wet of optimum.

Seed, Mitchell and Chan (1960) discuss the influence of structure, initial water content and dry density on the strength of compacted clays. As part of their study, they presented consolidated undrained triaxial test results for compacted silty clay which show the differences in stress-strain and pore pressure behaviour exhibited by specimens with flocculated and dispersed structures. The

soil tested by them is described in Table 2.1 and the results are given in Figure 2.1. The specimen which was compacted wet of optimum attains an axial strain of up to 14% prior to reaching failure, at the maximum principal effective stress ratio, whereas the specimen compacted dry of optimum reaches a strain of only about 3% at failure. These results indicate that larger deformations would be exhibited by an embankment constructed of soil compacted wet of optimum.

2.2.2 Influence of Compacted Water Content and Dry Density

2.2.2.1 Unconsolidated Undrained Strength of Compacted Clay

Seed, Mitchell and Chan also present unconsolidated undrained triaxial test results which show the relationship between dry density, water content and strength for partially saturated Vicksburg silty clay prepared by kneading compaction. Figure 2.2 indicates that the undrained shear strength of the soil, compacted under various foot pressures, is more related to the as compacted water content than to the as compacted dry density for water contents of optimum or greater. At water contents of less than optimum both the as compacted dry density and water content influence the undrained shear strength significantly.

Casagrande and Hirschfeld (1960) also conducted an investigation on the influence of the as compacted dry

density and water content on the stress-deformation and strength characteristics of compacted silty clay. As part of their investigation they ran a series of unconsolidated undrained triaxial tests on partially saturated silty clay specimens with approximately the same Atterberg limits, grain size distribution and compaction curve as the fill soils being tested in this study. The index properties and compaction characteristics of the silty clay examined by Casagrande and Hirschfeld are given in Table 2.1.

Their study showed that on the wet side of optimum the unconsolidated undrained shear strength at a given water content increases only slightly with an increase in the as compacted dry unit weight of the soil. The test results presented in support of this conclusion are given in Figure 2.3. They show that the variations in the dry densities of the specimens have a greater affect on shear strength when sheared under a confining stress of 100 kPa than under a confining stress of 400 kPa. This is due to the fact that under high confining stresses, the specimems become fully saturated, except at low water contents of less than about 14%. Consequently the void ratio and corresponding strength after application of the cell pressure depend only on the water content.

Unconsolidated undrained triaxial tests were also conducted on partially saturated silty clay specimens

compacted to 95% of the maximum standard compaction dry unit weight at water contents ranging from 13 to 19%. The variation in undrained shear strength with as compacted water content determined for the specimens subject to high enough confining stresses to become saturated is given in Figure 2.4. Comparison of Figures 2.3 and 2.4 shows that the undrained shear strength of the compacted silty clay tested by Casagrande and Hirschfeld is considerably more sensitive to changes in the as compacted water content than to changes in the as compacted dry density.

2.2.2.2 Consolidated Undrained Strength of Compacted Clayey Soil

To examine the effect of the compaction water content on the behaviour of clay specimens, Seed, Mitchell and Chan (1960) presented the results from consolidated undrained traixial tests with pore pressure measurements conducted on saturated silty clay specimens. Two groups of specimens were prepared by kneading and static compaction at various wet of optimum water contents. They were then allowed to consolidate under a back pressure, thus bringing the degree of saturation in the specimens up to 100%. The water contents before and after saturation are shown in Figure 2.5 for the specimens prepared by standard static compaction.

The stress-strain and pore pressure-strain curves obtained from the two sets of tests are shown in Figures 2.5 and 2.6. The water contents shown are those determined for the fully saturated specimens. The results indicate that relatively small variations in water content manifest considerable differences in the stress-strain behaviour and the pore pressures developed within the specimens at failure.

Lovell and Johnson (1981) also examined the relationship between the pore pressures developed at failure and the as compacted water contents and dry densities of compacted clay specimens subject to consolidated undrained triaxial tests. The soil tested by them is described in Table 2.1. A statistical analysis of the laboratory data obtained by the authors resulted in the following equation:

$$A_f = 1.79 - 0.00011\rho_d\sqrt{S_i} + 1.28\sigma_c'/\rho_d \qquad [2.1]$$

where A_f=estimated value of Skempton's A-paramter at failure (Skempton, 1954)

ρ_d=as-compacted dry density (kg/m^3)

S_i=initial degree of saturation (%)

σ_c'=isotropic consolidation stress (kPa)

The relationship between A_f and ρ_d determined from this equation is shown in Figure 2.7 for a constant σ_c' and

initial degrees of saturation varying from 70 to 90%. Figure 2.7a shows that for a given initial degree of saturation, as the density of the specimens increases A_f decreases. In other words, the denser specimens tend more towards dilation due to shearing and this is compensated for by a reduction in the pore pressures.

Lovell and Johnsons' statistical equation for A_f was checked against the consolidated undrained triaxial test data presented by Casagrande and Hirschfeld. Figure 2.8 shows the change in A_f with increasing confining stress calculated using Equation 2.1 for a dry density equal to 95% of the standard compaction maximum at various degrees of saturation. The measured values of A_f determined from the consolidated undrained traixial tests are also shown. Figure 2.8 indicates that the A_f parameters measured in the laboratory do not show good agreement with the theoretical relation developed by Lovell and Johnson for their soil. The compacted clay soil tested in this study will also be compared with Lovell and Johnsons' theoretical relation in Chapter 4.

Additional statistical analyses by Lovell and Johnson yielded an equation which relates the percent volume change due to back-saturation and consolidation of soil specimens to the as compacted dry density, initial degree of saturation and the isotropic consolidation pressure. The equation is given by:

$$\Delta V/V_o = 28.48 - 0.0000136(\rho_d)^2 + 0.0077 S_i \sqrt{\sigma_c} \qquad [2.2]$$

The relationship between $\Delta V/V_o$ and ρ_d as given by this equation for a constant initial degree of saturation and various confining stresses is shown in Figure 2.7b. A negative percent volume change represents net swell and a positive percent volume change represents net consolidation. Figure 2.7b shows that for a given confining stress, as the dry density of the specimens increase their potential for swell increases. However, for a constant dry density the specimens show more net consolidation as the confining stress increases.

Casagrande and Hirschfeld give the percent volume change undergone by their silty clay specimens during the consolidation phase of consolidated undrained triaxial tests. Figure 2.9 shows the measured percent volume change due to consolidation only, undergone by specimens compacted to the maximum standard compaction dry density at water contents of 13.3, 16.4 and 17.4%. The net theoretical percent volume change due to back-saturation and consolidation for these specimens as predicted by Lovell and Johnsons' equation is also shown with solid lines. It is apparent from Figure 2.9 that swell due to back-saturation has a significant effect on the final volume of a specimen after consolidation, especially under low confining stresses. Since

Casagrande and Hirschfeld did not give the volume changes due to back-saturation of their specimens the validity of Lovell and Johnsons' equation for their soil cannot be determined. However the trend of greater consolidation with an increase in water content is evident.

The consolidated undrained triaxial tests conducted by Lovell and Johnson on compacted clay specimens also showed that the effective stress cohesive strength of the Mohr-Coulomb failure envelope increases with increasing water content, for a constant initial void ratio. The statistical relationship established by them is given by:

$$c' = 1.71-3.83(w)\log(e_o) \qquad [2.3]$$

where c'=effective stress cohesive strength (kPa)

w=compaction water content (%)

e_o=initial void ratio

Equation 2.3 has been plotted for various values of e_o in Figure 2.7c. As indicated in Figure 2.7b, specimens compacted at a low water content have a greater swell potential and according to Figure 2.7c, they therefore have a lower effective stress cohesive strength. Lovell and Johnson also determined that the effective stress angle of frictional resistance was approximately

constant for the range of as compacted water contents and densities examined. Casagrande and Hirschfeld did not include cohesive strength intercepts with their results. However, Equation 2.3 will be compared with the consolidated undrained triaxial test data obtained from this study in Chapter 4.

2.3 Correlation between Shear Strength and Deformational Behaviour of Compacted Clayey Soil Under Laboratory and Field Conditions

2.3.1 Shear Strengths of Laboratory and Field Compacted Specimens

Holtz and Ellis (1963) conducted a series of triaxial tests on cohesive soil compacted in the field and in the laboratory to determine whether any differences in shear strength existed between the specimens. The soil studied by them is described in Table 2.1. Undisturbed block samples were removed near the surface of three compacted clay embankments. Specimens were trimmed from the block samples for testing. Additional soil was removed with the block sample and remoulded specimens were prepared by standard laboratory impact compaction methods and by a laboratory sheepsfoot compaction machine.

The results obtained from triaxial tests conducted on these specimens showed the following:

1. The field-compacted specimens tended to show only

slightly higher shear strengths than the specimens compacted in the laboratory using standard, static compaction methods. The specimens compacted in the laboratory with the sheepsfoot machine showed slightly lower strengths than either the standard laboratory-compacted or field-compacted specimens.

2. The strains at failure shown by the field-compacted specimens were equal or less than the failure strains exhibited by either of the laboratory-compacted specimens.
3. A trend in the pore pressures developed during shearing of specimens was not apparent.

Holtz and Ellis concluded that for the soils tested in their study, " the normal laboratory procedures used produce strength parameters which tend to be equal to or slightly conservative to the strength of the soils compacted in the field".

2.3.2 Modelling of Field Conditions

2.3.2.1 Drainage

Bjerrum and Simons (1960) showed that the effective stress angles of shear resistance determined from consolidated undrained and consolidated drained triaxial tests are approximately the same for many clays if failure is defined at the maximum principal effective stress ratio. The friction angles determined from drained and undrained tests for various specimens of

undisturbed and remoulded clay soil are given in Figure 2.10.

Although the angles of frictional resistance determined from consolidated drained and consolidated undrained triaxial tests are approximately the same, the stress-strain behaviour exhibited by specimens subject to these tests may differ considerably. Casagrande and Hirschfeld conducted both consolidated drained and consolidated undrained triaxial tests on silty clay compacted to 95% of the standard compaction maximum density at a water content of 19%. The stress-strain curves are shown in Figure 2.11 for confining stresses of 100 and 400 kPa.

The consolidated undrained stress-strain curves exhibit elastic-perfectly-plastic behaviour with a high initial tangent modulus. The consolidated drained stress-strain curves have a much lower initial tangent modulus and appear to express a hyperbolic shape. Moreover, the strains at failure are much larger for the drained tests because the strains measured during this test represent the sum of the volumetric strains and the shear strains (Lambe and Whitman, 1969). Volumetric strains are not permitted in consolidated undrained tests during shear. Therefore, if prediction of embankment deformations from triaxial data is required, the drainage conditions which exist in the field should be modelled in the laboratory.

2.3.2.2 Stress Paths

At the time of conducting this research the rate of construction of the test embankment to the final height of 12 m was unknown. Therefore, the stress paths which would be followed in the field were unknown and could not be modelled during laboratory shear strength and deformation testing. Therefore, to estimate the strength and deformational characteristics of the soils being used to construct the test fill, conventional triaxial and oedometer tests were conducted.

Table 2.1: Summary of Compacted Clayey Soils Studied by Various Authors

Reference	Soil Type	Wl (%)	Wp (%)	Ip (%)	%clay sizes	%silt sizes	%sand sizes	Ac	compaction method	w(opt) (%)	Pd(max) (g/cm3)
Seed et al (1960)	silty clay	38	24	14	24	69	7	0.7	Static	16.1	1.813
"	"	"	"	"	"	"	"	"	Kneading	17.2	1.761
Holtz & Ellis (1963)	Sherman Dam Clay	32	19	13	21	74	5	0.6	Standard	19.0	1.672
Lovell & Johnson (1981)	Highly Plastic Clay	53	22	31	-	-	-	-	Kneading	22.0	1.635
Casagrande Hirshfeld (1960)	Silty Clay	34	15	19	20	59	21	0.9	Standard	15.7	1.783
"	"	"	"	"	"	"	"	"	Harvard Miniature	16.0	1.770
Hofmann (1989)	Devon Clay	41	20	21	30	44	26	0.7	Kneading	21.0	1.678
Hofmann (1989)	Devon Silt	33	18	15	23	58	19	0.7	Kneading	17.0	1.817
Hofmann (1989)	Fill Shelby Tube	36	22	14	20	61	19	0.7	Field Sheepsfoot	-	-
Hofmann (1989)	Sandy Clay	39	18	21	-	-	40	-	-	-	-

Table 2.2: Comparison of Properties for Cohesive Soil Compacted Dry of Optimum and Wet of Optimum (Modified from Lambe, 1958b)

Property	Comparison
1. Structure	
a. Particle Arrangement	Dry side more random.
b. Water Deficiency	Dry side more deficient hence, imbibe more water, swell more, has lower pore pressure.
c. Permanence	Dry side structure sensitive to change.
2. Permeability	
a. Magnitude	Dry side more permeable.
b. Permanence	Dry side permeability reduced much more by permeation.
3. Compressibility	
a. Magnitude	Wet side more compressible in low pressure range, dry side in high pressure range.
b. Rate	Dry side consolidates more rapidly.
c. Rebound	Wet side rebound per compression greater.
4. Strength	
a. As-Moulded	
- undrained	Dry side much higher.
- drained	Dry side somewhat higher.
b. After Saturation	
- undrained	Dry side somewhat higher if swelling prevented; wet side can be higher if swelling permitted.
- drained	Dry side about the same or slightly greater.
c. Pore Water Pressure at Failure	Wet side higher.
d. Stress-Strain Modulus	Dry side much greater.
e. Sensitivity	Dry side more apt to be sensitive.

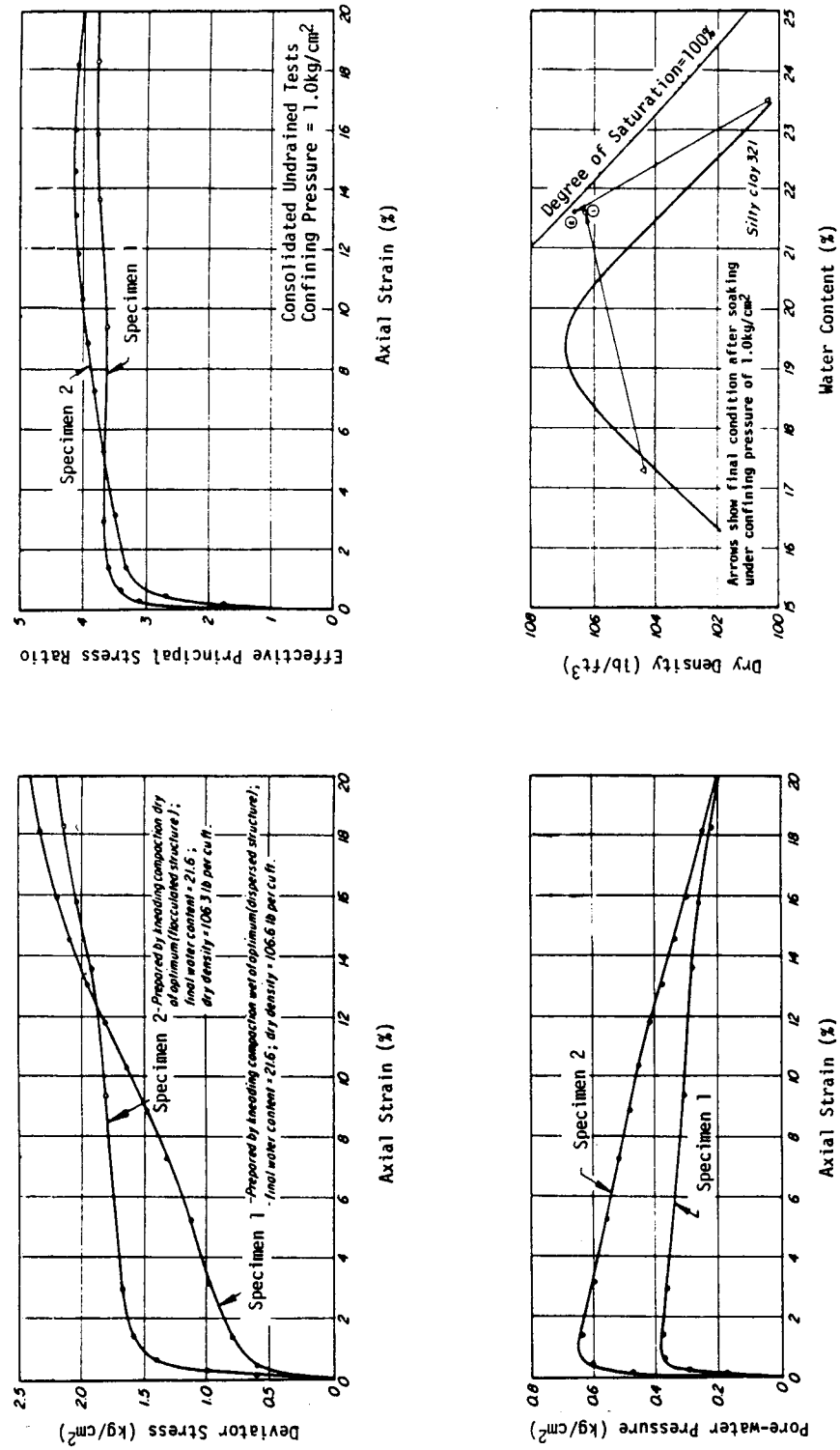

Figure 2.1: Influence of Compacted Structure on Stress-Strain Behaviour - CU Tests on Silty Clay (Modified from Seed et al., 1960)

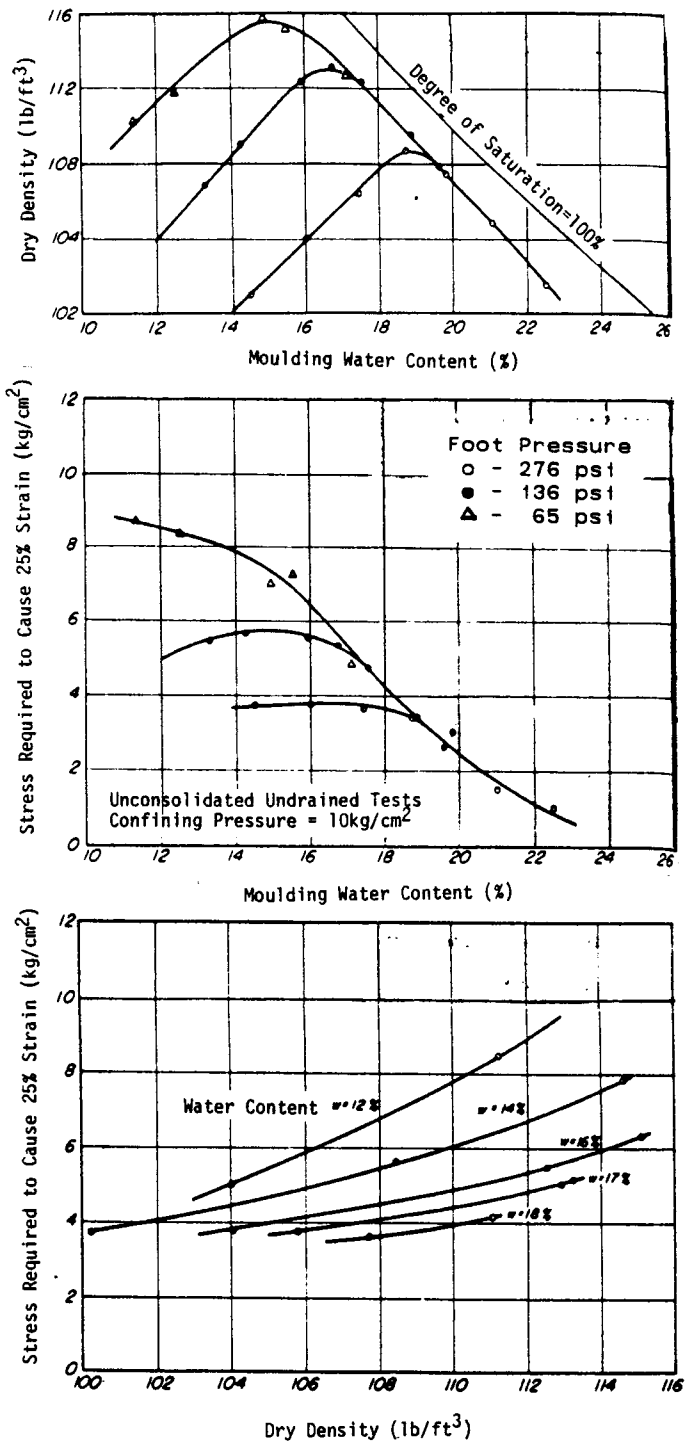

Figure 2.2: Influence of Compacted Water Content and Dry Density on Shear Strength - UU Tests on Silty Clay (Modified from Seed et al., 1960)

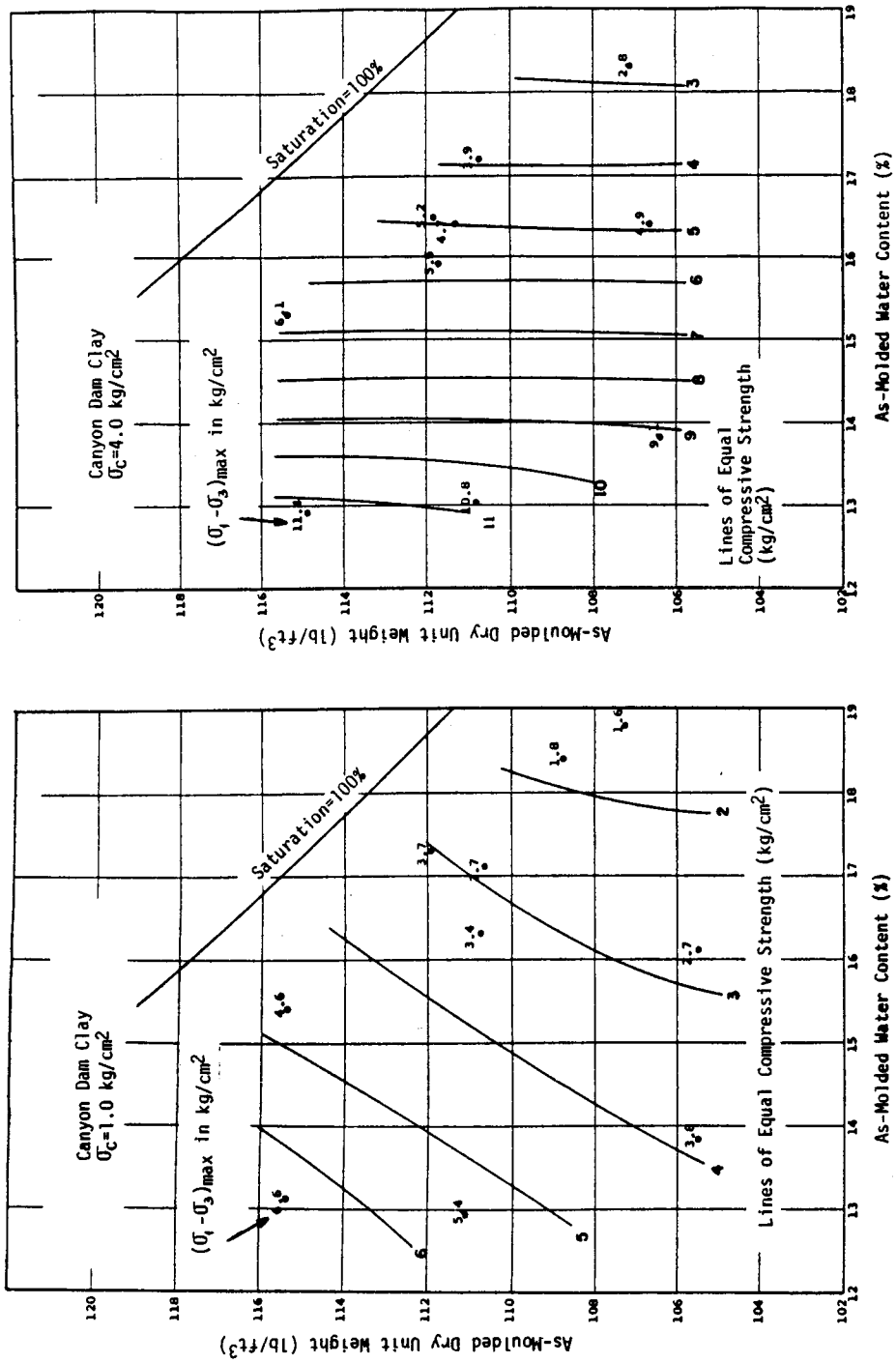

Figure 2.3: Influence of Compacted Dry Density on Shear Strength - UU Tests on Silty Clay (Modified from Casagrande & Hirschfeld, 1960)

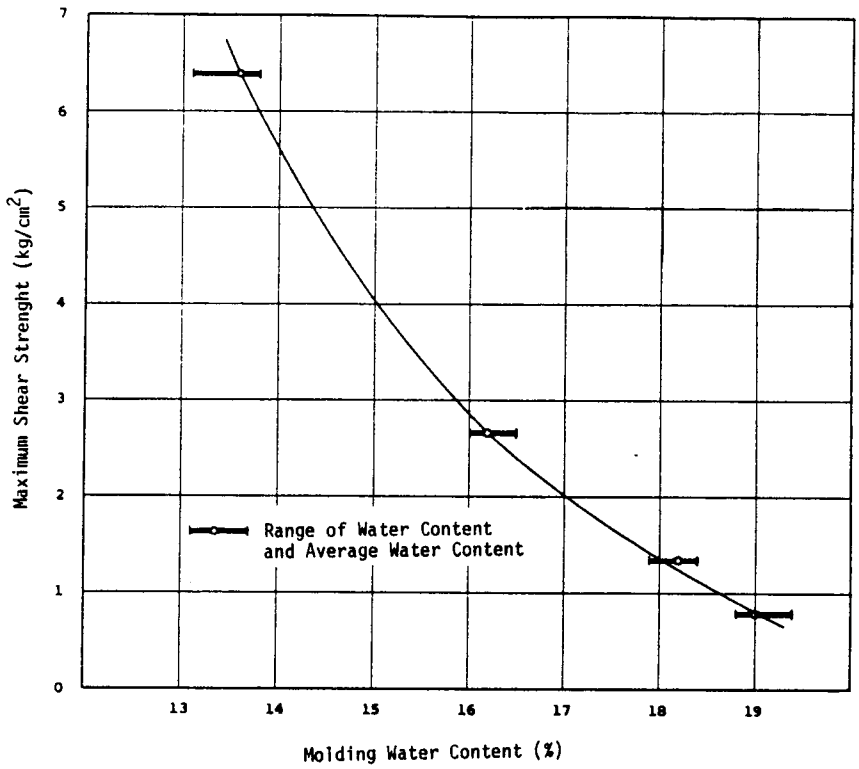

Figure 2.4: Influence of Compacted Water Content on Shear Strength - UU Tests on Silty Clay (Modified from Casagrande & Hirschfeld, 1960)

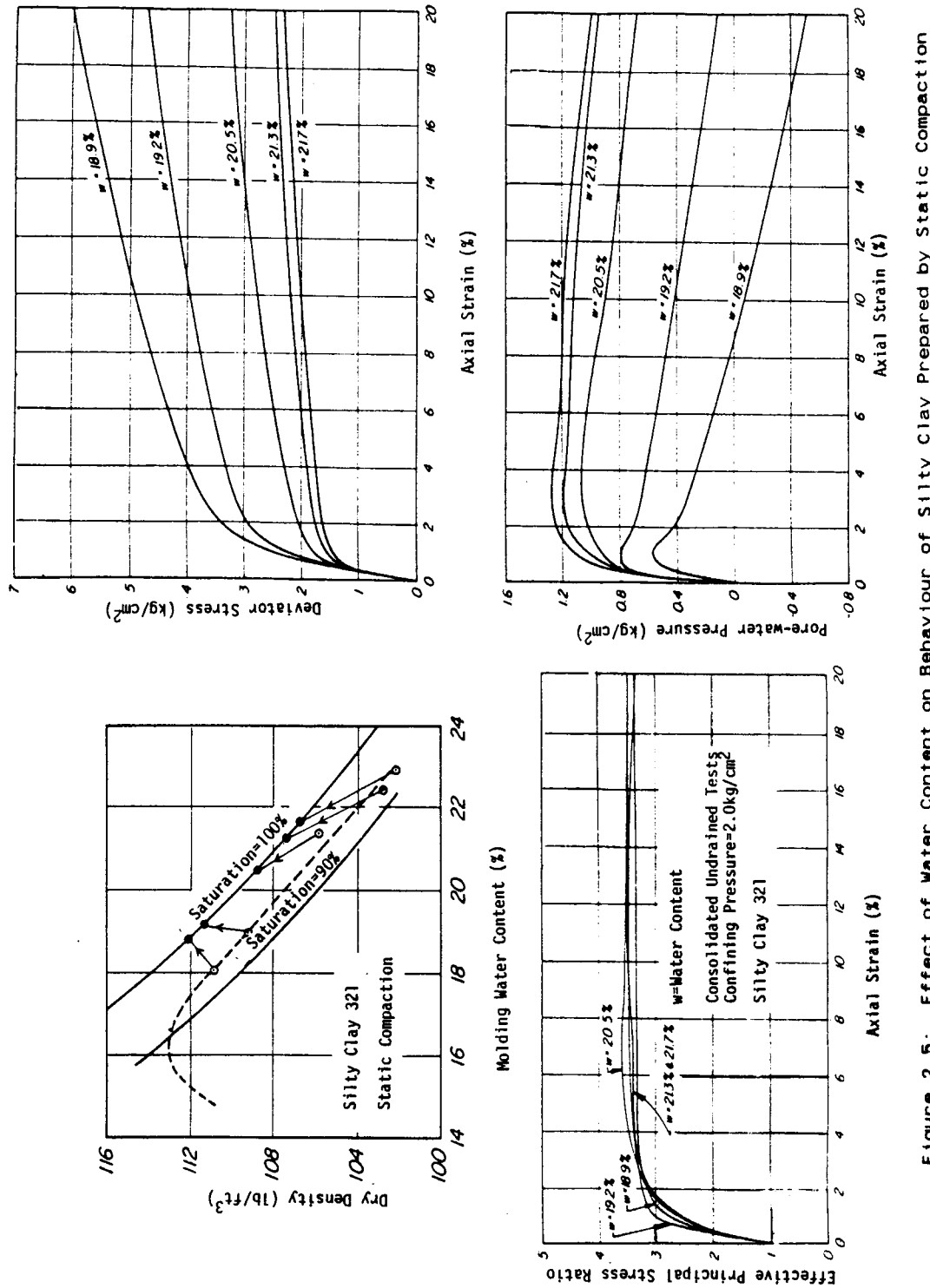

Figure 2.5: Effect of Water Content on Behaviour of Silty Clay Prepared by Static Compaction (Modified from Seed et al., 1960)

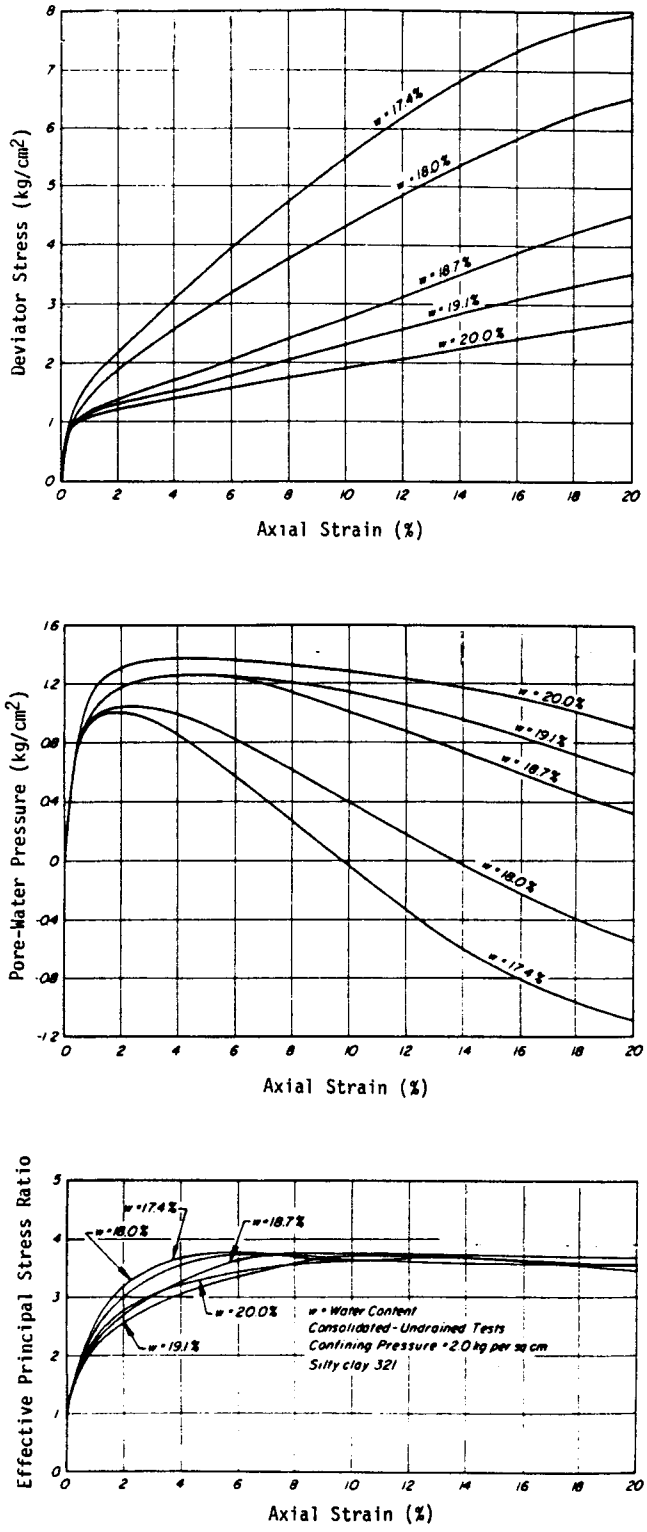

Figure 2.6: Effect of Water Content on Behaviour of Silty Clay Prepared by Kneading Compaction (Modified from Seed et al., 1960)

a)

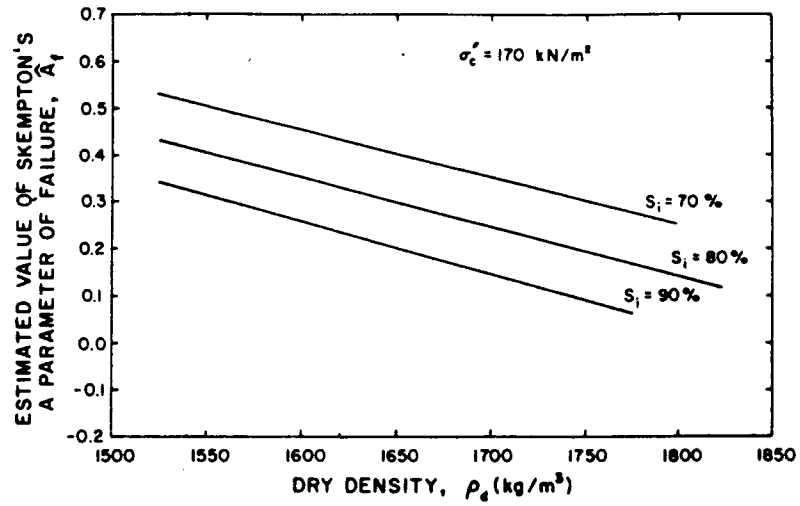

b)

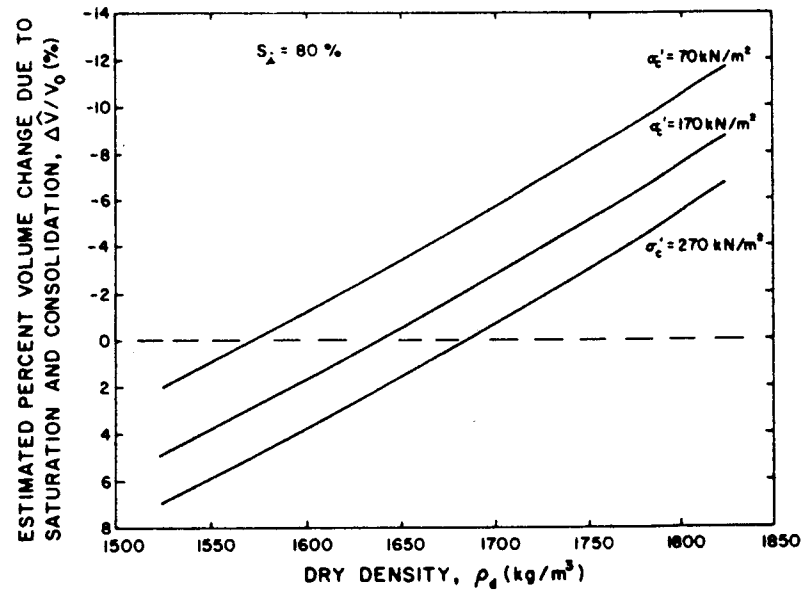

c)

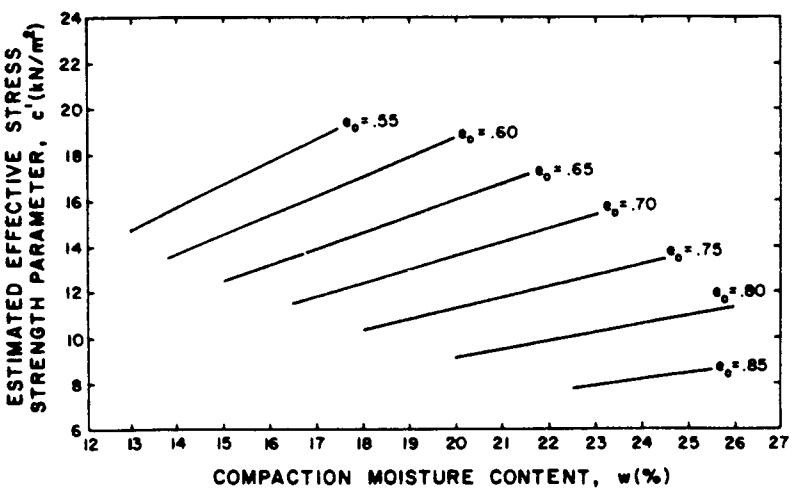

Figure 2.7: Statistical Relations Developed by Lovell and Johnson for Compacted Silty Clay (Modified from Lovell and Johnson, 1981)

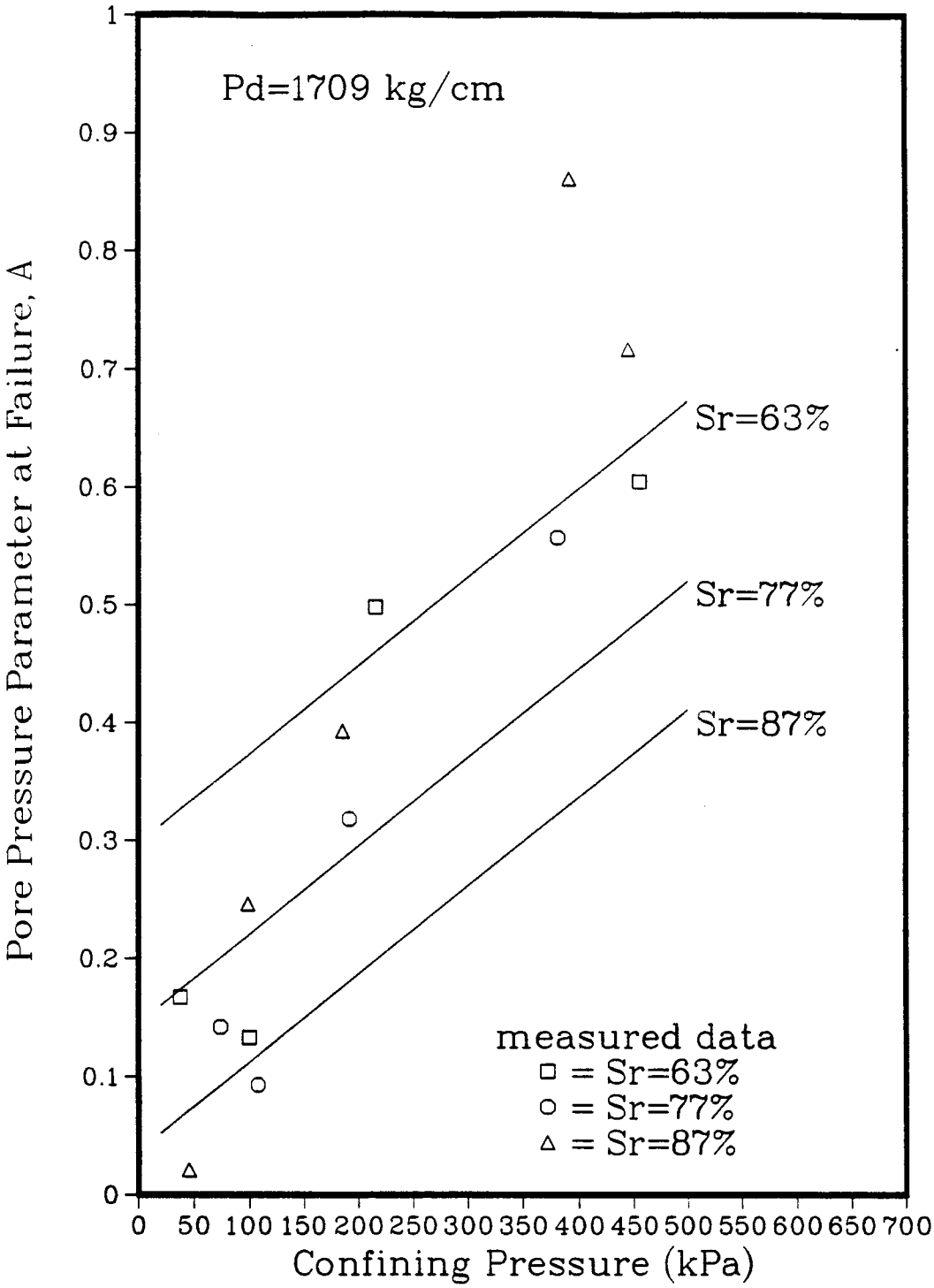

Figure 2.8 : Calculated and Measured Values of A from Casagrande & Hirschfelds' data

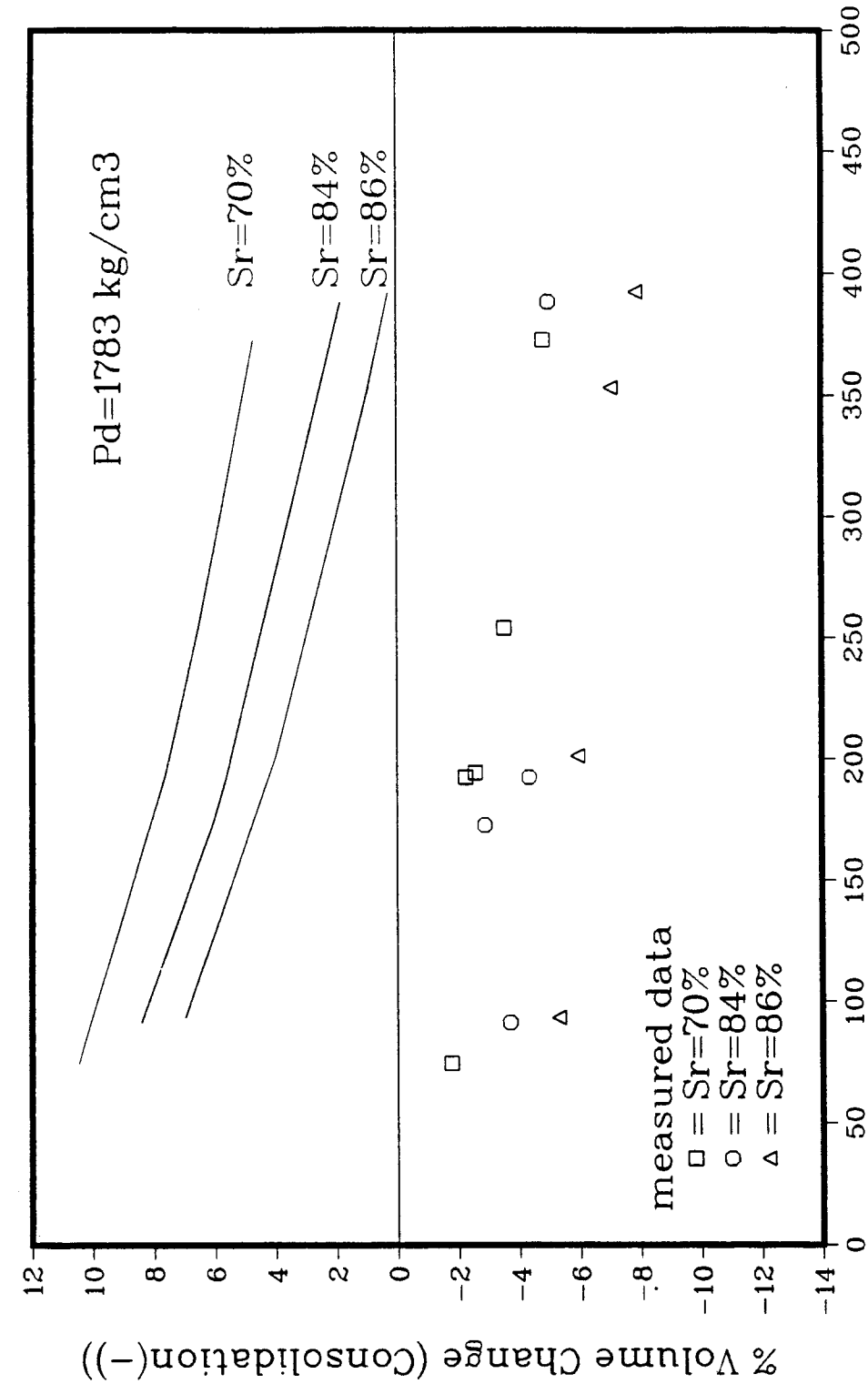

Figure 2.9: Calculated & Measured Values of V/Vo from Casagrande & Hirschfelds' Data

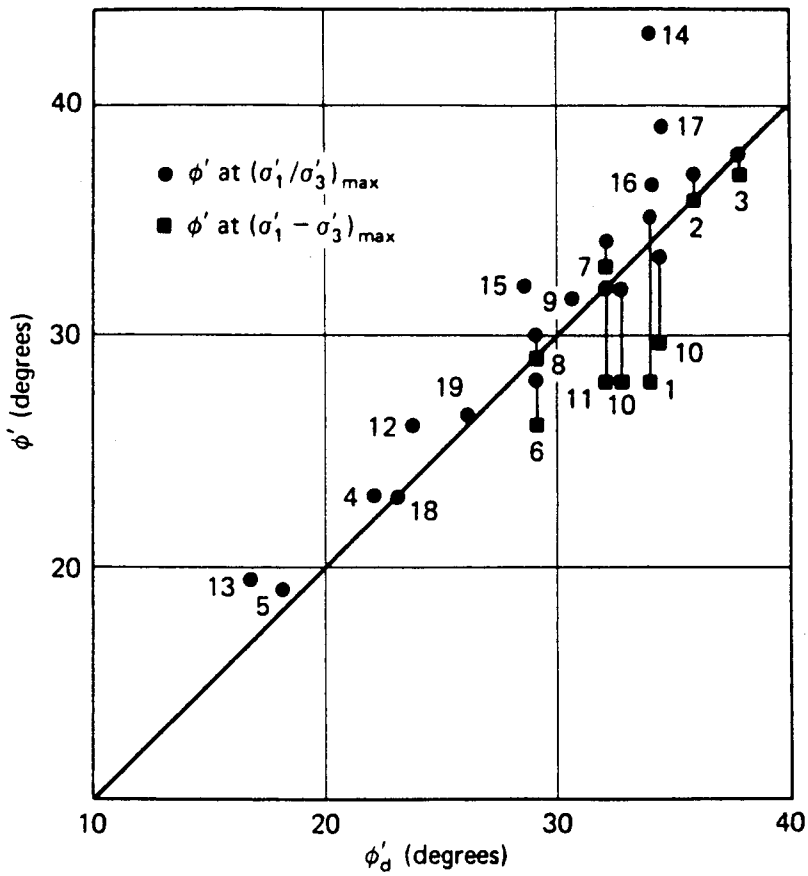

Type of Clay	State*	Reference
1 Cornwall	U	Kenney
2 Cornwall	R	Kenny
3 Bersimis	R	Kenney
4 Weald	R	Henkel
5 London	R	Henkel
6 Oslo	U	N.G.I.
7 Fredrikstad	U	N.G.I.
8 Lodalen	U	N.G.I.
9 Fornebu	U	N.G.I.
10 Drammen	U	N.G.I.
11 Okernbraten	U	N.G.I.
12 Seven Sisters	U	Casagrande and Rivard
13 North Ridge	U	Casagrande and Rivard
14 Organic	U	Casagrande
15 Boston Blue	U	Casagrande
16 Weymouth	U	Hirschfeld
17 New Haven	U	Hirschfeld
18 Haslemere	R	Skempton and Bishop
19 Wiener Tegel	R	Hvorslev

* U = undisturbed
R = remoulded

Figure 2.10 : Relationship between Od Determined from CD Triaxial Tests and ϕ' Determined from CU Tests with Pore Pressure Measurements (Modified from Bjerrum and Simons, 1960)

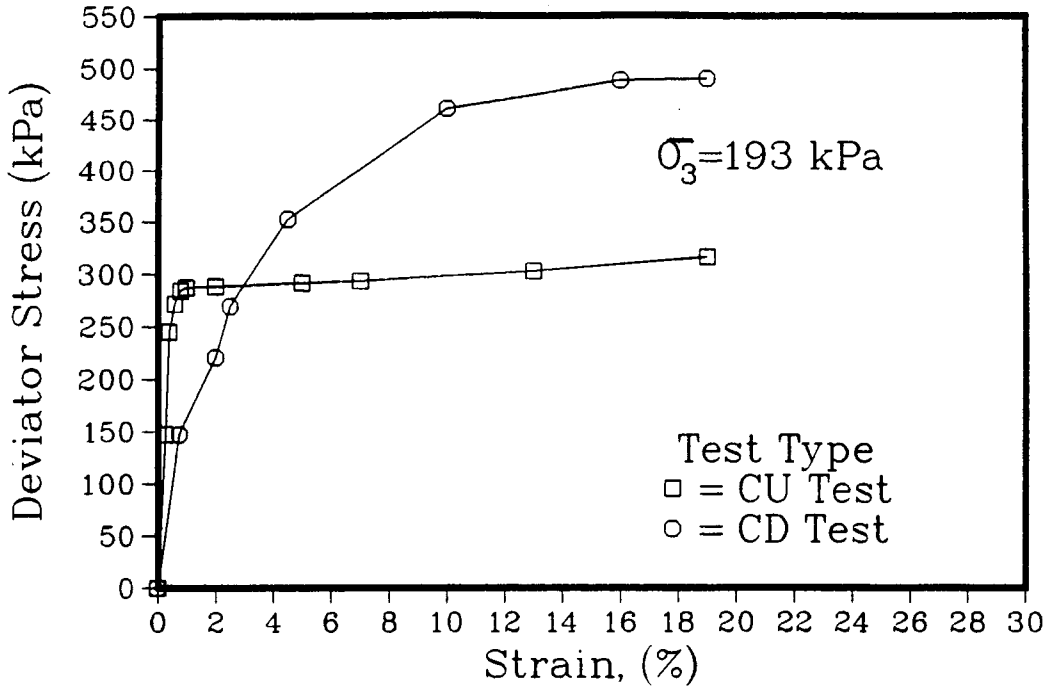

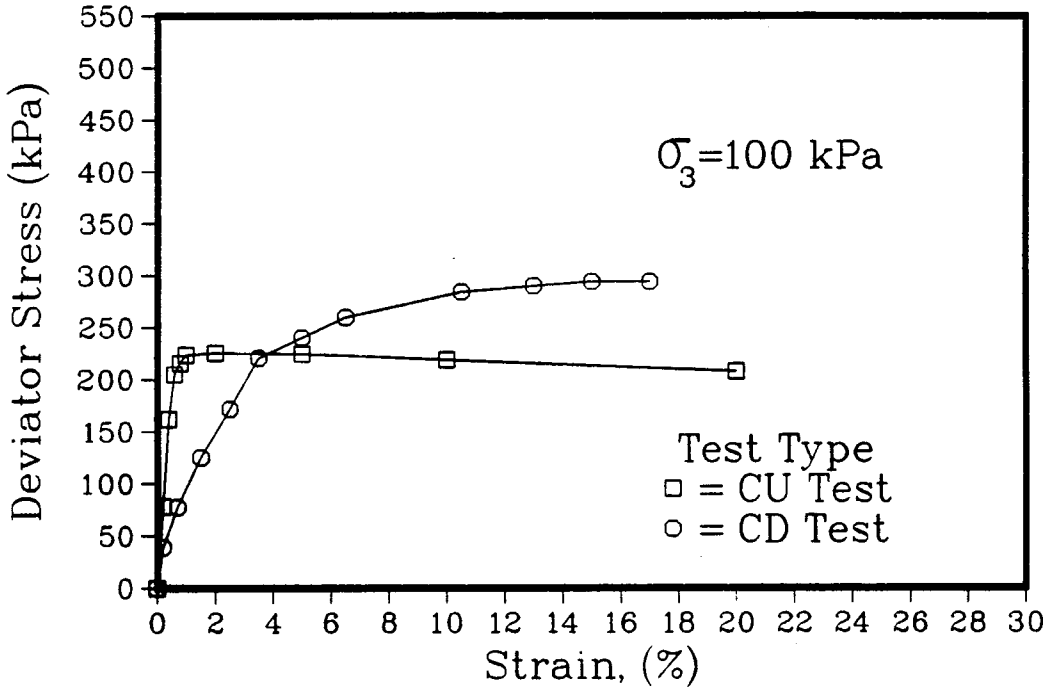

Figure 2.11: CU & CD Stress–Strain Curves (Modified from Casagrande and Hirschfeld, 1960)

3. CHARACTERISTICS OF THE FOUNDATION AND FILL SOILS

3.1 Introduction

The recent geological history of the Devon area will first be reviewed to assess the stress histories of the surficial deposits. The particular strata of the test fill foundation soil determined from a drilling and sampling program undertaken at the site will then be presented. The soil units identified during drilling will be correlated with those units for which the geological history has been established. This will aid in determining which materials have been consolidated under loads of a lesser magnitude than those induced by the test embankment and therefore may deform significantly under its weight.

Additional undisturbed foundation soil samples will be described. These include a block sample removed from a test pit near the test fill site and Shelby tube samples obtained by Alberta Transportation on the north side of the North Saskatchewan River along the new alignment of Highway 60. The foundation soil samples whose properties are considered relevant for the prediction of embankment deformations will be characterized in terms of their Atterberg limits and grain size curves.

To characterize the borrow soil available to build the test fill, a bulk sample of loose soil was removed from the site. The Atterberg limits, grain size curve and compaction curve will be presented and discussed. Once construction of

the embankment was underway, thin-walled tube samples were taken along the center lines of each quadrant for every second lift of compacted soil. A bulk sample of the compacted fill was also removed at an elevation of 3.0 m from the south end of the test fill. The Atterberg limits and grain size curves established for the tube samples taken at a fill height of 1.67 m and for the bulk sample will be presented and compared with those determined for the fill soil prior to construction. The compaction curve obtained for the bulk sample will also be presented. The actual soil being used to construct the fill was analysed to determine whether or not its properties differed from the borrow soil which had been tested prior to construction of the test fill.

3.2 Regional Geology

Detailed descriptions of the bedrock and surficial geology of the Devon area are presented by Gabert (1968). The geological history and composition of each of the soil units identified by Gabert will be presented to aid in identifying which soil units may be significantly compressible under the weight of the test fill.

The bedrock in the Devon area is the lowest member of the Upper Cretaceous Edmonton Formation (Ower, 1958). It is composed of alternating bentonitic, carbonaceous shales and light grey sandstones. Coal seams of up to 0.6 m in thickness are also present.

Six distinct geological units may be indentified above the bedrock. Unit A, overlying the bedrock, is composed of Saskatchewn sands and gravels. This material was deposited as a river network cut down into the bedrock between 50,000 and 100,000 years ago. The test fill site is situated above one of the tributary valleys, therefore, boreholes drilled in the test fill foundation soil should reveal Saskatchewan sands and gravels over bedrock.

A period of glaciation followed during which a poorly sorted sheet of till, unit B, was deposited on the Saskatchewan sands and gravels. The grain size distribution of the till ranges from large granitic and gneissic boulders to fine silty clay material. Unit B is olive grey in colour. The deposit covers most of the area and is thickest above the buried valleys. This basal till sheet is most likely heavily overconsolidated due to the high loads placed on the soil by the ice.

As the glacier began to retreat well-bedded silts, sands and gravels were laid down by melt water to form unit C. The ice advanced a second time to cover the glaciofluvial deposit with the till composing unit D. Unit D is made up of poorly sorted material containing an abundance of coal and is olive grey in colour. The till deposit is thickest over depressions in the bedrock surface. Like unit B, this material is also a basal till and is probably heavily overconsolidated. The sand lying directly beneath unit D may also have been compacted by the weight of the glacier.

The till of unit D is overlain by the glaciolacustrine sediments of Lake Edmonton. The sediments forming unit E range from very well-bedded sand, silt and clay to till-like material deposited by melting ice floating in Lake Edmonton. The grain size distribution of unit E ranges from fine material near the bottom of the unit to coarse material near the top. The upper part of unit E is composed of sand or silty sand. The history of unit E suggests that the soil is normally consolidated. However, in some areas wind moulded the sand deposits of unit E into large dunes of up to 15 m in height. The presence of one such sand dune adjacent to the test fill site indicates that the local glaciolacustrine sediments may have become overconsolidated as the dune covered the area and then migrated. Air photos show numerous sand dunes in the surrounding region which have now been stabilized by vegetation.

3.3 Sampling of the Foundation Soil

3.3.1 Shelby Tube Samples

Four boreholes were drilled in the foundation soil at the test fill site with a wet rotary drill rig. The locations of these holes are presented in Figure 3.1. Standard penetration tests and undisturbed thin-walled tube samples were taken alternatively between 1 and 10 m below the ground surface. Split spoon samples were obtained from the standard penetration tests for index tests and natural

water contents. Shelby tubes, 73 mm ($2^{7}/_{8}$") in diameter by 0.61 m (2') long, were pushed into the soil below the bottom of the washed-out drill holes to obtain undisturbed tube samples. The tube samples were later extruded for triaxial and oedometer tests.

The boreholes were logged in the field as drilling progressed by examining the split spoon samples and the exposed ends of the tube samples. The strata identified in each borehole are shown in Figure 3.2. The logs indicate that each of the soil units are approximately continuous over the region of the test fill foundation. The changes in natural water content and blow count with depth are plotted in Figure 3.3 along with the average boundaries of each soil unit. The plot represents data obtained from all four boreholes.

The uppermost 4.6 m of soil consists of a sandy silt to silty clay. The material is brown in colour with some grey pockets. Silty clay was not clearly distinguishable in boreholes 3 and 4, although the sandy silt unit became more fine grained with depth. The average blow count of the upper 4.6 m indicates that the material is of medium consistency. Table 3.1, after Peck et al. (1974), relates the blow count values of clayey soils with degrees of consistency. Figure 3.3 shows a decrease in the water content of the unit above about 2 m, suggesting the presence of a desiccated crust. The ground water table exists at about elevation 697.3, 5 m below the ground surface at the test fill site. According to

Gaber's findings, the sandy, clayey silt is a glaciolacustrine sediment of Lake Edmonton. Although lake sediments are usually normally consolidated, it was noted in the previous section that this material may have been overconsolidated by sand dunes that once moved across the area.

The silt is underlain by a stiff to very stiff, grey clay till. The water content decreases with depth through this unit from 35% to 15% and then remains fairly constant with depth. The stiffness of this material and the fact that it is a basal till suggests that the unit is heavily overconsolidated.

A medium dense, grey silty sand is situated between 7 and 8 m below the ground surface. This unit was not detected in borehole 4 due to a loss of samples at 6.4 m and between 8 and 9 m.

A very stiff, grey clay till is situated beneath the grey sand. The thickness of this unit appears to vary from about 0.5 to 1.5 m across the site. Gabert indentified this unit as a basal till, hence, it is also most likely heavily overconsolidated.

Beyond about 9 to 10 m a very dense grey sand was identified. This was classified as Saskatchewan sands and gravels by Gabert. It was not possible to remove samples from the unit due to its high density. Consequently, drilling was stopped at about 10 m in boreholes 1, 3 and 4. In borehole 2, however, drilling was continued down to

clayshale bedrock at 27 m, without sampling. Examination of the material removed as drilling progressed showed that the grey sand was continuous to bedrock.

Figure 3.3 shows that the N values of the foundation strata increase with depth beyond 6 m to attain a blow count of about 90 at 9 m. From this information and consideration of the recent geological history of the surficial deposits it was estimated that only the top 6 m of foundation soil would compress significantly under the weight of the test fill. Consequently, the stress-strain and settlement characteristics of only the sandy, clayey silt foundation soil was determined by laboratory testing. The elevations and sample numbers of the tube samples extruded, wrapped and stored in a moisture room for laboratory testing are given in Table 3.2. The Atterberg limits and grain size curves established for these samples will be presented in Section 3.5 of this chapter.

3.3.2 Undisturbed Block Sample

Two test pits were dug with a backhoe in the locations shown in Figure 3.1. A large undisturbed block sample of sandy, clayey silt was removed from the floor of test pit 1 at a depth of 4.5m below the ground surface (approximate elevation of 697.5m). Vertical rust stained fissures at a spacing of approximately 10 to 15 cm and horizontal rust stained fissures at a spacing of about 15 cm were evident throughout the sample. The fissures were tight but the block

tended to fall apart along the fissures when samples were being cut. The fissures indicate that the soil has undergone some degree of stress relief and is therefore, overconsolidated. The block sample showed distinct horizontal laminations suggesting, in agreement with Gabert's assessment, that the deposit is lacustrine in nature. The Atterberg limits and grain size curve were established for the block sample. It was then wrapped in plastic and stored in a moisture room for later testing.

3.3.3 Tube Samples Obtained by Alberta Transporation and Utilities

Alberta Transportation and Utilities drilled and logged a total of 70 boreholes at various locations along the new alignment of Highway 60. Shelby tube samples were obtained from these holes. The soil descriptions and variation of natural water content and shear strength with depth have been compiled by Alberta Transportation and Utilities. Only those tests on the undisturbed foundation soil which are relevant to the test fill have been presented here. Figure 3.4 shows the average soil profile obtained from boreholes 27 and 28. Tube samples removed from these boreholes were used by Alberta Transportation and Utilities for consolidated undrained triaxial testing in their laboratory.

3.4 Classification of the Foundation Soil

The Atterberg limits and the percent composition determined for the various samples of foundation soil are given in Table 3.4. The Atterberg limit tests were conducted according to ASTM (American Society for Testing and Materials) designation D 4318-84. The grain size analyses were performed according to ASTM standard D 421-58.

The grain size curves established for tube samples 22 and 24 and for the block sample are shown in Figure 3.5. The distribution of sand, silt and clay-sized particles is similar for each of the three samples: the dominant particle size being silt. Although on the basis of the grain size curves, these soils would be classified as silt, the plastic and liquid limits (given in Table 3.4) show that the small fraction of clay-sized particles present have a significant influence on the behaviour of the soil.

Casagrande (1948) suggested that the clay minerals present in a soil may be identified by comparing the plasticity index and liquid limit of the soil to those of known minerals. Figure 3.6 shows the range of liquid limits and plasticity indicies determined for 5 different clay minerals and the Atterberg limits determined for the tube samples and block sample. It appears that the clay fraction of the silty foundation soil between 2.5 and 4.0 m below the ground surface may contain a significant amount of illite. Sedimentation of clay minerals such as illite may result in a flocculated structure (Holtz and Kovacs, 1981) which in

turn may effect the stress-strain behaviour of the soil unit containing the clay minerals. If this structure is disturbed during sampling of, for example, a lacustrine deposit, the true stress-strain behaviour of the in situ soil may not be obtained from laboratory testing.

X-ray diffraction tests were carried out on four samples of silty clay obtained from the test fill site to determine the mineral content. The test results, presented in Table 3.3, show that the clay fraction contains up to 50% illite and up to 60% montmorillonite.

Alberta Transportation and Utilities determined the Atterberg limits of Shelby tube samples obtained from borehole 28, at depths of about 10 m and 13 m, for triaxial testing. The liquid and plastic limits (given in Table 3.4) indicate that the soil in borehole 28, between10 and 14 m, behaves plastically over a much narrower range of water contents, and is therefore more silty than the foundation soil at shallower depths tested in this study. Since Alberta Transportation and Utilities did not conduct hydrometer tests on their soil, the grain size distributions cannot be compared.

3.5 Selection and Sampling of the Fill Soil

Figure 3.3 shows that approximately 6 different soil units may be found in the Devon area. Of these, the silty clay, clay and the grey clay till were available for construction of the test fill. Satisfying the objectives of

the test fill required that two criteria be met which depend upon the fill soil. Firstly, in order that the geogrids are loaded to their working stress level, a substantial amount of deformation must occur in the embankment. Secondly, the embankment must be homogeneous with respect to the shear strength of the fill soil, such that the behaviour of the slopes reinforced with different geogrids and the behaviour of the unreinforced slope can be compared. To satisfy these two requirements, the test fill must be built with a soil that strains a great deal under its own weight and one whose stress-strain behaviour will be consistent throughout the embankment.

The clay till is very dense and stiff and it was estimated that this soil would have a stiff modulus and a high shear strength. An embankment built of this material would not deform adequately. Therefore, this soil was not considered for construction of the test fill. The silty clay appeared to be softer than the till material and it had a high in situ water content. Therefore, it could be placed and compacted without the addition of water. This soil unit was also the most accessible since it was located between 1 and 5 m below the ground surface. Moreover, the vast amount of it available would mean that it could be used to build the entire embankment. Considering all of these factors, the silt was chosen as the soil to be used for construction of the test embankment.

In order to characterize the stress-strain behaviour of the sandy, clayey silt a large bag sample was removed from the borrow area, shown in Figure 3.1. Examination of this material showed that it was particularly clayey. The Atterberg limits, grain size curve and compaction curve were established for this soil. To establish the compaction specifications for the test fill, unconfined compression tests were then conducted on laboratory-compacted specimens to determine the variation in the undrained shear strength with changes in the initial water content and dry density.

During construction of the embankment two types of fill soil samples were obtained to determine the properties of the soil actually being used for construction and to establish the variability of those properties. 25.4 mm (1") diameter Shelby tube samples were removed from the field-compacted lifts of soil along the centerlines of each of the four test slopes. The Atterberg limits and grain size curve were established for the tube samples removed from the fill at an elevation of 1.67 m. The tube samples were stored in a moisture room for later testing to determine their unconfined compressive strength.

A large bag sample was also removed from the south end of the test fill at an elevation of 3 m. It was noted that this soil appeared slightly more coarse grained than that which had been analysed prior to construction of the test fill. A compaction curve was established for the loose sample of fill soil and compared with that initially

determined for the borrow soil. The soil was also characterized in terms of its Atterberg limits and grain size curve. Bag samples of sandy, clayey silt were also obtained by Alberta Transportation and Utilities from the borrow area to prepare compacted specimens for testing in their laboratory.

3.6 Classification of the Fill Soil

The Atterberg limits and particle size distributions determined for each of the fill soil samples are shown in Table 3.5. The grain size curves are given in Figure 3.7. The plasticity index and the percentage of clay sized particles determined for the borrow soil tested prior to construction are both higher than the values determined for the bag sample obtained from the south end of the test fill. According to the Unified Soil Classification System (U.S. Army Engineer Waterways Experiment Station, 1960) both soils would be considered as inorganic clays or silty clays of low to medium plasticity. However, the loose soil obtained from the test fill contains 15% more silt-sized particles. For clarity, this soil will be referred to as silt while the borrow soil will be referrred to as clay for the remainder of this study.

In general, there does not appear to be any significant difference in either the liquid or plastic limits of any of the fill soil samples. The grain size distributions also agree closely although the tube samples contain more silt

and less sand that either of the silt or clay samples. The clay material contains about 10% more clay-sized particles than the silt material or tube soil samples. Alberta Transportation and Utilities' soil contains more sand but the percentages of silt and clay sized particles are unknown. These differences in the grain size distributions may be a source of disagreement between the shear strengths determined for each of the fill soils. The liquid limits and corresponding plasticity indicies have been plotted in Figure 3.6. The points plotted for each of the fill soil samples fall between the range of values for illite and montmorillonite.

3.6.1 Fill Soil Compaction Curves

Bobey (1987) established compaction curves for the clay fill soil being used to construct the test embankment using both kneading and dynamic compaction. Figure 3.8 shows the compaction curves obtained. The two compaction methods resulted in essentially the same relation between dry density and water content. Holtz and Ellis (1963) showed that dynamic compaction in the laboratory results in specimens with the same stress-strain behaviour as field-compacted specimens. Since kneading and dynamic compaction result in the same compaction curve, it was assumed that remoulded specimens could be prepared in the laboratory by kneading compaction and that these specimens would be representative of the soil compacted in the field.

The kneading compaction curves established for the silt and clay fill soils are shown in Figure 3.9. Comparison of the compaction curves for the two soils shows that although the Atterberg limits and grain size distributions of the clay and silt fill soils are similar, the compaction curves differ significantly. For a given water content, the same amount of compaction effort will result in much denser silt specimens than clay specimens. The optimum water content determined for the silt fill soil is 16.6% and the maximum dry density is 1.82 g/cm^3 while the optimum water content of the clay is 20.5% and the maximum dry density is 1.68 g/cm^3. The differences in strength of the two samples compacted at the same water content will be discussed in Chapter 4.

Table 3.1: Clay Soil Properties Based on Penetration Resistance (Modified from Peck et al., 1974)

Number of Blows per ft, N	Consistency
Below 2	Very Soft
2 - 4	Soft
4 - 8	Medium
8 - 15	Stiff
15 - 30	Very Stiff
Over 30	Hard

Table 3.2: Shelby Tube Samples Extruded for Laboratory Testing

Hole Number	Tube Number	Tube Elevation (meters) Top	Bottom	Elevation of ground surface (meters)	Depth below ground surface (meters)
1	4	699.1	699.5	701.8	2.50
1	6	698.1	698.6	701.8	3.45
2	22	699.3	699.8	702.5	2.95
2	24	698.4	698.8	702.5	3.90
3	42	699.3	699.7	702.0	2.50
3	44	698.5	699.0	702.0	3.25
4	64	698.2	698.6	701.9	3.50

Table 3.3 : Clay Minerals Contained in the Clay Fraction of the Silty Clay Soil at the Test Fill Site

Sample #	Illite (% of clay fraction)	Montmorillonite (% of clay fraction)	Kaolinite (% of clay fraction)
1	30	60	10
2	30	60	10
3	45	40	15
4	50	30	20

Table 3.4: Atterberg Limits and Grain Size Distributions of Foundation Soil Samples

Soil	Depth (m)	Wn(%)	Wl(%)	Wp(%)	Ip(%)	%Sand	%Silt	%Clay	Ac
BH2 Tube 22 Tube 24	 3.0 3.9	 33.0 31.0	 34.7 39.7	 25.6 22.2	 9.1 17.5	 2 28	 74 62	 24 10	 0.38 1.75
Block Sample	4.5	36.4	46.7	21.5	25.2	5	75	20	1.26
AB.T. BH28 BH28	 10.06 13.11	 18.0 20.0	 29.0 24.4	 19.9 21.0	 9.1 3.4	-	-	-	-

Table 3.5: Atterberg Limits and Grain Size Distributions of Fill Soil Samples

Soil Type	Wn (%)	Wl (%)	Wp (%)	Ip (%)	%sand	%silt	%clay	Ac
Clay	- - -	42.3 40.0 40.0	20.7 19.6 19.2	21.6 20.4 -	28 25 -	44 43 -	28 32 -	0.77 0.64 -
Silt	- -	33.3 -	18.1 -	15.2 -	22 23	60 57	18 20	0.84 -
Tube Soil	20.0 19.1 -	37.4 34.5 -	20.9 23.0 -	16.5 11.5 -	5 20 20	73 62 61	22 18 19	0.75 0.64 -
Sandy Clay	19.0	39.0	17.5	21.5	40	-	-	-

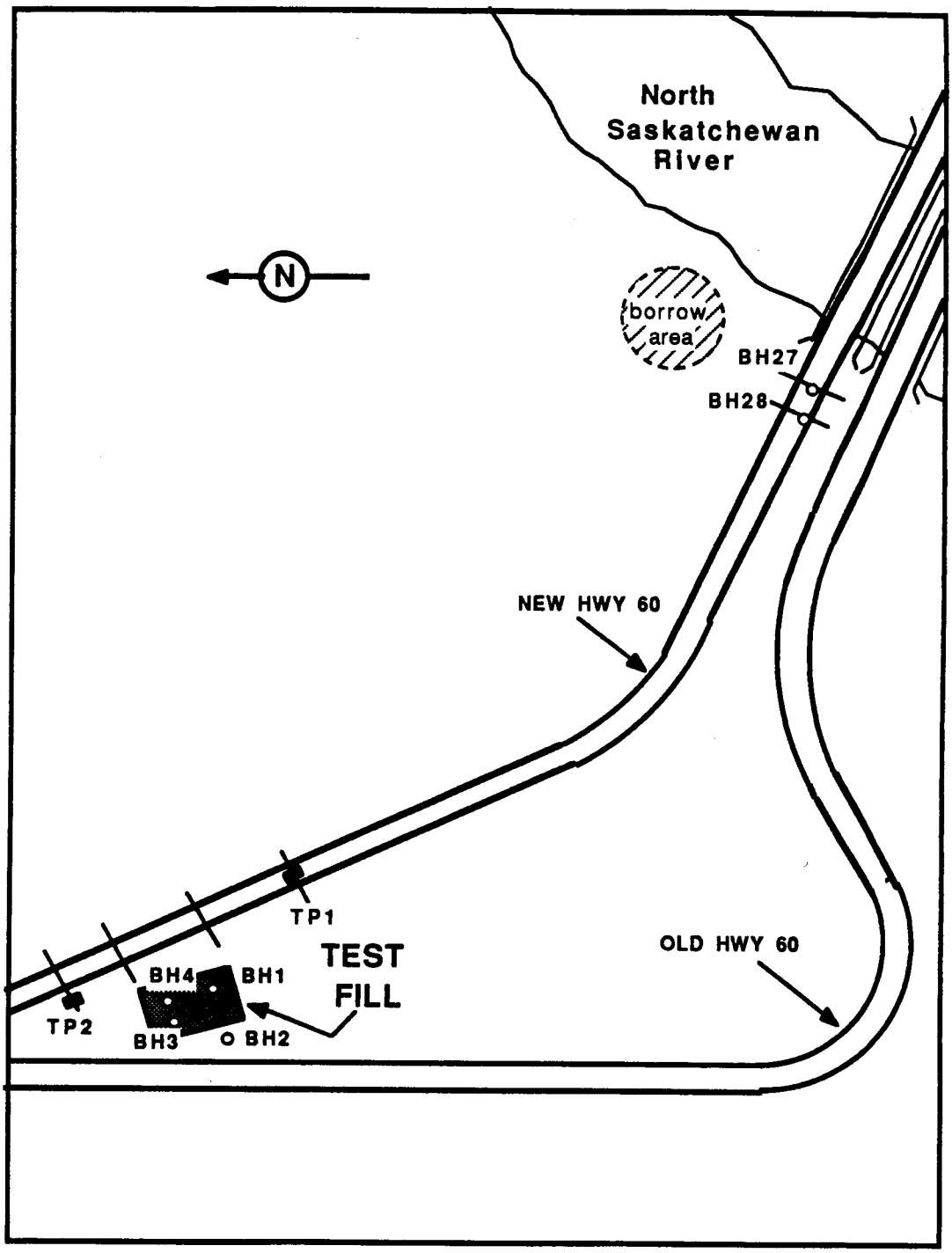

Figure 3.1: Location of Boreholes and Test Pits

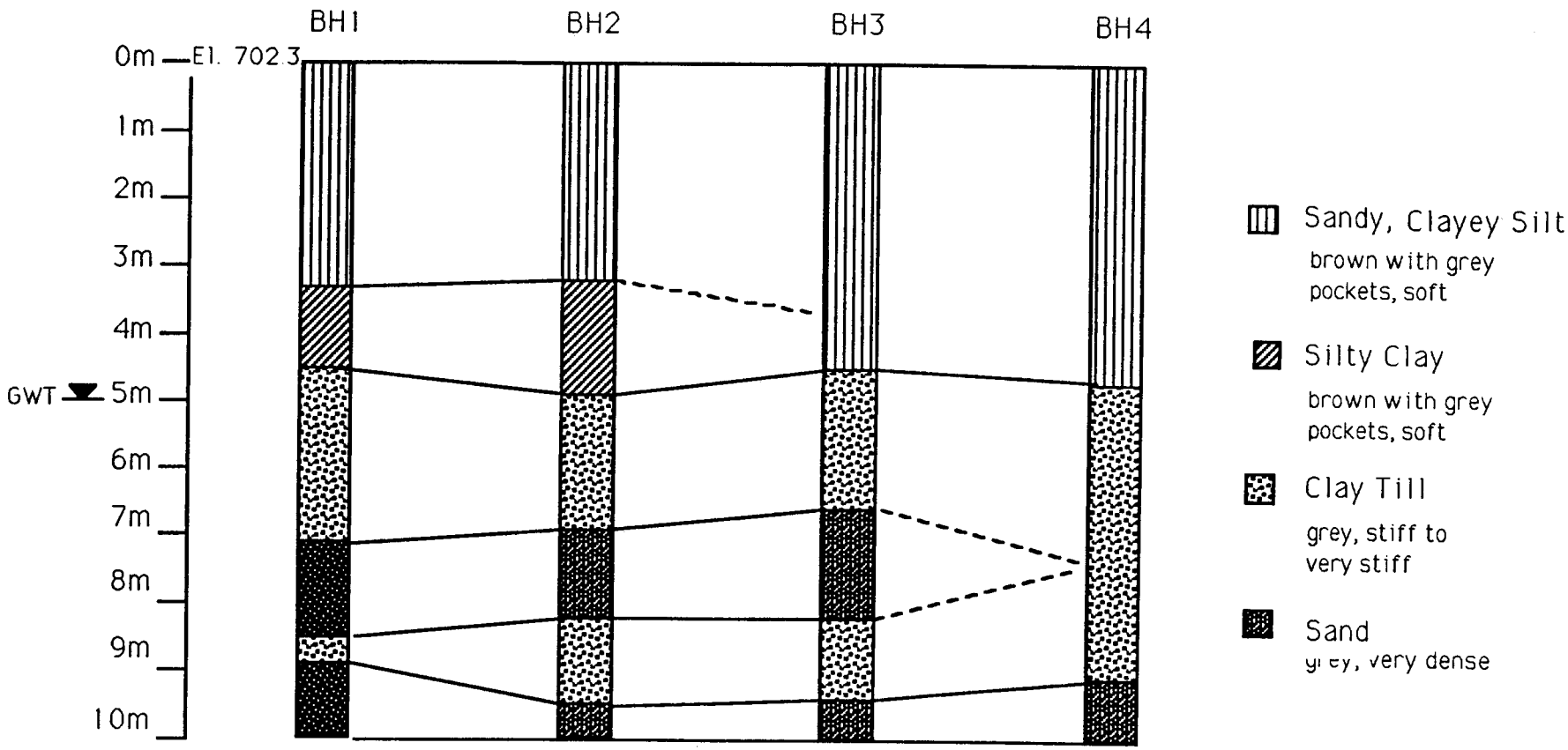

Figure 3.2: Boreholes Drilled in the Test Fill Foundation

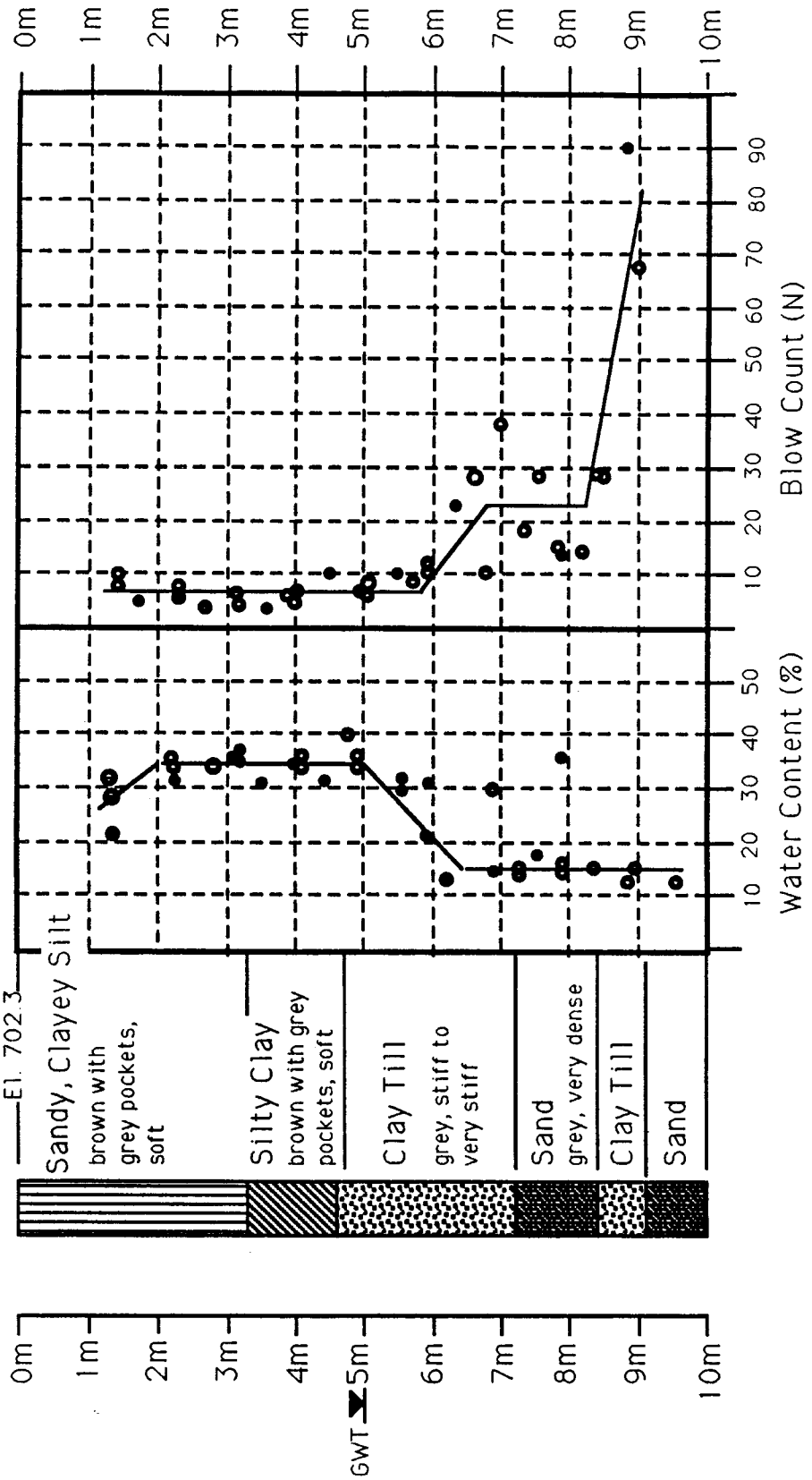

Figure 3.3: Average Borehole Data

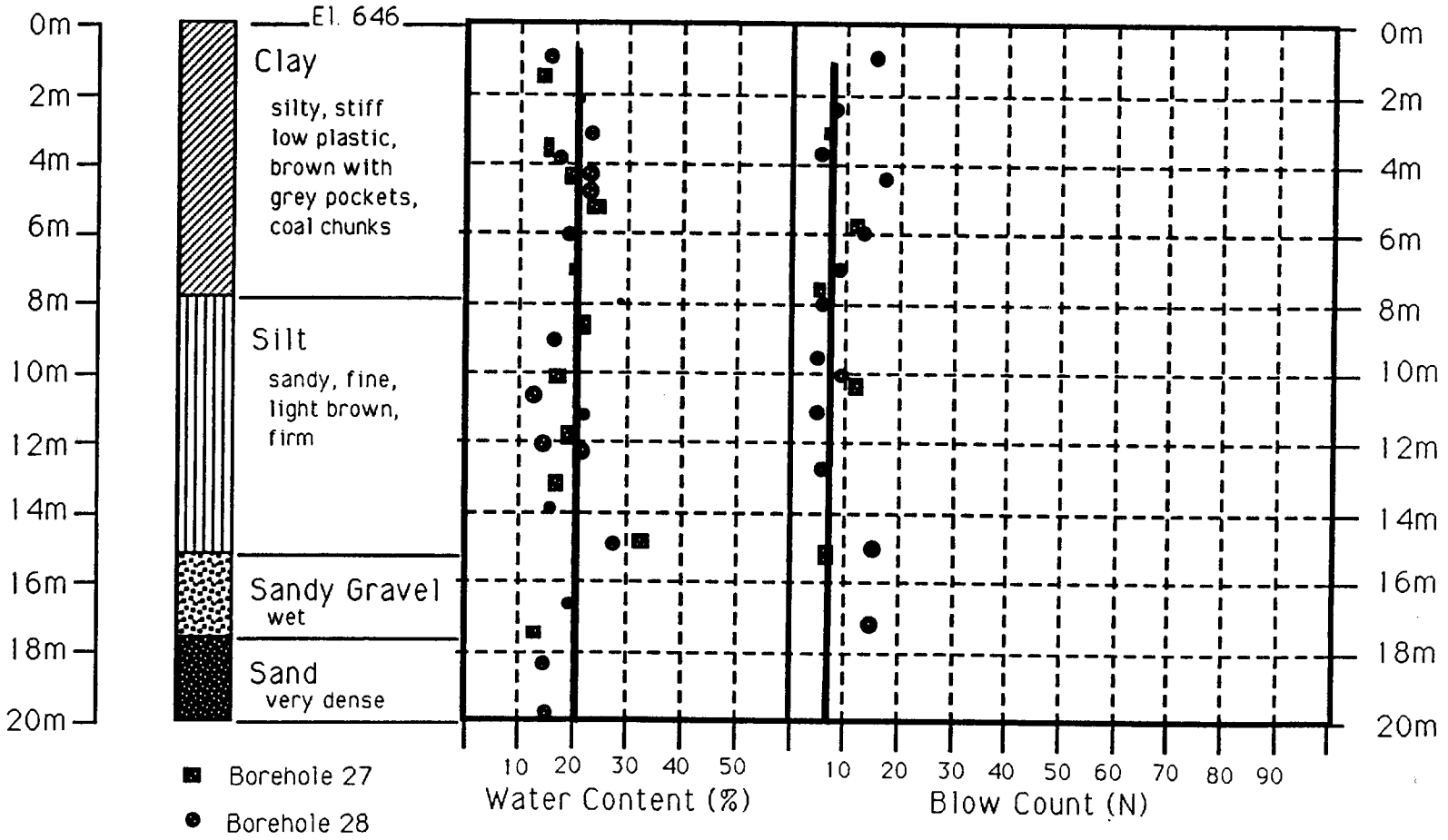

Figure 3.4: Borehole Information Obtained by Alberta Transportation and Utilities

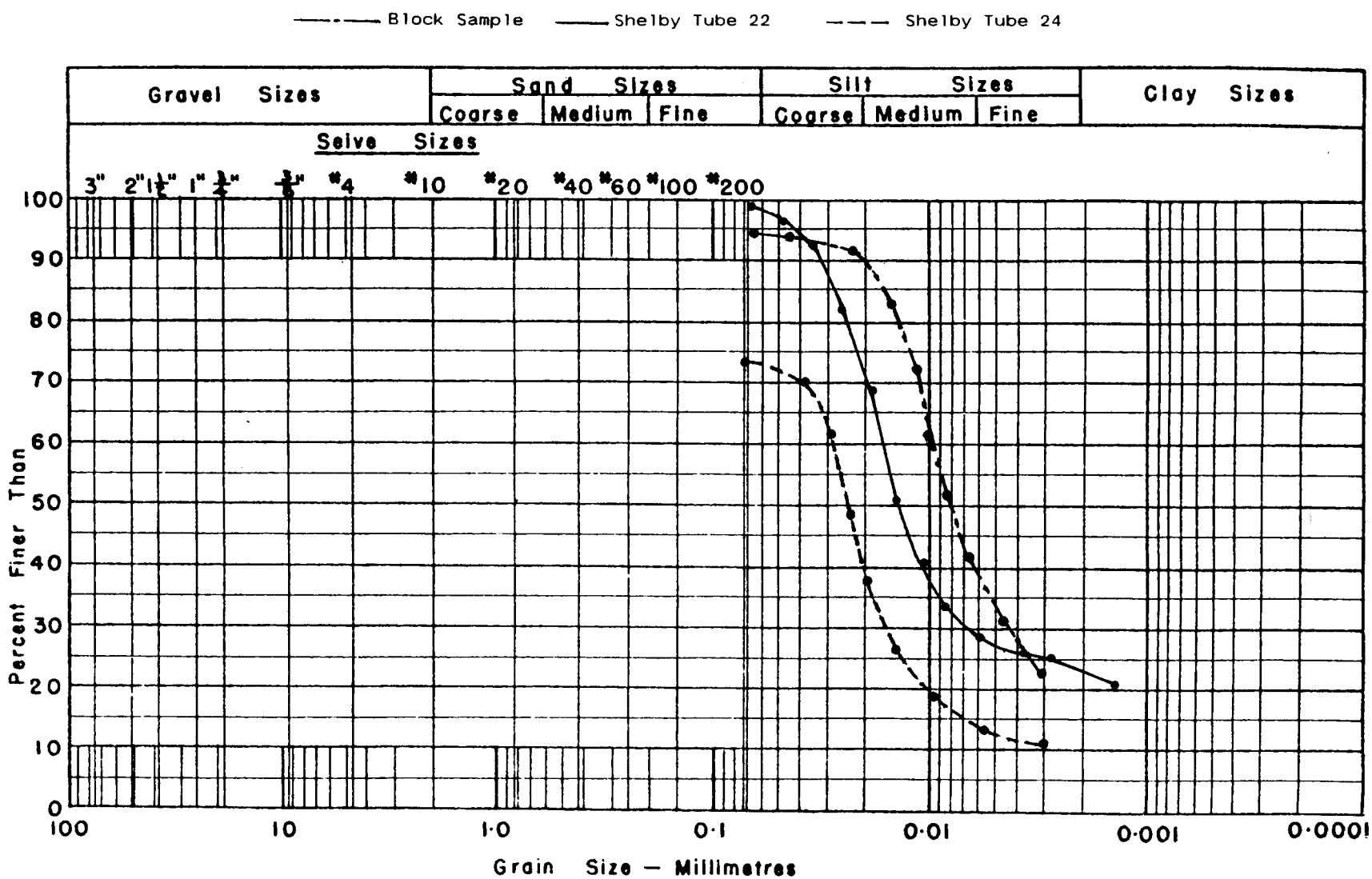

Figure 3.5: Grain Size Curves Determined for Foundation Soil Samples

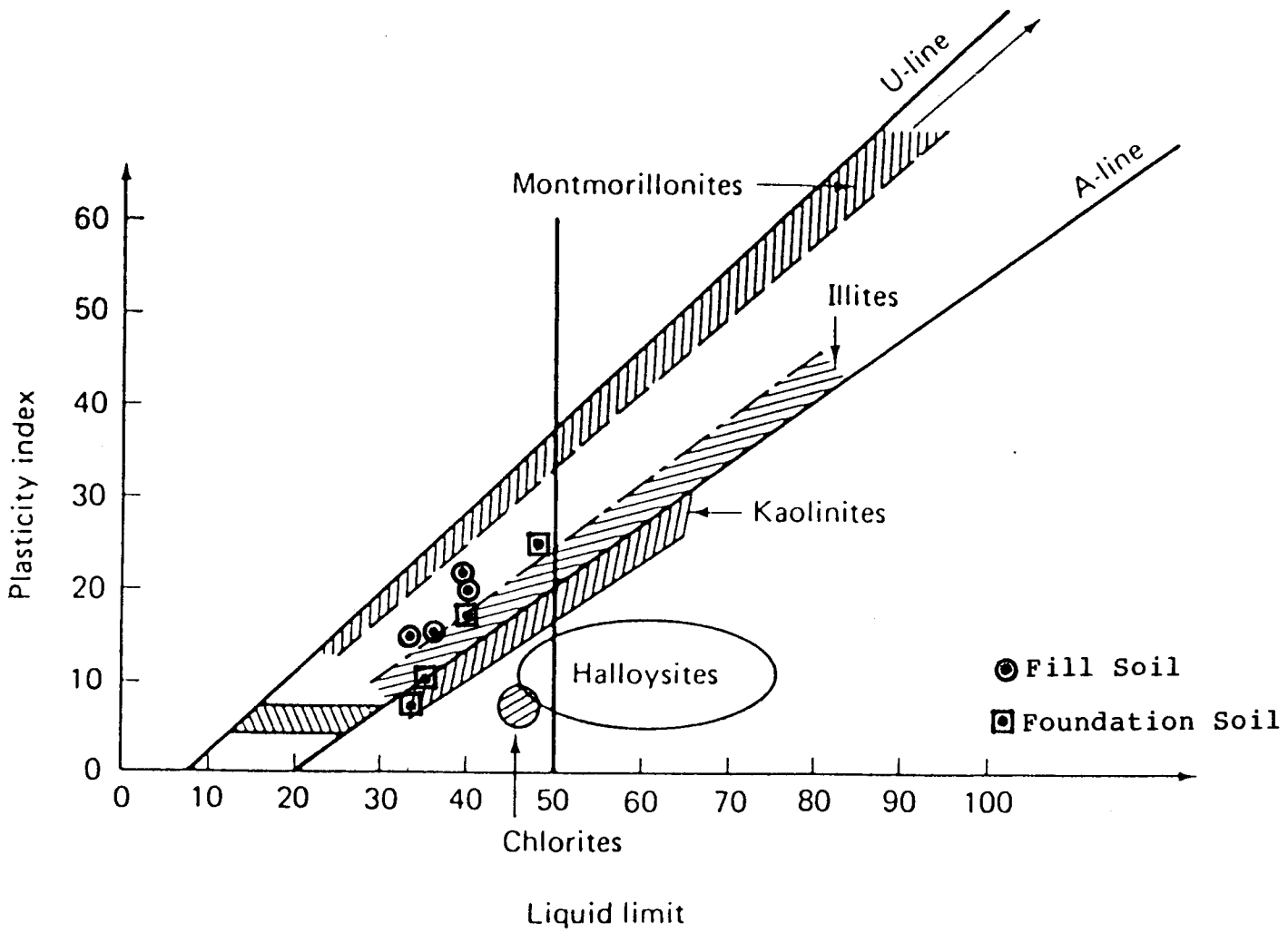

Figure 3.6: Location of Common Clay Minerals on Casagrande's Plasticity Chart (Modified from Holtz and Kovacs, 1981)

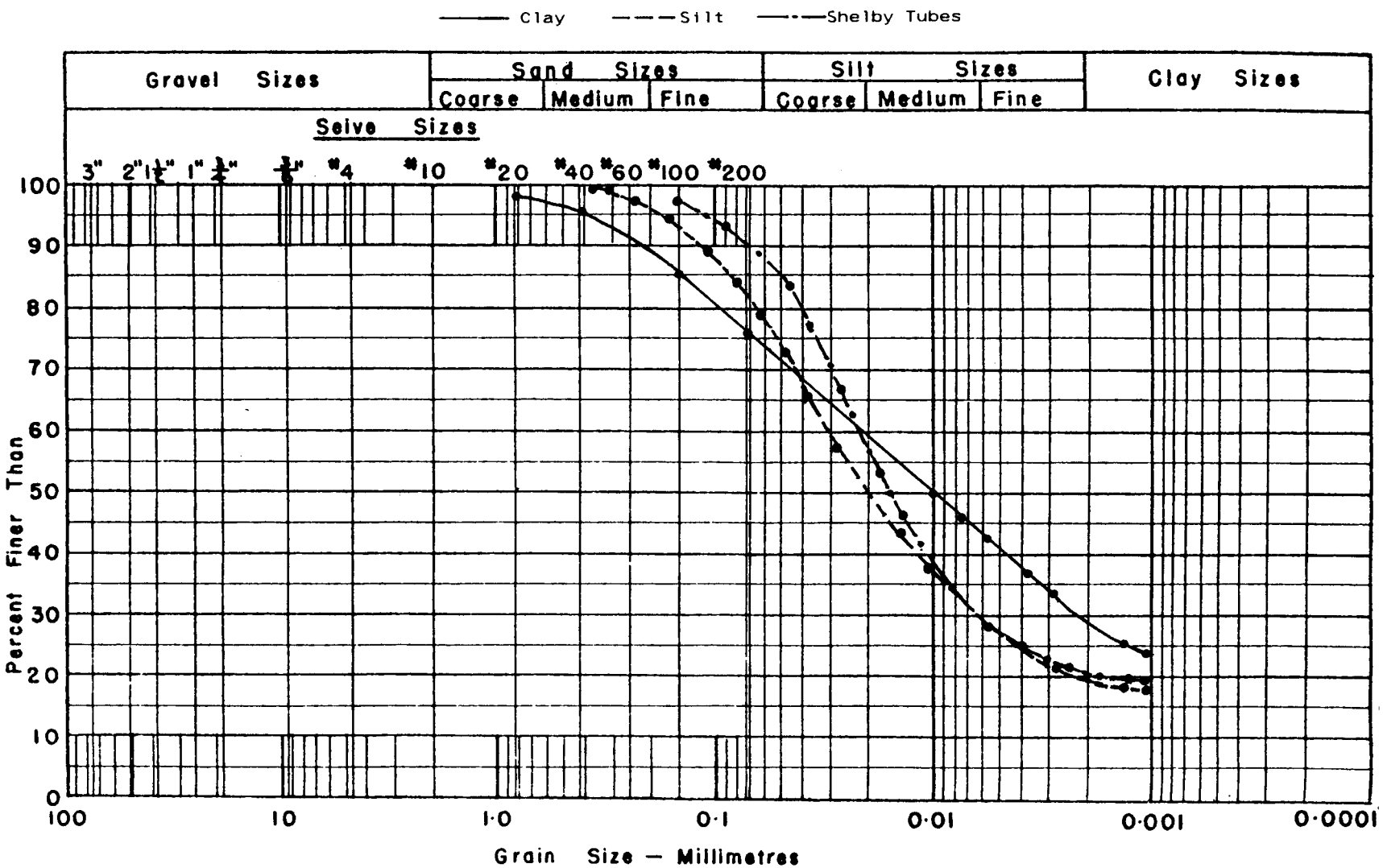

Figure 3.7: Grain Size Curves Determined for Fill Soil Samples

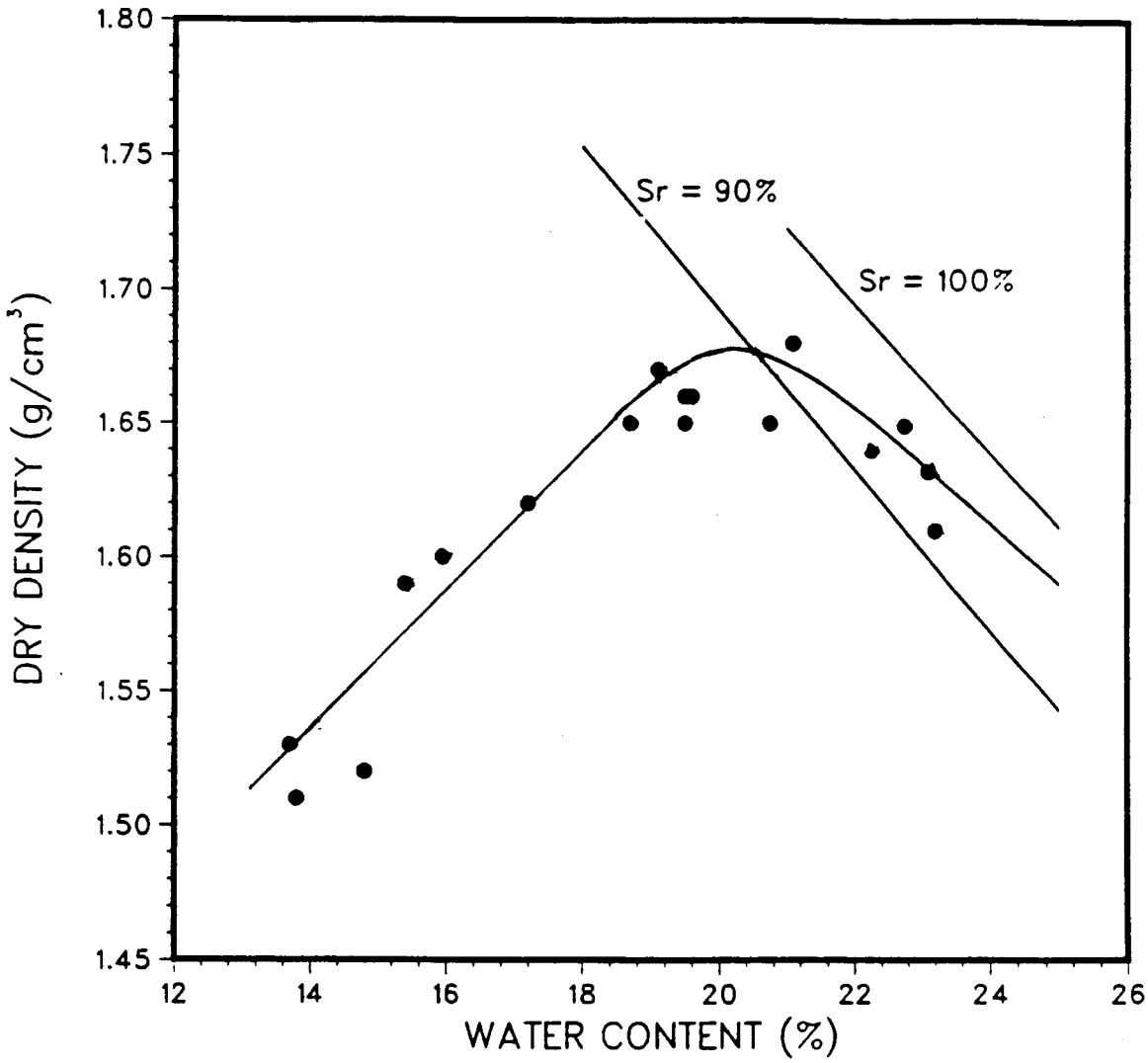

Figure 3.8: Compaction Curves Determined for Clay Fill Soil (Modified from Bobey, 1988)

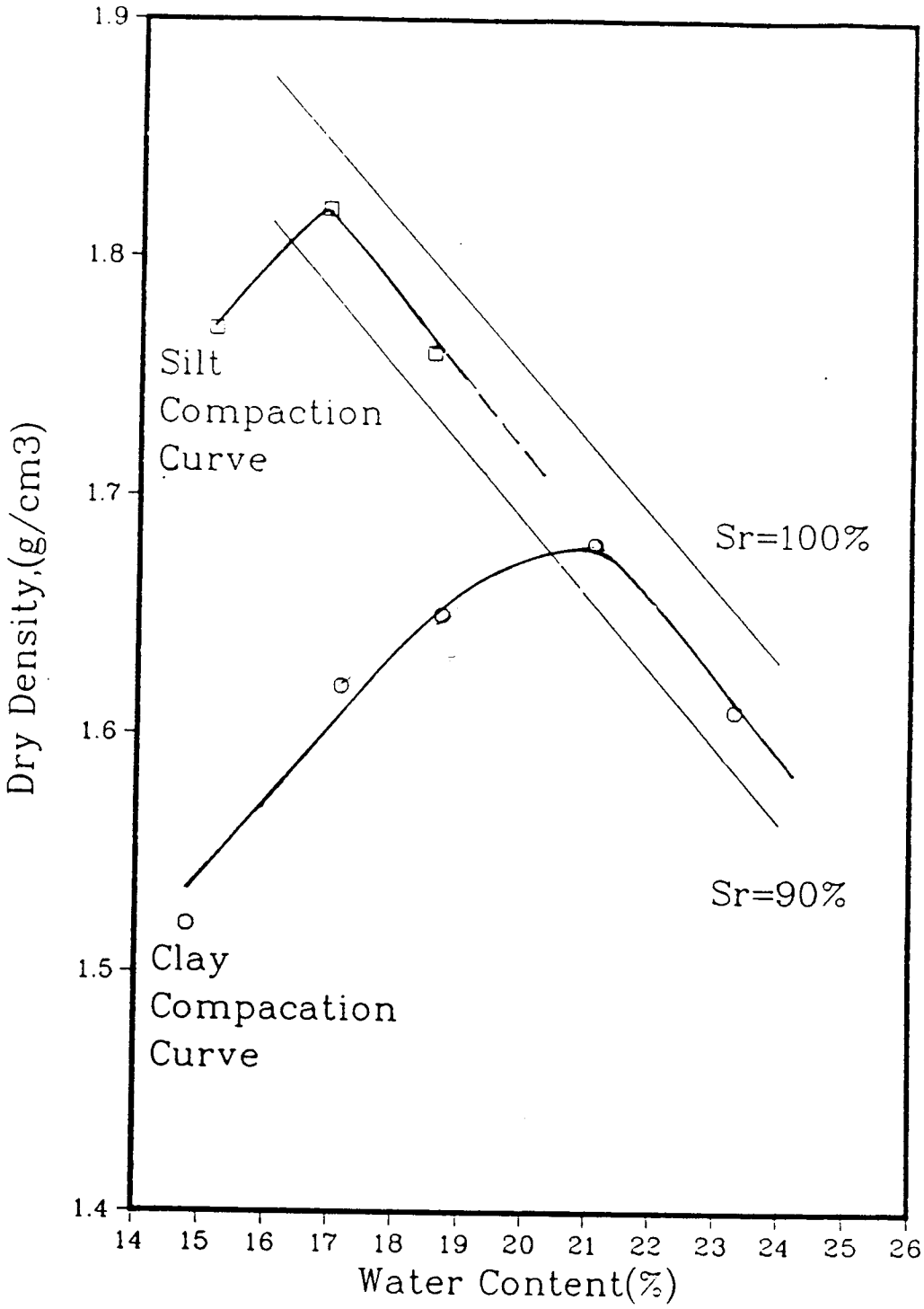

Figure 3.9: Comparison of Silt and Clay Compaction Curves

4. LABORATORY TESTING OF FILL SOIL

4.1 Introduction

The shear strength and stress-strain properties were determined for a range of fill soils through laboratory testing to allow the following:

1. Selection of the appropriate soil for construction of the test fill, based on the criteria that the soil deform significantly, thereby stressing the geogrids.
2. Prediction of the long-term and short-term factors of safety against a shear failure in the unreinforced slope of the test fill using limit equilibrium analyses.
3. Prediction of the deformation of the unreinforced slope of the test fill using a finite element analysis.

The laboratory tests performed to establish the required soil parameters included unconfined compression tests, unconsolidated undrained and consolidated undrained triaxial tests with pore pressure measurements and consolidated drained triaxial tests. The unconfined compression tests were conducted to determine the affect of variations in the density, degree of saturation and water content on the undrained shear strength and stress-strain behaviour of the fill soil. Unconsolidated undrained triaxial tests with pore pressure measurements were conducted to determine the pore pressure response of the test fill soil to undrained loading prior to consolidation. Consolidated undrained triaxial tests were conducted with

pore pressure measurements to determine the frictional and cohesive effective stress parameters and pore pressure response of the fill soil after a certain amount of consolidation has taken place in the embankment. Consolidated drained tests were conducted to determine the long-term stress-strain behaviour of the fill soil and to obtain the parameters necessary for conducting the long-term deformation analysis.

These laboratory tests were performed on different fill soil materials to establish the range of shear strength and stress-strain properties that must be considered for the stability and deformational analyses of the test fill. Clay and silt fill soil specimens were prepared for testing at 3% wet of their optimum water contents. Sandy clay fill soil specimens were also tested by Alberta Transportation and Utilities at the optimum water content and maximum dry density. The results from these tests will be included here since they represent an upper bound to the shear strengths which may exist in the field due to compaction at a lower water content. The index properties and grain size curves of the various fill soils tested have been presented in Chapter 3. A summary of the laboratory tests conducted on each of the different fill soils is given in Table 4.1. The detailed results obtained from each set of tests conducted on the various fill soils will be presented and discussed in this chapter.

4.2 Unconfined Compression Tests

Unconfined compression tests were conducted, according to ASTM designation D 2166-66, on compacted specimens of clay and silt fill soil to determine how the compressive strength and stress-strain behaviour of the soils vary with changes in water content and density. The specimens were prepared by standard laboratory static compaction (kneading) techniques at various moisture contents under a foot pressure of 690 kPa (100 psi). Two 38 mm (1.5") outer diameter Shelby tubes were pushed into each compaction mould. They were then extruded to obtain specimens for unconfined compression tests. Because the same compaction effort was used on the soils at different water contents, the resulting densities of the specimens vary with water content.

Casagrande and Hirschfeld (1960) showed that the undrained shear strength of the silty clay, compacted wet of optimum, tested by them depended strongly upon the as compacted water content and to a lesser degree upon the as compacted dry density. Based on the details of their information, given in Section 2.2.2.1, it may be assumed that the variation in shear strength of the fill soils tested in unconfined compression as part of this study, depend only upon the water content of the specimens, provided that the water content is wet of optimum.

4.2.1 Compacted Clay Fill Soil

Unconfined compression tests were conducted on ten specimens with water contents ranging between 14 and 22% and corresponding densities of between 1.49 and 1.68 g/cm^3. The stress-strain curves obtained from the tests are presented in Figure 4.1 and the variation of maximum shear strength with water content and dry density is given in Figure 4.2. Table 4.2 gives the specimens' characteristics prior to testing and the stress and strain values at failure. The as compacted dry densities could not be calculated because the extruded specimens were not weighed prior to testing. Hence, the dry densities shown in the table have been obtained from the clay compaction curve, given in Chapter 3, which corresponds to the specimens' measured water contents.

Figure 4.2 shows that the maximum shear strength of the soil increases with increasing water content up to a water content of about 16.5% and then decreases with any further increase in water content. For a constant dry density, the undrained shear strength of a soil usually decreases with any increase in water content. However, the trend shown here may be due to the fact that the dry density of the clay increases up to a water content of about 20%, which causes an increase in shear strength. The specimens compacted at a water content of 14.3% exhibit brittle stress-strain curves, while the specimens compacted at water contents of 18% or greater, curve gently to a maximum shear stress at a high percent strain and then gradually drop off.

Ideally, the test fill should be constructed such that it will deform excessively without undergoing a shear failure; brittle stress-strain behaviour of the fill soil would not be acceptable. The results obtained from the unconfined compression tests therefore indicate that the clay fill soil must be compacted wet of its optimum water content of 20.5%, to ensure that the embankment will deform significantly when loaded to stress levels near the peak shear strength. The variation in the maximum undrained shear strength with water content for these tests will be discussed in greater detail in Section 4.2.3 along with the results obtained from the unconfined compression tests conducted on the silt fill soil.

4.2.2 Compacted Silt Fill Soil

Unconfined compression tests were conducted on five silt specimens at moisture contents ranging from 14.6% to 19.0% with corresponding dry densities ranging from 1.73 to 1.81 g/cm^3. Figure 4.3 shows the stress-strain curves obtained from these tests and Figure 4.2 gives the variation of the maximum undrained shear strength with water content and dry density. Table 4.3 gives the specimens' conditions prior to testing and the stress and strain values at failure. The densities given in the table have been obtained from the silt compaction curve, given in Chapter 3, at the measured water contents of the specimens.

Figure 4.2 shows that the shear strength increases with increasing water content and dry density up to a water content of about 16% and then decreases with the addition of more water, in a manner similar to that exhibited by the clay fill soil. The specimens compacted at a water content of about 14.7% show a brittle failure as did the clay fill soil. The strain at failure for all tests increases with increasing water content and it is only at a water content of 18%, which is 1% wet of the optimum for the silt, that the soil begins to strain significantly before the peak deviator stress is reached.

As was found for the clay fill soil, the unconfined compression test results indicate that the silt must be compacted in the field at a water content which is wet of its optimum of 16.6% to ensure that the test fill soil will deform significantly as the factor of safety of the slope approaches 1.0. The variation in undrained shear strength with water content will be compared with that for the clay in the next section wherein the compaction specifications for the test fill will be discussed.

4.2.3 Compaction Specifications for the Test Fill

It was decided that the compaction specifications should be established such that a factor of safety against a shear failure in the embankment, immediately after construction, of slightly greater than 1.0 would be attained. The stresses in the embankment would thus approach

the peak undrained shear strength of the fill soil. For a fill compacted wet of optimum, the stress-strain curves obtained from the unconfined compression tests indicated that significant deformations should occur in the embankment under these conditions.

Using Taylor's stability chart (1937), with $\phi=0^{\circ}$, the factors of safety against an undrained shear failure for various embankment geometries and undrained shear strengths were assessed. It was found that an undrained shear strength of about 50 kPa would yield a factor of safety of 1.2 for a 12 m high embankment with 1:1 side slopes. Therefore, 50 kPa was chosen as the design undrained shear strength for the compaction specifications.

Figure 4.2 shows that an undrained shear strength of 60 to 40 kPa corresponds to a water content of between about 22 and 24% on the compaction curve (Figure 4.21). These water contents correspond to a dry density of between about 1.66 and 1.59 g/cm^3 for the clay fill soil. Unconfined compression tests were not conducted on silt specimens with a range of water contents high enough to bring the undrained shear strength down to 50 kPa. Therefore, it was necessary to establish the compaction specifications for construction of the test fill based on the data obtained for the clay fill soil until further testing of the silt fill soil could be completed.

Since the borrow soil used for construction of the first 3 m of the test fill was particulary clayey, it was

initially specified that the fill be compacted to densities ranging from 1.66 to 1.59 g/cm^3 at corresponding water contents of between 22 and 24%. However, in order to ensure that an undrained shear strength of about 50 kPa would be maintained throughout the embankment, regardless of potential variations in the silt content of the fill, more detailed compaction specifications were required. Hence, additional undrained shear strength tests were conducted on not only the silty fill soil, but also on the clay fill soil and on 38 mm (1.5") diameter Shelby tube samples taken directly from each compacted lift of the embankment. Unconsolidated undrained triaxial tests were conducted on these specimens rather than unconfined compression tests to determine the undrained shear strengths. This was done such that the effects of increasing confining stress and of back-saturation on the undrained shear strengths of the fill specimens could also be determined.

4.3 Unconsolidated Undrained Triaxial Tests

Immediately after construction of a fill, before the soil has had a chance to consolidate, the pore water pressures are highest. Under these conditions, the undrained shear strength parameters of the soil may be used to calculate the factor of safety against a shear failure occuring in the embankment or to model the unconsolidated undrained load-deformation behaviour for finite element analyses.

The undrained shear strength parameters may be determined from unconsolidated undrained triaxial tests. If pore pressures are measured, only one effective stress Mohr circle will be obtained from several specimens subject to different confining stresses. Consequently, a unique effective stress cohesive strength and friction angle cannot be obtained. However, the undrained shear strength, determined from the total stress failure envelope, may be used along with the pore pressure ratios, r_u, determined from the pore pressure measurements taken during testing, in order to conduct effective stress limit equilibrium or deformational analyses.

Unconsolidated undrained tests were first conducted on Shelby tube specimens obtained from the compacted embankment. The locations and elevations from which the specimens were removed are given in Figure 4.4. The tests were performed to determine the variability of shear strength throughout the embankment and to establish the effect on shear strength of saturating specimens with a back pressure.

The development of pore pressures during undrained loading may be affected by back-pressure saturation of the soil. Skempton's (1954) Equation (4.1), relates induced pore pressure to changes in total stress.

$$\Delta u = B(\Delta\sigma_1 + A(\Delta\sigma_1 - \Delta\sigma_3)) \qquad [4.1]$$

The B-parameter is equal to 1.0 for fully saturated soil and less than 1.0 for partially saturated soil. Hence, the pore pressures which develop in a fully saturated specimen will be greater than those that would develop in a partially saturated specimen. The effective stress acting on the soil skeleton would therefore be less in a fully saturated specimen, thus resulting in a lower shear strength. The extent to which changes in the degree of saturation affect the undrained shear strength of the fill soil will be examined in the following sections.

Unconsolidated undrained tests were first conducted on Shelby tube specimens obtained from the compacted embankment. The locations and elevations from which the specimens were removed are given in Figure 4.4. The tests were performed to determine the variability of shear strength throughout the embankment and to establish the effect on shear strength of saturating specimens with a back pressure.

Unconsolidated undrained tests were conducted on laboratory compacted clay and silt fill soils to determine the range of undrained shear strength parameters that could be expected for the two soils. The tests were conducted according to ASTM designation D 2850-82. The soils were compacted by standard laboratory static compaction at water contents of between 20 and 24% to simulate field conditions. 25 tamps were applied to each of 3 soil layers under a foot pressure of 690 kPa (100 psi). 38 mm (1.5") diameter Shelby

tubes were pushed into the soil contained in the standard compaction mould. These specimens were then extruded for unconsolidated undrained triaxial tests.

Alberta Transportation and Utilities also conducted unconsolidated undrained tests on sandy clay fill soil, compacted in the laboratory at 100% of the maximum standard compaction density at the optimum water content. Back pressures were not used to saturate the samples; consequently, pore pressures were not measured. The results from these tests will be presented here as they represent a possible upper limit to the shear strength and lower limit to the deformation characteristics of the fill soil being used to construct the test embankment.

4.3.1 Shelby Tube Samples Obtained from the Test Fill

To determine the variability of shear strength across a compacted lift of the test fill, 9 unconsolidated undrained triaxial tests were conducted on specimens removed from various locations across the test fill at an elevation of 1.67 m. 5 specimens were obtained 10 m west of the fill centerline and 4 were obtained 12 m east of the fill centerline, as shown in Figure 4.4. Both sets of specimens were tested without the application of a back pressure.

To determine the affect of back-saturation on the undrained shear strength of the fill soil, four specimens were removed from the embankment at an elevation of 2.33 m, along a line 12 m east of the centerline. The locations from

which the specimens were removed are also shown in Figure 4.4. Unconfined compression tests were conducted on these specimens and the results will be compared to those obtained from the first two sets of tube samples tested in the following sections.

The water contents and densities of all 13 tube samples tested are plotted in Figure 4.5 with respect to the laboratory compaction curves established for the clay and silt fill soils. The points for all but specimen UU5 fall between the silt and clay compaction curves with degrees of saturation between 90 and 100%.

4.3.1.1 Samples From 1.67m Elevation, 10m W of CL

The stress-strain curves obtained from specimens UU1 to UU5 removed at an elevation of 1.67 m, 10 m west of the test fill centerline are shown in Figure 4.6. Table 4.4 gives the specimens' characteristics prior to testing and the stress and strain conditions at failure. Table 4.4 shows that the specimens did not differ significantly in their initial water content, dry density, void ratio or degree of saturation. Specimen UU5 was, however, slightly drier and had a lower degree of saturation. These factors may have contributed to the higher strength exhibited by specimen UU5. The percent strain reached by each specimen at the peak undrained shear stress cannot be commented on because loading of specimens UU1, UU2 and UU3 was stopped at a strain of 15%, before the stress-strain curves reached a peak.

Assuming that the as compacted specimens were similar, the stress-strain curves show that the peak strength and initial tangent modulus increase with increasing confining pressure. The total stress p-q plot, given in Figure 4.7, shows more clearly the increase in sample strength with confining pressure. The failure envelope on the p-q plot is referred to as the K_f line and represents the best fit line through the data points.

The K_f line drawn in Figure 4.7 is not horizontal due to the fact that the application of a confining stress brought about an increase the density of the specimens until the confining stress was high enough to compress all the air in the voids and completely saturate the soil. The apparent total stress friction angle calculated from the slope of the K_f line is 4.82° and the apparent total stress cohesive strength calculated from the intercept of the K_f line is 76.3 kPa. The results from these tests will be compared later in this section with those derived from the unconsolidated undrained tests conducted on the specimens obtained from another location and from those subject to a back pressure.

4.3.1.2 Samples From 1.67m Elevation, 12 m E of CL

The stress-strain curves obtained for specimens UU6 to UU9, taken from an elevation of 1.67 m, 12m east of the fill centerline are given in Figure 4.8. The

specimens' characteristics prior to testing and the stress and strain conditions at failure are given in Table 4.5. Specimen UU8, confined under a stress of 160 kPa, failed prematurely due to flaws present in the specimen. Therefore, the results from this test were not considered. The stress-strain curves of specimens UU6 and UU9 are very similar while specimen UU7 shows a much higher initial tangent modulus and peak strength. The initial water content, dry density, void ratio or degree of saturation of specimen UU7 are not significantly different from those of specimens UU6 and UU9. It is therefore difficult to explain why the specimen confined under a stress of 80 kPa is much stronger than the specimen confined under a stress of 240 kPa. Specimen UU7 may have contained more sand than the other samples, which would have contributed to a greater shear strength.

Figure 4.9 shows the total stress p-q plot obtained from these tests. It was not possible to define the K_f line due to the scatter in the data. Hence, the apparent failure envelopes for these specimens and the first set of tube samples tested cannot be compared. However, the undrained shear strengths of individual specimens subject to the same confining stresses may be compared.

Comparison of Table 4.4 and 4.5 shows that the average initial water content, dry density, void ratio and degree of saturation of the first and second sets of

unconsolidated undrained triaxial tests are very similar. The scatter in the undrained shear strength, for samples subject to the same confining stress, therefore, indicates that differences in the grain size distribution and/or clay mineral content must have existed between the specimens. The results from these two sets of tests show that close control of the type of fill soil being placed in the field and the corresponding compaction requirements specified for each type of soil must be exercised if homogeniety with respect to shear strength within the embankment is to be maintained.

4.3.1.3 Samples From 2.33m Elevation, 12m E of CL

Unconsolidated undrained triaxial tests were conducted on specimens UU10 to UU13 obtained at an elevation of 2.33 m, 12 m east of the fill centerline. The locations of these specimens are given in Figure 4.4. The specimens were allowed to saturate under a back pressure of 600 kPa for 24 hours. B-tests (Bishop and Henkel, 1962) were conducted to confirm whether or not the specimens had become fully saturated. The B-test results will be presented later in this section. The drainage valves were then closed and the samples were sheared under various confining stresses. The results obtained from these tests will be compared to the results obtained from the tests conducted on the unsaturated specimens.

Figures 4.10 and 4.11 show the stress-strain curves and pore pressure-strain curves obtained from the back-saturated specimens. The specimens' conditions prior to testing and the stress, strain and pore pressure conditions at failure are included in Table 4.6. The pore pressure parameter, B, shown in Table 4.6, was equal to 1.0 for all tests, indicating that a back pressure of 600 kPa was sufficient to fully saturate the specimens.

The pore pressures developed in the specimens, shown in Figure 4.11, are positive at small strains. The pore pressures of the specimens confined under cell pressures of 0, 160, and 240 kPa become negative beyond a strain of about 6% and continue to decrease steadily with increasing strain. This indicates that the specimens are tending to dilate at strains of greater than 1% to 4%. The pore pressure developed in the specimen confined under 80 kPa remained positive up to about 14% strain and then grew negative with increasing strain. It is not apparent from the as compacted dry densities, water contents or degrees of saturation why the behaviour of the specimen confined under 80 kPa differed slightly from the other specimens. Table 4.6 shows that the pore pressures at failure were all negative and in general, became more negative with increasing confining stress. The continually decreasing negative pore pressures act to increase the effective

stresses in the specimens, thereby making them stronger as the soil continues to strain.

Ideally, specimens which are 100% saturated and compacted to the same density should exhibit the same shear strength when subject to an unconsolidated undrained triaxial test, regardless of the confining pressure (Lambe and Whitman, 1969). The Mohr circles at failure will therefore have the same diameter for any confining stress and a horizontal failure envelope will result.

Figure 4.10 shows that specimens UU11 and UU12 expressed stress-strain curves of a similar shape, which reached approximately the same peak stress. The initial tangent modulus of specimen UU13 is about the same as those obtained for specimens UU11 and UU12 but, the peak stress attained is 80 kPa higher. The results from specimen UU10 are questionable due to flaws in the specimen. However, there does appear to be an increase in undrained shear strength with confining stress.

The total stress p-q plot for these specimens is given in Figure 4.12. The results from specimen UU10 have been ignored and an envelope through the points obtained for specimens UU11, UU12 and UU13. Since the initial water content, dry density and void ratio of the specimens were the same and since they were all completely saturated prior to shearing, according to Lambe and Whitman (1969), a horizontal failure envelope

would be expected. There is, however, an apparent increase in the peak strength of these samples with confining stress. This may be due to differences in the materials composing the specimens. The total stress friction angle calculated from the k_f line is 5° and the total stress cohesive strength intercept is 100 kPa. This cohesive strength intercept is greater than that determined for the specimens obtained from an elevation of 1.67m, 10 m W of the centre line of the embankment, tested without back saturation. The partially saturated specimens would be expected to show a greater strength due to the fact that smaller pore pressures would be developed. However, this anomoly may have resulted because the fully saturated specimens contained a greater percentage of sand particles.

The maximum deviator stress and corresponding strain at failure for a given confining stress have been compared in Table 4.7 for the partially and fully saturated tube specimens tested. The table shows that the maximum shear strength and the strain at failure attained by the fully saturated and partially saturated specimens under each confining stress appear to be very similar. That is, increasing the degree of saturation of the specimens from the average field value of 92% to 100% by back-saturation, did not change the effective stress conditions during testing enough to reduce the shear strength. Comparison of the shapes of the

stress-strain curves for each set of tests also shows that the stress-strain behaviour is not influenced by back-saturating the soil. Therefore, it was concluded that back-saturating specimens during triaxial testing did not result in a reduction of the shear strength or a change in the stress-strain behaviour and all further triaxial testing was conducted under a back pressure to aid in the measurement of pore pressures.

4.3.2 Compacted Clay Fill Soil

Four unconsolidated undrained triaxial tests with pore pressure measurements were conducted on laboratory-compacted specimens of clay fill soil. Unfortunately, specimens UU14, UU16 and UU17 were not weighed prior to testing so the densities, void ratios and percent saturation could not be calculated. However, the water content and density of specimens UU15 have been plotted on the clay compaction curve in Figure 4.5. The density of specimen UU15 is greater than would be expected from the clay compaction curve at a water content of 24%.

Figures 4.13 and 4.14 show the stress-strain and pore pressure-strain curves obtained from these tests. Table 4.8 gives the specimens' characteristics prior to testing and the stress, strain, and pore pressure conditions at failure. Figure 4.13 shows that the specimens tested under confining stresses of 80, 160 and 240 kPa showed approximately the same stress-strain behaviour. This is to be expected from

specimens with the same initial water content, dry density and void ratio that have been fully saturated. Specimen UU14, under zero confining stress, peaked at only half the shear stress of the other samples due to flaws present in the specimen. Hence, the results obtained from specimen UU14 will not be considered. The strains reached at failure by clay specimens UU15, UU16 and UU17 are greater than 18%. This indicates that the test fill slopes may deform considerably in their undrained state before consolidation commences.

The total stress p-q plot obtained from these tests is given in Figure 4.15. The points plotted in Figure 4.15 define a horizontal k_f line with an undrained shear strength intercept of 76 kPa, which represents the average peak strength of specimens UU15, UU16 and UU17. The undrained cohesive strength intercept of the failure envelope for the back-saturated field specimens was about 25 kPa greater than the strength determined for the clay. This is most likely due to the fact that the field-compacted specimens had an average water content of 20.5% and an average density of 1.70 g/cm^3 while the clay specimens had an average water content of 23.0% and an average density of approximately 1.65 g/cm^3. It was shown in Chapter 2 that compacted clayey soils with higher dry densities and lower water contents are stronger. These results indicate that the test fill soil compacted to a height of 2.33 m has been placed at water contents which may be too low. To attain the design

undrained shear strength of about 50 kPa, the fill soil should have been compacted at a higher water content of about 24%.

The pore pressure behaviour during shearing of specimens UU14 through UU17 is dissimilar. The pore pressure at failure measured for specimen UU17 is about 30 to 40 kpa higher than the pore pressures measured for the other samples. The effective stress p-q plot for these tests, given in Figure 4.16, shows more clearly that the pore pressure response measured in specimen UU17 was questionably high. In general, the effective stress paths do not show good agreement as would be expected from the results of unconsolidated undrained triaxial tests conducted on saturated specimens with the same initial dry density and water content and it is suspected that the pore pressure measurements taken during this set of tests were not accurate.

The specimens were set up with a porous stone and filter paper at each end and a filter paper wrapped around the circumference. Drainage was not allowed during the test and pore pressures were measured at the bottom end of the sample through the porous stone. The pressures at the base of the specimen may have been different from those generated near the failure zone of the sample unless a slow enough strain rate was used to allow for equilization of pore pressures throughout the specimen. A strain rate of 0.76 mm/min was used to shear the specimens. However, according

to Bishop and Henkel (1964) a strain rate of 0.05 mm/min should be used for compacted soil such as the fill material used here in order to ensure uniformity of pore pressures throughout the specimen.

4.3.3 Compacted Silt Fill Soil

Four unconsolidated undrained triaxial tests were conducted on the laboratory compacted silt fill soil. The water contents and densities of the specimens have been plotted with the compaction curves established for the clay and silt fill soils in Figure 4.5. The points for the silt specimen fall on either side of the 100% saturation line, in between the compaction curves determined for the clay and silt soils.

Figures 4.17 and 4.18 show the stress-strain and pore pressure-strain curves obtained from these tests. The stress-strain curves have a shape which is different from those obtained for the clay soil. The initial tangent modulus of the silt stress-strain curves is very steep. A sharp break in the curve occurs at a strain of less than 2%. The deviator stress then increases with increasing strain in almost a straight line up to a peak at a strain of 18% or more. This behaviour suggests that a definite structure is set up by compaction of the silt which is broken down at a very low percent strain. Deviator stresses of greater than about 40 kPa would have to exist in the slopes of the test embankment if it were built with the silt fill before soil

strains of greater than 2% would occur.

Table 4.9 gives the specimens' characteristics prior to testing and the stress, strain and pore pressure conditions at failure. Specimen UU20 had a lower initial water content, a higher initial dry density and a lower void ratio than specimens UU18, UU19 and UU21. These factors may have contributed to the slightly higher strength of specimen UU20.

Figures 4.19 and Figure 4.20 show the total and effective stress p-q plots determined for these tests. The unconsolidated undrained shear strength for this set of tests has been taken as 73 kPa, which is the average shear strength of the four specimens tested. This agrees closely whith the unconsolidated undrained shear strength determined for the clay fill soil and is therefore about 25 kPa less than the undrained cohesive strength intercept determined for the back-saturated field-compacted specimens. The clay fill was compacted at a higher water content, to a slightly lower density and a higher void ratio than the silt fill soil. However, the unconsolidated undrained shear strengths of the clay and silt fill soils, compacted with the same effort, are the same. It may therefore be concluded that if the clay fill is compacted in the field at a 2 to 3% higher water content than the silt fill, then a homogeneous undrained shear strength will be achieved.

In section 4.2.3 compaction specifications for the test fill were established based on the unconfined compression

tests conducted on the clay fill soil specimens. However, the compaction specifications must be broad enough to ensure a homogeneous shear strength regardless of an increase in the silt content of the fill soil. The unconsolidated undrained triaxial tests conducted here showed that the silt fill soil must be compacted in the field at a water content of between about 20 and 22% to attain an undrained shear strength of 75 kPa or less. The silt fill compaction curve, given in Figure 4.21, shows that water contents of 20 to 22% correspond to densities of 1.71 to 1.66 g/cm^3.

The complete compaction specifications therefore included: a water content of between 22 and 24% with corresponding dry densities of 1.66 and 1.59 g/cm^3 for the clay fill soil and a water content of between 20 and 22% with corresponding dry densities of 1.71 and 1.66 g/cm^3 for the silt fill soil. These specifications are shown on the fill soil compaction curves in Figure 4.21. The construction supervisor was required to qualitatively assess the silt content of the fill soil being placed in the field and then exercise some judgement as to where the compacted water contents and densities should fall within the specified range.

The average undrained shear strength of about 74 kPa determined from the unconsolidated undrained triaxial tests for the silt and clay soils is higher than the design undrained shear strength of 50 kPa. The 50 kPa shear strength gives a factor of safety of about 1.2 against a

shear failure in the unreinforced slope. Consequently, if the clay cannot be compacted in the field at a water content of greater than about 23% and the silt cannot be compacted at a water content of greater than about 21%, the factor of safety in the unreinforced slope of the test fill may be substantially higher than 1.0. Detailed limit equilibrium analyses based on the soil parameters obtained from the laboratory testing will be presented in Chapter 6.

Although the undrained shear strengths of the 2 soils are the same, the stress-strain behaviour differs significantly at strains of less than approximately 10%. For example, Figure 4.22 shows that under a confining stress of 80 kPa, a strain of 6% corresponds to a principal stress difference of about 98 kPa for the clay and about 58 kPa for the silt. Consequently, the strains which are induced in a layer of geogrid in the test embankment will depend upon the type of fill soil in which the geogrid has been installed.

The stress-strain curves (Figure 4.10) obtained for the back-saturated, field-compacted specimens illustrate the potential for dissimilar stress-strain behaviour due to differences in the silt content of the fill soil. The shape of the stress-strain curve obtained for specimen UU10 of the back-saturated, field-compacted specimen is similar to those obtained for the laboratory-compacted silt fill soil. Specimens UU11, UU12 and UU13 on the other hand, express stress-strain curves which are similar to those obtained for the laboratory-compacted clay fill soil. This suggests that

specimen UU10 may have contained more silt than specimens UU11, UU12 and UU13.

The unconsolidated undrained triaxial tests with pore pressure measurements were conducted to aid in predicting the pore pressure response of the test fill to undrained loading prior to consolidation. In general, the pore pressures in all but two of the fill soil specimens rose to between 10 and 20 kPa at strains of less than about 5% and then decreased to about -25 kPa at failure. Therefore, immediately after placement of a lift of soil positive pore pressures will most likely develop, thereby reducing the effective stresses in the slope. However, the positive pore pressures are not excessively high, thus, a great deal of time will not be required to allow for pore pressure dissipation if necessary. Of course, the actual time required will depend upon the permeability of the fill soil. The consolidation rate of the fill soil will be examined in Section 4.4 wherein consolidated undrained triaxial test results will be presented.

4.3.4 Compacted Sandy Clay Fill Soil

Three unconsolidated undrained triaxial tests were conducted by Alberta Transportation and Utilities on sandy clay compacted to the maximum standard compaction density at the optimum water content. The specimens were subject to confining stresses of 69, 138 and 207 kPa. The resulting stress-strain curves are shown in Figure 4.23. Table 4.11

shows the sample conditions prior to testing and the stress and strain conditions at failure. Pore pressures were not measured by Alberta Transportation and Utilities during their unconsolidated undrained triaxial testing because the specimens were not fully saturated with a back pressure.

The stress-strain curves have a steep initial tangent modulus up to deviator stresses of between 60 and 80 kPa. The deviator stress continues to increase without reaching a peak value up to a strain of 15% were the tests where stopped. The shapes of the stress-strain curves are similar to those obtained for the clay fill soil, however, the shear strengths are much higher. This is most likely due to the fact that the sandy clay specimens were compacted to the maximum dry density and optimum water content.

The total stress failure envelope established by Alberta Transportation and Utilities is given in Figure 4.24. Since a back pressure was not used to saturate the specimens, a horizontal failure envelope was not obtained. The total stress friction angle calculated from the slope of the k_f line is 6.4° and the total stress cohesive strength is 113.7 kPa. These values, along with the average initial water contents, dry densities, void ratios and degrees of saturation of the specimens tested by Alberta Transporation and Utilities have been compared to those obtained from the tests conducted on the unsaturated, field-compacted soil in Table 4.12.

The total stress angle of frictional resistance determined for the sandy clay is only about 1.5° higher than that found for the first set of Shelby tube fill soil specimens. However, the total stress cohesive strength is about 37 kPa higher. This suggests that decreasing the water content, void ratio and degree of saturation and increasing the dry density of the fill soil greatly increases its cohesive strength and has very little effect on the frictional resistance.

4.3.5 Summary of UU Triaxial Test Results

Unconsolidated undrained triaxial tests were conducted on three sets of Shelby tube samples obtained from the test fill at elevations of 1.67 m and 2.33 m. The samples obtained from an elevation of 2.33 m were subject to a back-pressure to fully saturate the soil. The undrained shear strengths of the unsaturated specimens, subject to the same confining stress, showed a considerable amount of scatter due to differences in silt content. This indicates that close control of the type of fill soil being placed in the field and the corresponding compaction requirements specified for each type of soil must be exercised to maintain a homogeneous undrained shear strength within the test embankment. The unconsolidated undrained triaxial tests conducted on the specimens subject to a back-pressure showed that neither the undrained shear strength nor the stress-strain behaviour was affected by saturation of the

soil prior to shearing. This is most likely due to the fact that the average degree of saturation of the soil compacted in the field is 92%.

Unconsolidated undrained triaxial tests were also conducted on silt and clay fill soil specimens compacted in the laboratory to determine whether the two soils behave differently under undrained loading. It was concluded from the tests that if the clay fill soil is compacted at a 2 to 3% higher water content than the silt fill soil, then a homogeneous undrained shear strength will be achieved. The complete compaction specifications include a water content of between 22 and 24% at a corresponding dry density of between 1.66 and 1.59 g/cm^3 for the clay fill soil and a water content of between 20 and 22% at a corresponding dry density of between 1.71 and 1.66 g/cm^3 for the silt fill soil. Although the undrained shear strengths of the two soils are the same, the stress-strain behaviour differs significantly at strains of less than 10%. Silt specimens show approximately twice as much strain as clay specimens at the same stress level. Consequently, the strains which are induced in a layer of geogrid in the test embankment will depend upon the type of fill soil in which the geogrids have been installed.

The pore pressure-strain curves showed that the more silty soil has a greater tendency to dilate during shearing as indicated by the large negative pore pressures. All but two of the fill soil specimens subject to unconsolidated

undrained triaxial tests, with the application of a back-pressure, exhibited a rise in pore pressure up to between 10 and 20 kPa at strains of less than 5%, followed by a decrease in pore pressure to approximately -25 kPa at failure. Therefore, immediately after placement of a lift of soil during construction of the embankment positive pore pressures will most likely develop.

4.4 Consolidated Undrained Triaxial Tests

Due to the need for evaluating the pore pressure response during shear, consolidated undrained triaxial tests with pore pressure measurements were conducted on the clay and silt fill soils. The results from these tests will be presented and discussed in this section.

Compacted clay and silt specimens were prepared for the consolidated undrained triaxial tests in the same manner as those prepared for the unconfined compression tests. The consolidated undrained tests were conducted in accordance with the procedures outlined by Bishop and Henkel (1962). The specimens were allowed to saturate under a back pressure for 24 hours prior to consolidation. Once primary consolidation was complete the specimens were sheared without allowing drainage and pore pressure measurements were taken.

Alberta Transportation and Utilities also conducted consolidated undrained triaxial tests on compacted sandy clay fill soil. The specimens were compacted to the maximum

standard compaction density and the optimum water content. Hence, they represent an upper limit to the long-term undrained shear strength and a lower limit to the stress-strain behaviour of the fill soil. The results from these tests will be presented in this section along with those obtained in this study.

Failure during consolidated undrained triaxial tests with pore pressure measurements may be defined as either the maximum deviator stress or as the maximum principal effective stress ratio (Bjerrum and Simons, 1960). For consolidated drained tests these two points coincide because the pore pressures are zero throughout the test, hence, the effective minor princpal stress in constant. However, for undrained tests with pore pressure measurements the maximum deviator stress and the maximum principal effective stress ratio occur at different points on the stress-strain curve. The maximum deviator stress will be the same whether it is expressed in terms of total or effective stress. This point corresponds to some amount of strain, regardless of the pore pressures developed during axial loading . The principal effective stress ratio depends upon the pore pressures generated during shear and therefore, the point at which the maximum ratio is reached depends upon the pore pressure conditions.

From triaxial tests conducted on various clays, Bjerrum and Simons (1960) showed that the effective stress angle of shear resistance determined from a consolidated undrained

test with pore pressure measurements, where failure is defined as the maximum principal effective stress ratio, agrees with that determined from a consolidated drained test. These results were discussed in Chapter 2 (Figure 2.10). Consequently, where possible, the maximum principal effective stress ratio was taken as the failure criterion for the consolidated undrained triaxial tests. The failure stresses, defined by this point, were used to define the failure envelopes for the soils subject to these tests.

4.4.1 Compacted Clay Fill Soil

Nine consolidated undrained triaxial tests with pore pressure measurements were conducted on laboratory compacted clay fill soil under a back pressure of 400 kPa. The specimens were compacted, at an average water content of 24%, to an average dry density of 1.59 g/cm^3.

The consolidation curves obtained from the consolidation phase of the consolidated drained triaxial tests conducted on the fill soil specimens have not been included here. However, Table 4.13 gives the coefficients of consolidation calculated for the specimens and the time to reach 90% completion of primary consolidation. The average t_{90} for the clay fill was 55 minutes and the average coefficient of consolidation was 4.14E-3 cm^2/s.

The percent volume change during consolidation has been plotted against the consolidation pressure for each specimen in Figure 4.25. The percent volume change remains fairly

constant at approximately -1% up to a consolidation stress of 100 kPa and then becomes more negative with a further increase in consolidation stress. Figure 4.25 indicates that average all-round preconsolidation pressure due to compaction of the soil in the laboratory is about 100 kPa. Rivard and Goodwin (1978) showed that no significant difference in the preconsolidation stresses induced by laboratory compaction or field compaction exists for glacial or alluvial clays. Hence, it may be assumed that if the average of σ_1, σ_2 and σ_3 existing in the test fill due to the weight of the soil is greater than about 100 kPa, volume changes of between 2 and 7% will result, depending upon the particular stress level.

The stress-strain and pore pressure-strain curves obtained from the consolidated undrained triaxial tests conducted on the clay fill are shown in Figures 4.26 and 4.27. Table 4.14 gives the specimens' characteristics prior to testing, the moisture content after consolidation and the stress, strain and pore pressure conditions at failure. Failure has been defined at the point where the principal effective stress ratio is a maximum. This point is shown on each of the stress-strain curves.

In some cases the maximum principal effective stress ratio occurs at up to 6% less strain than the maximum deviatoric stress. Hence, the choice of the failure criteria used to interpret the consolidated undrained triaxial test results is important in that the strains at failure may be

over estimated if the maximum deviator stress is used as the failure criterion. In the field the stability of the test fill will be gauged indirectly by the strains taking place in the soil, as measured by slope indicators and magnetic extensometers. Hence, if the failure strains are over estimated the strains measured by the field instrumentation may not appear to be critical, yet a shear failure may be about to occur.

The stress-strain curves exhibit a high initial tangent modulus. Beyond about 2% strain, the stress rises slowly with increasing strain up to failure. The specimens consolidated under higher confining pressures are denser and therefore, as shown in Figure 4.26, are stiffer and have a higher shear strength. The peak in the deviator stress of the specimens consolidated under stresses between 150 and 203 kPa occurs at strains of between 5 and 11%. The stress-strain curves of the samples consolidated at stresses of 125 kPa or less, do not exhibit a peak in the deviator stress even at strains of up to 24%.

These test results suggest that the undrained stress-strain behaviour of the soil will differ throughout the test fill, depending upon the degree of confinement. Confinement of the soil in the center of the embankment near the base will be greatest and here the soil will take on large deviator stresses up to failure and then will begin to shed load as the strain increases. The soil under lower confining stresses, near the slope face, will reach failure

under smaller stresses at a high percent strain and then will continue to strain indefinitely under the failure stress.

Figure 4.27 shows that the pore pressures developed during shearing increase with an increase in confining stress. The pore pressures rise sharply below 5% strain and then slowly begin to decrease throughout the rest of the test. Figure 4.28 shows that Skempton's pore pressure parameter, A_f, (Skempton, 1954) measured at failure during the tests increases approximately linearly from about 0.02 to 0.50 with increasing confining pressure.

Lovell and Johnson (1980) developed a relation which shows that Skempton's A-parameter at failure is largely a function of the final void ratio, e_f, reached after the consolidation phase of a consolidated undrained triaxial test conducted under a back pressure. They also stated that A_f is probably related to the degree of overconsolidation produced by compaction. The theoretical relation has been plotted in Figure 4.28 by substituting the average as compacted dry density, the average initial degree of saturation and the confining pressure for each of the specimens into Lovell and Johnsons' Equation (2.1).

The A_f-parameters determined from the triaxial tests increase more quickly with confining stress than the theoretical relation predicts. This discrepency may be due to differences between the compacted clay tested in this study and the compacted soil examined by Lovell and Johnson.

However, the laboratory data suggests that an increase in the consolidation pressure for a constant initial void ratio and initial degree of saturation represents a reduction in the overconsolidation ratio and, as shown in Figure 4.29 (Bishop and Henkel, 1962), this produces an increase in A_f. Consequently, the pore pressures will be greatest in the lower central region of the embankment where the confining stresses are highest.

The total and effective stress p-q plots are shown in Figures 4.30 and 4.31. The design total stress friction angle calculated from the slope of the K_f line is 17.6° with no obvious range of values. The design total stress cohesive strength calculated from the intercept of the k_f line is 23 kPa with a possible range from 23 to 24 kPa. The design effective stress friction angle and cohesive strength determined from the effective stress p-q plot are 28° and 10 kPa, respectively. Scatter in the test data suggests that the effective stress cohesive strength may lie between approximately 8 and 14 kPa, with no apparent variation in the effective stress frictional strength. The total and effective stress shear strength parameters determined for the clay fill soil will be compared with those obtained for the silt fill soil in the next section.

4.4.2 Compacted Silt Fill Soil

Five consolidated undrained triaxial tests with pore pressure measurements were conducted on laboratory compacted

silt fill soil under a back pressure of 600 kPa. The specimens were compacted to an average density of 1.71 g/cm^3 at an average water content of 19.6%. Note that these specimens are more dense and dryer than those prepared with the clay soil. However, both sets of specimens were compacted to the density and water content specified on their respective compaction curves, at about 3% wet of the optimum water contents.

The coefficients of consolidation and times required to compete 90% of the primary consolidation calculated from the consolidation phase of the consolidated undrained traixial tests are given in Table 4.13. The average coefficient of consolidation for the silt fill soil was 6.88E-3 cm^2/s. The silt specimens reached t_{90} faster than the clay specimens with an average time of 33 minutes although they had a lower void ratio. This is most likely due to the fact that the pores between the silt particles are larger, thus the specimens have a higher permeability. The percent volume change undergone by the silt specimens during consolidation has been plotted against the consolidation pressure in Figure 4.32. The data is somewhat scattered due to differences in the initial compacted dry desities. The percent volume change which takes place in the silt specimens appears to be less sensitive to the consolidation pressure than was found for the clay specimens. Beyond a confining stress of about 60 kPa, increasingly larger changes in volume occur within the silt specimens. More data

points are required to better define the relationship between the percent volume change undergone by the silt specimens and the consolidation stresses, although it does appear that a smaller load is required to break down the structure of the silt specimens than the clay specimens.

The stress-strain and pore pressure-strain curves obtained from these consolidated undrained tests are shown in Figures 4.33 and 4.34. Table 4.15 gives the specimen properties prior to testing, the moisture content after consolidation and the stress, strain and pore pressure conditions at failure, where failure has been defined as the point at which the principal effective stress ratio is a maximum. The failure points have been identified on the stress-strain curves.

The stress-strain curves show a high initial tangent modulus and then turn abruptly at less than 2% strain to continue upwards in a straight line angled at about 45°. It is interesting to note that the shapes of these stress-strain curves are similar to those obtained from the unconsolidated undrained triaxial tests conducted on similar silt specimens. Hence, the soil structure which is set up during compaction must not be altered significantly during the consolidation phase of the consolidated undrained triaxial tests.

The failure points on the stress-stain curves, defined by the maximum principal effective stress ratio, occurs at between 13 and 21% strain for all specimens. These failure

strains are higher than those reached by the clay specimens. The stress-strain curves obtained for the silt specimens consolidated under higher stresses do not show a peak . Rather, the deviatoric stress seems to increase steadily up to and beyond strains of 28%. Figure 4.35 shows the difference in shape of the stress-strain curves obtained for the clay and silt specimens under consolidation pressures of 50 and 200 kPa. Note that for a confining stress of 200 kPa a strain of 6% corresponds to a deviator stress of about 213 kPa for the clay soil and a deviator stress of only about 168 kPa for the silt soil. Therefore, higher loads will be required in the clay fill in the field to generate strains equivalent to those occuring in the silt fill.

Figure 4.34 shows that the pore pressures developed in the silt specimens increased with the application of higher confining stresses, except for the specimen CU12, consolidated under a stress of 50 kPa. Specimen CU12 had a higher density than the other specimens. This may have resulted in a greater tendency for dilation during shear which in turn, would have caused the developement of large negative pore pressures to resist dilation. The shapes of the pore pressure-strain curves for the clay and silt fill soils are very similar, as shown in Figure 4.36. However, the pore pressures at failure developed in the clay under confining stresses of 125 and 200 kPa were higher than the pore pressures reached at failure in the silt. Consequently, the A-parameters at failure calculated for the clay at high

confining stresses are greater.

Figure 4.37 shows the relationship between A_f and confining stress exhibited by the silt fill soil. The theoretical relationship between A_f and confining stress, calculated using Lovel and Johnsons' Equation 2.1 for the degrees of saturation and dry densities of the silt specimens is also shown in Figure 4.37. The slopes of the measured and theoretical relationships between A_f and confining stress are similar. However, the measured values of A_f are approximately 0.1 higher. Figure 4.37 indicates that the pore pressures generated in the silt specimens due to shear stress are not very sensitive to increases in confining stress. Comparison of these results with those obtained for the clay fill show that the pore pressures which develop in response to shear stresses may be slightly higher in the clay fill than in the silt fill soil.

The total and effective stress p-q plots derived from these tests are shown in Figures 4.38 and 4.39. The design total stress friction angle calculated from a line drawn through the total stress failure points is 20.5° and the total stress cohesive strength intercept is 22 kPa. Since very little scatter in the data exists, ranges of shear strength parameters were not estimated. The design effective stress friction angle of the silt is 27° with a possible range from 26 to 27 kPa. The design effective stress cohesive strength is 20 kPa with a possible range from 20 to 25 kPa. The total and effective stress strength parameters

determined for the silt specimens are similar to those obtained for the clay specimens. However, the design effective stress cohesive strength of the clay is equal to only half of that determined for the silt. Consequently, effective stress limit equilibrium analyses conducted using each set of parameters established for the two soils would result in higher factors of safety for the silt fill soil. The shear strength parameters determined for the various fill soils will be compared and commented on later in the Chapter.

4.4.3 Compacted Sandy Clay Fill Soil

Three consolidated undrained triaxial tests were conducted by Alberta Transportation and Utilities on sandy clay fill soil. Although the specimens were subject to a back pressure of only 275 kPa, B-tests showed that it was sufficient to fully saturate the specimens.

The coefficients of consolidation and times to reach 90% consolidation calculated for these specimens are given in Table 4.13. The sandy clay specimens consolidated more slowly than either the clay or silt specimens. The average t_{90} of the sandy clay specimens was 191 minutes, which is 136 minutes greater than the average t_{90} for the clay specimens. Since the distribution of grain sizes less than 0.06 mm was not determined for this soil it is difficult to explain why consolidation of the sandy clay specimens took longer.

Figure 4.40 shows the stress-strain curves obtained from these tests. The specimen characteristics prior to testing and after consolidation are given in Table 4.16 along with the stress, strain and pore pressure conditions at failure where failure has been defined at the maximum principal effective stress ratio. The specimens were compacted to the maximum dry density and optimum water content but attained shear strengths similar to those of the less-dense clay and silt specimens. For example, Figure 4.41 shows that the specimens prepared at the maximum dry density and consolidated under a confining pressure of 207 kPa failed at a deviator stress of about 260 kPa. The clay specimens confined under cell pressures of 200 and 203 kPa failed at deviator stresses of 230 and 258 kPa, respectively. The silt specimen confined under a stress of 200 kPa failed at a deviator stress of 285 kPa. The shape of the stress-strain curves resulting from the consolidated undrained tests conducted by Alberta Transportation resemble more closely those obtained from tests conducted on the clay specimens. A steep initial portion of the stress-strain curve is observed at less than 2% strain, followed by a gradual increase in stress with increasing strain.

The total and effective stress frictional and cohesive strength parameters obtained from Alberta Transportation and Utilities' tests agreed closely with the parameters obtained from the clay and silt soils. The total and effective stress p-q plots are given in Figures 4.42 and 4.43. The design

total angle of frictional resistance determined from Alberta Transportation's tests was 16° and the design total cohesive strength was 38 kPa with a possible range in cohesive strength from 38 to 41 kPa. The design effective angle of frictional resistance was 27° and the design effective cohesive strength was 24 kPa with a possible range from 24 to 26 kPa. These values will be compared in the next section with those obtained for the clay and silt fill soils along with the results from the consolidated drained tests conducted on the clay fill soil.

4.5 Consolidated Drained Triaxial Tests

The long-term stability and deformational characteristics of the unreinforced slope of the test fill will be governed by the consolidated drained behaviour of the fill soil. It has been shown by Bjerrum and Simons (1960) that the effective stress frictional and cohesive strength parameters determined from consolidated drained and consolidated undrained tests are the same for many soils. However, it was shown in Chapter 2 that the shape of the stress-strain curves obtained from the two types of tests may differ significantly. This is due to the fact that both volumetric and shear strains are measured during drained tests while only shear strains are measured during undrained tests. Therefore, to establish the stress-strain behaviour induced by axial loading under drainage conditions similar to the long term conditions which may be present in the

field, consolidated drained triaxial tests were conducted on the fill soil.

It should be noted that true modelling of the stress paths followed by the soil in the embankment would be considerably more complicated. Eisenstien and Law (1979) showed that the ratio of the minor and major principal stress increment, K, for most elements of soil in an embankment during construction falls within a narrow range and may be considered approximately constant. In the zone through which a critical slip circle may pass, K is about 0.40. Consequently, in order to model the stress path which occurs due to the addition of compacted lifts of soil, a triaxial test should be conducted wherein the confining stress is increased by 0.40 times the axial stress throughout the test. Furthermore, to model construction of an embankment in stages, a specimen must be subject to a series of undrained load steps in the triaxial apparatus with σ_3/σ_1 equal to 0.40, where full consolidation is allowed to take place at the end of each load step. Tests such as these have not been conducted for this thesis as it was not known at the time of performing the laboratory testing program that the test fill would be constructed in stages over a three year period.

4.5.1 Compacted Clay Fill Soil

Consolidated drained triaxial tests were conducted on 3 specimens of clay fill to establish the stress-strain

behaviour of the soil for use in the long term finite element analysis. The specimens were prepared in the same manner as those prepared for the unconfined compression tests. The consolidated drained tests were conducted in accordance with the procedures outlined by Bishop and Henkel (1962). The specimens were saturated with a back pressure of 600kPa, consolidated under various cell pressures and then sheared slowly under drained conditions while volume change measurements were recorded.

The clay specimens were compacted with an average water content of 21% and an average density of 1.65 g/cm^3. The water content used was 2% lower that that used for the clay specimens prepared for the consolidated undrained triaxial tests, however, it matches more closely the water content of the fill soil placed in the field up to a height of 6m.

The stress-strain curves and volume change versus strain curves derived from these tests are shown in Figures 4.44 and 4.45. Table 4.17 shows the specimens' conditions prior to testing and the stress, strain and volume change conditions at failure.

The stress-strain curves appear to be hyperbolic in shape. Since the consolidated drained tests could represent the long term loading and drainage conditions of the fill soil, the stress-strain curves obtained from these tests were modelled for the finite element analysis. It was therefore important to comfirm whether or not they could be represented with a hyperbola.

The equation for a hyperbola is given by:

$$\frac{\epsilon_1}{(\sigma_1-\sigma_3)} = \frac{\epsilon_i}{(1/E_i)+(\epsilon_1/(\sigma_1-\sigma_3)_{ult})} \qquad [4.2]$$

Equation 4.5 may be rewritten as:

$$(\sigma_1-\sigma_3)=(1/E_i)+(\epsilon_1/(\sigma_1-\sigma_3)_{ult}) \qquad [4.3]$$

Hence to confirm whether or not the triaxial data follows a hyperbolic curve, $\epsilon_1/(\sigma_1-\sigma_3)$ was plotted against ϵ_1. The transformed triaxial test data, shown in Figure 4.46, follows an approximately straight line, thus indicating that the stress-strain curve is approximately hyperbolic. The intercept of the line represents $1/E_i$ and the slope of the line represents $1/(\sigma_1-\sigma_3)_{ult}$. The parameters used for the finite element analysis from the hyperbolic models of the consolidated drained stress-strain curves will be discussed in more detail in Chapter 6.

The volume change versus axial strain curves given in Figure 4.45 shows that the specimens first contracted and then dilated at high strains. This behaviour agrees with that exhibited by the pore pressures developed during undrained shear. The amount of contraction which occurred in

the specimens at low strains increased with increasing confining pressure, whereby the specimen confined under a stress of 160 kPa underwent a maximum negative volume change of 1.1%. It may be concluded from the small volume changes measured during drained shear and the small A-parameters calculated at failure during undrained shear, that neither excessively high pore pressures nor large volume strains will occur in the test fill due to shear stress alone.

The total/effective stress p-q plot derived from the consolidated drained tests is shown in Figure 4.47. The design effective stress friction angle and cohesive strengths calculated from the K_f line are 27° and 20 kPa, respectively. Figure 4.47 shows that the friction angle may range from about 27° to 28° and the cohesive strength may vary from 23 to 27 kPa, depending upon how the failure envelope is fit through the data. However, the values of the strength parameters measured for the drained tests appear to fall within the values established from the undrained triaxial tests. The results obtained from the consolidated undrained and consolidated drained triaxial tests conducted on various samples of fill soil will be discussed in the next section.

4.6 Summary of the CU and CD Triaxial Test Results

Table 4.18 gives both the design values and range of frictional and cohesive strength parameters determined for each of the different fill soils from drained and undrained

triaxial tests. Comparison of the results obtained from the consolidated undrained tests shows that the total and effective stress friction angles do not appear to be affected by differences in the initial compacted water content and dry density of the soils tested. However, both the total and effectivestress cohesive strengths appear to increase with increasing initial dry density.

The conclusions drawn for the consolidated undrained effective stress parameters are substantiated by the results obtained by Lovell and Johnson (1980), given in Chapter 2. They stated that the effective friction angle was essentially constant for the range of compaction conditions (p_d and w) investigated for Saint Croix clay and that the effective stress strength intercept was a function of the intial void ratio of the as compacted conditions. Table 4.18 shows that ϕ' determined for each of the fill soils tested here did not change. The statistical equation developed by Lovell and Johnson, which relates c' to the as compacted dry density and water content, shows that as the dry desity increases, or the initial void ratio decreases, the effective stress cohesive strength increases.

The effective stress cohesive strengths obtained from the consolidated drained triaxial tests have been plotted in Figure 4.48. The theoretical relationship between the effective stress cohesive strength and the as compacted water content for various as compacted void ratios was also determined for the specimens using Lovell and Johnsons'

Equation 2.3. Both the measured data and theoretical predictions show that as the initial void ratio decreases, or as the initial dry density increases, the effective stress cohesive strength intercept increases. c' determined from the consolidated undrained failure envelope for the clay fill is equal to about half of the value predicted with Lovell and Johnsons' relation. Otherwise, the measured data falls within reasonable limits of the theoretical curves. Assuming that the shear strength parameters of the fill soils tested in this study and by Alberta Transportation and Utilities are functions of the initial dry density and water content, in a manner similar to that described by Lovell and Johnson, then over compaction of soil in the field at a given water content will result in an increase in the cohesive strength of the soil but will not affect the frictional resistance.

The effective frictional strength determined from the consolidated drained triaxial tests agrees with that established from the undrained tests. However, although the densities of the specimens subject to drained shearing are intermediate to the clay and silt specimens sheared without allowing drainage, the effective cohesive strength is not intermediate to the values established for the less dense clay and the more dense silt. This anomoly may be due to a greater percentage of clay sized particles in the specimens sheared under drained conditions. A grain size curve was not established for these specimens, hence a definite conclusion

cannot be drawn.

The stress-strain curves obtained from the consolidated drained triaxial tests conducted on the clay fill soil are similar to those obtained from the consolidated undrained tests conducted on the same soil. However, Table 4.18 shows that the deviator stresses reached at failure were considerably higher in the drained tests than those reached in the undrained tests. This is most likely due to the initially higher dry density of the specimens subject to consolidated drained tests. Table 4.18 also shows that the initial tangent modulii of the drained stress-strain curves appear to be intermediate to those obtained for the undrained tests conducted on the clay and silt fill soils. This again may be due to the fact that the densities to which the clay specimens were compacted for drained testing were intermediate to the densities to which the clay and silt specimens were compacted to for undrained testing.

It was shown in Chapter 2, Section 2.3.2.1, that the shapes of the stress-strain curves obtained from consolidated drained and undrained triaxial tests may differ considerably if the volume change undergone during drained shear is significant. However, comparison of the undrained and drained stress-strain curves obtained for the clay fill soil in this study shows that very little difference in shape exists. This indicates that the volume changes which occurred during drained shear were not large. This is supported by Figure 4.43 which shows that the maximum

negative volume change which occurred at failure of the sample confined under a cell pressure of 160 kPa was only about 1.1%. Therefore, the deformations which take place in the test embankment due to shear stresses will most likely be insignificant.

In order to conduct stability and deformational analyses on the test fill, shear strength parameters and stress-strain curves were chosen for the fill soil from the laboratory test results presented in this chapter. The parameters selected to characterize the fill soil behaviour in the field under different drainage conditions will be discussed in Chapter 6 along with similar considerations for the foundation soil.

Table 4.1: Summary of Tests Conducted on Compacted Fill Soil Specimens

Specimen Type	Unconfined Compression	Unconsolidated Undrained Triaxial (Sr≠100%)	Unconsolidated Undrained Triaxial (Sr=100%)	Consolidated Undrained Traixial (Sr=100%)	Consolidated Drained Triaxial (Sr=100%)
Clay	X	-	X	X	X
Silt	X	-	X	X	-
Tube Samples:					
1.67m;10mW Cl	-	X	-	-	-
1.67m;12mE Cl	-	X	-	-	-
2.33m;12mE Cl	-	-	X	-	-
Sandy Clay	-	X	-	X	-

Table 4.2: Unconfined Compression Tests on Clay Fill Soil (strain rate = 0.71 mm/min)

NOTE: Dry desities were obtained from the compaction curve for the clay soil.

Specimen	qu1	qu2	qu3	qu4	qu5	qu6	qu7	qu8	qu9	qu10
W(%)	14.3	14.5	16.8	16.7	18.1	18.0	20.1	19.9	22.1	22.0
Pd(g/cm)	1.49	1.49	1.60	1.60	1.64	1.64	1.68	1.68	1.66	1.66
e	0.812	0.812	0.688	0.688	0.646	0.646	0.607	0.607	0.627	0.627
Sr(%)	47.5	47.5	65.6	65.2	75.6	75.2	89.4	88.5	95.2	94.8
$\sigma_1 f$(kPa)	130	149	230	200	180	194	126	134	89	76
εf(%)	4.3	3.8	7.7	7.5	12.8	11.5	19.7	15.9	26.5	23.0

Table 4.3: Unconfined Compression Tests on Silt Fill Soil

NOTE: Dry desities were obtained from the compaction curve for the clay soil.

Specimen	qu11	qu12	qu1	qu14	qu15
W(%)	14.7	14.9	15.9	16.0	18.1
Pd(g/cm)	1.73	1.75	1.81	1.81	1.75
e	0.561	0.543	0.492	0.492	0.543
Sr(%)	70.3	73.6	87.3	87.3	94.5
$\sigma_1 f$(kPa)	147	197	208	210	142
εf(%)	3.9	5.1	15.0	13.1	19.6

strain rate = 0.71 mm/min

Table 4.4: Data from UU Tests on Tube Samples (1.67 m elevation, 10 m W CL)

Specimen	UU1	UU2	UU3	UU4	UU5
Cell Press. (kPa)	0	80	160	240	240
Back Press. (kPa)	0	0	0	0	0
W(%)	21.1	21.1	20.7	20.7	19.6
Pd(g/cm3)	1.68	1.70	1.70	1.71	1.66
e	0.63	0.61	0.61	0.60	0.64
Sr(%)	91.4	94.4	92.6	94.2	83.6
$(\sigma_1 - \sigma_3)f$ (kPa)	166	182*	178*	244	271
Uf(kPa)	-	-	-	-	-
εf(%)	12.7	15.0	15.0	14.0	21.7

Strain rate = 0.76 mm/min
* Failure has been defined at 15% strain

Table 4.5: Data from UU Tests on Tube Samples (1.67 m elevation, 12 m E CL)

Specimen	UU6	UU7	UU8	UU9
Cell Press. (kPa)	0	80	160	240
Back Press. (kPa)	0	0	0	0
W(%)	19.6	19.1	21.9	20.6
Pd(g/cm3)	1.70	1.72	1.68	1.71
e	0.60	0.58	0.63	0.59
Sr(%)	88.7	89.0	95.2	94.0
$(\sigma_1 - \sigma_3)f$ (kPa)	156	286*	116**	152
Uf(kPa)	-	-	-	-
εf(%)	20.4	15.0	9.2	20.5

Strain rate = 0.76 mm/min
* Failure has been defined at 15% strain
** Results are suspect due to flaws in the sample

Table 4.6: Data from UU Tests on Tube Samples (2.33 m elevation, 12 m E CL)

Specimen	UU10	UU11	UU12	UU13
Cell Press. (kPa)	0	80	160	240
Back Press. (kPa)	600	600	600	600
W(%)	21.5	20.8	20.4	20.4
Pd(g/cm3)	1.70	1.69	1.72	1.70
e	0.61	0.62	0.59	0.60
Sr(%)	96.1	92.3	94.8	90.9
$(\sigma_1 - \sigma_3)f$ (kPa)	129**	235	244	274*
Uf(kPa)	-6.7	-27.0	-24.0	-45.0
εf(%)	15.0	20.7	16.4	15.0
B	1.0	1.0	1.0	1.0
A	-0.052	-0.115	-0.098	-0.164

Strain rate = 0.76 mm/min
* Failure has been defined at 15% strain
** Results are suspect due to flaws in the sample

Table 4.7: Comparison of Failure Parameters from UU Tests Conducted on Tube Samples

SIGMA 3 (kPa)	1.67m; 10mW CL (Sr≠100%)		1.67m; 12mE CL (Sr≠100%)		2.33m; 12mE CL (Sr=100%)	
	$(\sigma_1-\sigma_3)f$ (kPa)	εf (%)	$(\sigma_1-\sigma_3)f$ (kPa)	εf (%)	$(\sigma_1-\sigma_3)f$ (kPa)	εf (%)
0	166	12.7	156	20.4	-	-
80	182	15.0	286	15.0	235	20.7
160	178	15.0	-	-	244	16.4
240	244 271	14.0 21.7	152 -	20.5 -	274 -	15.0 -

Note: The deviator stresses and strains at failure have not been included in the table for those specimens whose results are suspect.

Table 4.8: Data from UU Tests on Clay Fill Soil

Specimen	UU14	UU15	UU16	UU17
Cell Press. (kPa)	0	80	160	240
Back Press. (kPa)	600	600	600	600
W(%)	22.6	24.3	24.2	23.6
Pd(g/cm)	-	1.651	-	-
e	-	0.635	-	-
Sr(%)	-	103.0	-	-
$(\sigma_1-\sigma_3)f$ (kPa)	77**	153	140	165
Uf	-4.3	2.0	-10.0	34.0
εf	15	28	27	18
B	1.0	1.0	1.0	1.0
A	-0.056	0.013	-0.071	0.206

** Results are suspect due to flaws in the sample

Table 4.9: Data from UU Tests on Silt Fill Soil

Specimen	UU18	UU19	UU20	UU21
Cell Press. (kPa)	0	80	160	240
Back Press. (kPa)	600	600	600	600
W(%)	21.3	21.7	20.3	21.8
Pd(g/cm)	1.724	1.696	1.740	1.698
e	0.566	0.592	0.552	0.590
Sr(%)	101.6	99.0	99.3	99.8
$(\sigma_1 - \sigma_3)f$ (kPa)	142	158	172	116
Uf	-29	-30	-29	-25
εf	20	30	20	31
B	1.0	1.0	1.0	1.0
A	-0.204	-0.190	-0.169	-0.216

Strain rate = 0.76 mm/min

Table 4.10: Comparison of Pore Pressures Developed in Fill Soil Samples During UU Triaxial Tests

Fill Soil	Pd(g/cm3)	W(%)	U=2%(kPa)	Uf(kPa)
Clay				
0 kPa	-	22.6	0.0	-4.3
80 kPa	1.65	24.3	16.0	2.0
160 kPa	-	24.2	-2.0	-10.0
240 kPa	-	23.6	33.0	34.0
Silt				
0 kPa	1.72	21.3	-6.0	-29.0
80 kPa	1.70	21.7	1.5	-30.0
160 kPa	1.74	20.3	3.0	-29.0
240 kPa	1.70	21.8	-1.0	-25.0
Tube Samples				
0 kPa	1.70	21.5	0.5	-6.7
80 kPa	1.69	20.8	17.5	-27.0
160 kPa	1.72	20.4	19.0	-24.0
240 kPa	1.70	20.4	16.0	-45.0

Table 4.11: Data from UU Tests conducted on Sandy Clay fill soil

Specimen	UU22	UU23	UU24
Cell Press. (kPa)	69	138	207
Back Press. (kPa)	0	0	0
W(%)	16.3	16.6	16.7
Pd(g/cm)	1.819	1.799	1.803
e	0.500	0.518	0.514
Sr(%)	90.0	87.5	88.7
$(\sigma_1 - \sigma_3)f$ (kPa)	273	289	309
Uf(kPa)	-	-	-
εf	14.4	14.4	14.8

Strain rate = 0.76 mm/min

Table 4.12: Comparison of Undrained Shear Strength Parameters for Partially Saturated Fill Soil

Fill Soil	Tube Samples from Test Fill		Compacted Sandy Clay
	1.67m 10mW CL	1.67m 12mE CL	
W(%)	20.6	20.3	16.5
Pd(g/cm)	1.69	1.70	1.81
e	0.62	0.60	0.51
Sr(%)	91.2	91.7	88.7
ϕ(deg)	4.8	-	6.4
C(kPa)	76.3	-	113.7
εf(%)	15.7	16.3	14.5

Table 4.13: Consolidation Parameters for Fill Soils Determined from CU Triaxial Tests

Soil Type	Sigma 3 (kPa)	Cv (cm2/s)	t90 (min)
Clay	25	32x10e-4	64
	50	-	-
	75	-	-
	100	42x10e-4	52
	125	56x10e-4	40
	150	-	-
	175	43x10e-4	56
	200	34x10e-4	64
	203	-	-
Silt	20	-	-
	35	73x10e-4	35
	50	91x10e-4	23
	125	57x10e-4	36
	200	54x10e-4	39
Sandy Clay	69	0.7x10e-4	144
	138	0.5x10e-4	266
	207	0.6x10e-4	164

Table 4.14 : Data from CU Traixial Tests Conducted on Clay Fill Soil

Specimen	CU1	CU2	CU3	CU4	CU5	CU6	CU7	CU8	CU9
Cell Press. (kPa)	25	50	75	100	125	150	175	200	203
Back Press. (kPa)	400	400	400	400	400	400	400	400	400
Wo(%)	21.3	25.1	24.3	23.6	23.7	23.0	22.9	23.1	22.5
Wf(%)	24.0	24.2	24.0	24.0	24.4	24.0	24.0	23.1	24.0
Pd(g/cm3)	1.604	1.581	1.592	1.575	1.541	1.622	1.592	1.601	1.594
e	0.665	0.689	0.677	0.695	0.733	0.646	0.677	0.668	0.675
Sr(%)	94.7	92.7	94.5	90.6	87.7	99.1	92.9	90.9	94.9
$(\sigma_1 - \sigma_3)f$ (kPa)	100	104	125	143	165	187	211	230	258
$(\sigma_1'/\sigma_3')f$	5.46	3.81	3.60	6.02	3.40	3.37	4.26	3.36	2.30
Uf(kPa)	2.4	12.6	27.0	71.7	56.0	71.0	110.3	102.7	91.0
εf(%)	3.0	6.1	7.0	4.4	13.7	7.0	5.2	10.1	11.0
B	1.0	1.0	1.0	1.0	1.0	1.0	1.0	1.0	1.0
A	0.024	0.121	0.216	0.501	0.339	0.380	0.523	0.446	0.353

Strain rate=0.15 mm/min

Table 4.15 : Data from CU Triaxial Tests Conducted on Silt Fill Soil

Specimen	CU10	CU11	CU12	CU13	CU14
Cell Press. (kPa)	20	35	50	125	200
Back Press. (kPa)	600	600	600	600	600
Wo(%)	20.1	20.1	19.3	19.3	19.3
Wf(%)	21.3	21.7	-	-	-
Pd(g/cm3)	1.70	1.70	1.74	1.73	1.68
e	0.571	0.571	0.535	0.543	0.589
Sr(%)	91.5	91.5	94.4	92.3	85.8
$(\sigma_1 - \sigma_3)f$ (kPa)	85	93	178	197	285
$(\sigma_1'/\sigma_3')f$	8.98	6.12	4.00	3.35	3.07
Uf(kPa)	9.4	16.8	-9.5	41.1	62.5
$\varepsilon f(\%)$	15.5	14.0	16.5	20.6	17.2
B	1.0	1.0	1.0	1.0	1.0
A	0.111	0.181	-0.053	0.209	0.220

Strain rate = 0.15 mm/min

Table 4.16 : Data from CU Tests Conducted on Sandy Clay Fill Soil

Specimen	CU15	CU16	CU17
Cell Press. (kPa)	69	138	207
Back Press. (kPa)	276	276	276
Wo(%)	17.1	17.1	17.1
Wf(%)	18.4	18.0	17.6
Pd(g/cm)	1.797	1.792	1.782
e	0.519	0.523	0.532
Sr(%)	89.9	89.2	87.8
$(\sigma_1 - \sigma_3)f$ (kPa)	137	197	263
$(\sigma_1'/\sigma_3')f$	5.42	3.73	3.46
Uf(kPa)	38	66	100
$\varepsilon f(\%)$	2.07	4.59	7.19
B	0.98	0.98	1.00
A	0.277	0.335	0.380

Strain rate = 0.76 mm/min

Table 4.17 : Data from CD Triaxial Tests Conducted on Clay Fill Soil

Specimen	CD1	CD2	CD3
Cell Press. (kPa)	40	80	160
Back Press. (kPa)	600	600	600
Wo(%)	20.9	20.9	20.9
Wf(%)	24.0	22.9	21.0
Pd(g/cm)	1.656	1.663	1.637
e	0.631	0.624	0.650
Sr(%)	89.5	90.5	86.9
$(\sigma_1 - \sigma_3)f$ (kPa)	147.3	246.4	328.8
$(\sigma_1'/\sigma_3')f$	4.68	4.08	3.05
(V/Vo)(%)	0.46	0.57	-0.68
εf	11.5	13.2	16.5

Strain rate = 0.009 mm/min(?)

Table 4.18 : Summary of CU and CD Triaxial Test Results

Soil Type	Clay Fill (CU)	Silt Fill (CU)	Sandy Clay (CU)	Clay Fill (CD)
Pd(ave)g/cm	1.589	1.703	1.790	1.652
Wo(ave)%	23.3	19.7	17.1	20.9
e(ave)	0.681	0.562	0.491	0.616
ϕ(deg)				
range	17.7-17.6	20.5-20.5	16.0-15.7	-
design	17.6	20.5	16.0	-
C(kPa)				
range	23.0-24.0	22.0-22.0	38.0-40.5	-
design	23.0	22.0	38.0	-
ϕ'(deg)				
range	30.0-30.0	27.0-25.9	27.0-27.0	28.1-27.3
design	30.0	27.0	27.0	27.0
C'(kPa)				
range	8.0-13.9	20.0-25.0	24.0-25.8	22.7-27.0
design	8.0	20.0	24.0	22.0

Table 4.19: Comparison of Parameters Obtained from CU and CD Triaxial Tests

Soil Type	Test Type	Dry Density (g/cm^3)	Confining Stress(kPa)	$(\sigma_1 - \sigma_3)f$ (kPa)	Ei (kPa)
Clay	CU	1.58	50	104	6350
		1.73	75	125	11000
		1.62	150	187	17000
Silt	CU	1.74	50	178	10750
		1.73	125	197	24150
		1.68	200	285	27700
Clay	CD	1.66	40	147	9200
		1.66	80	246	19850
		1.64	160	329	23600

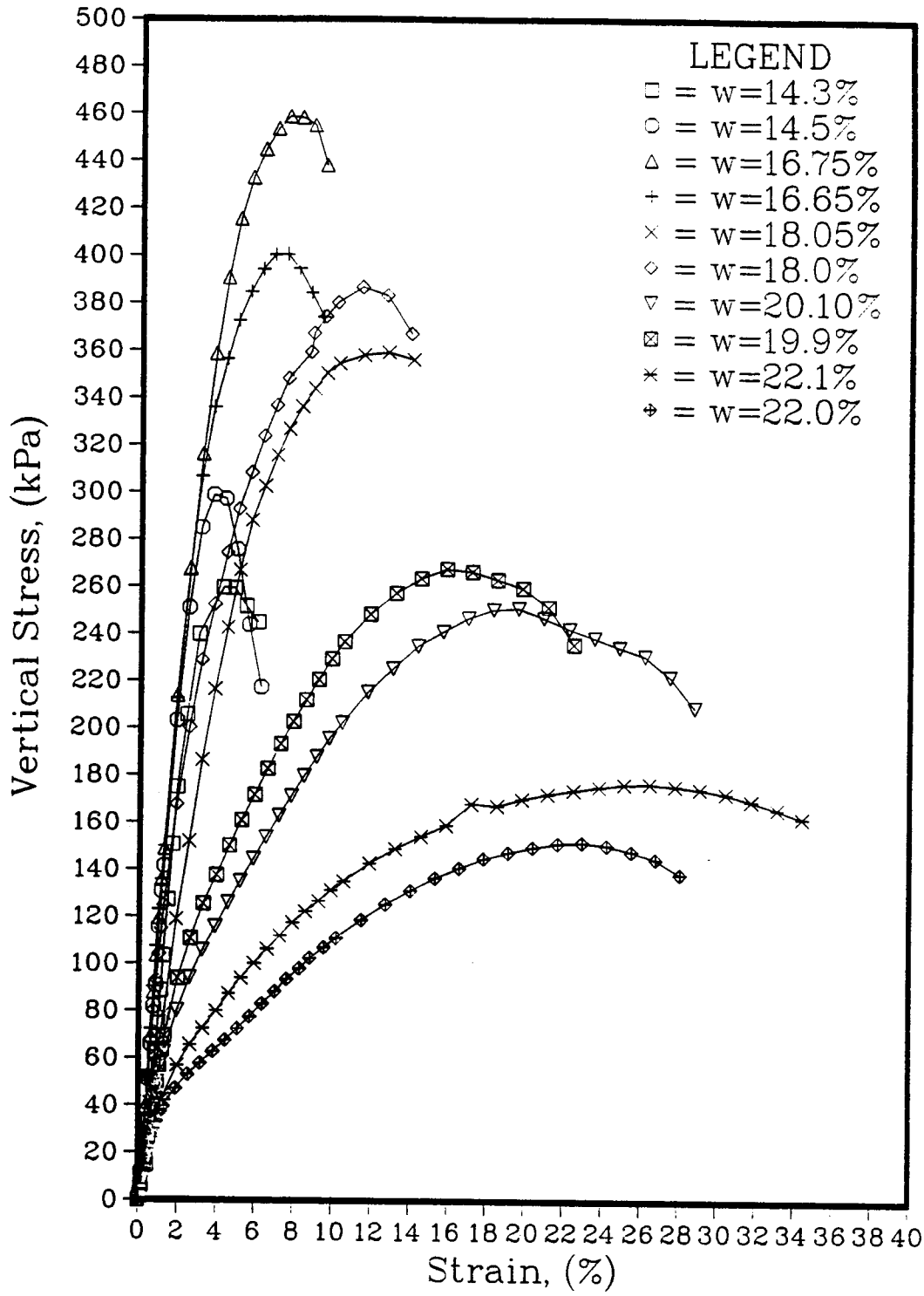

Figure 4.1: qu Tests on Clay Fill Soil

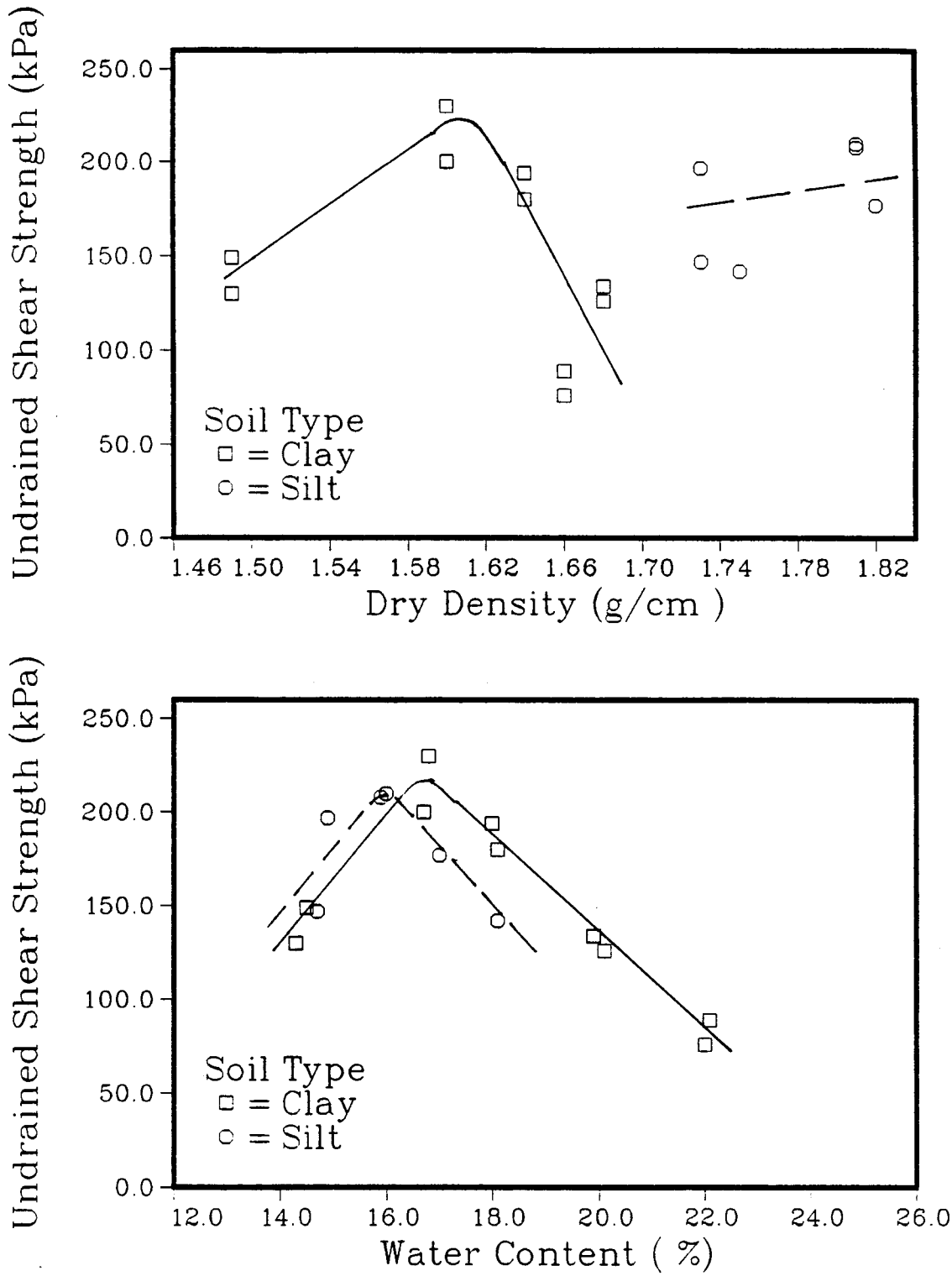

Figure 4.2: Data from qu Tests on Fill Soils

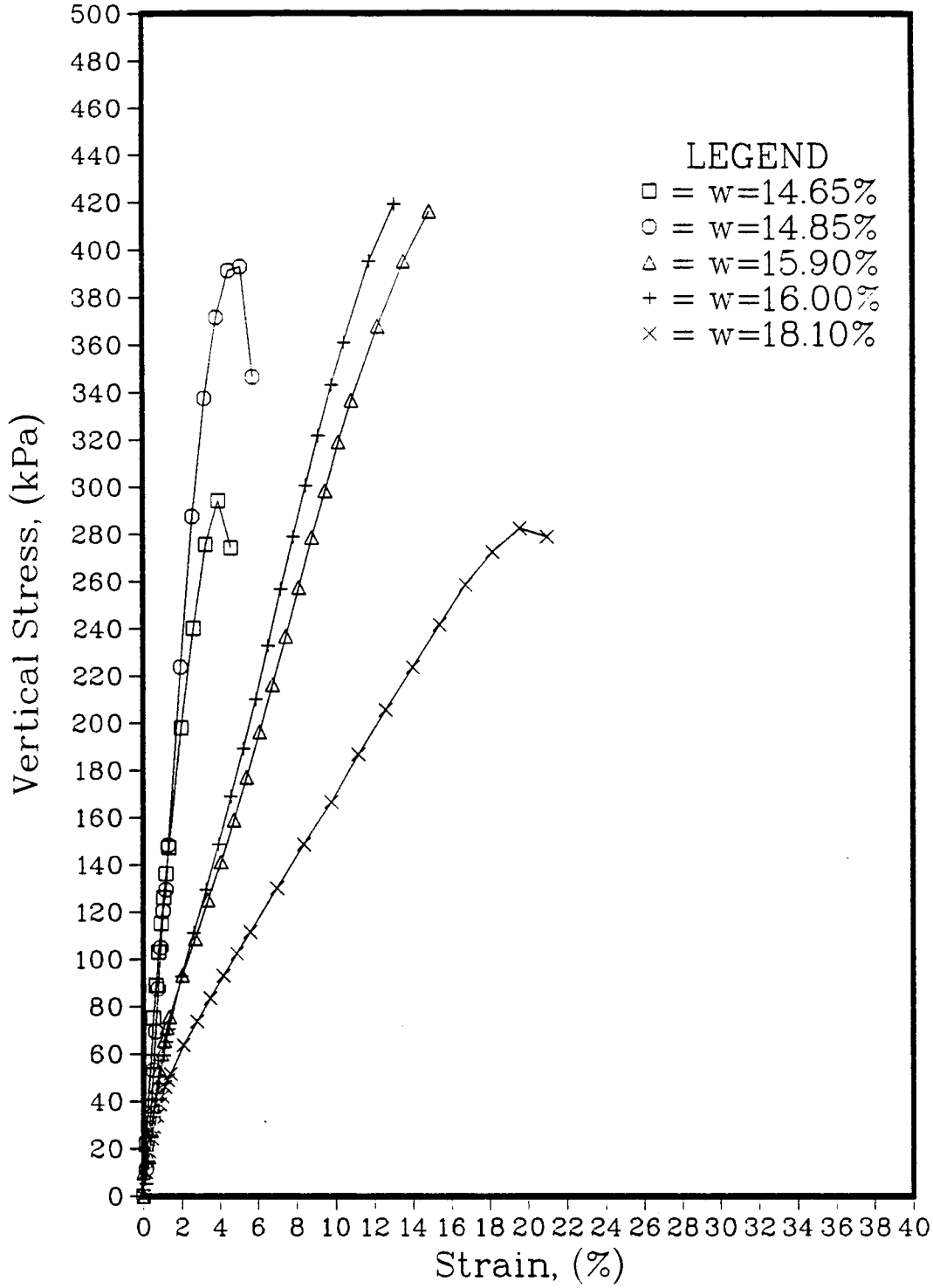

Figure 4.3: qu Tests on Silt Fill Soil

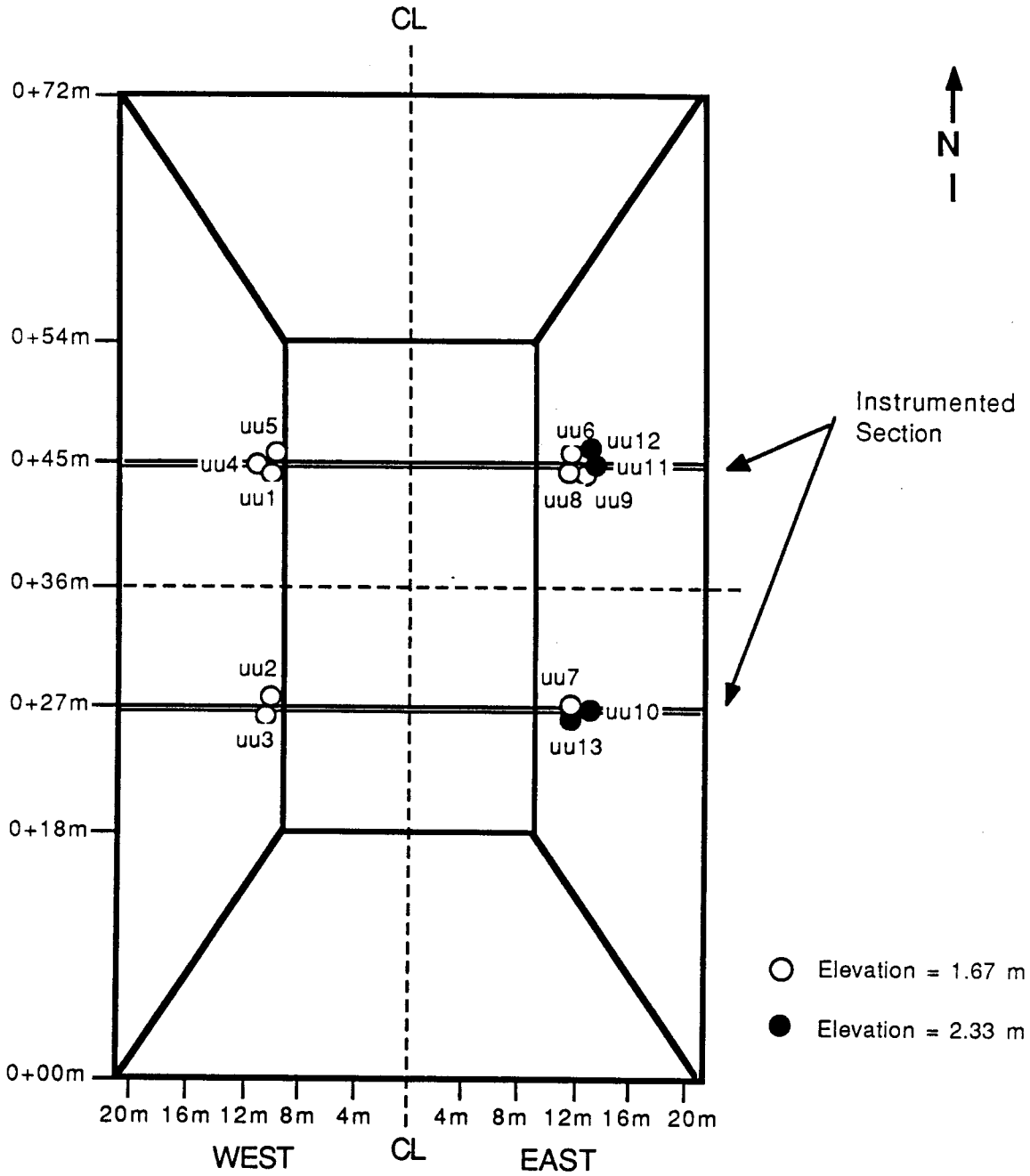

Figure 4.4 : Plan View of Test Fill Indicating Location of Tube Samples

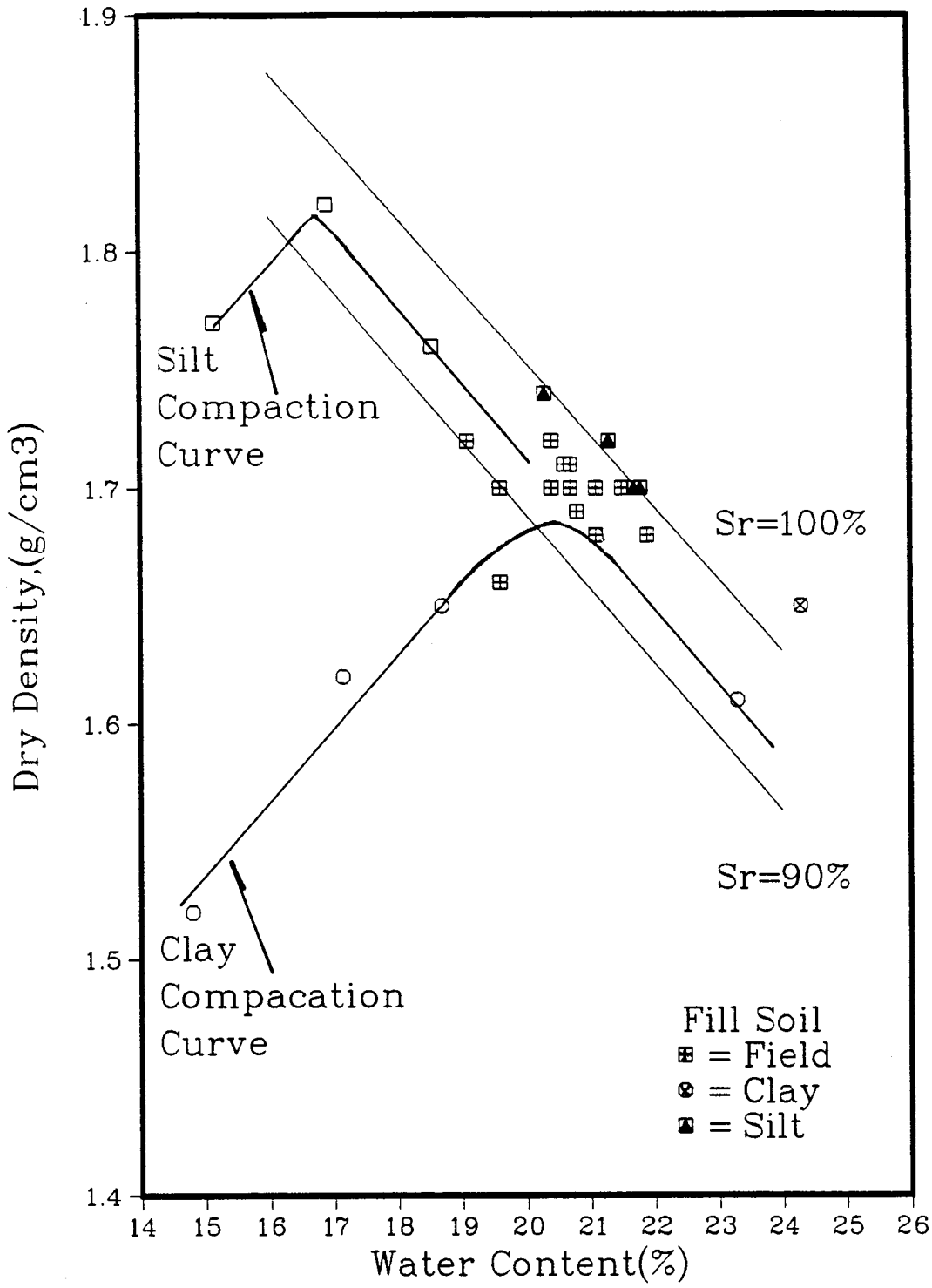

Figure 4.5: Fill Soil Specimens with Respect to Original Compaction Curves

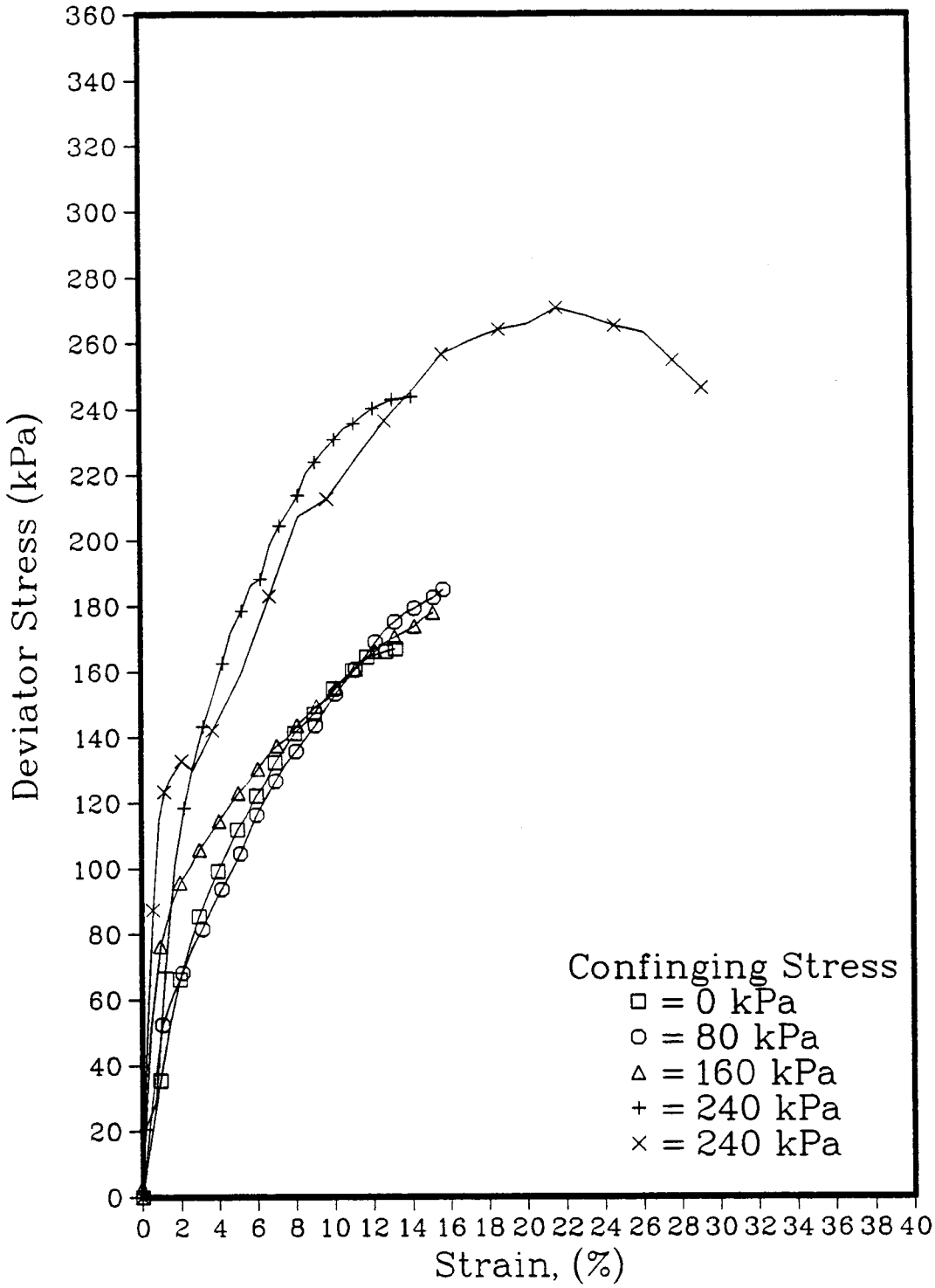

Figure 4.6: UU Triaxial Tests on Tube Fill Soil
(1.67m elevation, 10m W of CL)

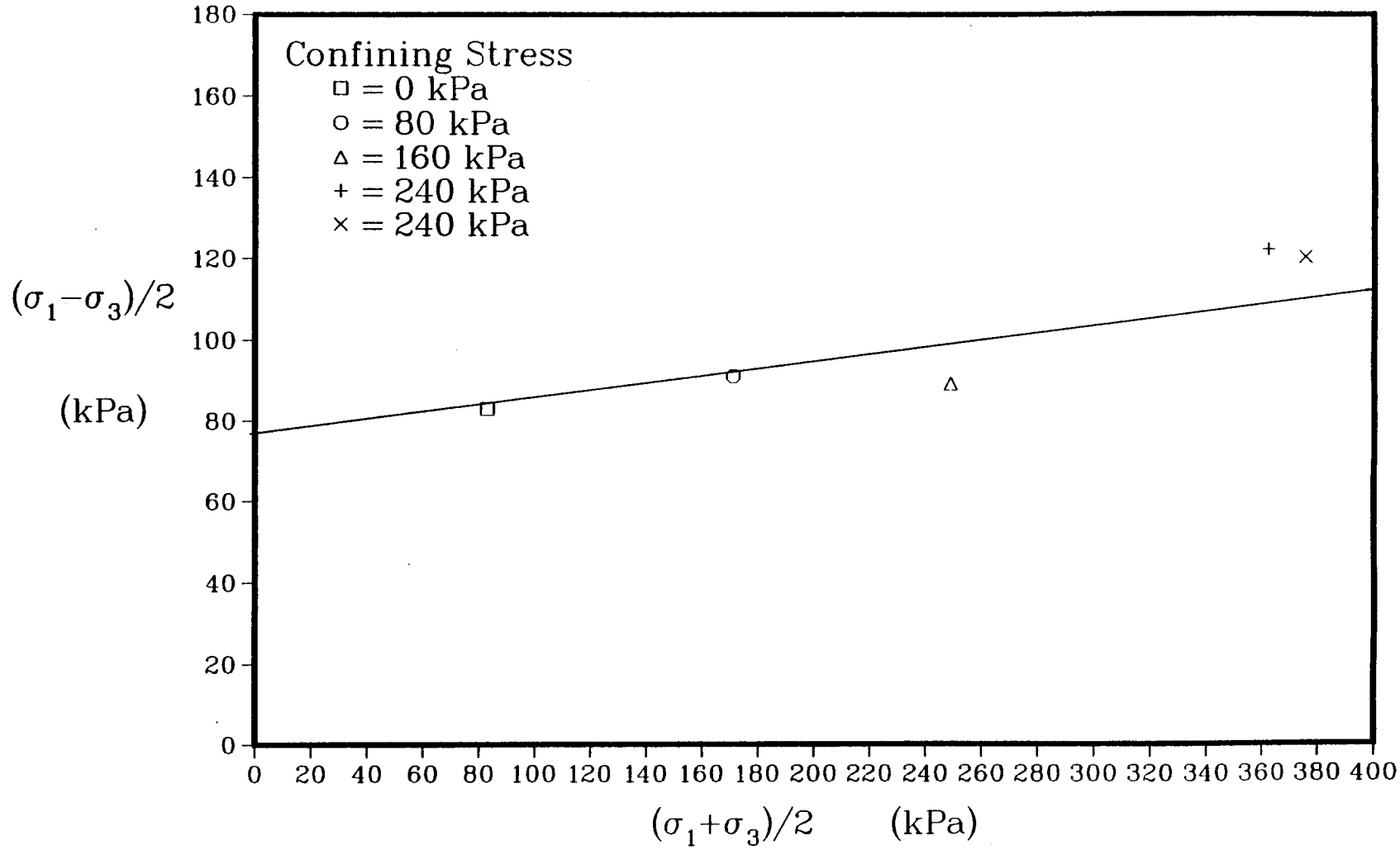

Figure 4.7: Total Stress P–Q Plot for Tube Fill Soil from UU Triaxial Tests (1.67m; 10m W CL)

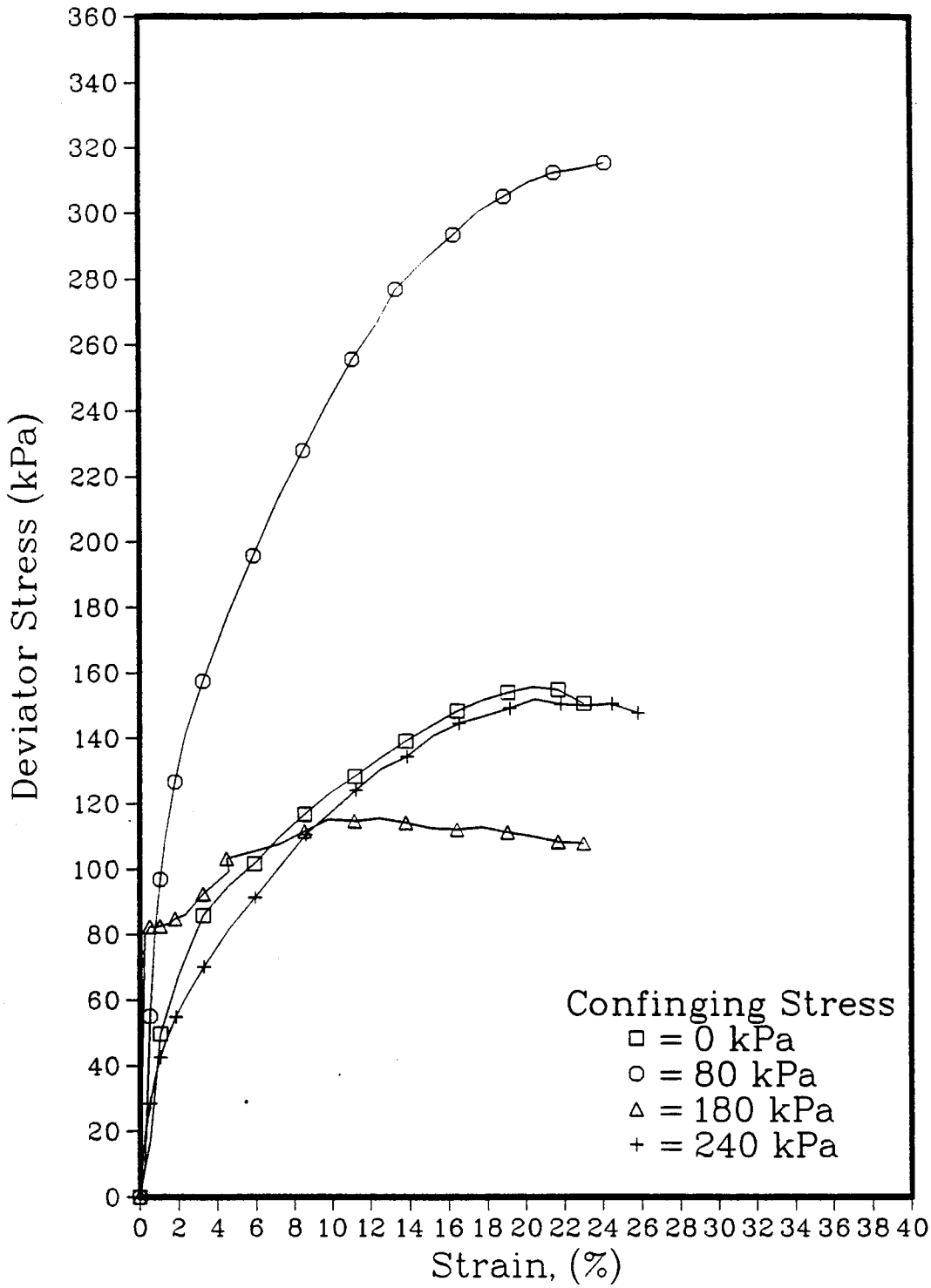

Figure 4.8: UU Triaxial Tests on Tube Fill Soil
(1.67m elevation, 12m E of CL)

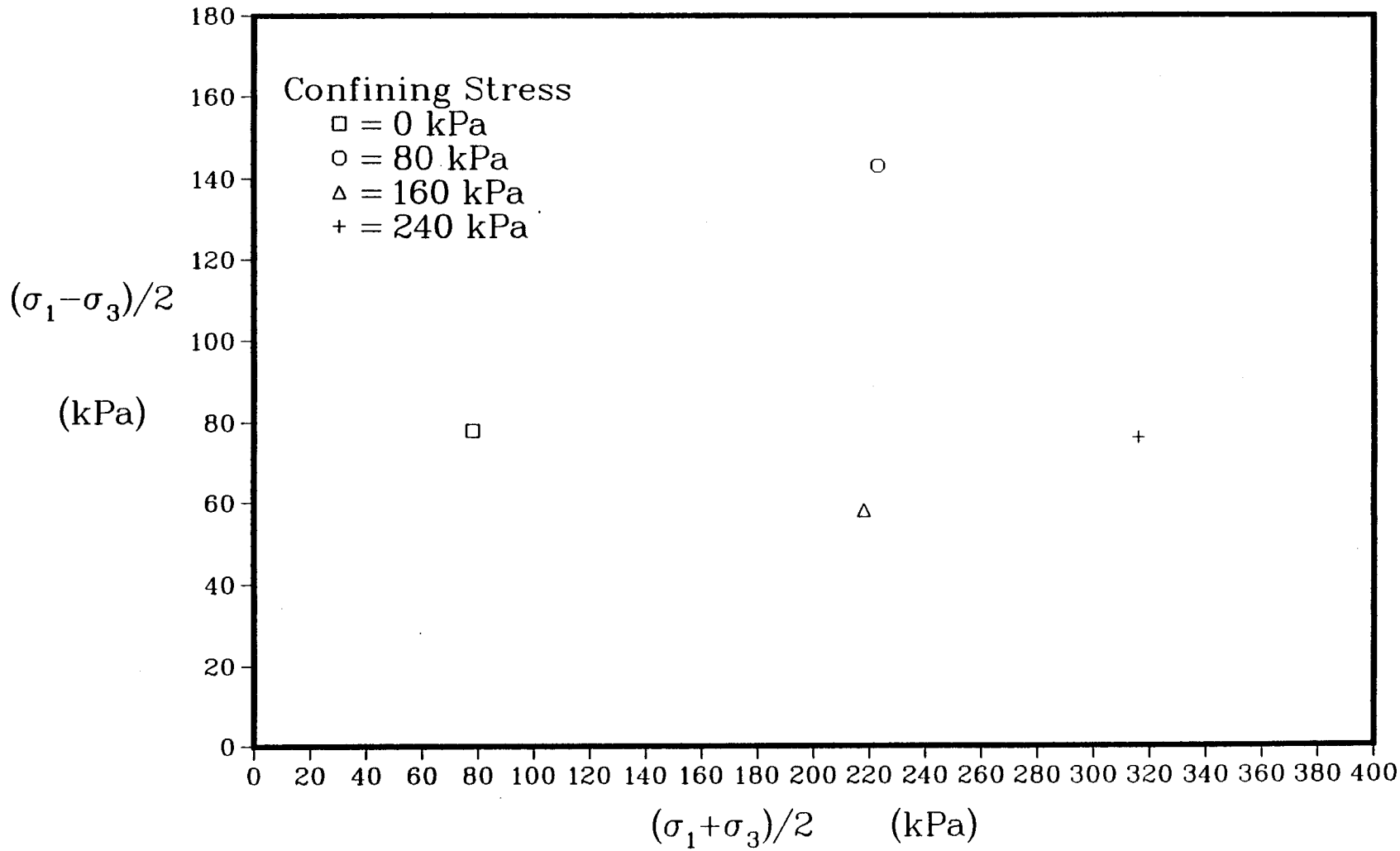

Figure 4.9: Total Stress P–Q Plot for Tube Fill Soil From UU Triaxial Tests (1.67m; 12m E CL)

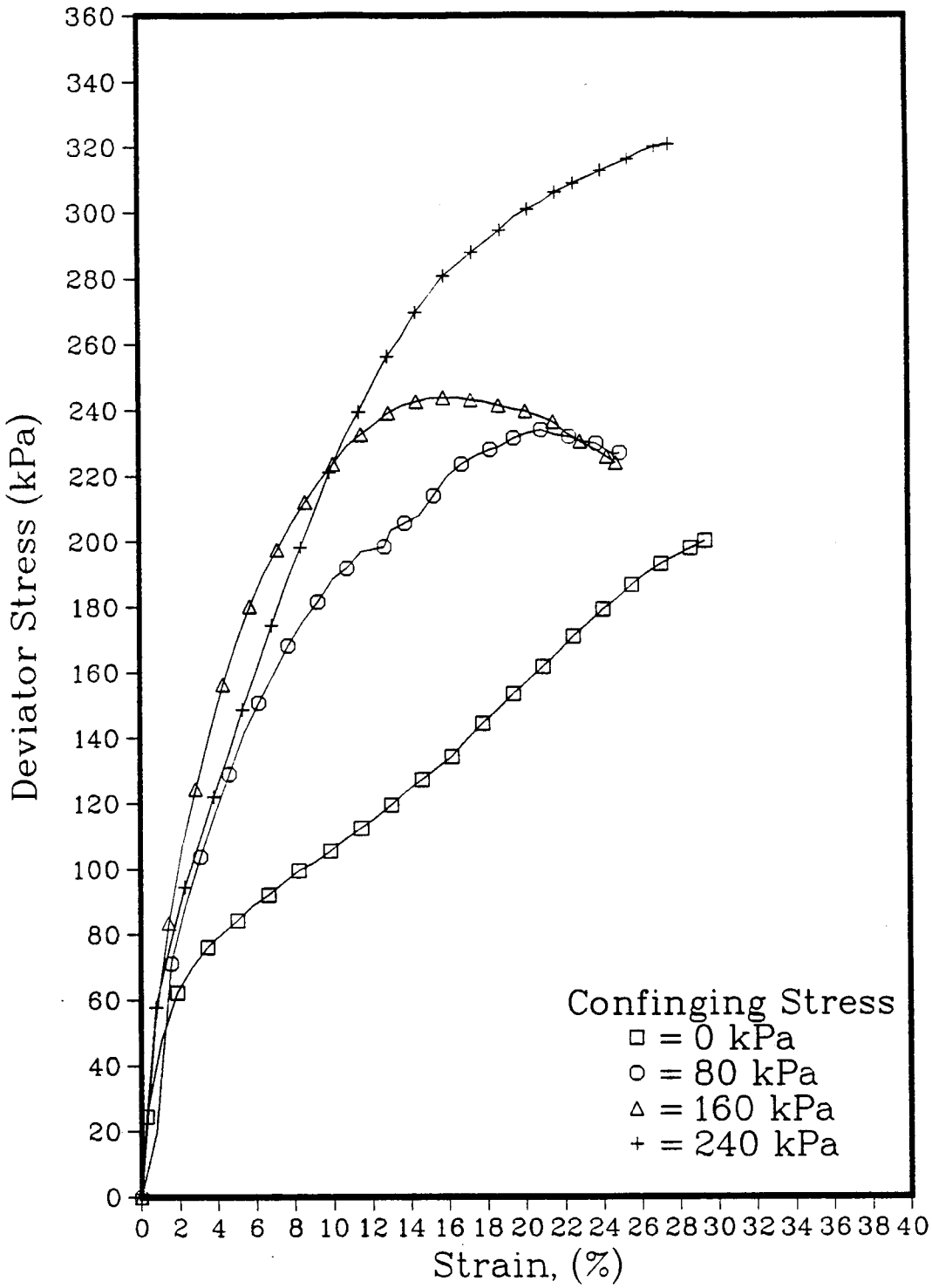

Figure 4.10: UU Triaxial Tests on Tube Fill Soil (2.33m elevation, 12m E of CL)

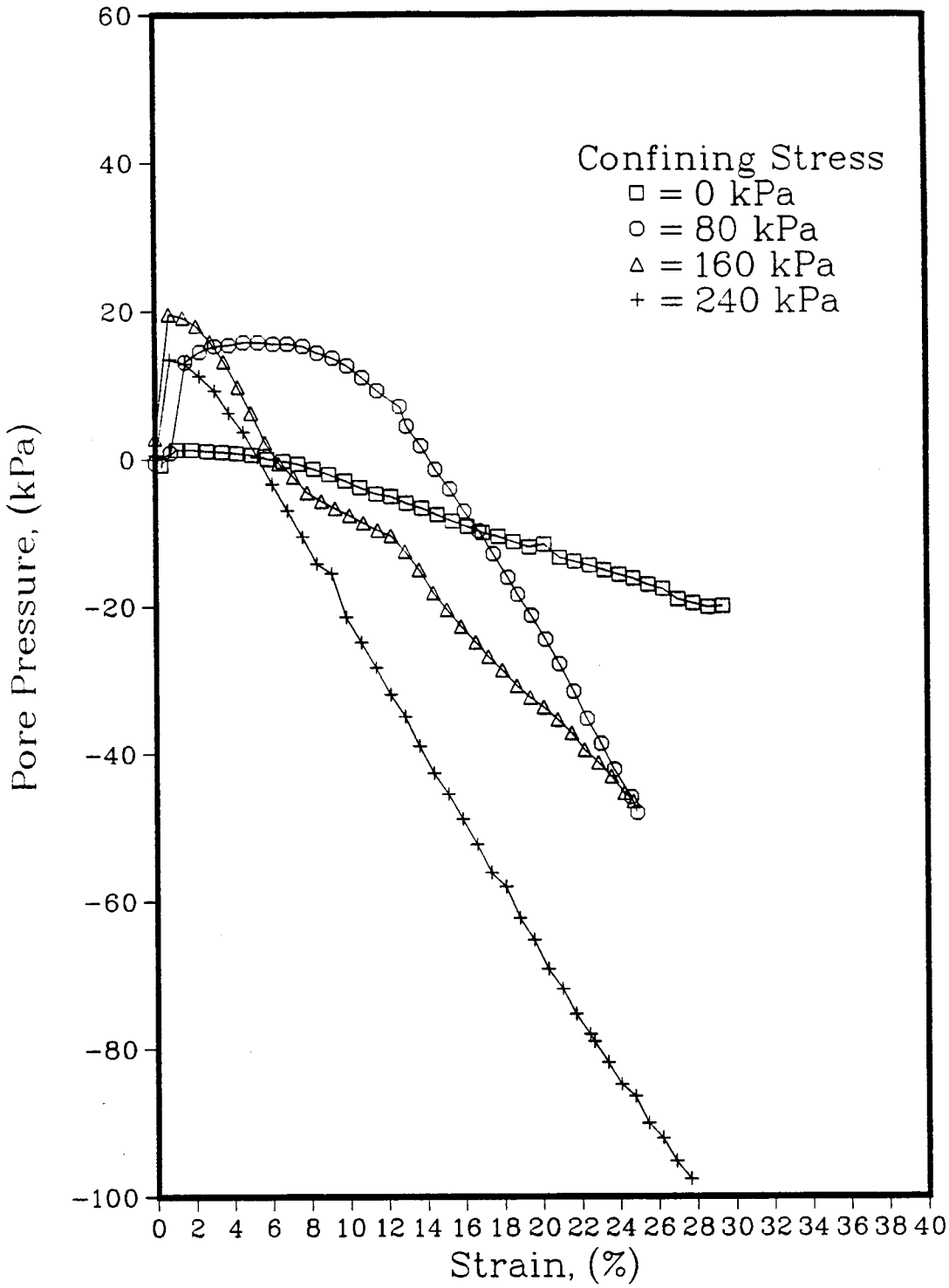

Figure 4.11: UU Triaxial Tests on Tube Fill Soil (2.33m elevation, 12m E of CL)

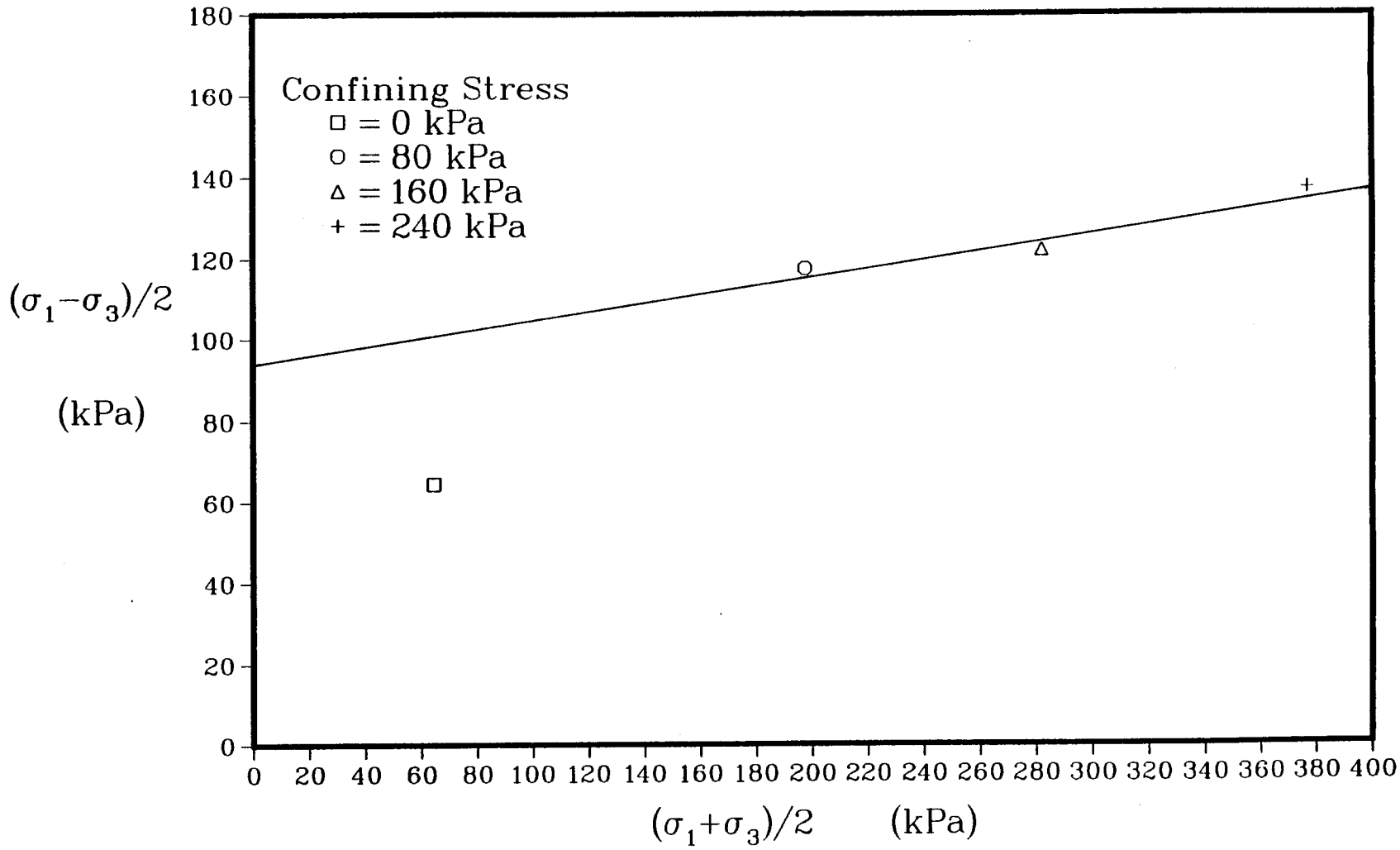

Figure 4.12: Total Stress P–Q Plot for Tube Fill Soil From UU Triaxial Tests (2.33m; 12m E CL)

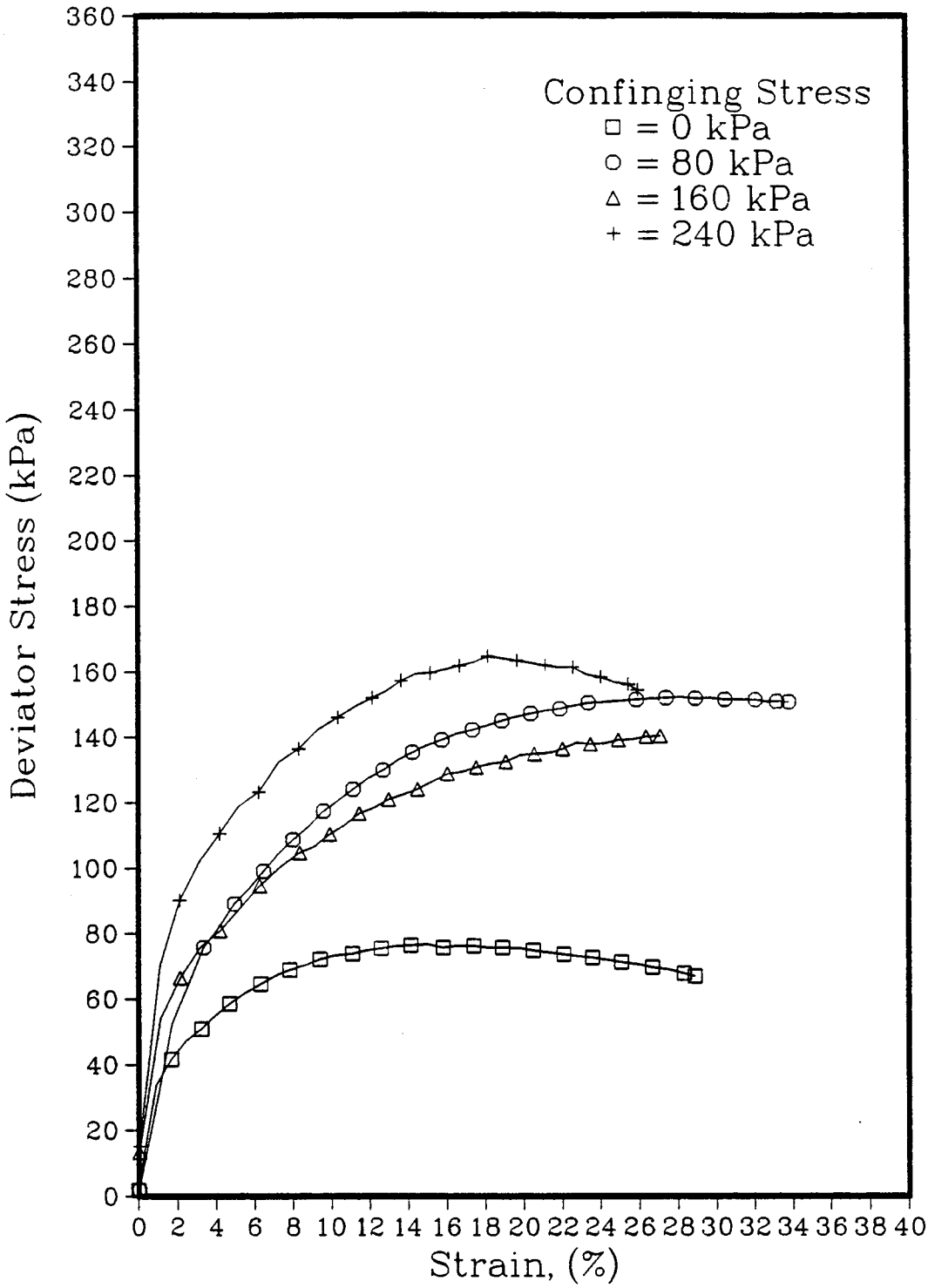

Figure 4.13: UU Triaxial Tests on Clay Fill Soil

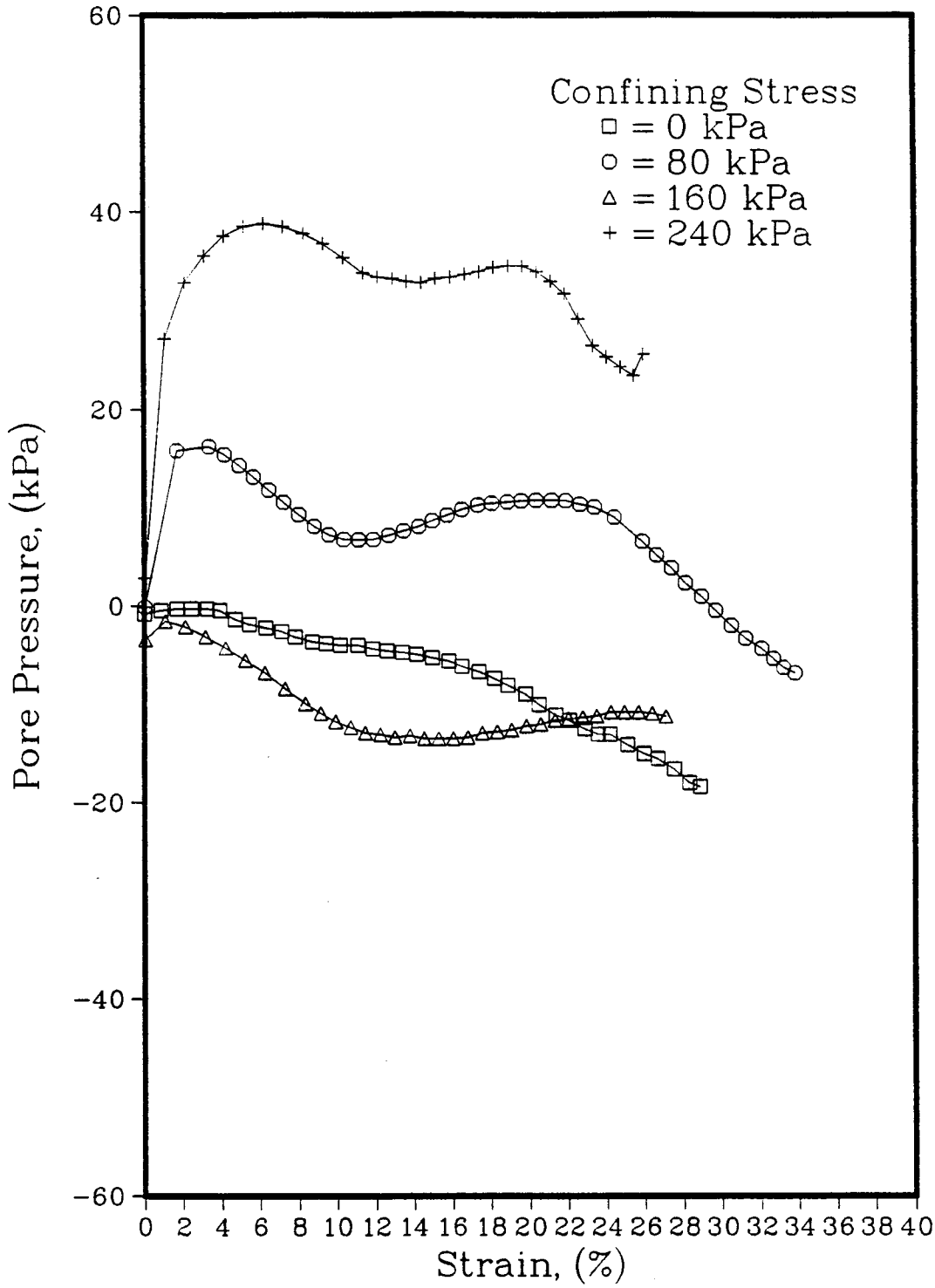

Figure 4.14: UU Triaxial Tests on Clay Fill Soil

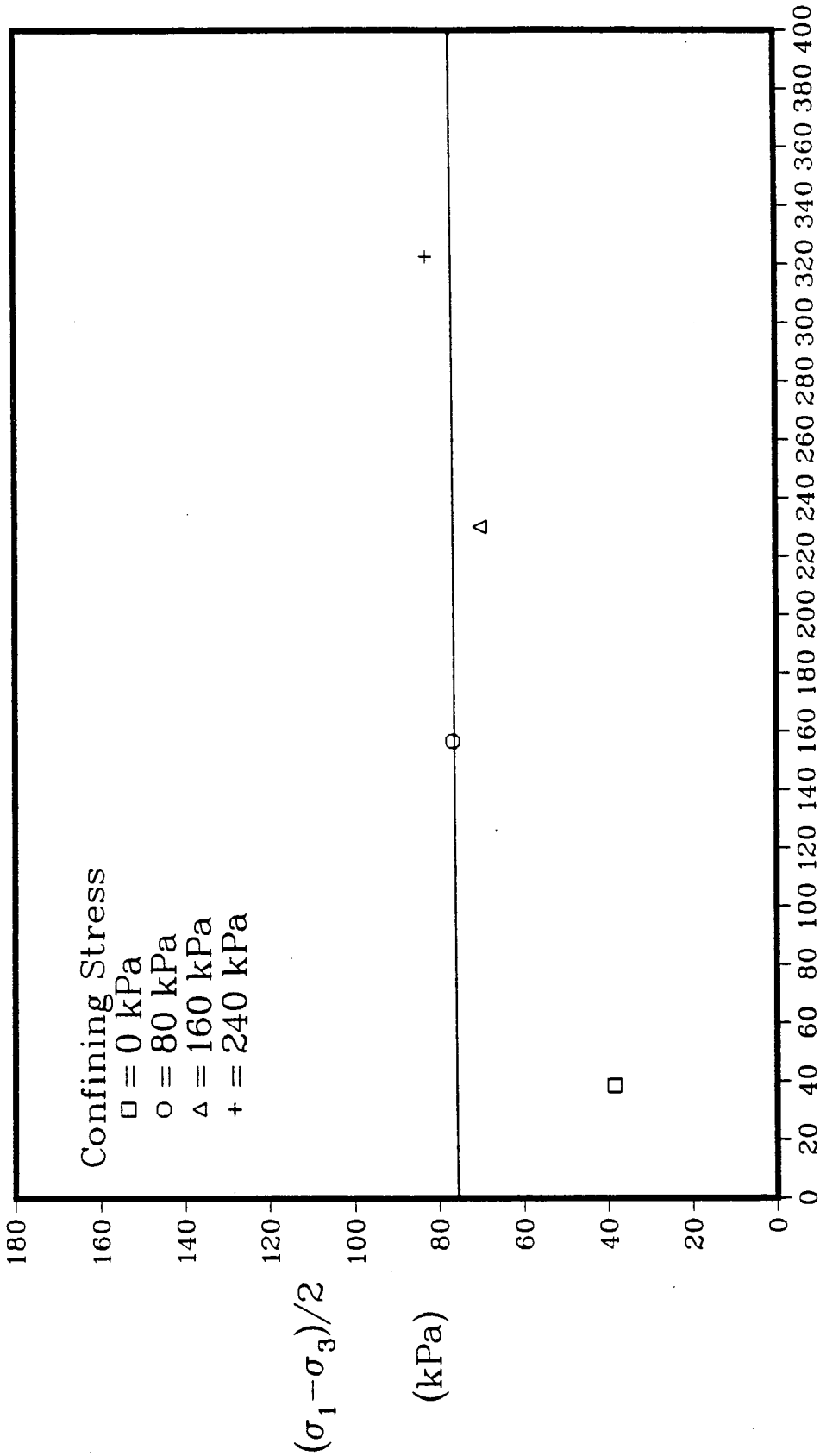

Figure 4.15: Total Stress P–Q Plot for Clay Fill Soil From UU Triaxial Tests

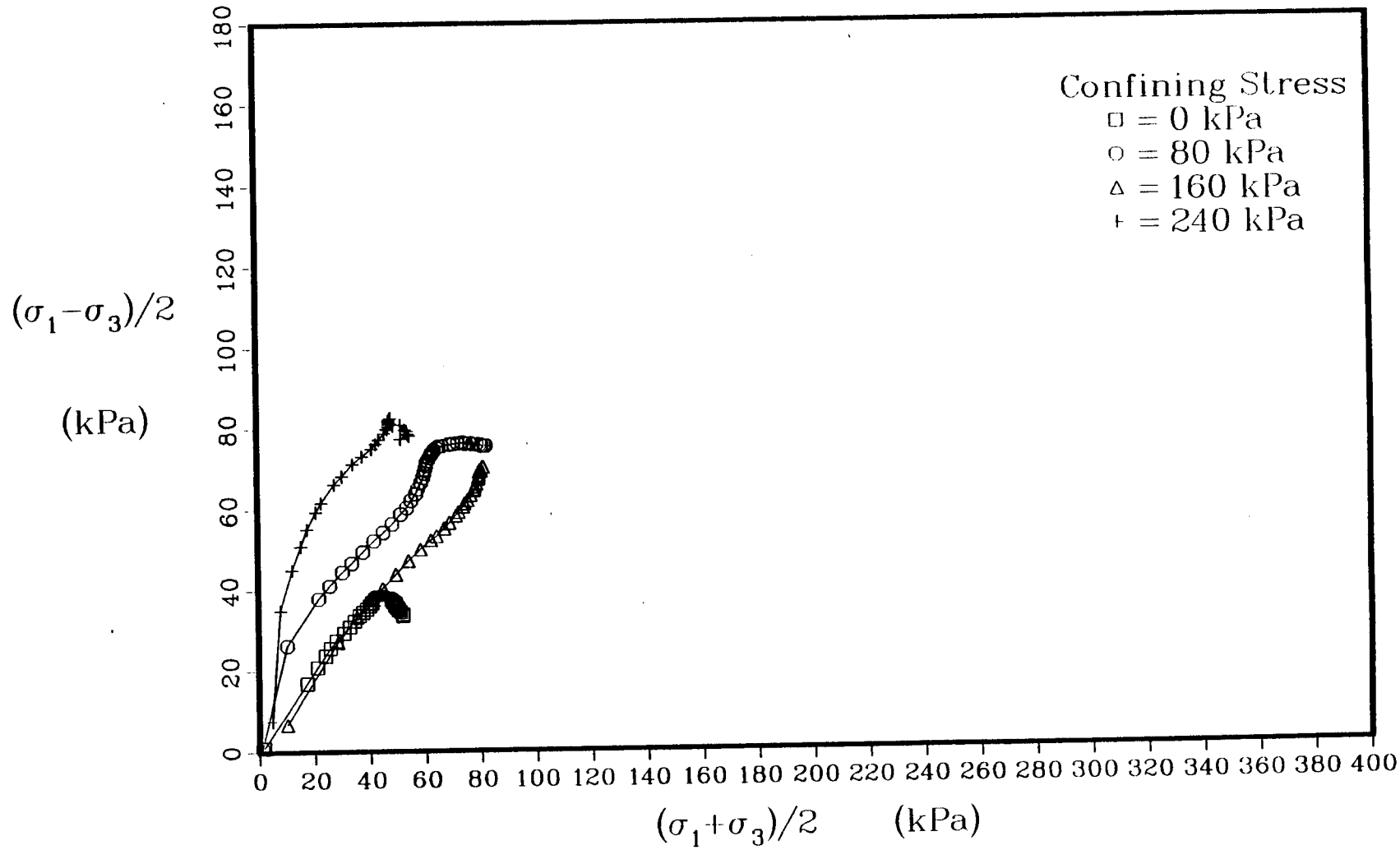

Figure 4.16: Effective Stress P–Q Plot for Clay Fill Soil From UU Triaxial Tests

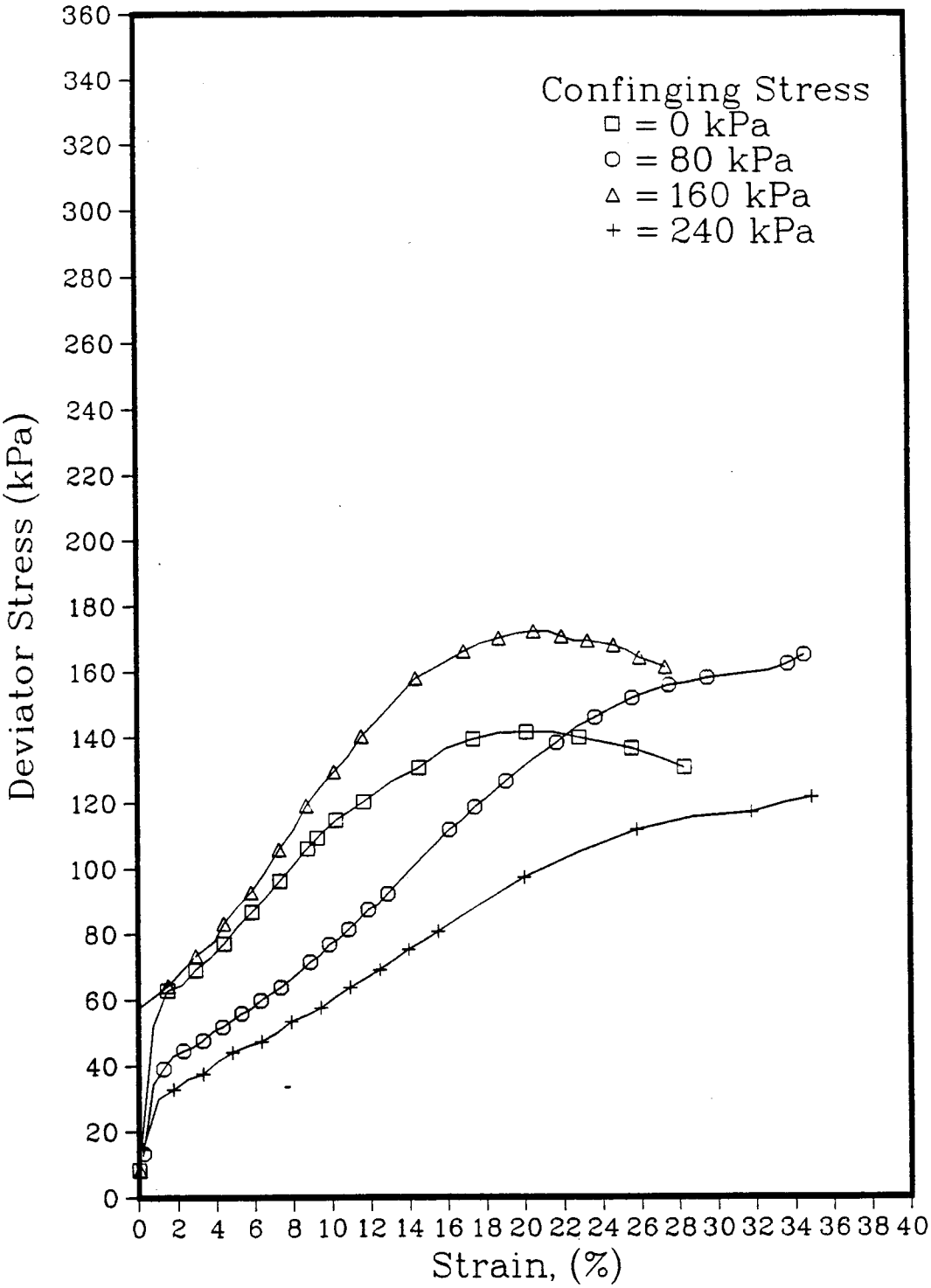

Figure 4.17: UU Triaxial Tests on Silt Fill Soil

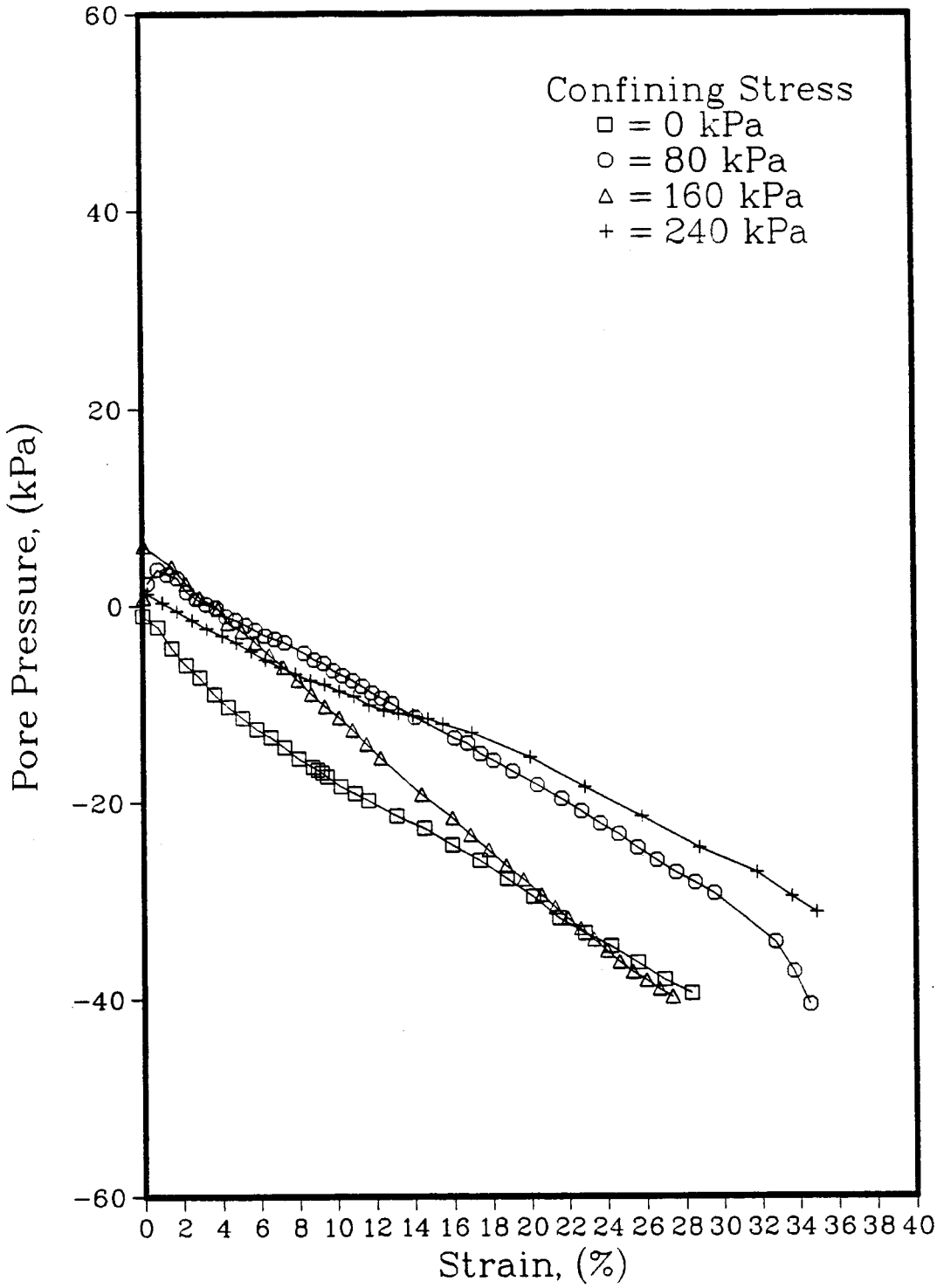

Figure 4.18: UU Triaxial Tests on Silt Fill Soil

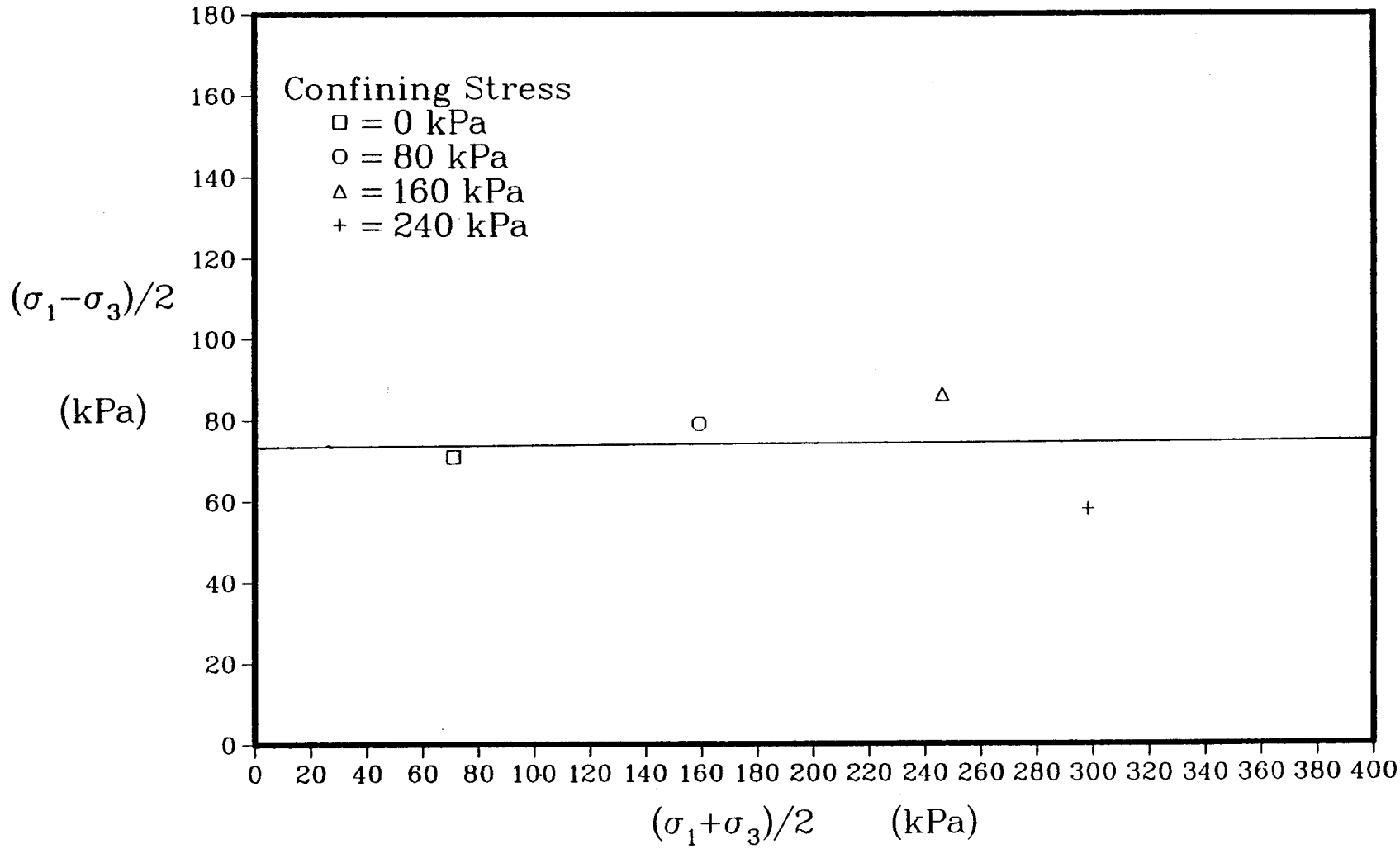

Figure 4.19: Total Stress P–Q Plot for Silt Fill Soil From UU Triaxial Tests

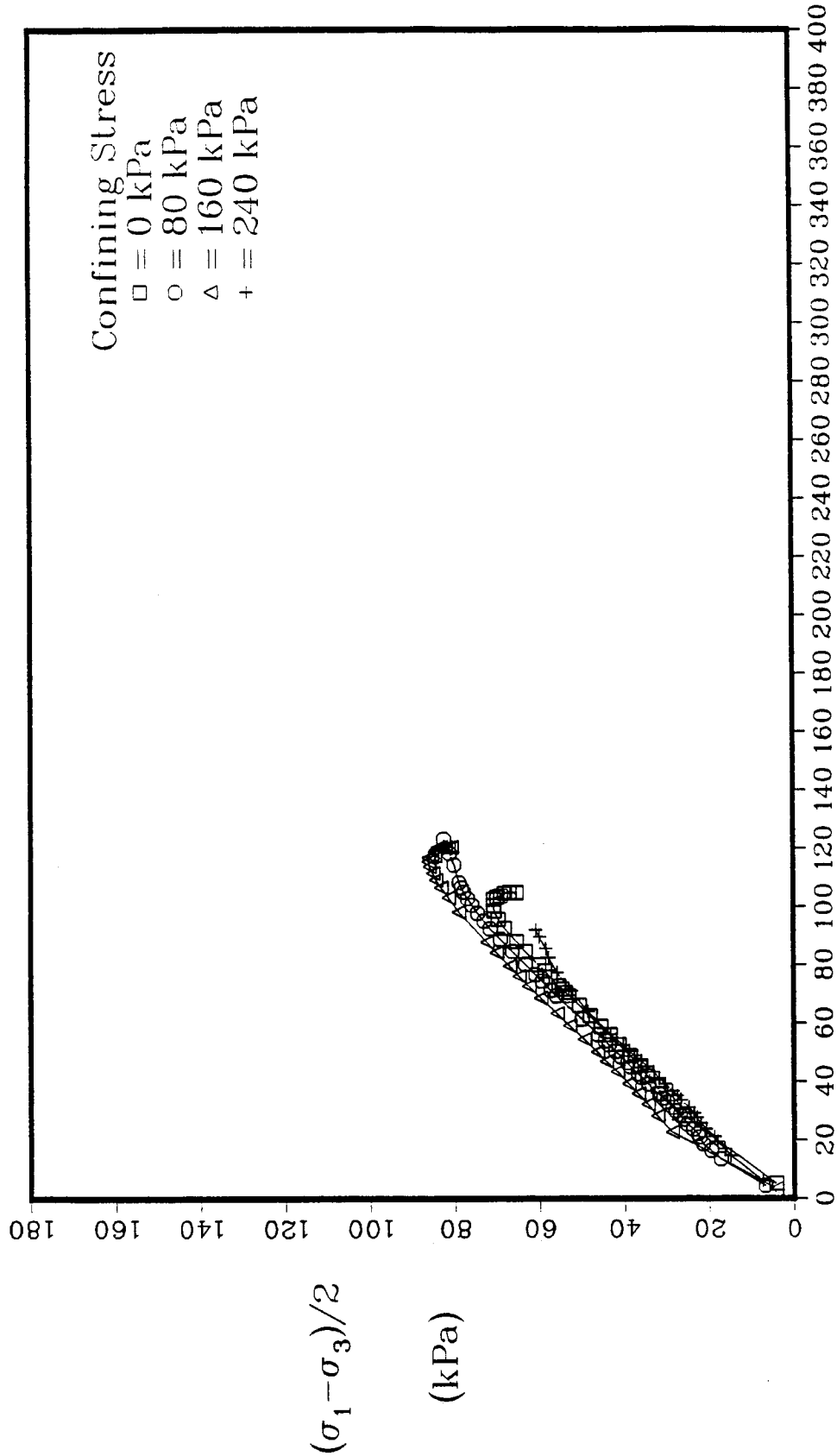

Figure 4.20: Effective Stress P–Q Plot for Silt Fill Soil From UU Triaxial Tests

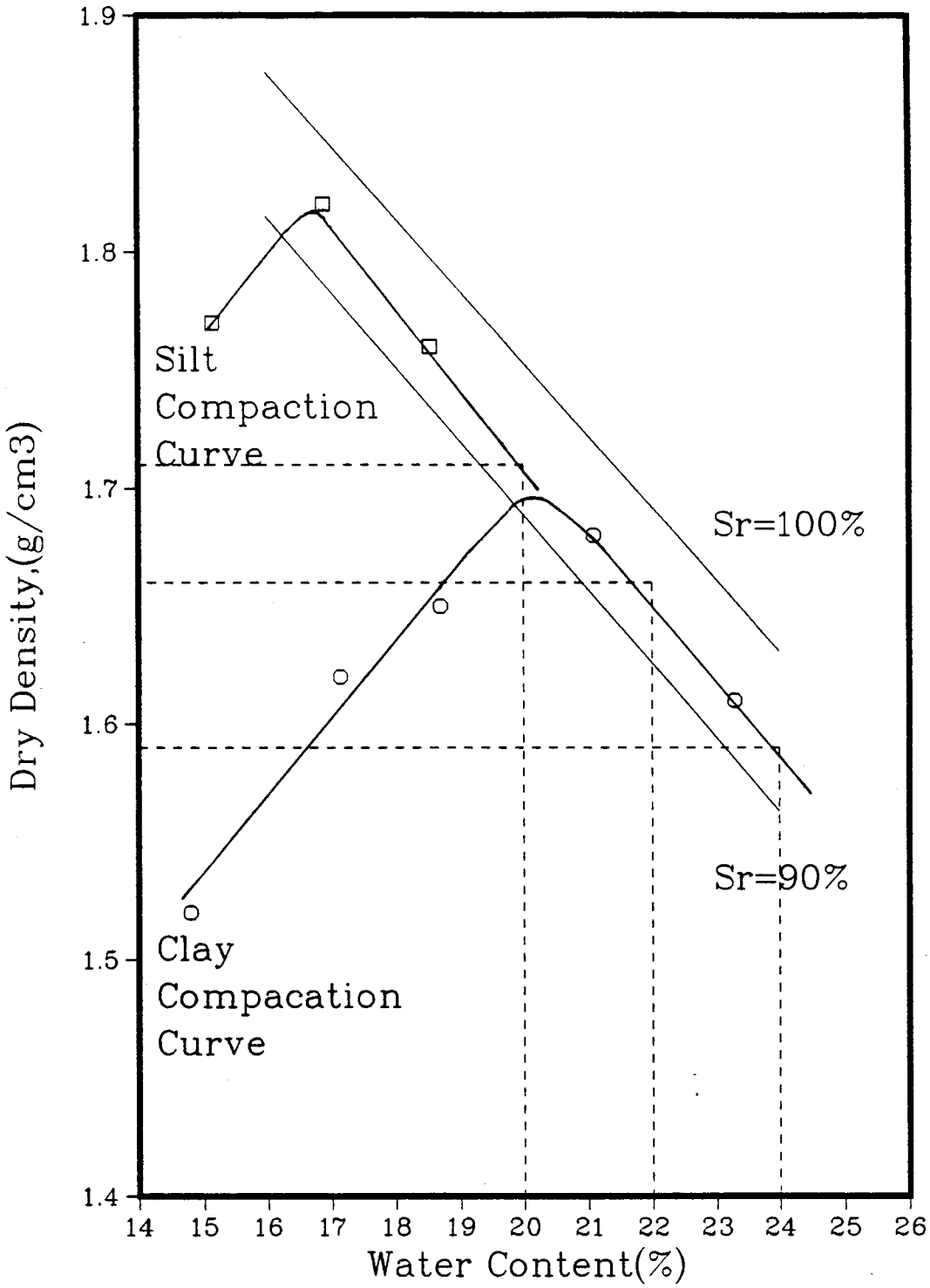

Figure 4.21: Compaction Curves for Fill Soils

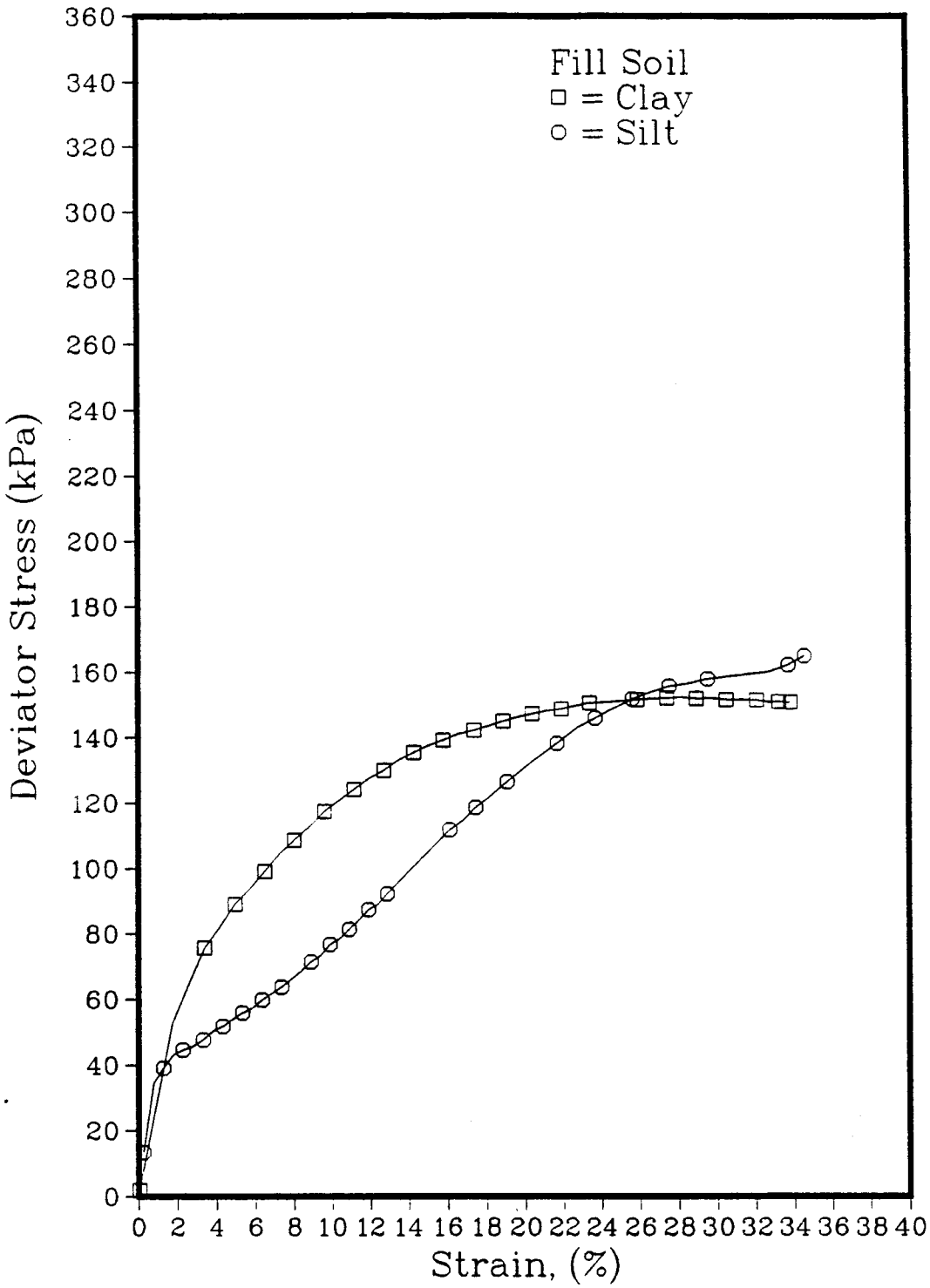

Figure 4.22: Comparison of UU Test Results for Silt & Clay Fill Soils Confined Under 80 kPa

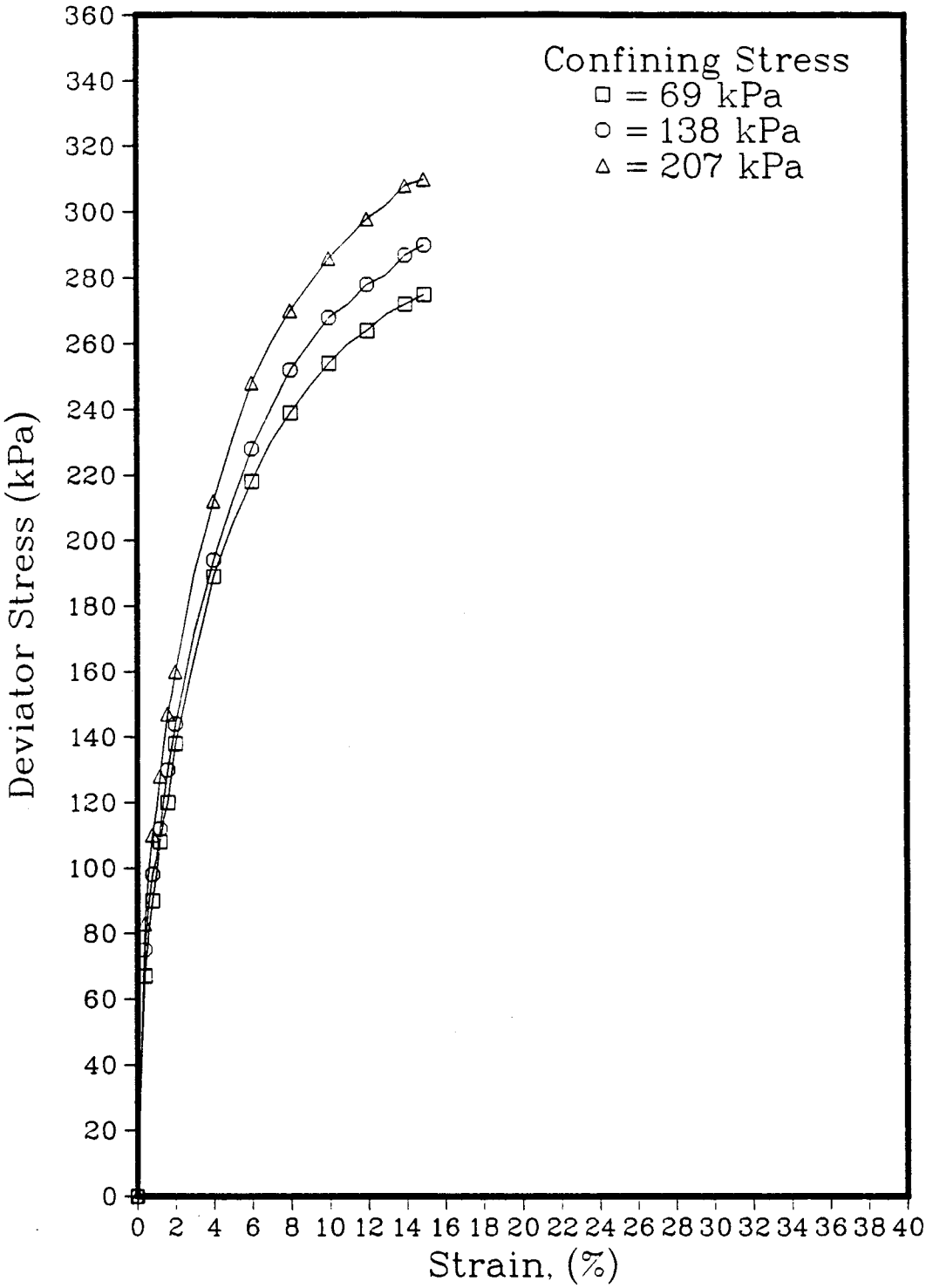

Figure 4.23: UU Triaxial Tests on Sandy Clay Fill Soil

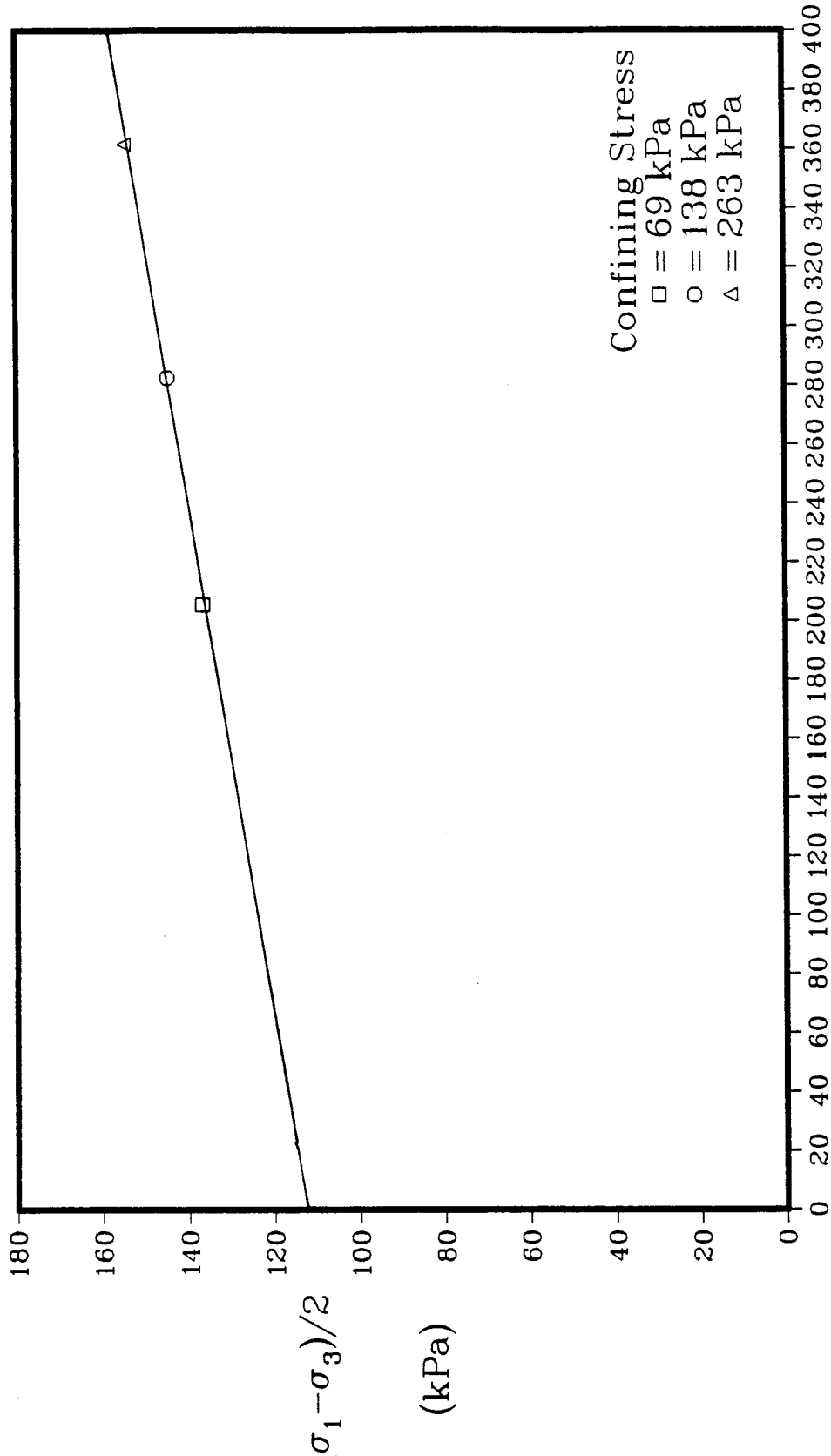

Figure 4.24: Total Stress P–Q Plot for Sandy CLay Fill Soil from UU Triaxial Tests

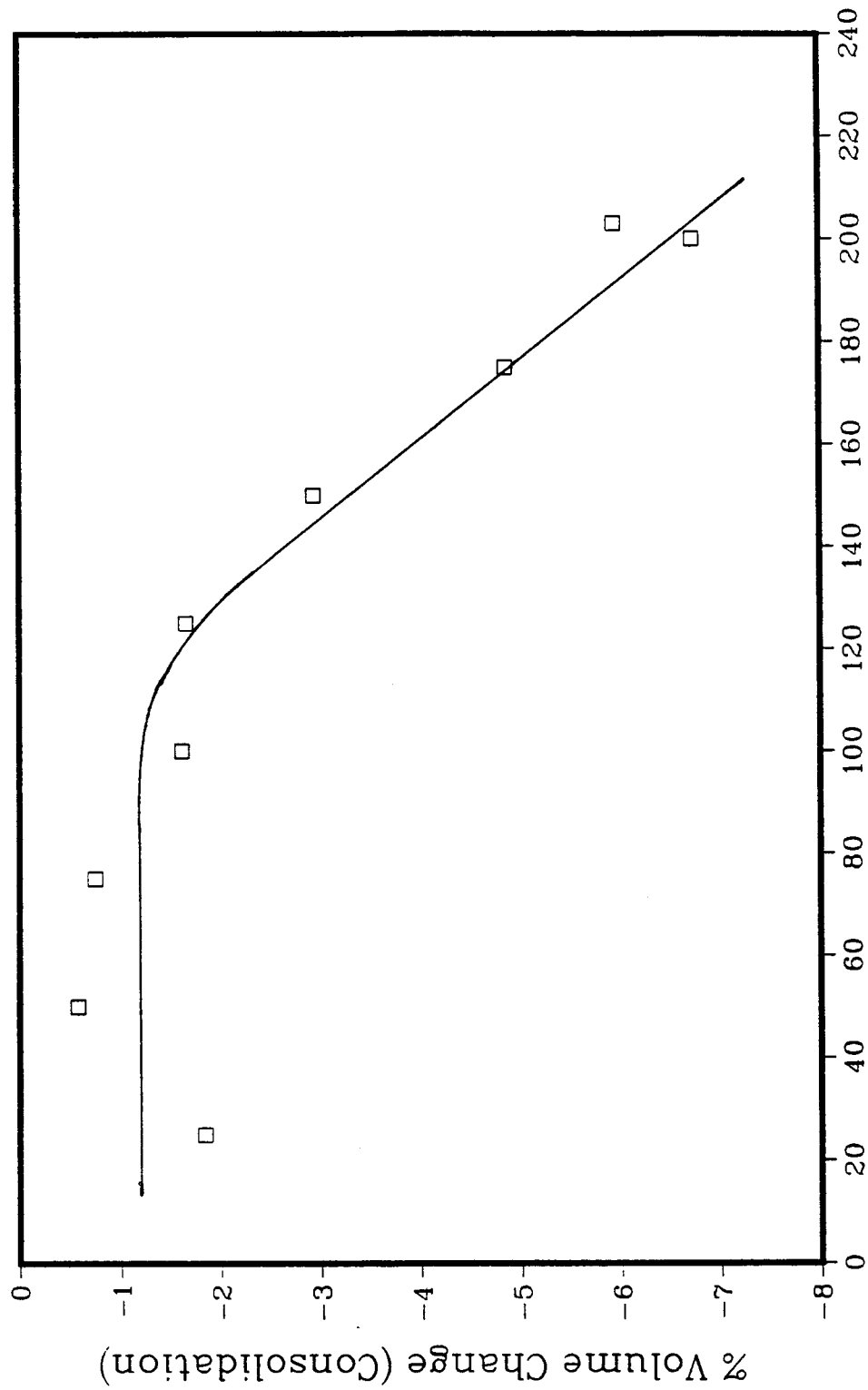

Figure 4.25: Volume Change During Consolidation of Clay Fill

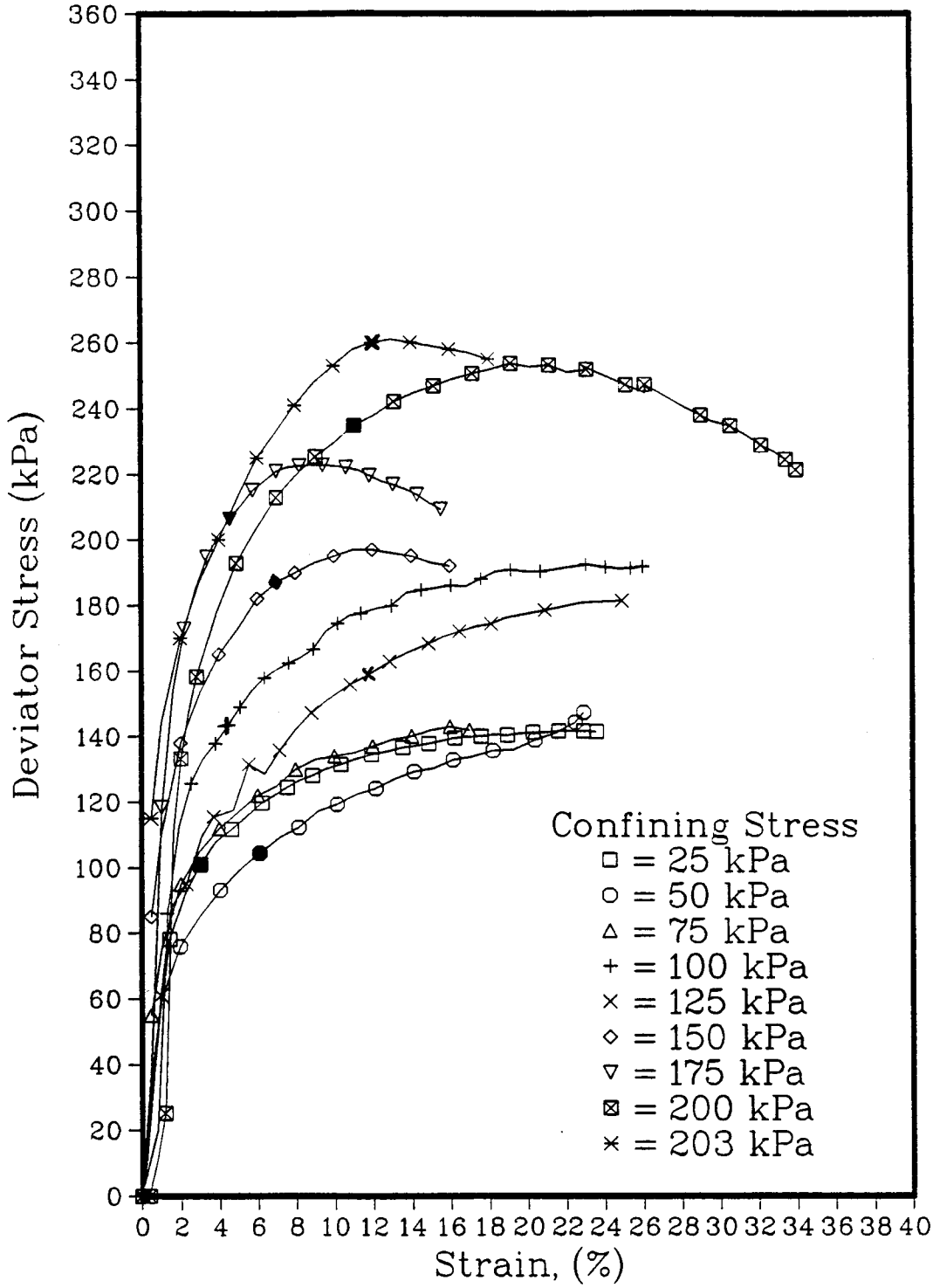

Figure 4.26: CU Triaxial Tests on Clay Fill Soil

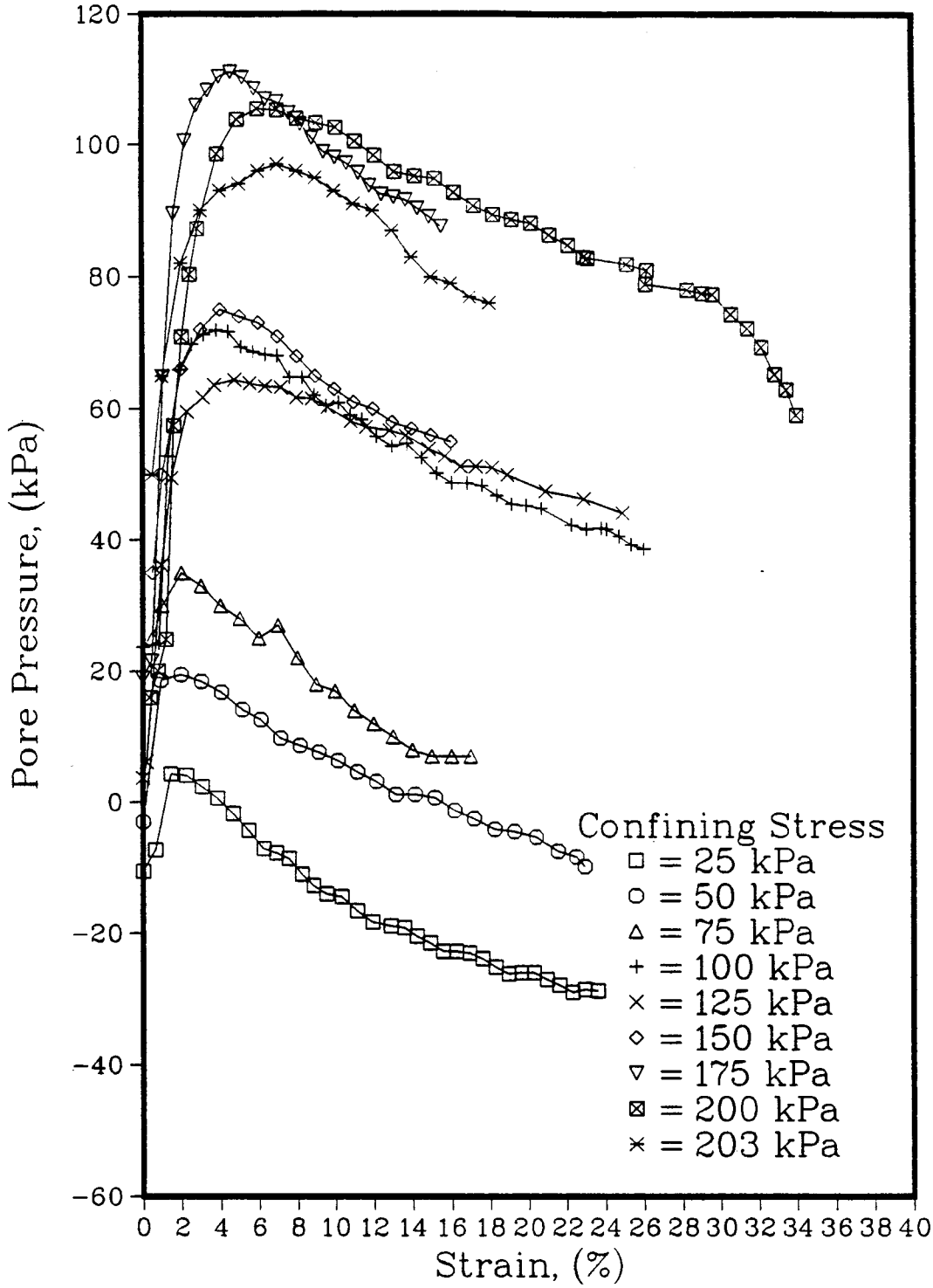

Figure 4.27: CU Triaxial Tests on Clay Fill Soil

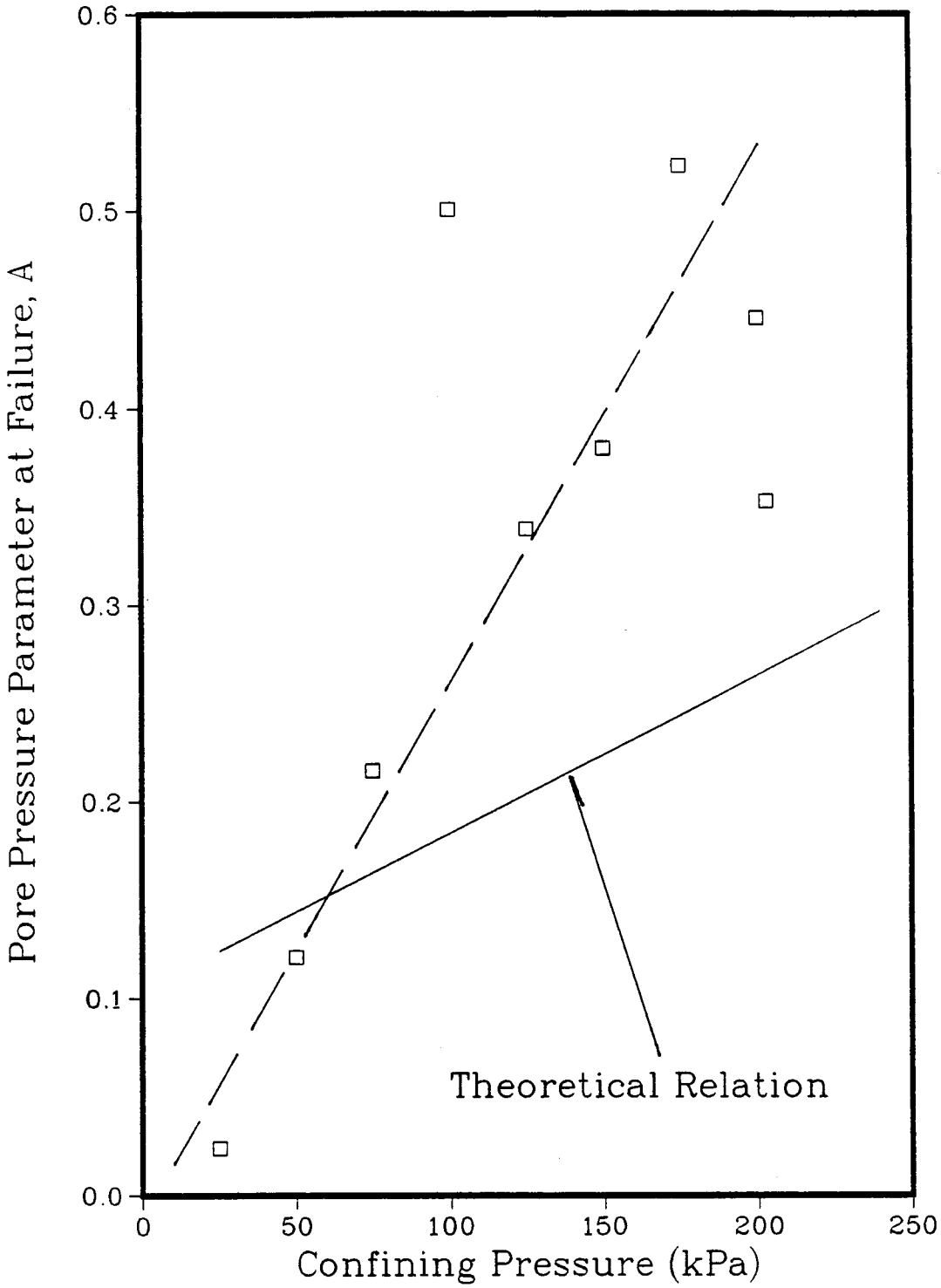

Figure 4.28: Calculated and Measured Values of A_f from CU Tests Conducted on Clay Fill

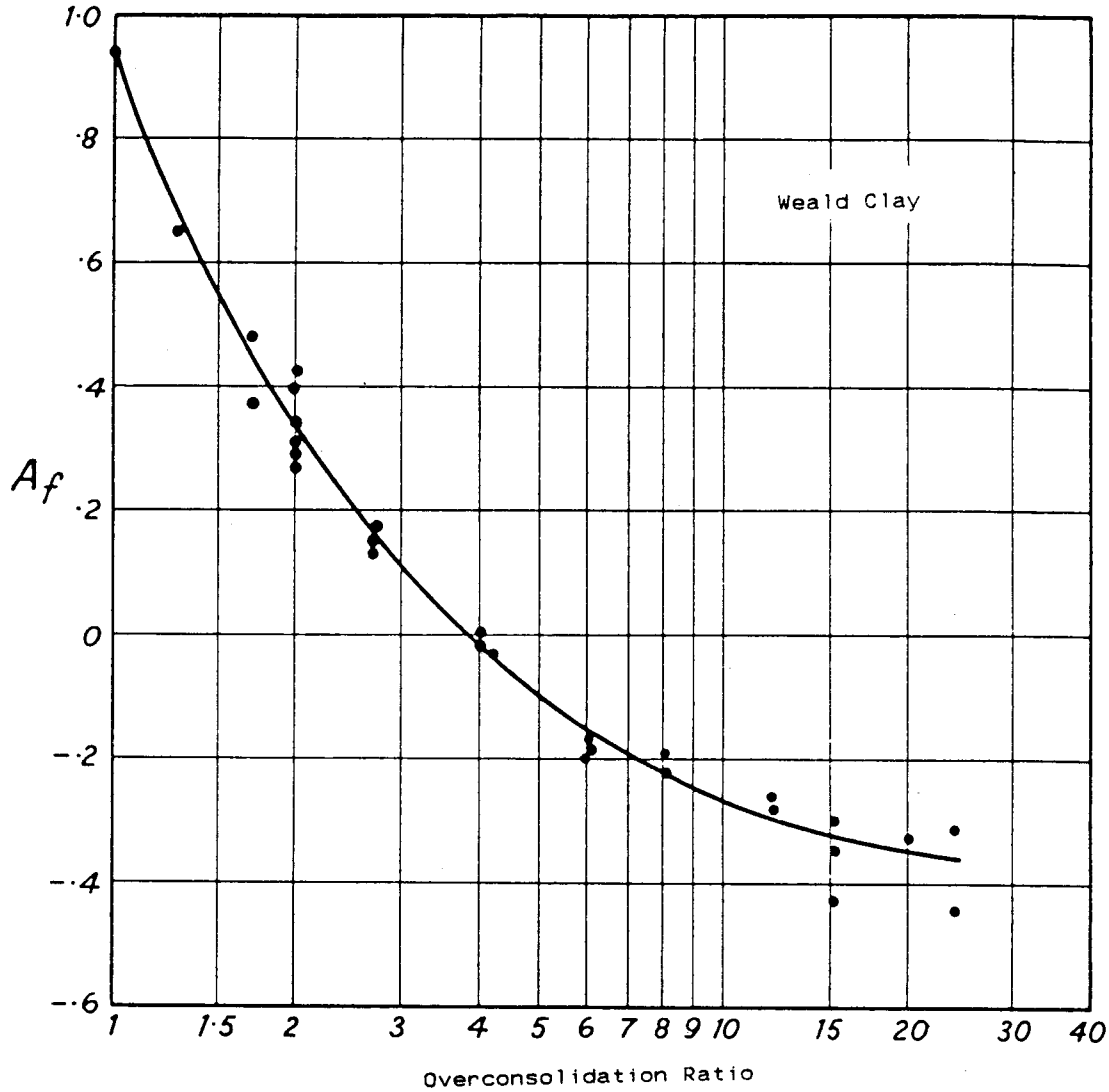

Figure 4.29 Variation of Skemptons Pore Pressure Parameters at Failure, A_f, with the OCR (Modified from Bishop and Henkle, 1962)

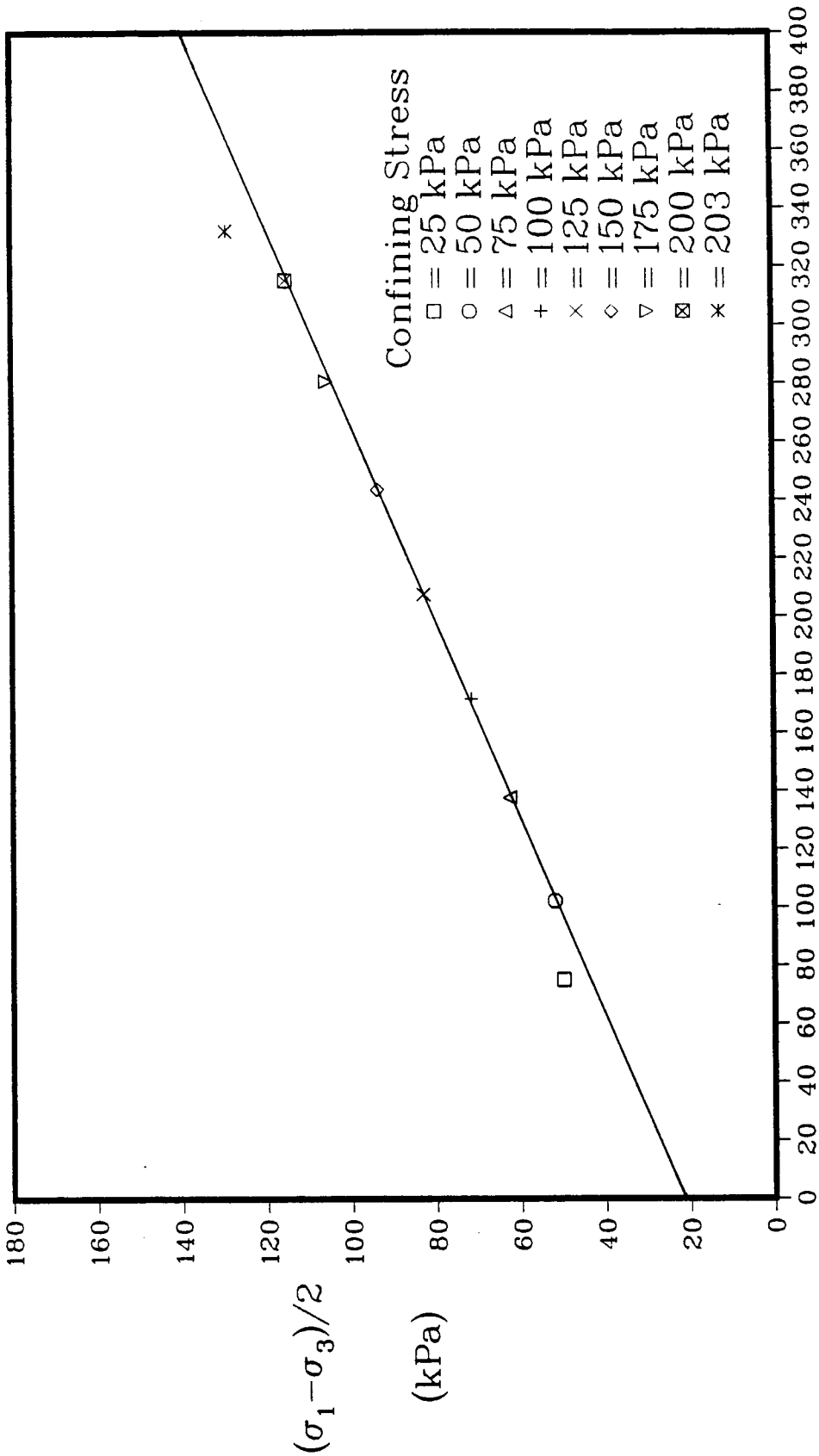

Figure 4.30: Total Stress P–Q Plot for Clay Fill Soil from CU Triaxial Tests

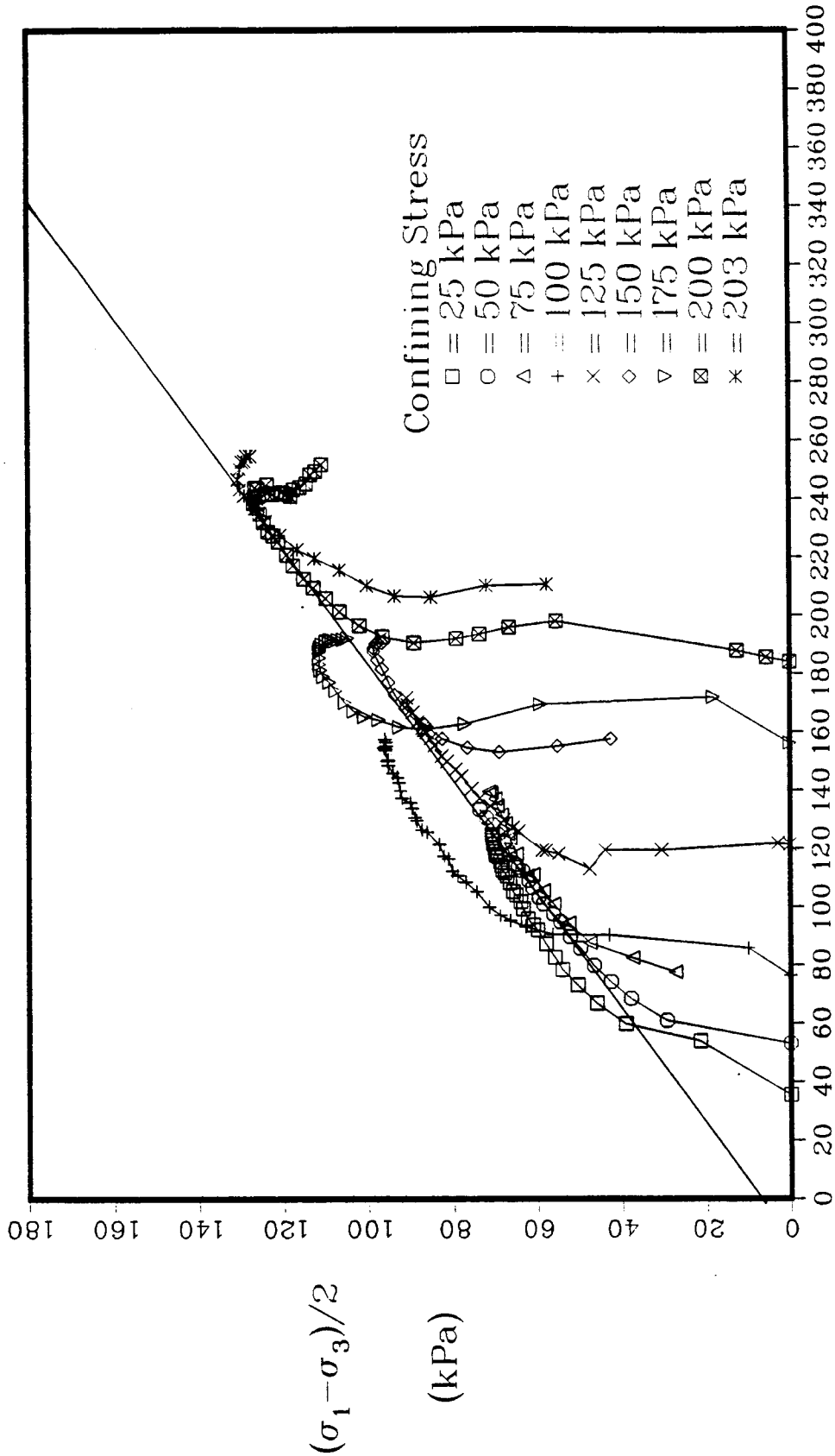

Figure 4.31: Effective Stress P–Q Plot for Clay Fill Soil

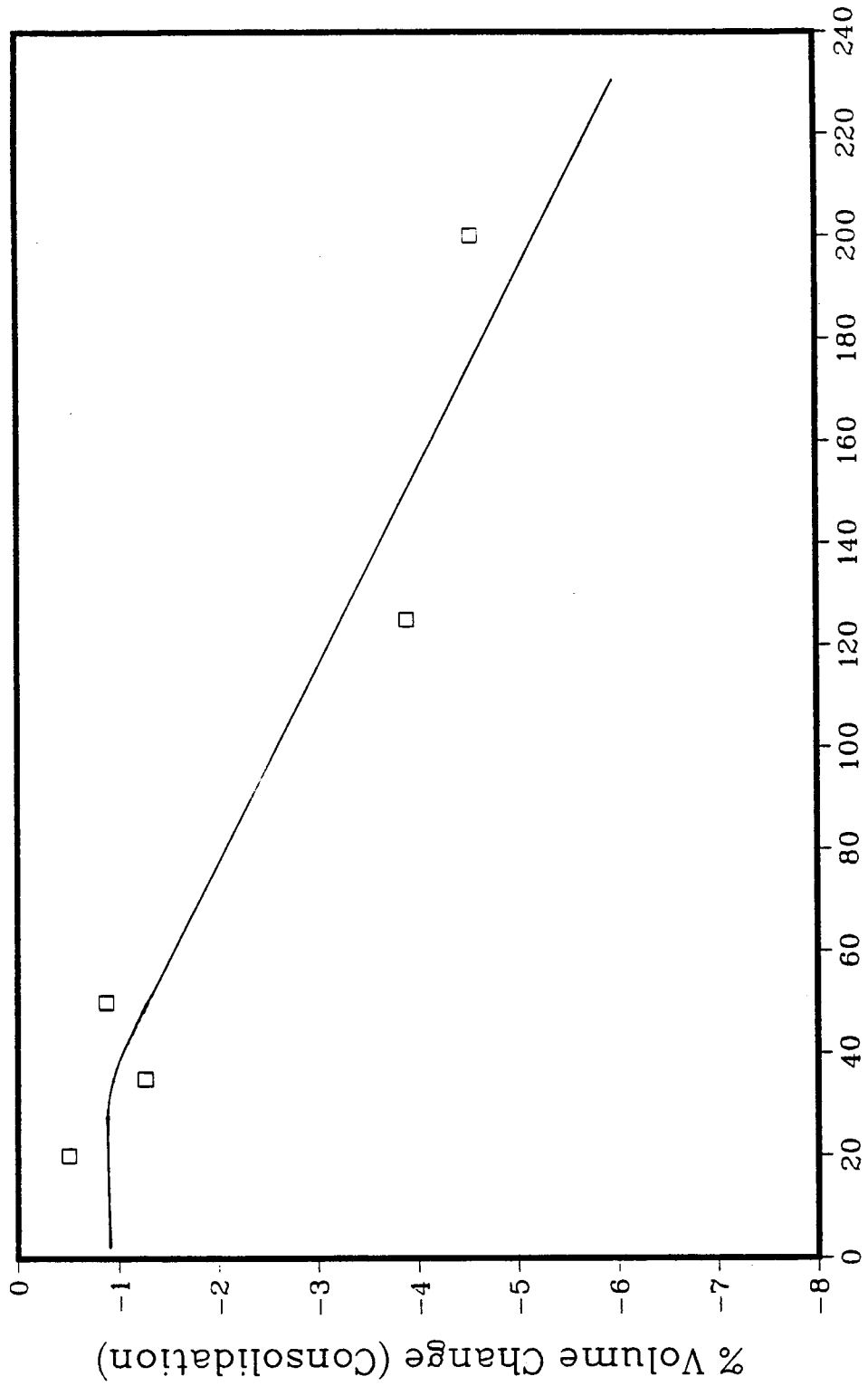

Figure 4.32: Volume Change During Consolidation of Silt Fill

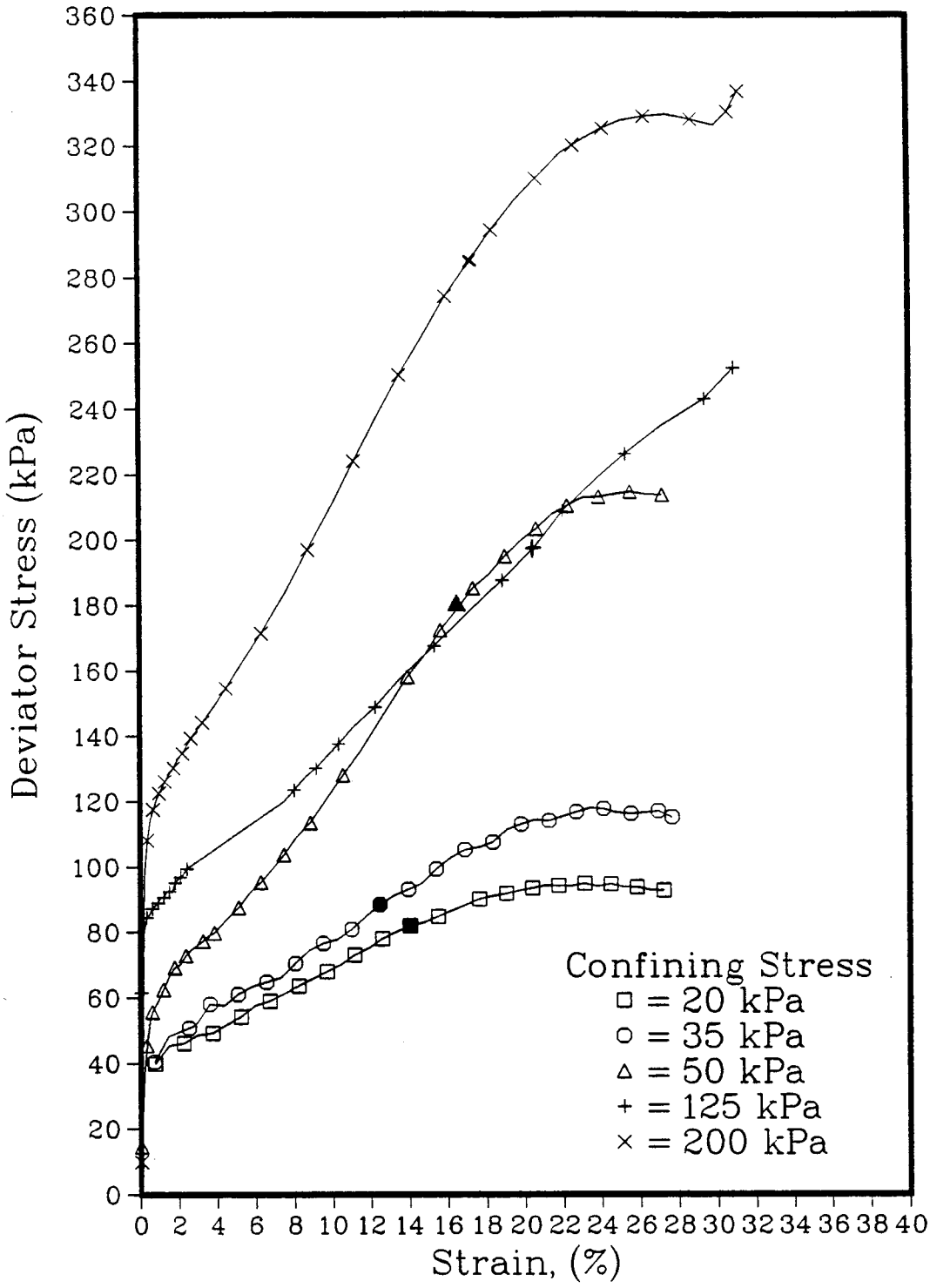

Figure 4.33: CU Triaxial Tests on Silt Fill Soil

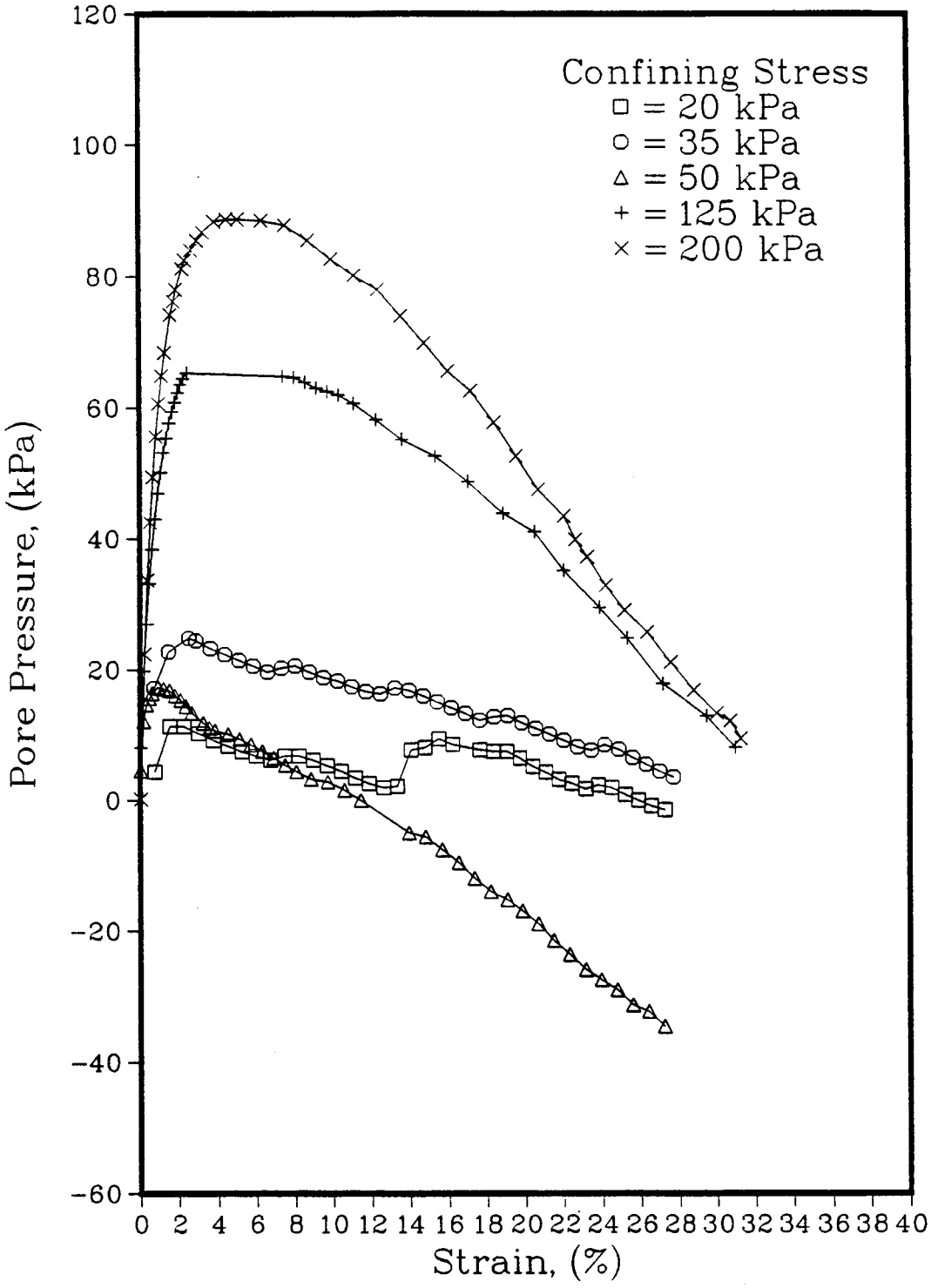

Figure 4.34: CU Triaxial Tests on Silt Fill Soil

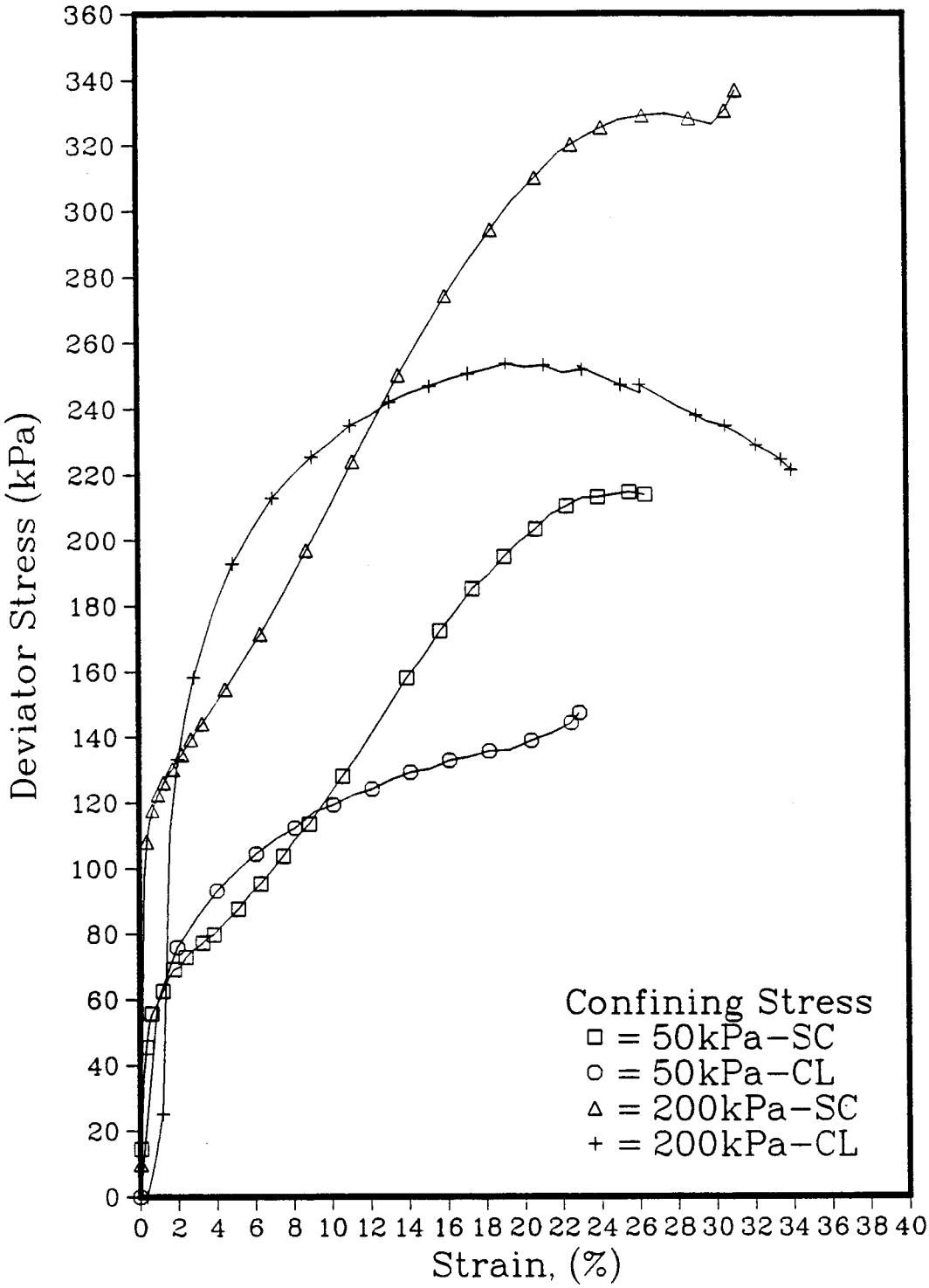

Figure 4.35: Stress–Strain Curves for Clay & Silt Specimens from CU Triaxial Tests

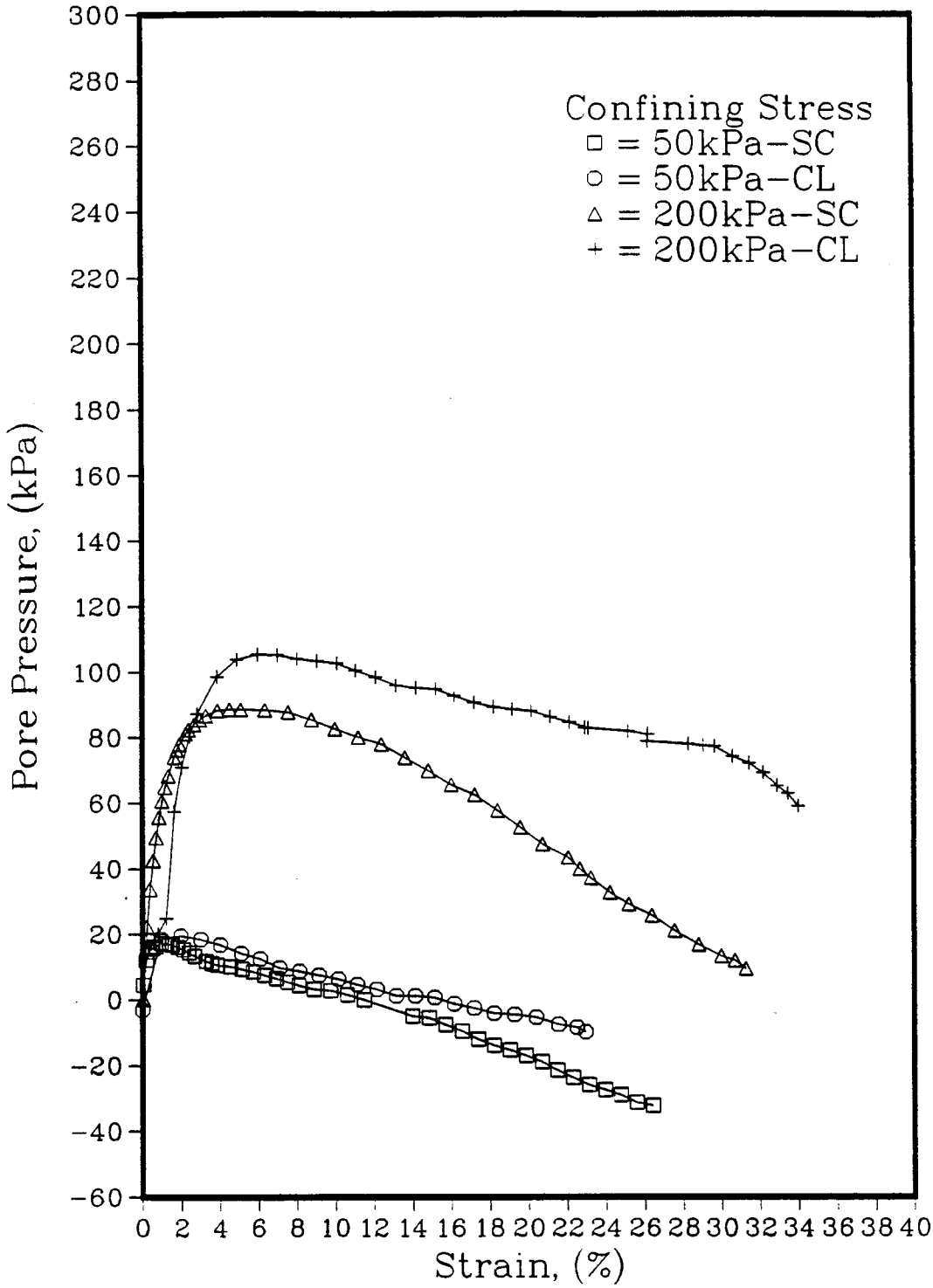

Figure 4.36: Pore Pressure–Strain Curves for Clay & Silt Specimens from CU Triaxial Tests

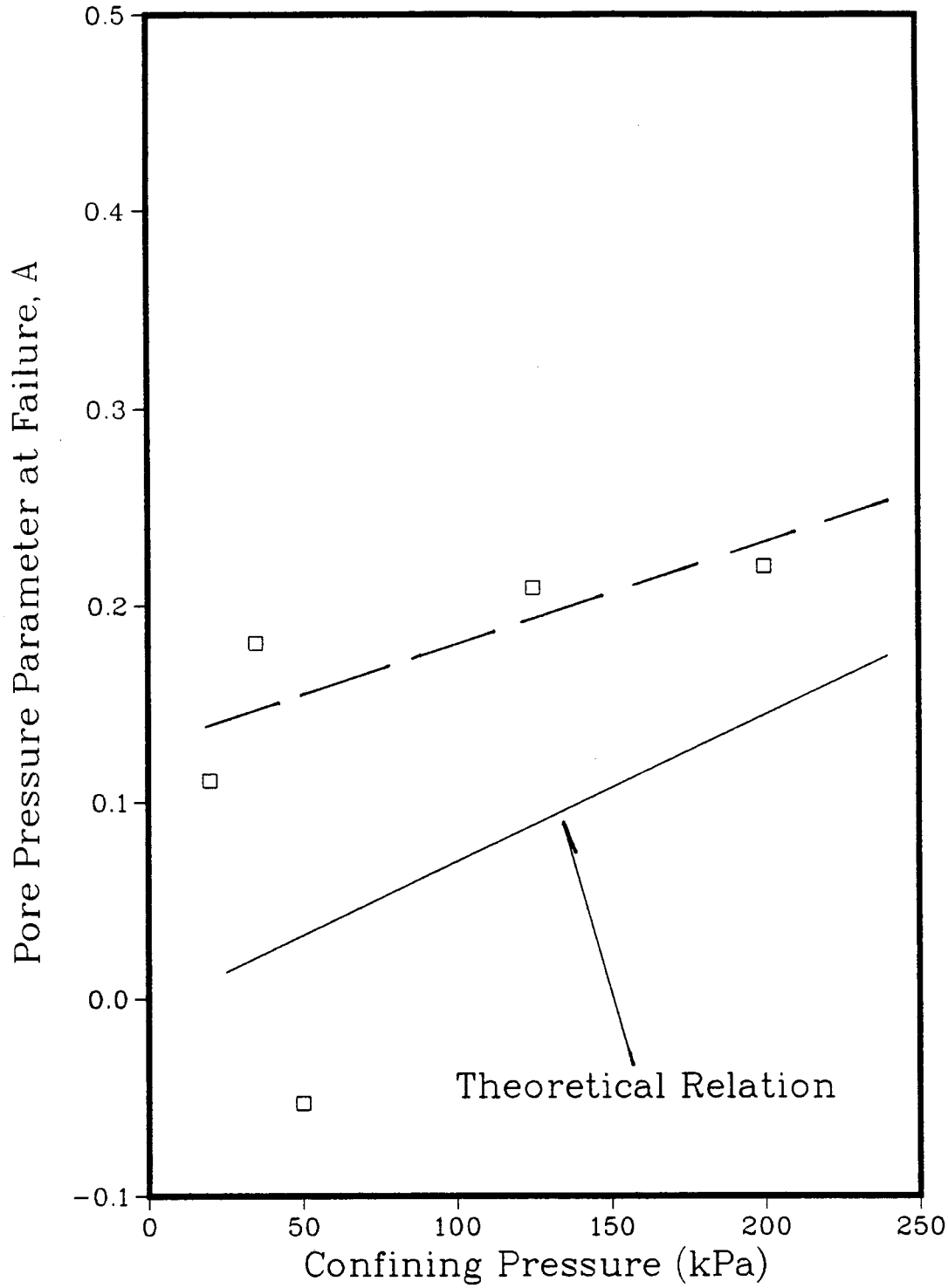

Figure 4.37: Calculated and Measured Values of A_f from CU Tests Conducted on Silt Fill

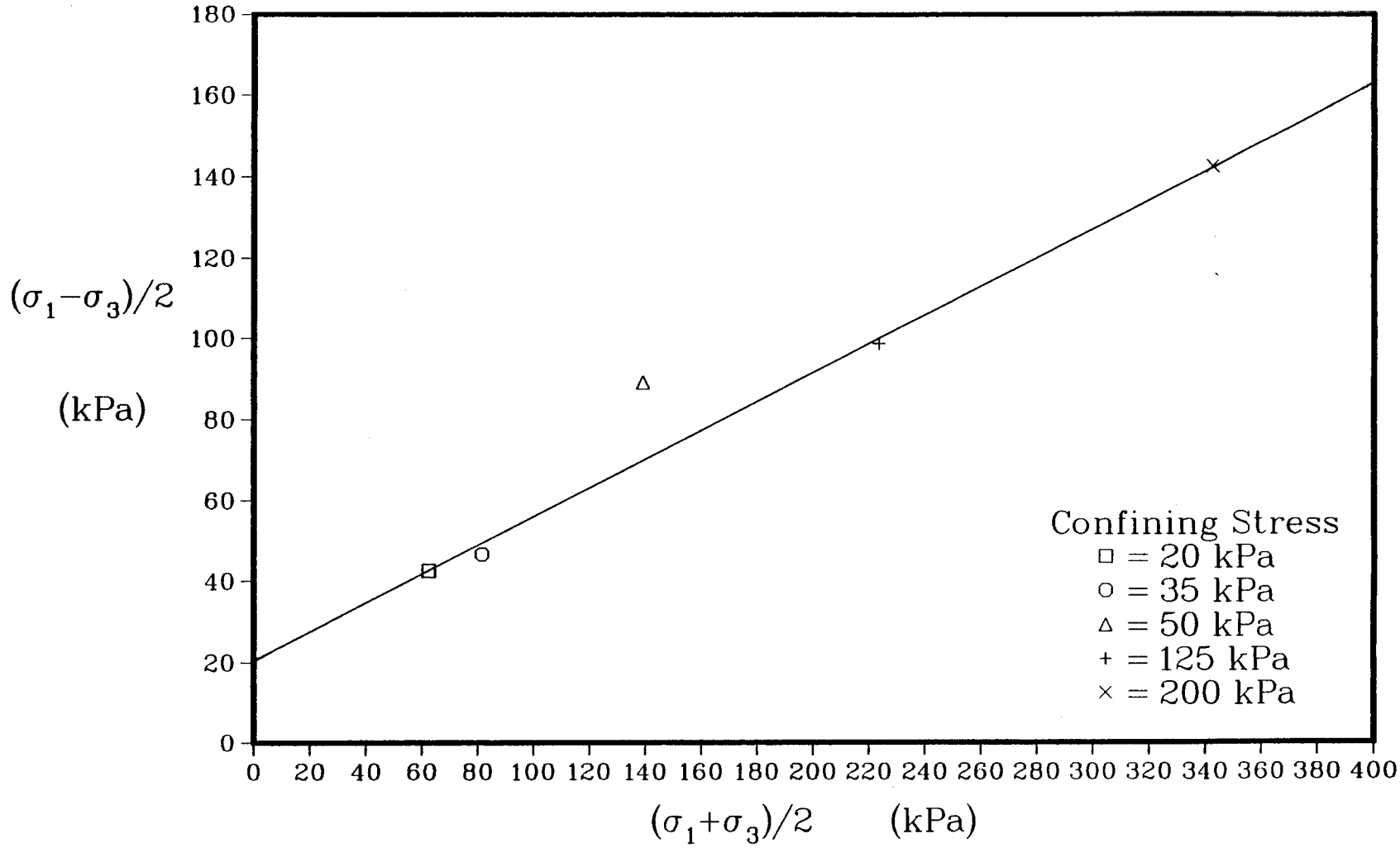

Figure 4.38: Total Stress P–Q Plot for Silt Fill Soil from CU Triaxial Tests

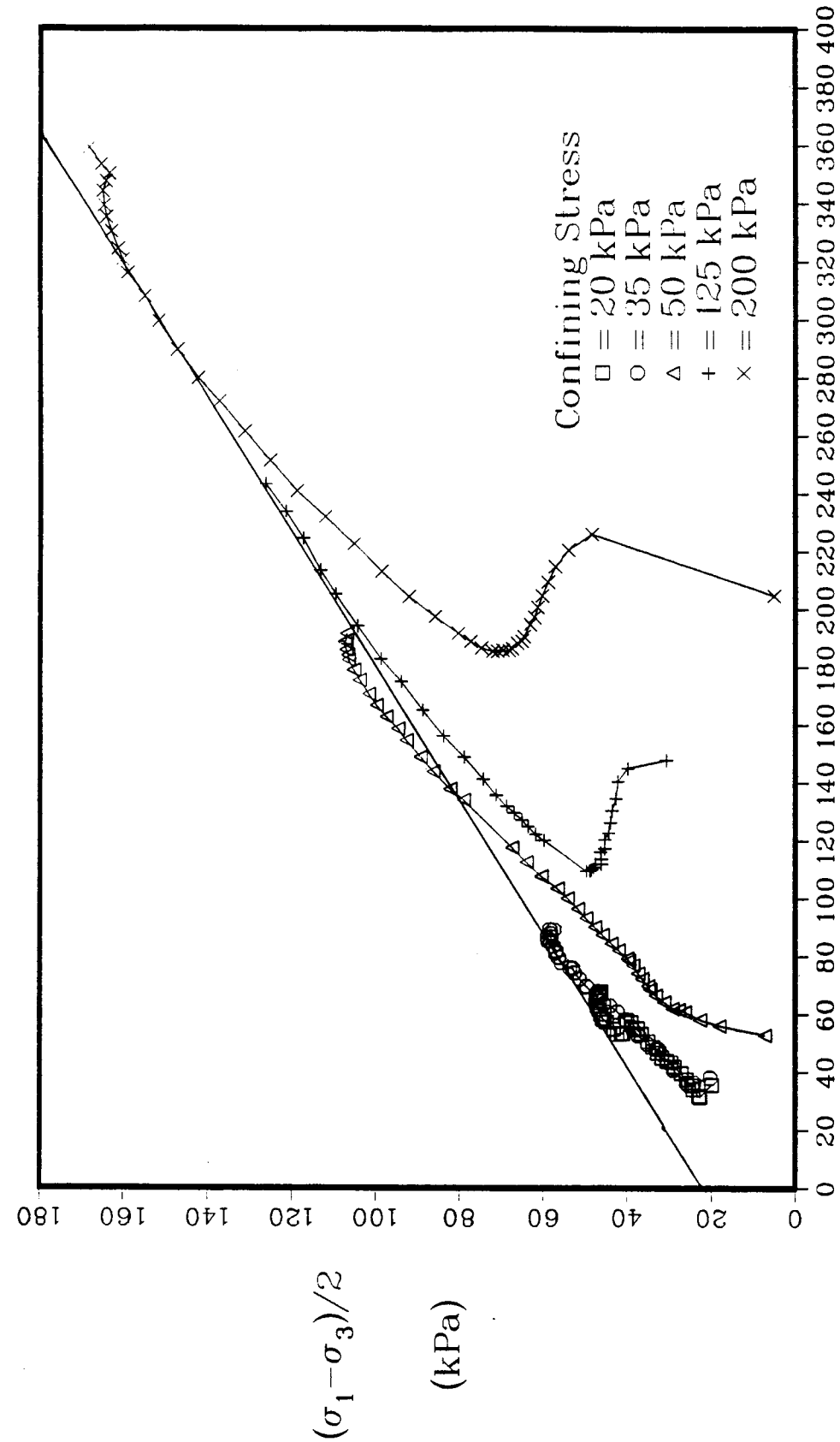

Figure 4.39: Effective Stress P–Q Plot for Silt Fill Soil

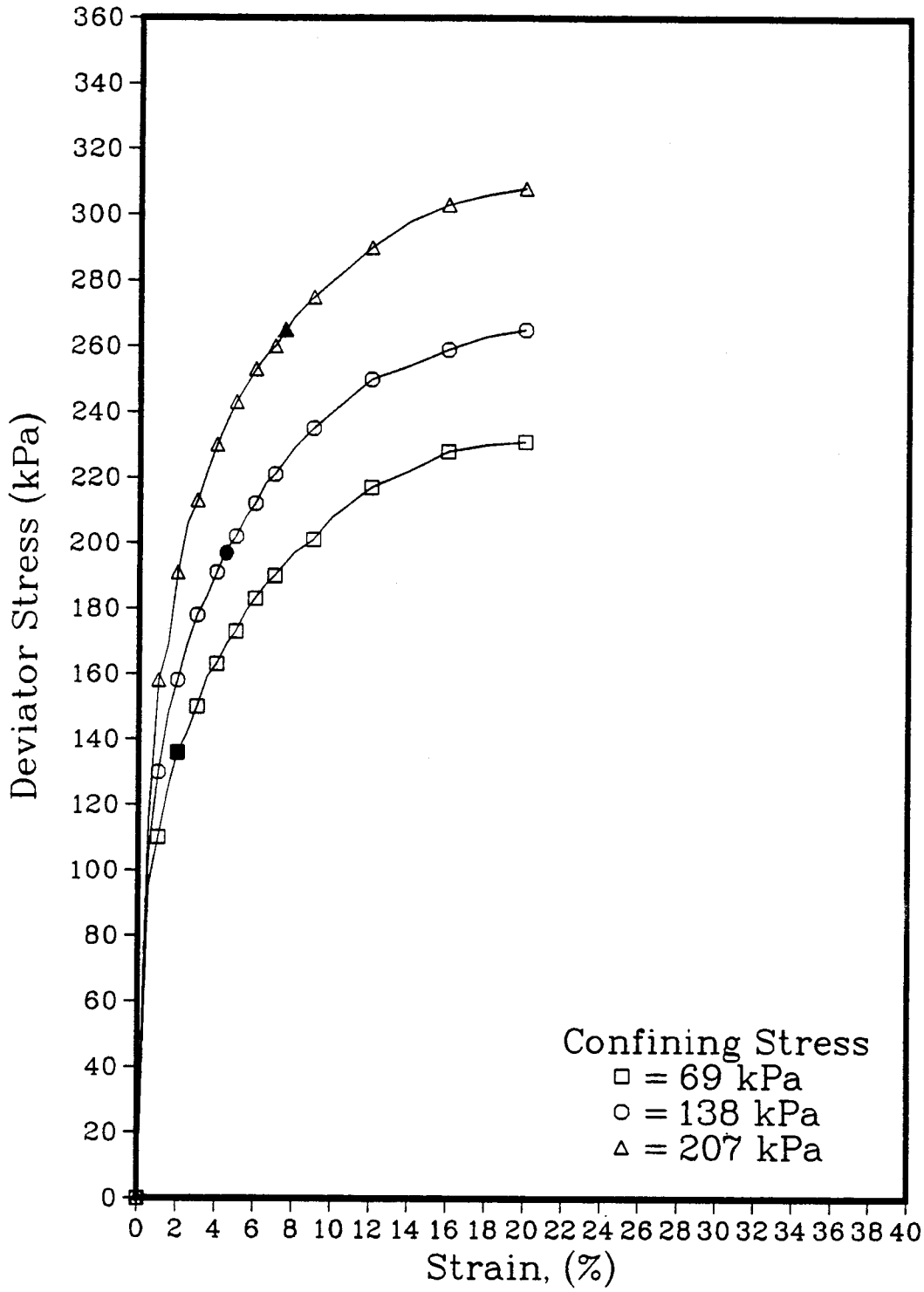

Figure 4.40: CU Triaxial Tests on Sandy Clay Fill Soil

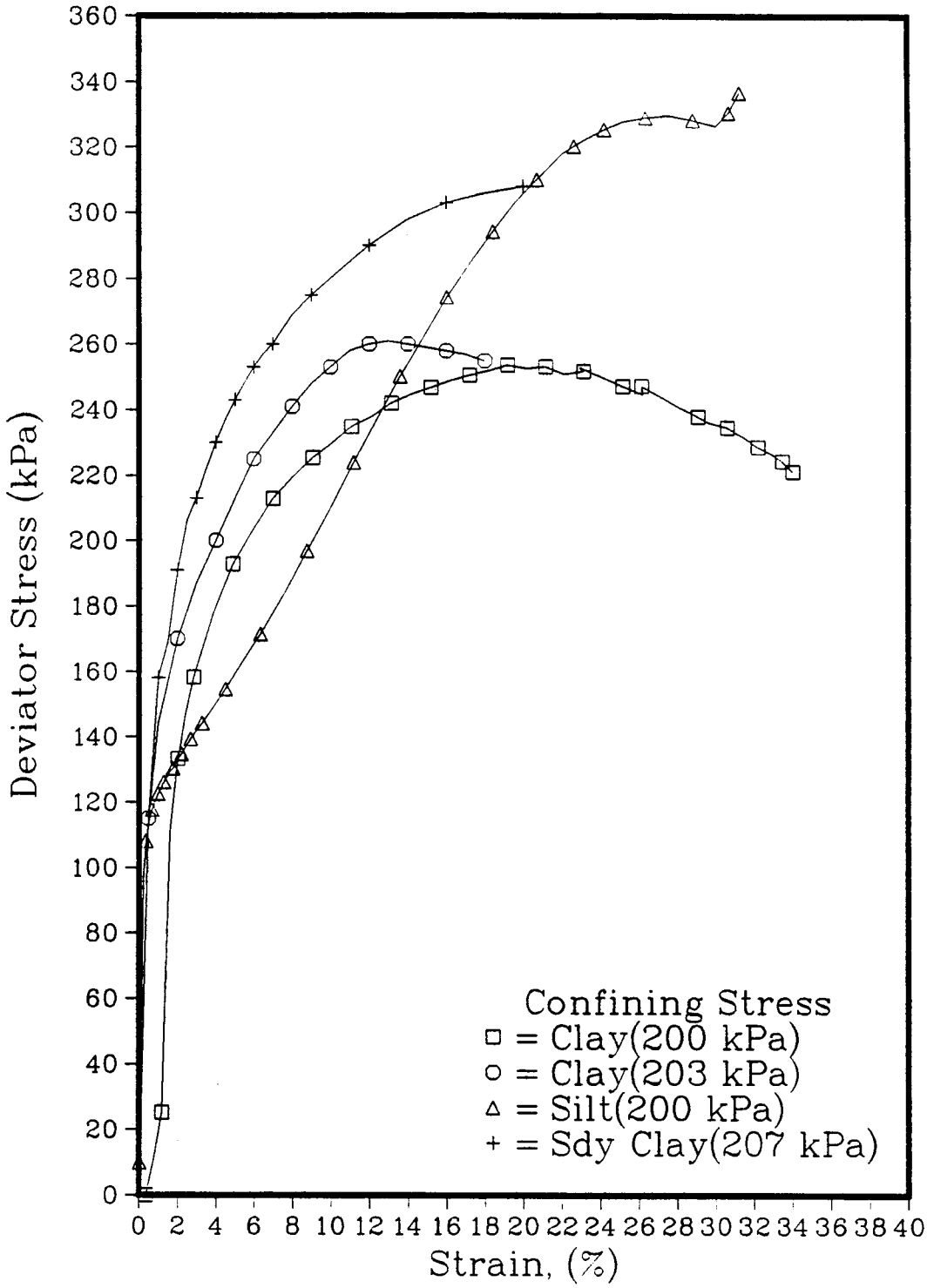

Figure 4.41: Comparison of Stress–Strain Curves from CU Tests on Different Fill Soils

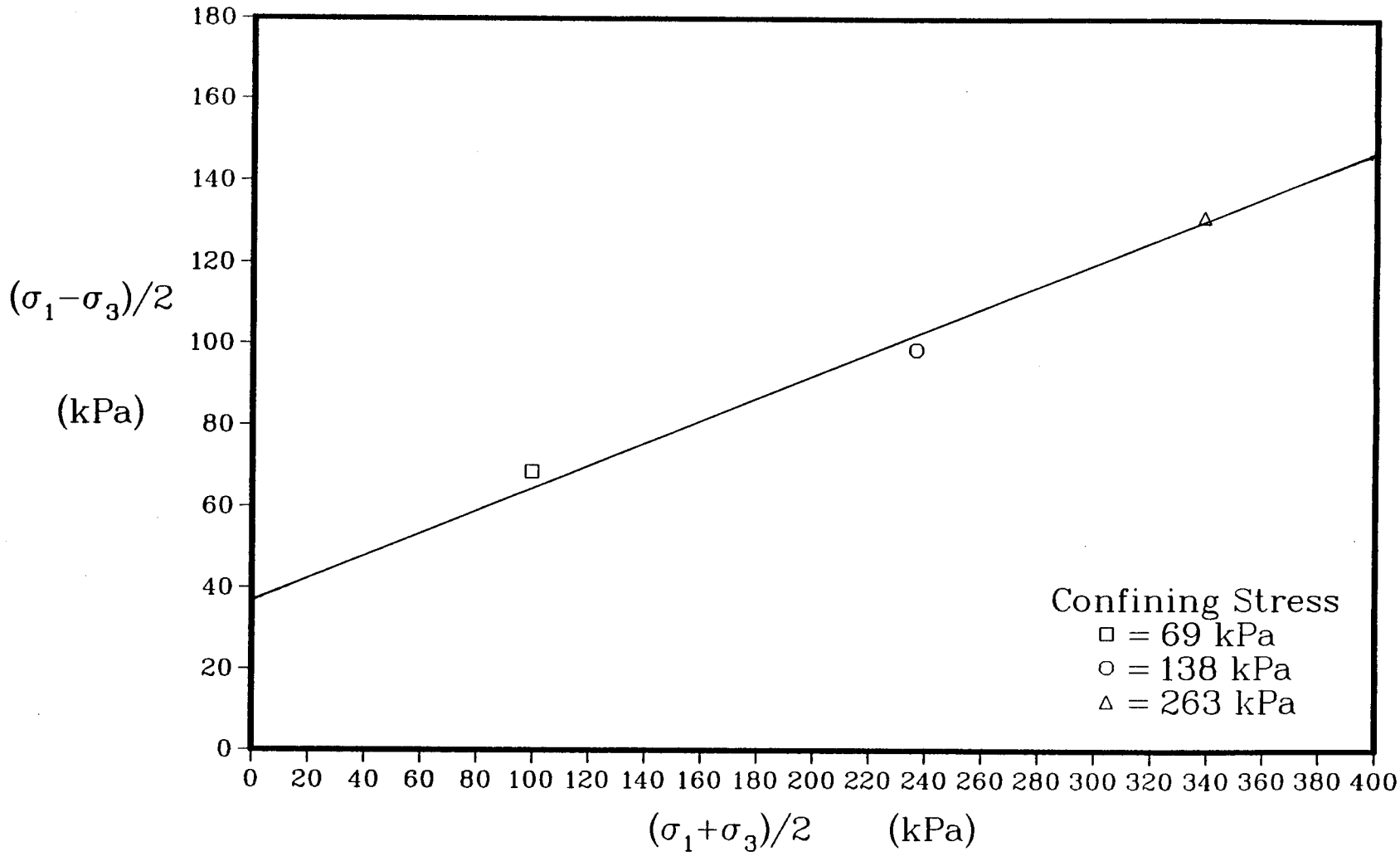

Figure 4.42: Total Stress P–Q Plot for Sandy Clay Fill from CU Triaxial Tests

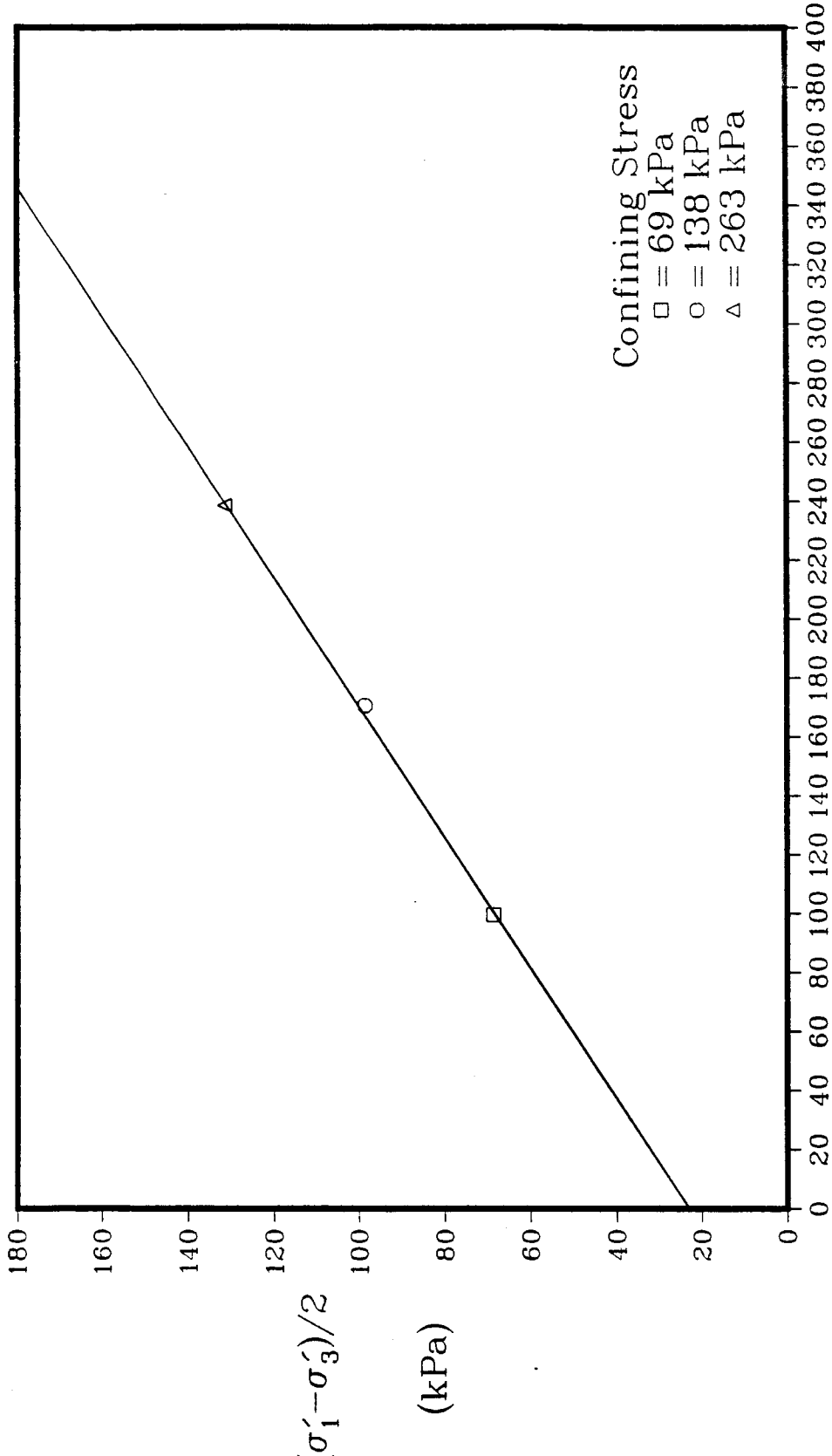

Figure 4.43: Effective Stress P–Q Plot for Sandy Clay Fill from CU Triaxial Tests

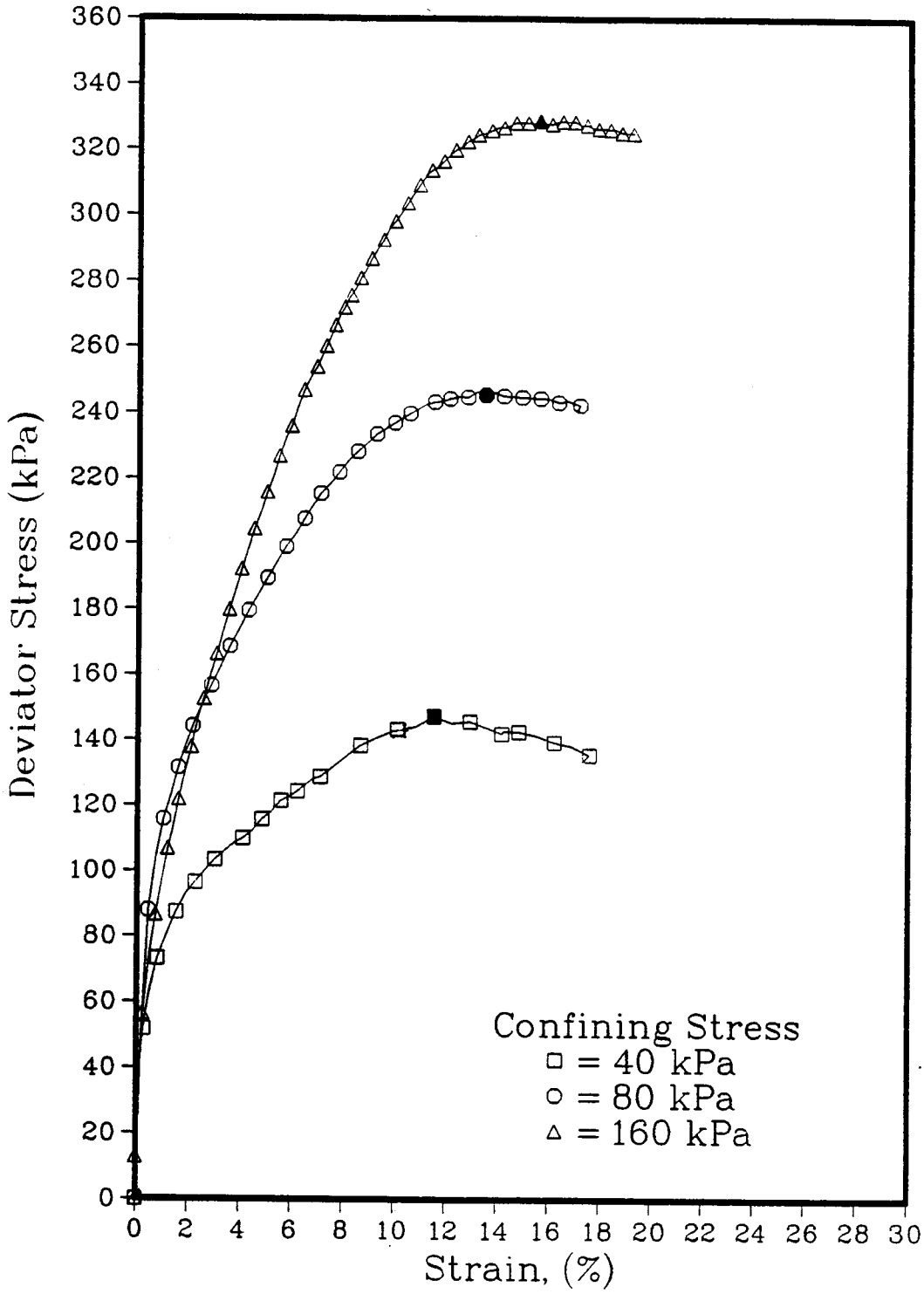

Figure 4.44: CD Triaxial Tests on Clay Fill Soil

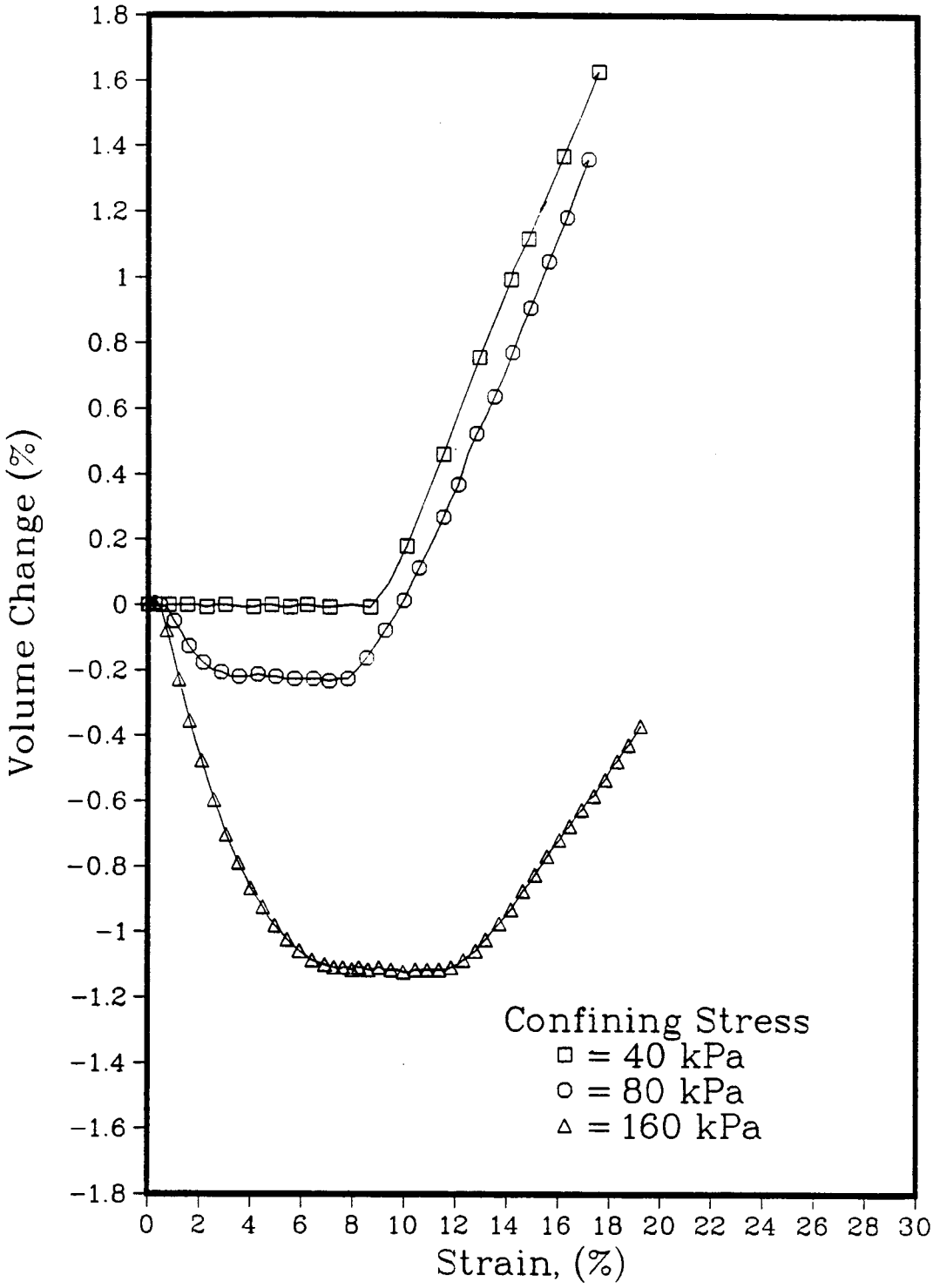

Figure 4.45: CD Triaxial Tests on Clay Fill Soil

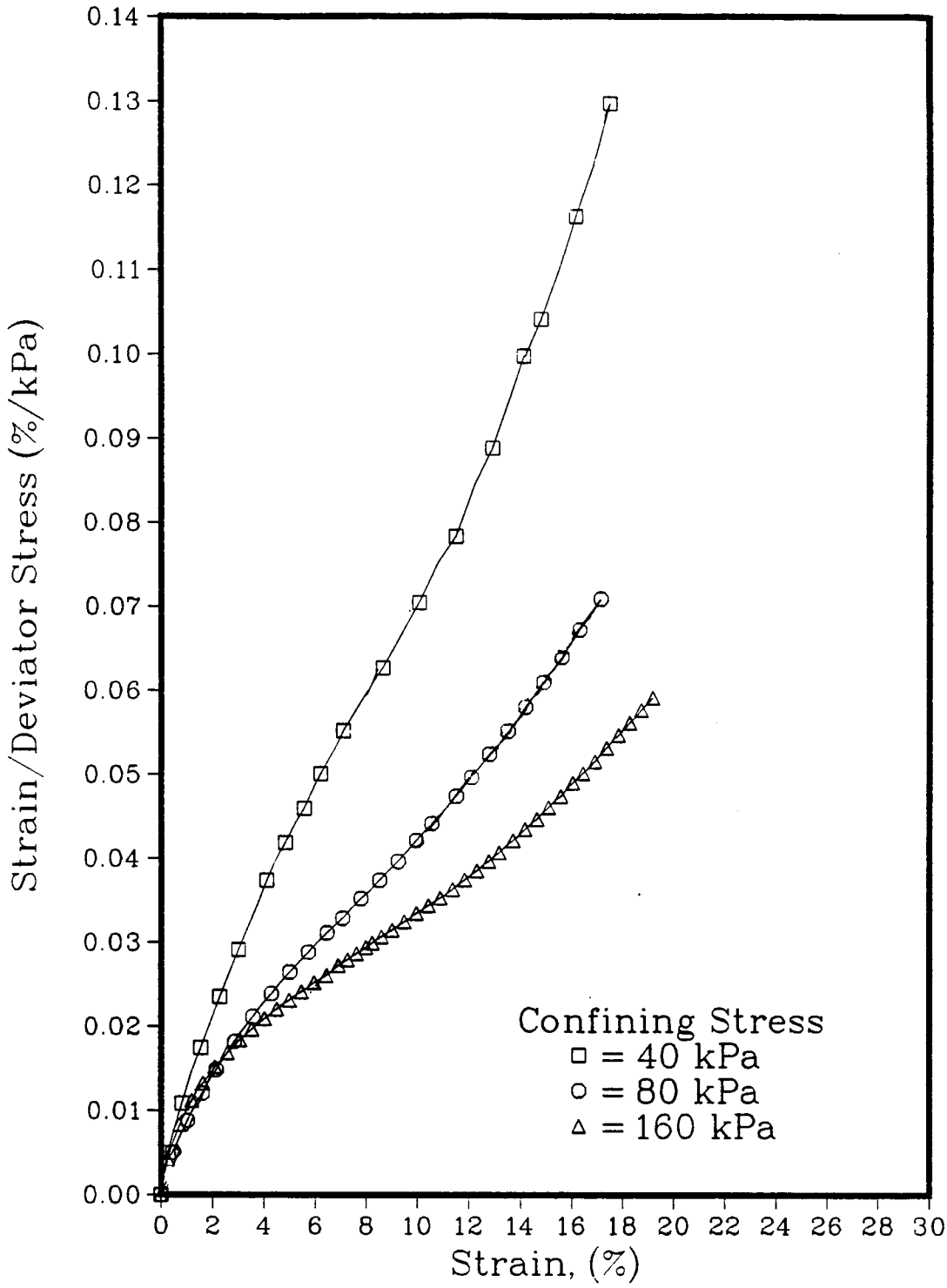

Figure 4.46: Transformed CD Triaxial Test Data Obtained for Clay Fill Soil

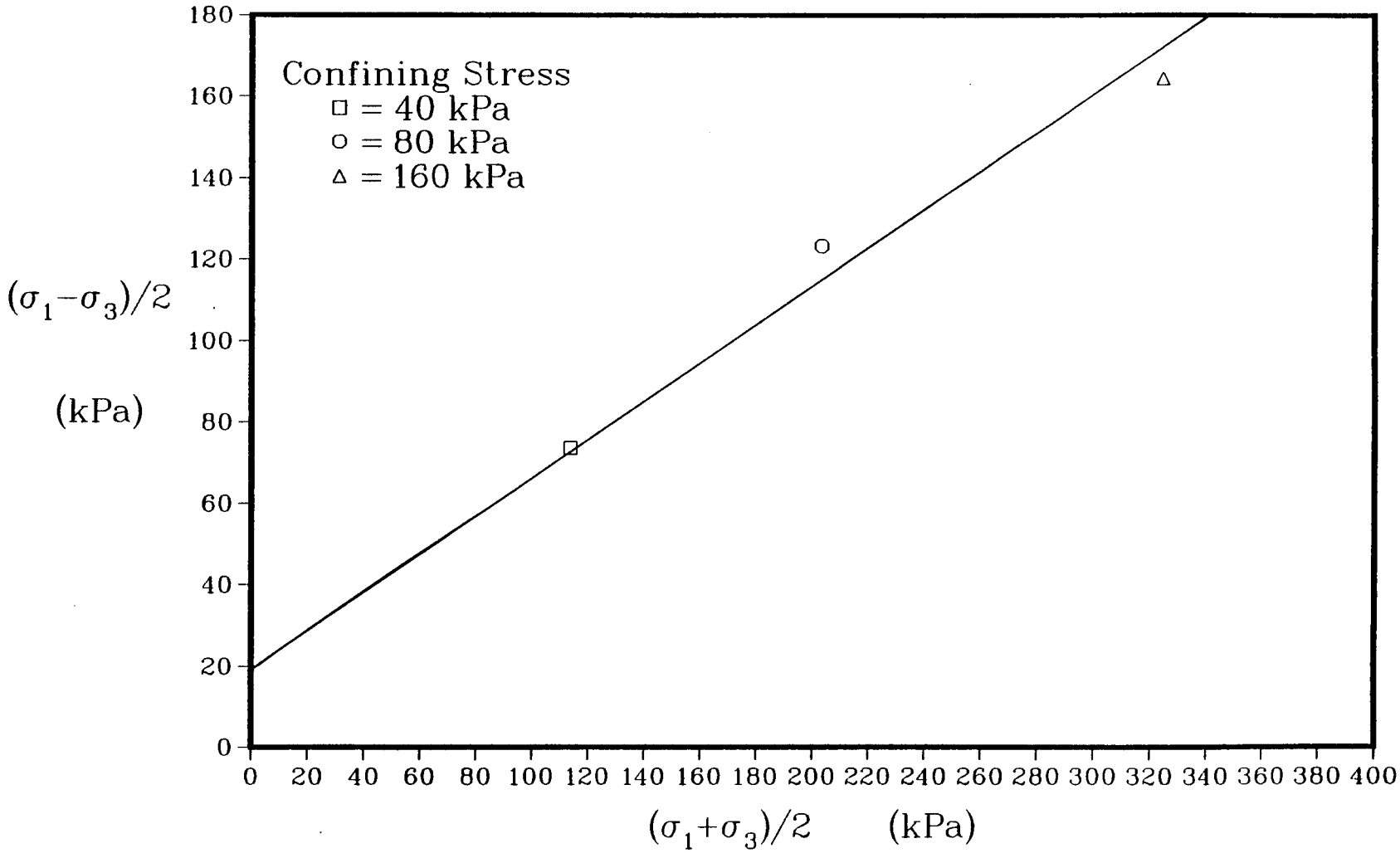

Figure 4.47: Total & Effective Stress P–Q Plot
for Clay Fill Soil

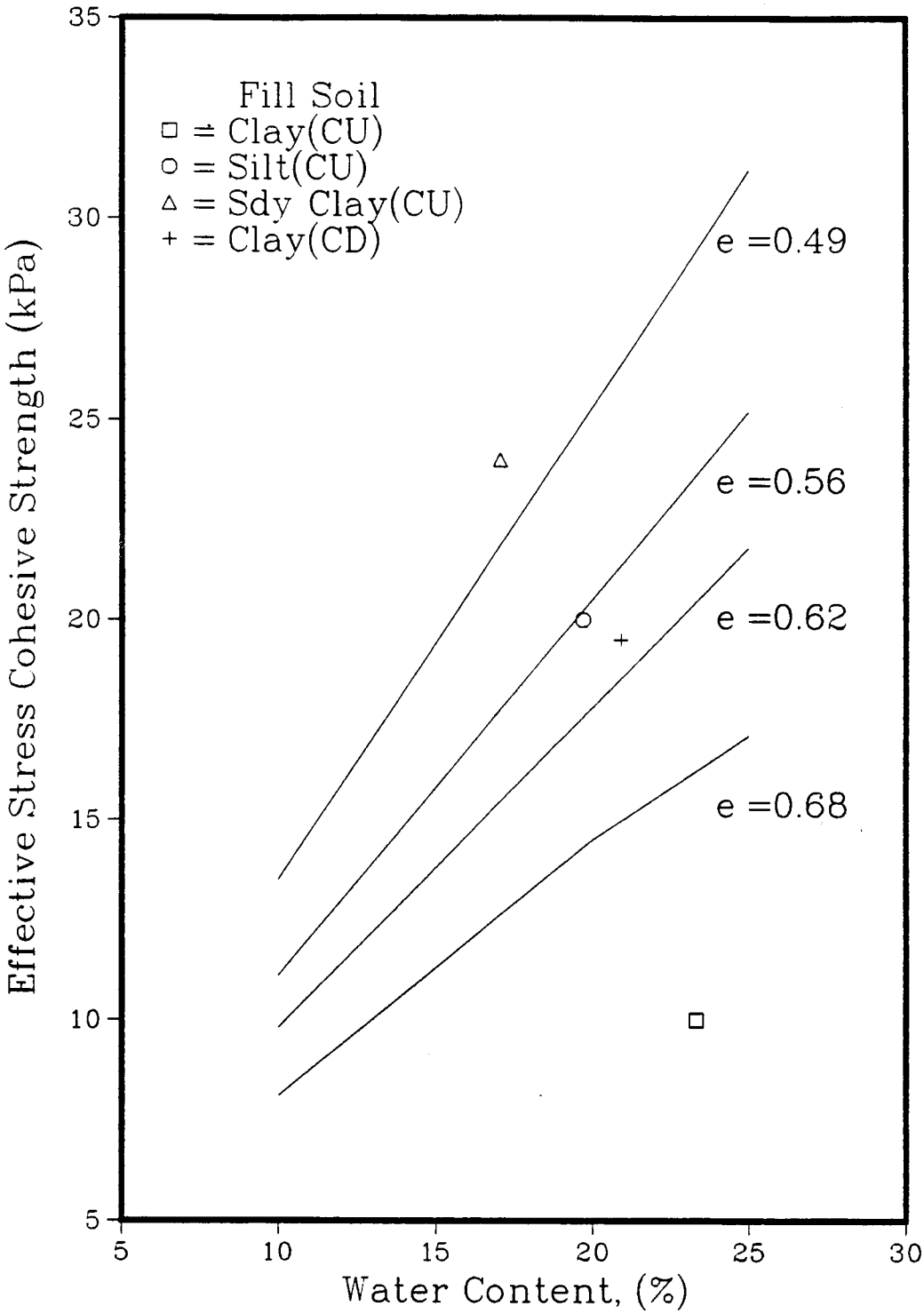

Figure 4.48: Theoretical and Measured Values of c'

5. LABORATORY TESTING OF FOUNDATION SOIL

5.1 Introduction

In order to conduct stability and deformational analyses on the unreinforced slope of the test fill it was necessary to determine the shear strength and stress-strain properties of the foundation soil through laboratory testing. Standard penetration tests conducted during the foundation drilling program, described in Chapter 3, showed that beyond a depth of 6 m the soil becomes very stiff. Hence, determination of the shear strength and the stress-strain properties of only the top 6 m of foundation soil was considered necessary in order to analyze the critical stability and deformational characteristics of the test fill.

Consolidation tests were conducted on the block and Shelby tube specimens obtained from the site to determine the consolidation rate, preconsolidation stress and permeabiltiy of the foundation soil. The information obtained from these tests was also required for settlement calculations and to assess the dissipation rate of excess pore pressures. Consolidated undrained triaxial tests with pore pressure measurements were conducted on the block and Shelby tube specimens to determine the pore pressure behaviour and the effective stress parameters required for the limit equilibrium and finite element analyses. Table 5.1 summarizes the various tests conducted on each of the

foundation soil samples. The results obtained from these tests will be presented and discussed in this Chapter.

5.2 Consolidation Tests

The test fill is 12 m high with a base dimension of 42 m by 72 m, a crest dimension of 18 m by 36 m, side slopes of 1:1 and end slopes of 1.5:1. Hence, the embankment covers a large area and the consolidation of the foundation soil beneath the center of the fill may be considered as one-dimensional under the major part of the embankment. Figure 5.1 shows the distribution of stresses acting on the foundation soil due to the weight of the embankment. Beneath the slopes of the test fill, the foundation soil is subject to overburden stresses which decrease as the overlying fill height decreases. Consequently, consolidation of the foundation soil in this region should rigorously be treated as two-dimensional. However, the consolidation problem may be simplified by considering the test fill as a right prism with dimensions of 30 m by 54 m and consolidation of the soil beneath the prism may be idealized as one-dimensional.

The oedometer may be used to simulate one-dimensional compression of soil in the laboratory. Consolidation tests were conducted according to ASTM standard D 2435-80 using a floating-ring oedometer. Specimens, 25.4 mm (1") high by 63.5 mm (2.5") in diameter, were carved from the block sample, described in Section 3.3, for the oedometer. Consolidation tests were conducted on specimens with

laminations running both horizontally and vertically. vertically laminated specimens were tested to determine the horizontal permeability of the soil unit. Tube samples 22 and 42 obtained from depths of 2.95 and 2.50 m below the original ground surface were extruded and trimmed to a height of 25.4 mm (1") and a diameter of 63.5 mm (2.5") for the oedometer.

5.2.1 Block Sample

5.2.1.1 Horizontally Laminated Specimens

Two horizontally laminated block sample specimens were subject to a load sequence chosen with small load increments in the range of stresses, between 60 and 300 kPa, expected to be induced on the foundation soil by the test fill. The specimens were allowed to consolidate, or swell, for 24 hours under each load increment. The log-time and square-root-time consolidation curves for specimens 1 and 2, under consolidation loads of 500 and 800 kPa, are shown in Figures 5.2 to 5.4. The consolidation curves obtained for all other load steps are given in Appendix A.

The relationship between the vertical deformations and the log of time for clay is usually highly non-linear and express 3 different deformation phases. Upon loading, immediate undrained settlement takes place. Then, as pore water is expelled and the effective stress slowly increases, primary consolidation occurs.

This is characterized by a relatively sharp reduction in the void ratio over a period of time governed by the permeability of the soil. During the last stage, called secondary consolidation, the void ratio continually decreases under a constant effective stress due to creep of the soil particles. However, the consolidation curves obtained for the block sample specimens do not clearly exhibit these three phases.

The immediate and the primary settlement of the horizontally laminated block specimens took place within five minutes after the application of each load. The times to complete 90% of the primary consolidation under each load step, calculated using Taylor's square-root-time fitting method (1948), are given in Table 5.2. Due to the rapid primary consolidation phase, the vertical strain versus log-time plots are essentially straight lines governed by secondary consolidation. Consequently, it was only possible to determine the coefficient of consolidation, c_v, for these specimens from the vertical strain versus the square-root-time plots. It was difficult in some cases to calculate c_v from the curves obtained for low normal stresses. Hence, the values given in Table 5.4 for loads of 60 to 200 kPa are somewhat questionable.

The following relation may be used to calculate the time required for the foundation soil beneath the test fill to complete 90% of the primary consolidation:

$$\left[\frac{t_{90}}{H^2}\right]_{lab} = \left[\frac{t_{90}}{H^2}\right]_{field} \qquad [5.1]$$

where H=length of the drainage path

The borehole logs given in Chapter 3 show that the ground water table was located about 5 m below the original ground surface prior to construction of the test fill. However, the ground water table may rise locally due to the presence of the embankment and the 6 m of compressible silty clay foundation soil directly beneath the fill may become completely saturated due to capillary rise. In this case, the average drainage path in the field would be 3m, down to the till unit beneath the compressible silty clay where excess pore pressures are not generated. From the laboratory data obtained for the specimens subject to normal loads of between 200 and 300 kPa, an average value for t_{90} of 2.1 minutes was chosen for a drainage length of 2.5 cm. Substituting the appropriate values into Equation 5.1 yields a field value for t_{90} of 21 days.

If the foundation soil is not saturated, the distance to a free draining boundary will be considerably shorter, hence the time to complete 90% of the primary consolidation will be less. In addition, if construction of the embankment proceeds slowly, the foundation soil will have time to drain as the fill

height increases. Hence, using a t_{90} of 1.44 minutes for primary consolidation of the laboratory specimens under a normal stress of 60 kPa would result in a lower t_{90} calculated for the field.

The change in void ratio undergone by each specimen in a 24 hour period under each load step has been plotted in Figures 5.6 and 5.7. The preconsolidation stresses were determined from the plots using the Casagrande construction technique. Preconsolidation stresses of 550 and 365 kPa were determined for specimens 1 and 2, respectively. These stresses are greater than the stress of about 300 kPa that would be exerted on the foundation soil, 3 m beneath the embankment by a fill of 12 m in height. Therefore, excessively large settlements of the foundation soil would not be expected.

The compression and recompression indicies were also calculated from the void ratio versus effective stress plots for each specimen under various stress ranges. These parameters are given in Table 5.5 along with the secondary compression indicies established from the log-time and square-root-time consolidation curves.

The recompression indicies were determined from the unloading part of the void ratio versus effective stress plots for a stress range from 20 to 500 kPa as shown in Figures 5.6 and 5.7. According to Leonards (1976), the recompression index should be determined for a stress

range which is slightly less than the preconsolidation stress or between the current in situ stress, σ'_{vo}, and the stress expected to be applied in the field, $\Delta\sigma_v$, by, in this case, the test embankment. The value of the recompression index depends upon the stress at which the rebound-reload cycle starts. The recompression indicies calculated for the unloading stage from the virgin compression curve, as shown in Figures 5.6 and 5.7, are probably greater than those that would be calculated for a stress range of between σ'_{vo} and $\Delta\sigma_v$. Therefore, settlements calculated based on the recompression indicies given in Table 5.5 are most likely too large.

Since the overburden stress induced by the test fill is less than the foundation soil's preconsolidation stress, the recompression index was used to calculate settlement due to primary consolidation. Using the expression:

$$s_c = c_r \left[\frac{H_o}{1+e_o}\right] \log\left[\frac{\sigma'_{vo}+\Delta\sigma}{\sigma'_{vo}}\right] \qquad [5.2]$$

where H_o=initial thickness of compressible soil layer

e_o=void ratio determined in the laboratory under a normal load of 60 kPa

σ'_{vo}=initial overburden stress

$\Delta\sigma_v$=increase in overburden stress due to theweight of the embankment

An average settlement of 10.5 cm was calculated. This settlement is not significant compared to the height of the test fill.

In order to calculate the permeability of the block sample soil, a representative coefficient of consolidation had to be chosen. Due to the shape of the consolidation curves obtained for normal stresses equal to the stress which would be applied by the test embankment, c_v values could not be calculated with confidence from these curves. The consolidation curves obtained for loads which are greater than the preconsolidation stress exhibited the shape typical for clay and c_v values could be calculated relatively well. Therefore, the coefficients of consolidation quoted in Table 5.5 are those obtained from consolidation under stresses of 500 and 800 kPa. The c_v values calculated for the high normal stresses are probably lower than those that would be calculated for normal stresses of 200 kPa.

The average permeability of the two horizontally laminated block sample specimens calculated using the c_v values determined for normal loads of 500 and 800 kPa is 1.3×10^{-7}cm/s. According to Holtz and Kovacs (1981), a silty clay with a permeability of 10^{-7}cm/s would be classified as practically impervious. However, this number would most likely be higher under lower normal stresses. It was shown, using Equation 5.1, that even

for the worst case where the 6 m of compressible foundation soil is completely saturated, it would take only up to 21 days for primary consolidation to be complete.

5.2.1.2 Vertically Laminated Specimens

One-dimensional consolidation tests were also conducted on two vertically laminated specimens carved from the block sample. These tests were conducted to determine the horizontal permeability of the stratified foundation soil. The consolidation curves obtained for specimens 1 and 2 under normal stresses of 500 and 800 kPa are shown in Figures 5.8 to 5.11. The consolidation curves obtained for all other normal loads are given in Appendix A. The times required to reach 90% of the primary consolidation under each load step are given in Table 5.3. Under normal stress of 500 kPa or less, the values of t_{90} are all less than 5 minutes.

Figures 5.12 and 5.13 show the void ratio versus normal load curves obtained from each set of tests. The preconsolidation stresses calculated for the vertically bedded specimens are 335 and 385 kPa. The horizontal and vertical preconsolidation stresses are approximately the same, indicating that K_o for the silty clay foundation soil was close to 1.0 at the time that the soil unit was subject to its maximum stress. Table 5.5 shows the consolidation indicies obtained from these tests. The coefficients of consolidation and the permeabilities

given in Table 5.5 have been determined based on consolidation of the soil under normal loads of 500 and 800 kPa. The coefficient of consolidation and the coefficient of permeability may be higher than the values that would be determined under the actual field stress of approximately 240 kPa. However, due to the shape of the consolidation curves under low normal stresses, it was not possible to calculate values of c_v accurately for the lower stress range. The average horizontal permeability of the foundation soil determined for normal stresses of 500 and 800 kPa is 5.3×10^{-7}cm/s. This is approximately 4 times greater than the vertical permeability determined for the same normal stresses. Higher horizontal permeabilities are expected since the pore water can escape more quickly along lamination planes than across them.

5.2.2 Tube Samples

Three one-dimensional consolidation tests were conducted on specimens trimmed from Shelby tubes 22 and 42. The tube samples were obtained from depths of 3.0 and 2.5 m, respectively. A seating load of 5 kPa was applied to each specimen before the dial gauge was set to zero. The specimens were then loaded to the in-situ vertical effective stress of about 50 kpa and allowed to consolidate for 24 hours. This procedure is recommended by Holtz and Kovacs (1981). The loading sequences applied to each specimen were

chosen such that the preconsolidation stress of approximately 350 to 500 kPa could be well defined.

Two of the specimens were allowed to consolidate for 24 hours under each load step. The load increments placed on the third specimen were applied only until primary consolidation was complete. Figures 5.14 to 5.19 show the consolidation curves obtained for each specimen under loads of 500 and 800 kPa. The vertical strain undergone by each specimen versus the log of time plots are essentially straight lines with no obvious phases of immediate or primary consolidation. It was, however, possible to approximate the times to complete 90% of the primary consolidation and the coefficients of consolidation from the strain versus the square-root of time plots. These values are given in Table 5.6. Comparison of the t_{90} values calculated for the horizontally laminated block specimens and the tube specimens under loads of 500 and 800 kPa shows that they are similar.

The coefficient of consolidation, c_v, calculated for the tube specimens under normal stresses of 500 to 800 kPa are about 3 times greater than those calculated for the block specimens. In other words, primary consolidation of the tube soil was complete in less time than it took for completion of primary consolidation of the block soil.

Figures 5.20 , 5.21 and 5.22 show the plots of void ratio versus applied effective stress determined for each specimen. The average preconsolidation stress derived from

the three tests is 445 kPa. This agrees with the average preconsolidation stress determined from the tests conducted on the horizontally laminated block sample specimens. Table 5.7 gives the calculated coefficients of consolidation, permeability, compression, recompression and secondary compression derived from the tube sample consolidation tests for various stress ranges.

The recompression indicies calculated for the shelby tube specimens were determined from rebound-reload cycles between the current effective overburden stress and the additional load expected to be induced by the test embankment. According to Leonards (1976), this procedure results in recompression indicies which approximate the actual in situ values. Therefore, the recompression indicies determined for the shelby tube specimens are probably more accurate than the those determined for the block sample specimens.

Comparison of Tables 5.4 and 5.7 shows that the coefficients of compression and recompression determined for the Shelby tube specimens are slightly lower than those determined for the horizontally laminated block specimens. Primary settlement calculations using the average recompression index obtained for the three shelby tube specimens, for a stress range of 50 to 300 kPa, resulted in an average settlement of 3.4 cm. This is considerably lower than the settlement of 10.5 cm previously calculated, due to the inaccurate recompression indicies determined for the

block sample specimens.

Although the permeability of the silty clay foundation soil is low, as shown in Table 5.7, primary consolidation of the laboratory tested specimens was complete in less than 5 minutes, under normal loads of up to 800 kPa. The drainage paths for the soil in the field are much longer than those for the laboratory specimens. However, construction of the fill is proceeding slowly, thus, the foundation soil will most likely consolidate as the embankment is being built and high excess pore pressures are not expected.

5.3 Consolidated Undrained Triaxial Tests

The consolidation tests indicated that the foundation soil may have time to drain during construction of the embankment, provided that it is built up slowly. However, in the event that the last 6 m of fill soil is placed quickly, consolidated undrained triaxial tests were conducted on saturated foundation soil specimens to assess the pore pressure behaviour during shearing.

Specimens, 7.6 cm (3") long by 3.8 cm (1") in diameter, were carved as needed from the block sample for triaxial testing. The specimens were cut vertically from the block sample such that the bedding planes were kept horizontal. Shelby tube samples 4, 6, 22, 24, 42, 44 and 64 were also extruded for triaxial testing. It was not possible to trim the extruded, 7.3 cm ($2^{7}/_{8}$") diameter, tube samples to the dimensions used for the block specimens because the soil was

very wet. Consequently, the tube samples were simply cut to a length of 15 cm such that the length to diameter ratio of 2:1 was retained for triaxial testing. The specimens were tested within 48 hours of being removed from the tubes and were stored in a moisture room in the interim.

Alberta Transportation and Utilities extruded Shelby tube samples obtained from borehole 28 at depths of between 10 and 14 m for triaxial testing. Specimens were trimmed to a length of 7.6 cm (3") and a diameter of 3.8 cm (1.5").

Consolidated undrained triaxial tests were conducted as described by Bishop and Henkel (1962). A back pressure of 400 kPa and a strain rate of 5.5% per hour were used on the tube samples taken in the foundation soil of the test fill. A back pressure of 300 kPa was used for the block sample specimens. The first block specimens was sheared under a strain rate of 17.7% per hour. A slower strain rate, which allowed the pore pressures to equilibriate throughout the soil during shearing, was then established for the remaining tests. Alberta Transportation and Utilities conducted consolidated undrained triaxial tests on similar soil with a back pressure of 200 kPa and strain rate of 1% per hour.

It will be seen that it is difficult to define failure consistently as the point at which the deviator stress is a maximum or at which the principal effective stress ratio is a maximum. This is due to the variable shape of the stress-strain curves and the behaviour of pore pressures during shear. In some cases the deviator stress does not

peak to define a maximum. Rather, the soil exhibits an elastic-perfectly plastic stress-strain curve. Failure for this type of behaviour may be defined at the maximum principal effective stress ratio, provided that the pore pressures induced during shear are not such that a maximum ratio is not attained or such that the minor principal effective stress becomes close to zero. If the minor principal effective stress becomes small, the principal effective stress ratio becomes a very large number, beyond which the ratio decreases. Hence, in this case the maximum ratio cannot be used to define failure. For situations where the soil exhibits elastic-perfectly plastic stress-strain behaviour, and the minor principal stress is small, failure may be taken as the point at which the vertical strain of the specimen increases under an approximately constant stress. It is important that one of the two failure criterions be used consistently for a set of tests to define the failure envelope of the soil correctly (Peck, 1960).

5.3.1 Shelby Tube Specimens

Eight consolidated undrained triaxial tests with pore pressure measurements were conducted on the tube specimens. The stress-strain and pore pressure-strain curves derived from these tests are given in Figures 5.23 and 5.24. Table 5.8 lists the sample conditions prior to shearing and the stress, strain, pore pressure and moisture conditions at failure. The deviatoric stresses shown in Table 5.8 are

those which correspond to the maximum principal effective stress ratio. The variation of the initial tangent modulus of the stress-strain curves with confining stress is given in Figure 5.25. In general, the intial tangent modulus increases with increasing confining stress. This indicates that when choosing an initial tangent modulus for the foundation soil finite element model, a modulus must be used which corresponds to the average confining stress existing in the foundation.

Table 5.8 shows that positive pore pressures were developed at failure for all of the tube specimens except specimen CU2. This indicates that the specimens were undergoing compression during shearing. Skempton's pore pressure parameter at failure (Skempton, 1954), A_f, is plotted against confining stress in Figure 5.26. Although the data is somewhat scattered, it apparent that A_f tends to increase with increasing confining stress. Hence, pore pressures which develop in the test fill foundation will be highest in the region directly beneath the center of the fill where the confining stress is greatest. The values of A_f attained for higher confining stresses also indicate that a slow strain rate would be required to allow for dissipation of excess pore pressures during a consolidated drained triaxial test.

Figures 5.27 and 5.28 give the total and effective stress p-q plots derived from the consolidated undrained triaxial tests. In Figure 5.27 the total stress values of p

and q have been plotted at failure for each of the specimens, where failure is taken as the maximum principal effective stress ratio. The design total stress friction angle, calculated from a line drawn through these points for 5 out of the 8 specimens tested, is 15° and the design total stress cohesive strength is 10 kPa. The total stress friction angle may vary from about 15° to 18° while the total stress cohesive strength may vary from 10 to 12 kPa, depending upon how the failure envelope is fit through the data. The design failure envelope drawn through the failure points on the effective stress plot for 5 out of the 8 specimens tested yields an effective stress friction angle of 33° with a possible range from 24° to 33°. The design effective stress cohesive strength is 6 kPa with a possible range of 6 to 17 kPa. Scatter of the test data led to a wide range of possible shear strength parameters.

The total stress failure points and the effective stress paths of specimens CU5, CU6 and CU7 fall well below the total and effective stress failure envelopes, respectively. A difference in the manner by which the weaker specimens failed during testing was apparent. Those specimens with lower than expected strengths failed along a distinct shear plane while the others barrelled excessively. Shear plane development usually occurs in dense soils while barrelling occurs during failure of loose soils (Holtz and Kovacs, 1981). However, Table 5.8 shows that specimens CU3, CU5 and CU7 were not any more dense that the other

specimens. It may be that these specimens contained a greater percentage of sand which reduced the tendency for plastic deformation under loading. These specimens may not have been able to maintain higher loads due to flaws in the specimens or misalignment with the loading ram. However, there was not any evidence to suggest that either of these conditions existed.

5.3.2 Block Specimens

Four consolidated undrained triaxial tests with pore pressure measurements were conducted on specimens carved from the block sample. Figures 5.29 and 5.30 show the resulting stress-strain and pore pressure-strain curves. Table 5.9 gives the sample descriptions prior to testing and the water content, stress, strain and pore pressure conditions at failure.

It was difficult to choose a consistent failure criterion for this set of tests. Specimen CU11 developed pore pressures during the early stages of shearing which were very close to the confining stress. Hence, the effective minor principal stress became very small and this in turn, caused the principal effective stress ratio to become very large at stains of only 0.6%. The principal effective stress ratio calculated for specimen CU12 peaked at a strain of 4%, dropped off and then continued to increase until shearing was stopped. Since the maximum principal effective stress ratio could not be determined for

2 of the 4 tests conducted, the maximum deviatoric stress was chosen as the failure criterion.

Figure 5.31 shows that the initial tangent modulus remained fairly constant with increasing confining stress unlike the behaviour exhibited by the tube specimens. The stress-strain curves rise steeply in a straight line up to about 2% strain and then break sharply to continue straining under a constant or gradually decreasing stress level. The behaviour of specimens CU9, CU10 and CU11 may be idealized as elastic-perfectly-plastic. The pore pressures developed during shearing of these samples also follow a similar pattern. They rise quickly at the beginning of the test and then level off at a constant pressure. Specimen CU12 does not behave in the same manner, for unknown reasons.

The shapes of the stress-strain and pore pressure-strain curves obtained for the tube specimens and block specimens differ slightly. The tube specimens appear to exhibit hyperbolic stress-strain curves while the block specimens show elastic-perfectly plastic behaviour. This is most likely due to differences in the structure of the samples. The elastic-perfectly plastic stress-strain curves show that at some critical load the structure of an in-tact specimen is broken down, such that the soil can no longer take on additional load. However, Shelby tube sampling ofter causes some disturbance of the in situ soil structure. Hence, a sharp break is not exhibited by the stress-strain curve of a specimen whose structure has already been broken

down. The effect of sample disturbance on the stress-strain behaviour of Chicago clay is shown in Figure 5.32 (modified from Peck, 1940).

As was the case for the tube specimens, Table 5.9 shows that the pore pressures developed at failure by the tube specimens were positive. This shows that the soil compresses during shear. The pore pressure parameter A_f has been plotted against confining stress in Figure 5.33. A_f increases with confining stress to reach a value of 0.827 under a stress of 275 kPa. This behaviour is similar to that exhibited by the tube specimens and shows that the pore pressures generated due to shear stresses will be highest in the lower, central region of the embankment, where the confining stress is greatest.

Figures 5.34 and 5.35 show the total and effective stress p-q plots. The design total stress friction angle is 13° and the design total stress cohesive strength is 25 kPa. A possible range in the total stress cohesive strength from 25 to 27 kPa may exist. The design effective stress friction angle is 24° with a possible range from 24° to 25° and the design effective stress cohesive strength is 23 kPa with a possible range from 23 to 25 kPa. The cohesive strength determined for the block specimens is considerably higher than that obtained for the tube specimens. Conversely, the frictional strength is lower. Considering that the soil type, moisture contents and densities of both sets of specimens are similar, the lower cohesive strength obtained

for the tube specimens suggests that they may have been significantly disturbed.

5.3.3 Additional Shelby Tube Specimens

Three consolidated undrained triaxial tests were conducted on tube specimens obtained from borehole 28 at a depth of 13 m by Alberta Tansportation and Utilities. The stress-strain and pore pressure-strain curves obtained from these tests are given in Figures 5.36 and 5.37. The sample conditions prior to testing and after consolidation are given in Table 5.10 along with the stress, strain, pore pressure and moisture conditions at failure.

The shapes of the stress-strain curves appear to be similar to those obtained from the tests conducted on the tube specimens discussed in Section 5.3.2. The tests conducted under a confining stress of about 100 kPa have very similar stress-strain curves and show almost the same deviatoric stress at failure. The total and effective stress p-q plots obtained from Alberta Transportation and Utilities' tests are given in Figures 5.38 and 5.39. The design total stress friction angle is 15° and the design total stress cohesive strength is 30 kPa with a possible range from 28 to 30 kPa. This friction angle agrees with that obtained for the tube specimens tested in this study, while the cohesive strength is considerably higher. Figure 5.39 shows that the design effective stress friction angle is 31° and the design effective stress cohesive strength is

0 kPa, with no range of values. The effective stress paramters are similar to those obtained for the tube specimens tested in this study.

5.3.4 Summary of Consolidated Undrained Triaxial Test Results

A summary of both the design values and range of total and effective stress strength parameters established for the block specimens and the two sets of tube specimens is given in Table 5.11. The failure envelope established for the block specimens has a much higher effective stress cohesive strength intercept than the intercepts determined for both sets of tube specimens. However, the shape of the stress-strain curves exhibited by the tube specimens showed that the soil structure appeared to be considerably disturbed. It was therefore decided that the effective stress strength parameters obtained for the block specimens are more representative of the field strength and these parameters were selected for the limit equilibrium analysis.

If construction of the test fill continues to proceed slowly, the stress-strain curves obtained from consolidated drained triaxial tests would more accurately model the field conditions than the stress-strain curves obtained from consolidated undrained tests. However, due to time constraints, limits had to be placed on the number and type of laboratory tests that could be conducted. Furthermore, it was not known at what rate the remaining 6 m of fill soil

would be placed on the embankment. Hence, whether or not excess pore pressures generated in the foundation soil would have time to dissipate during construction was not known. It was therefore decided that the stress-strain curves obtained from the consolidated undrained triaxial tests would be used for the finite element analysis as an approximation to the field behaviour.

Since volume change is not allowed during undrained tests, volume strains caused by shearing are not included in the stress-strain curves obtained from consolidated undrained triaxial tests. Hence, use of the undrained stress-strain curve for the finite element analysis will result in an under estimation of the foundation soil deformations. However, since the pore pressures developed during the undrained triaxial tests were not excessively high, the volume strains which would occur during a drained test would not be large. It is not expected that approximating the stress-strain behaviour of the foundation soil from undrained test data will introduce a significant amount of error in pediction of embankment deformations with finite elements.

Table 5.1: Summary of Tests Conducted on Foundation Soil Specimens

Specimen Type	Depth Below Ground Sfc (m)	Oedometer	CU Triaxial Tests
Block Specimens			
- horz. lmntd.	4.5	X	X
- vert. lmntd.	4.5	X	-
Tube Specimens			
- 4	2.50	-	X
- 6	3.45	-	X
- 22	2.95	X	X
- 24	3.90	-	X
- 42	2.50	X	X
- 44	3.25	-	X
- 64	3.50	-	X
- AB.T.28	10.06	X	X
- AB.T.28	13.11	X	X

Table 5.2: Consolidation Parameters Determined for Horizontally laminated Block Specimens

Specimen #	Load (kPa)	t90 (min)	Cv (cm2/s)	Mv (m2/KN)	K (cm/s)
1	60	1.44	0.0152	4.29E-4	6.39E-7
	100	2.89	0.0074	1.12E-4	8.13E-8
	200	1.96	0.0110	1.12E-4	1.21E-7
	300	2.89	0.0071	1.35E-4	9.40E-8
	500	1.96	0.0098	2.16E-4	2.08E-7
	800	2.89	0.0060	1.71E-4	1.01E-7
2	200	1.44	0.0145	7.20E-5	1.12E-7
	300	2.10	0.0098	7.29E-5	7.01E-8
	500	1.96	0.0102	1.06E-4	1.06E-7
	800	1.96	0.0096	1.10E-4	1.04E-7

Table 5.3: Consolidation Parameters Determined for Vertically Laminated Block Specimens

Specimen #	Load (kPa)	t90 (min)	Cv (cm2/s)	Mv (m2/KN)	K (cm/s)
1	60	3.24	0.0069	4.93E-4	3.34E-7
	100	3.61	0.0061	2.80E-4	1.67E-7
	200	4.00	0.0054	2.36E-4	1.25E-7
	500	4.00	0.0050	3.72E-4	7.31E-7
	800	8.40	0.0022	3.77E-4	4.75E-7
2	60	1.44	0.0155	1.45E-4	2.20E-7
	100	3.24	0.0069	2.08E-4	1.41E-7
	200	2.89	0.0076	1.82E-4	1.36E-7
	300	4.00	0.0054	2.85E-4	1.03E-7
	500	4.84	0.0043	2.65E-4	5.38E-7
	800	9.00	0.0022	2.79E-4	3.72E-7

Table 5.4: One-Dimensional Consolidation of Horizontally Laminated Foundation Soil Specimens

Parameter	Stress Range (kPa)	Specimen 1	Specimen 2
Wo(%)	-	39.4	34.2
Wf(%)	-	29.8	29.2
eo	-	1.107	1.140
ef	-	0.703	0.916
Sro(%)	-	104.3	84.0
Srf(%)	-	114.5	86.2
Pc'(kPa)+	-	365	550
Cc(lab)+	800-1600	0.588	0.482
Cr+	20-500	0.041	0.065
C +	100 200 300	0.0012 0.0034 -	- 0.0010 0.0030
t90(min)*	500 800	1.96 2.89	1.96 1.96
Cv(cm2/s)*	500 800	0.0098 0.0060	0.0102 0.0096
Mv(m2/kN)*	500 800	2.16E-4 1.71E-4	1.06E-4 1.10E-4
K(cm/s)*	500 800	2.08E-7 1.01E-7	1.06E-7 1.04E-7

+ Calculated based on void ratio
* Calculated based on deformations

Table 5.5: One-Dimensional Consolidation of Vertically Laminated Foundation Soil Specimens

Parameter	Stress Range (kPa)	Specimen 1	Specimen 2
Wo(%)	-	38.5	33.1
Wf(%)	-	-	-
eo	-	1.089	0.937
ef	-	0.794	0.708
Sro(%)	-	95.4	95.3
Srf(%)	-	-	-
Pc'(kPa)+	-	335	385
Cc(lab)+	800-1600	0.438	0.373
Cr+	20-500	0.054	0.013
C +	100 200	0.0017 0.0045	- -
t90(min)*	500 800	4.00 8.40	4.84 9.00
Cv(cm2/s)*	500 800	0.0050 0.0022	0.0043 0.0022
Mv(m2/kN)*	500 800	3.72E-4 3.77E-4	2.65E-4 2.79E-4
K(cm/s)*	500 800	7.31E-7 4.75E-7	5.38E-7 3.72E-7

+ Calculated based on void ratio
* Calculated based on deformations

Table 5.6: Times to Complete Consolidation Determined for Shelby Tube Foundation Soil Specimens

Specimen #	Load (kPa)	t_{90} (min)	t_{100} (min)
1	50	-	0.42
	100	-	0.33
	200	-	0.33
	300	-	0.50
	500	-	0.80
	800	-	0.80
2	50	-	-
	100	0.36	-
	200	0.49	-
	300	0.72	-
	500	0.72	-
	800	1.00	-
3	50	0.15	-
	100	-	-
	200	0.13	-
	300	0.15	-
	500	0.18	-
	800	0.25	-

Table 5.7: One-Dimensional Consolidation of Shelby Tube Foundation Soil Specimens

Parameter	Stress Range (kPa)	Specimen 1	Specimen 2	SAMPLE 3
Wo(%)	-	29.4	33.2	25.2
Wf(%)	-	33.9	25.2	23.1
eo	-	1.000	0.962	0.939
ef	-	0.840	0.683	0.628
Sro(%)	-	93.9	93.2	82.0
Srf(%)	-	109.0	107.7	100.0
Pc'(kPa)+	-	480	330	440
Cc(lab)+ Cc(field)+ Cc(field)+ Cc(field)+	500-1500 480-6455 330-9000 440-9748	0.462 0.499 - -	0.260 - 0.312 -	0.309 - - 0.386
Cr+	5-50 50-300	0.005 0.019	0.007 0.012	0.031 0.017
C +	100 200 300 500 800	0.006 0.004 0.002 0.009 0.012	0.002 0.004 0.005 0.006 0.007	- - - - -
t90(min)*	500 800	1.10 1.69	0.72 1.21	0.69 0.81
Cv(cm2/s)*	500 800	0.018 0.012	0.027 0.019	0.028 0.023
Mv(m2/kN)*	500 800	8.70E-5 1.20E-4	8.66E-5 7.14E-5	7.72E-5 8.54E-5
K(cm/s)*	500 800	1.51E-7 1.42E-7	2.29E-7 1.33E-7	2.14E-7 1.92E-7

+ Calculated based on void ratio
* Calculated based on deformations
Note: Secondary consoldiation of specimen 3 was not allowed

Table 5.8: Data from CU Triaxial Tests Conducted on Shelby Tube Foundation Soil Specimens

Specimen	CU1	CU2	CU3	CU4	CU5	CU6	CU7	CU8
Tube Number	44-2	22-2	44-1	42	6	4	64	22-1
Depth (m)	3.25	2.95	3.25	2.50	3.45	2.50	3.50	2.95
Cell Press. (kPa)	19	25	57	100	197	250	294	300
Back Press. (kPa)	400	400	400	400	400	350	400	400
Wo(%)	34.5	38.1	38.1	35.8	35.3	39.4	35.3	37.4
Wf(%)	32.2	33.1	36.8	32.7	33.3	28.6	29.6	30.1
Pd(g/cm)	1.401	1.271	1.327	1.377	1.369	1.387	1.380	1.305
e	0.928	1.124	1.035	0.961	0.972	0.947	0.957	1.067
Sr(%)	100.4	91.5	99.4	100.6	98.1	99.5	99.4	94.5
$(\sigma_1-\sigma_3)f$ (kPa)	44.4	82.6	96.4	157.6	102.9	291.1	169.1	247.1
$(\sigma_1'/\sigma_3')f$	6.16	3.86	2.75	3.79	1.80	3.59	1.79	3.66
Uf(kPa)	10.0	-3.9	1.7	43.5	69.4	135.1	80.1	207.1
$\varepsilon f(\%)$	3.4	5.0	5.2	7.4	8.1	11.4	7.4	8.4
B	1.0	1.0	1.0	1.0	1.0	1.0	-	1.0
A	0.225	-0.047	0.018	0.276	0.674	0.464	0.474	0.838

Table 5.9: Data from CU Triaxial Tests Conducted on Foundation Soil Block Specimens

Specimen	CU9	CU10	CU11	CU12
Cell Press. (kPa)	16	60	182	275
Back Press. (kPa)	300	300	300	300
Wo(%)	-	35.5	36.4	37.1
Wf(%)	38.1	37.3	36.6	37.4
Pd(g/cm)	-	1.346	1.326	1.316
e	-	1.006	1.037	1.052
Sr(%)	-	95.3	95.3	95.2
$(\sigma_1 - \sigma_3)f$ (kPa)	66.7	121.0	156.8	239.0
$(\sigma_1'/\sigma_3')f$	-	-	-	-
Uf(kPa)	11.6	33.3	124.5	197.7
$\varepsilon f(\%)$	2.9	2.1	6.9	1.5
B	1.0	1.0	1.0	1.0
A	0.174	0.275	0.794	0.827

Table 5.10: Data from CU Triaxial Tests Conducted on Foundation Tube Specimens from BH 28

Specimen	CU13	CU14	CU15
Cell Press. (kPa)	103	310	518
Back Press. (kPa)	207	207	207
Wo(%)	16.3	20.9	25.6
Wf(%)	33.3	32.2	28.6
Pd(g/cm)	1.597	1.674	1.859
e	1.603	1.699	1.894
Sr(%)	46.0	59.0	84.0
$(\sigma_1 - \sigma_3)f$ (kPa)	165	260	427
Uf(kPa)	40	214	363
$\varepsilon f(\%)$	8.3	8.9	8.1
B	0.42	0.30	0.47
A	0.242	0.823	0.850

Table 5.11: Frictional and Cohesive Strength Parameters Obtained from CU Triaxial Tests Conducted on Foundation Soil Specimens

Specimen Type	C (kPa)	ϕ (degrees)	C′ (kPa)	ϕ' (degrees)
Block				
range	25.0-26.7	13.0-13.0	23.0-25.3	24.0-24.8
design	25.0	13.0	23.0	24.0
Tube				
range	10.0-11.6	15.0-18.0	6.0-16.5	33.0-24.4
design	10.0	15.0	6.0	33.0
Tube (AB.T.U)				
range	28.0-30.0	15.5-15.0	0.0-0.0	31.0-31.0
design	30.0	15.0	0.0	31.0

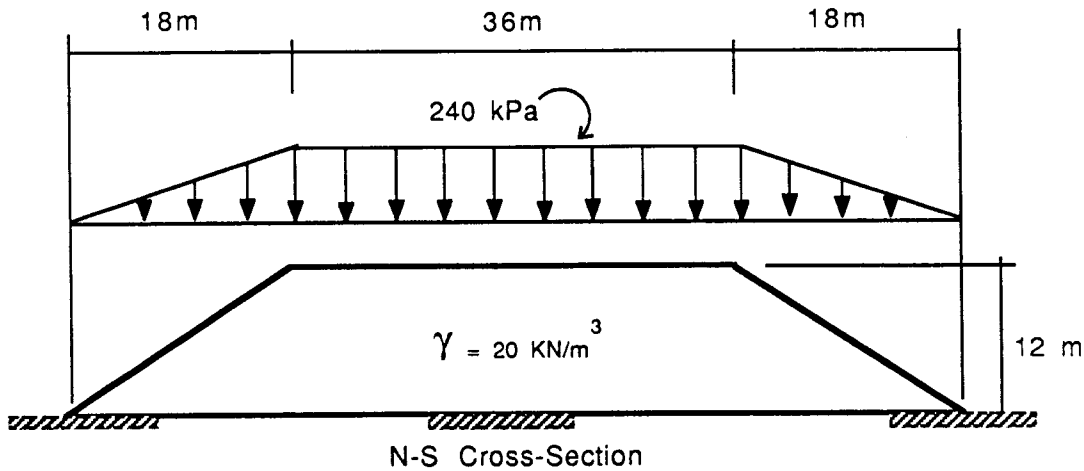

N-S Cross-Section

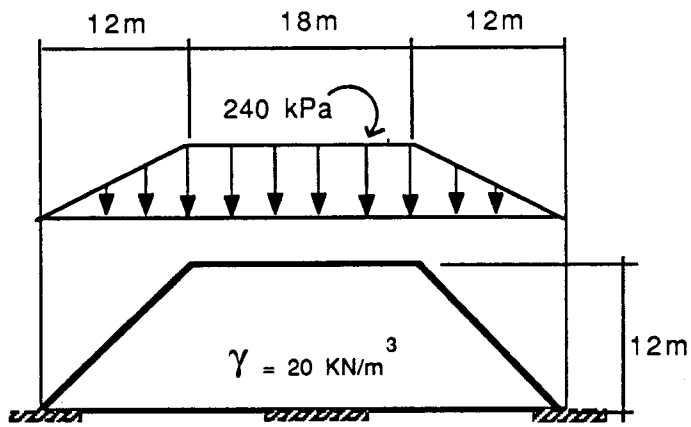

E-W Cross-Section

Figure 5.1: Surcharge Stresses Acting on Foundation Soil Due to the Weight of the Test Fill

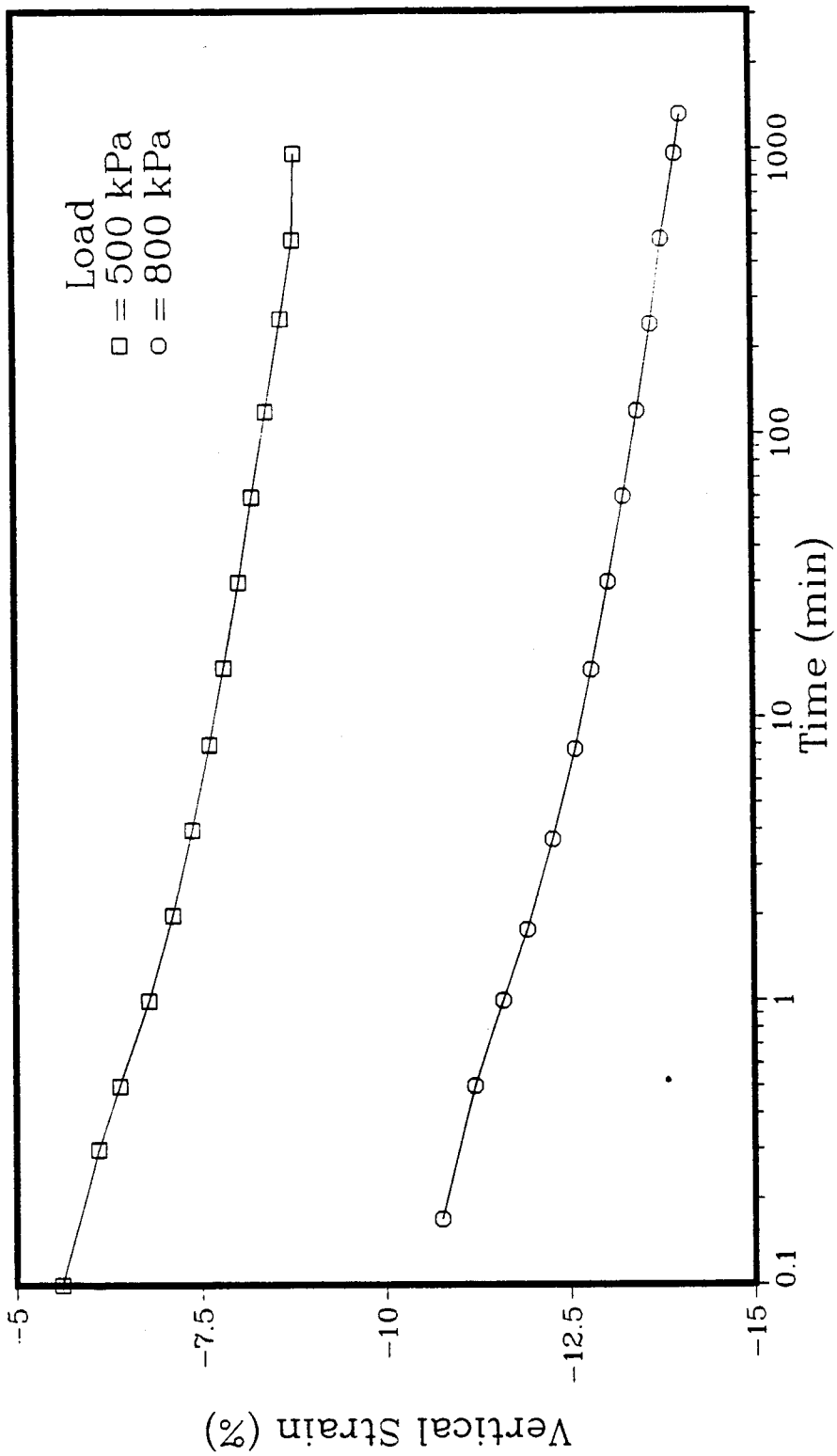

Figure 5.2: Consolidation of Horizontally Laminated Block Specimen #1

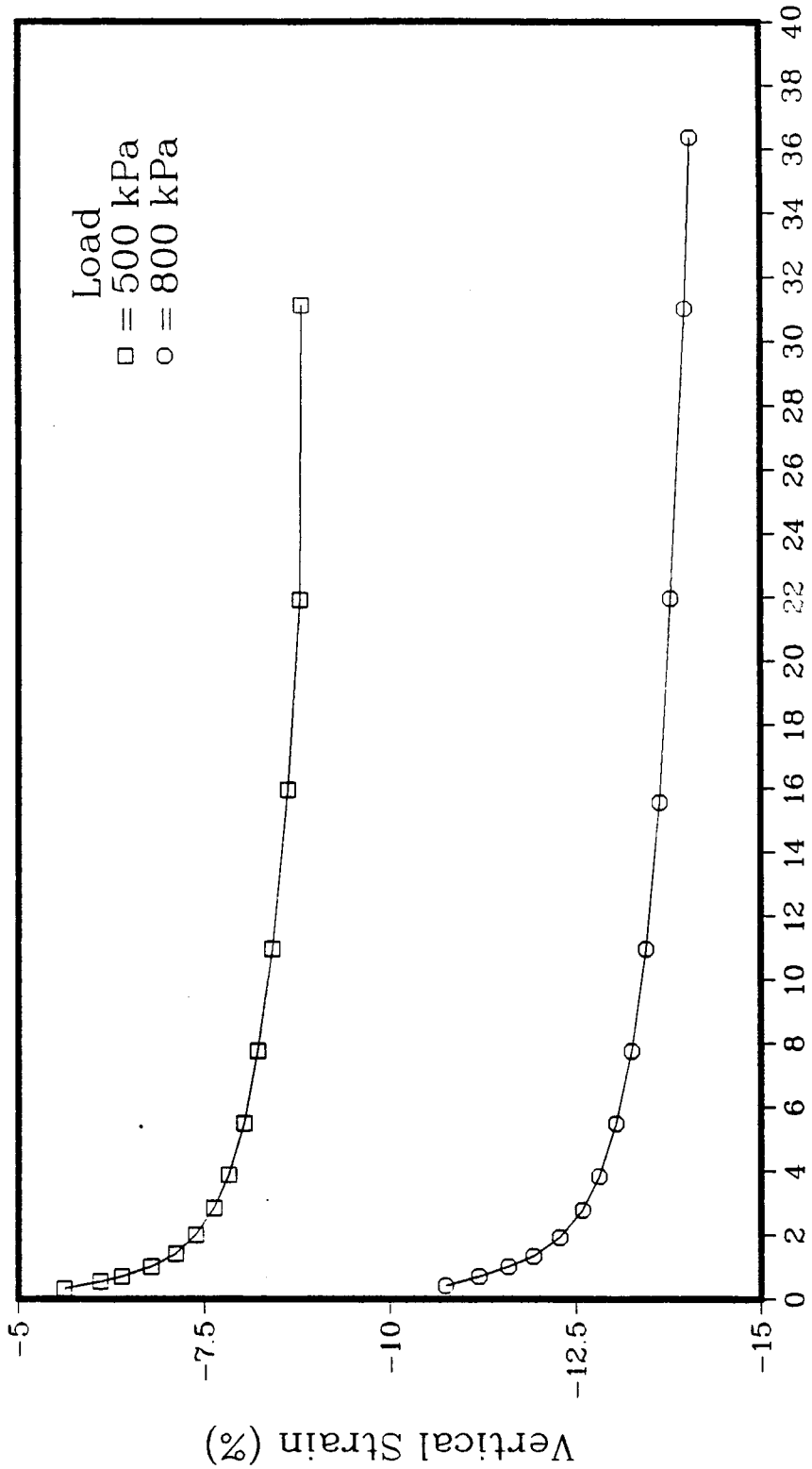

Figure 5.3: Consolidation of Horizontally Lamimated Block Specimen #1

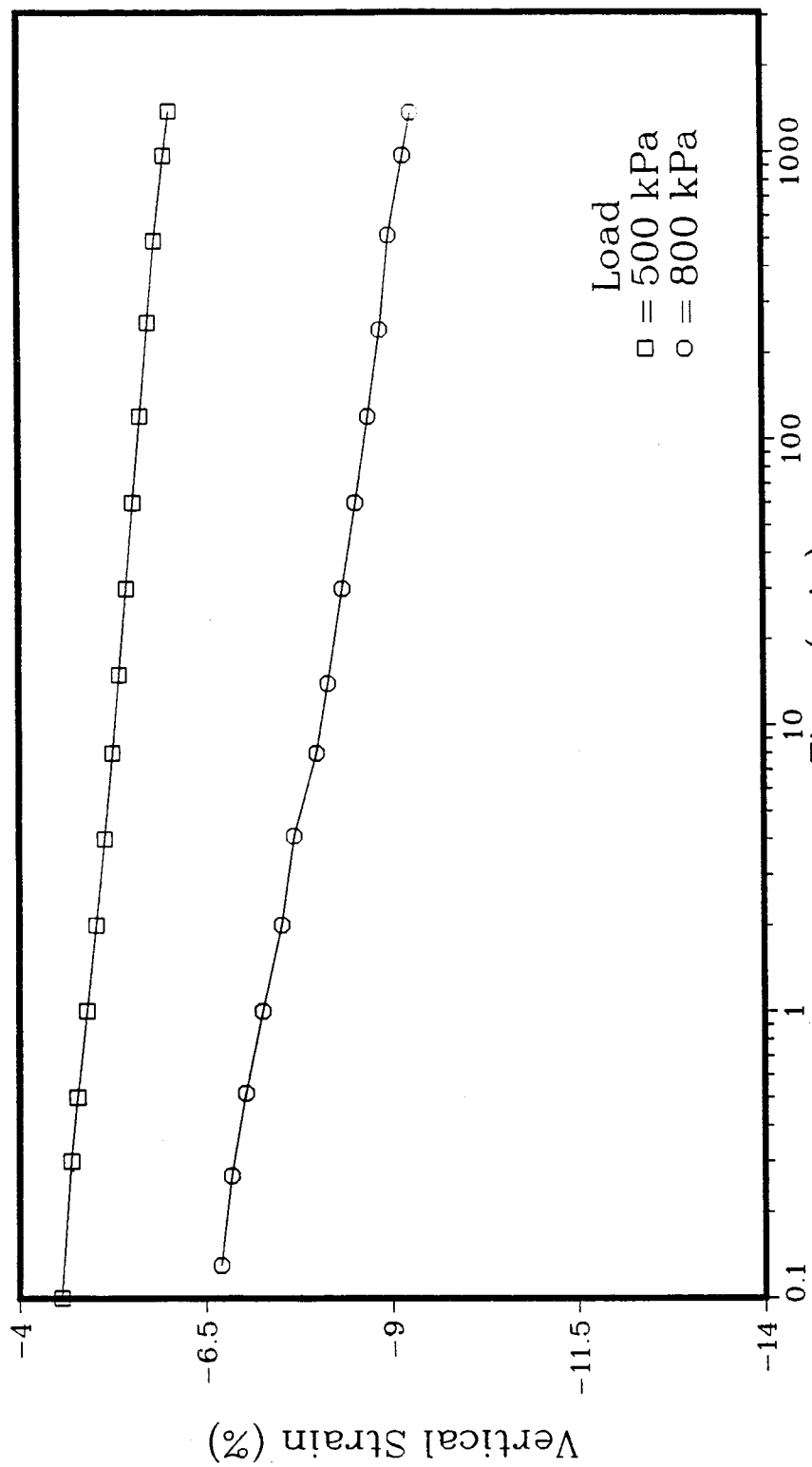

Figure 5.4: Consolidation of Horizontally Laminated Block Specimen #2

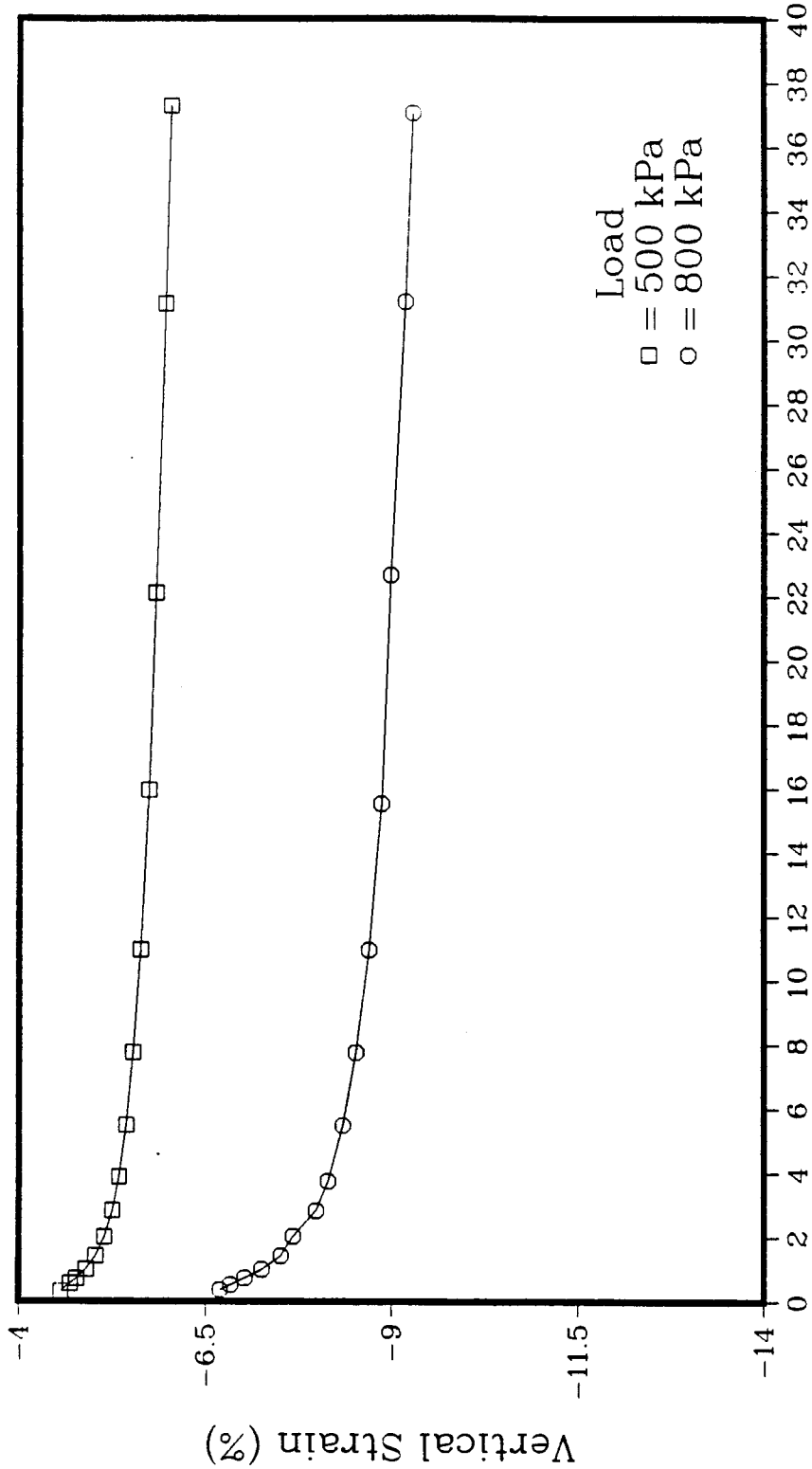

Figure 5.5: Consolidation of Horizontally Laminated Block Specimen #2

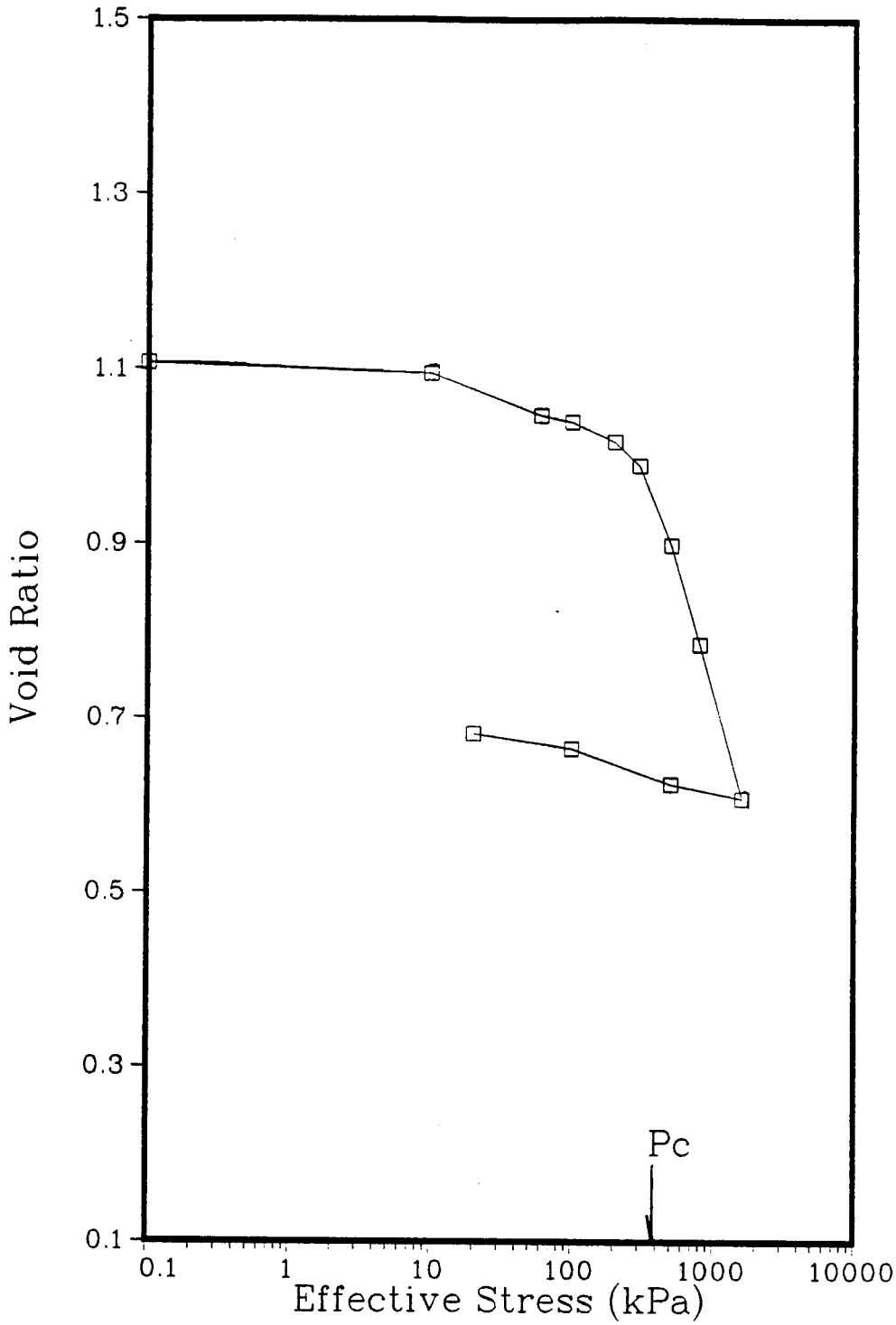

Figure 5.6: Consolidation of Horizontally Laminated Block Specimen #1

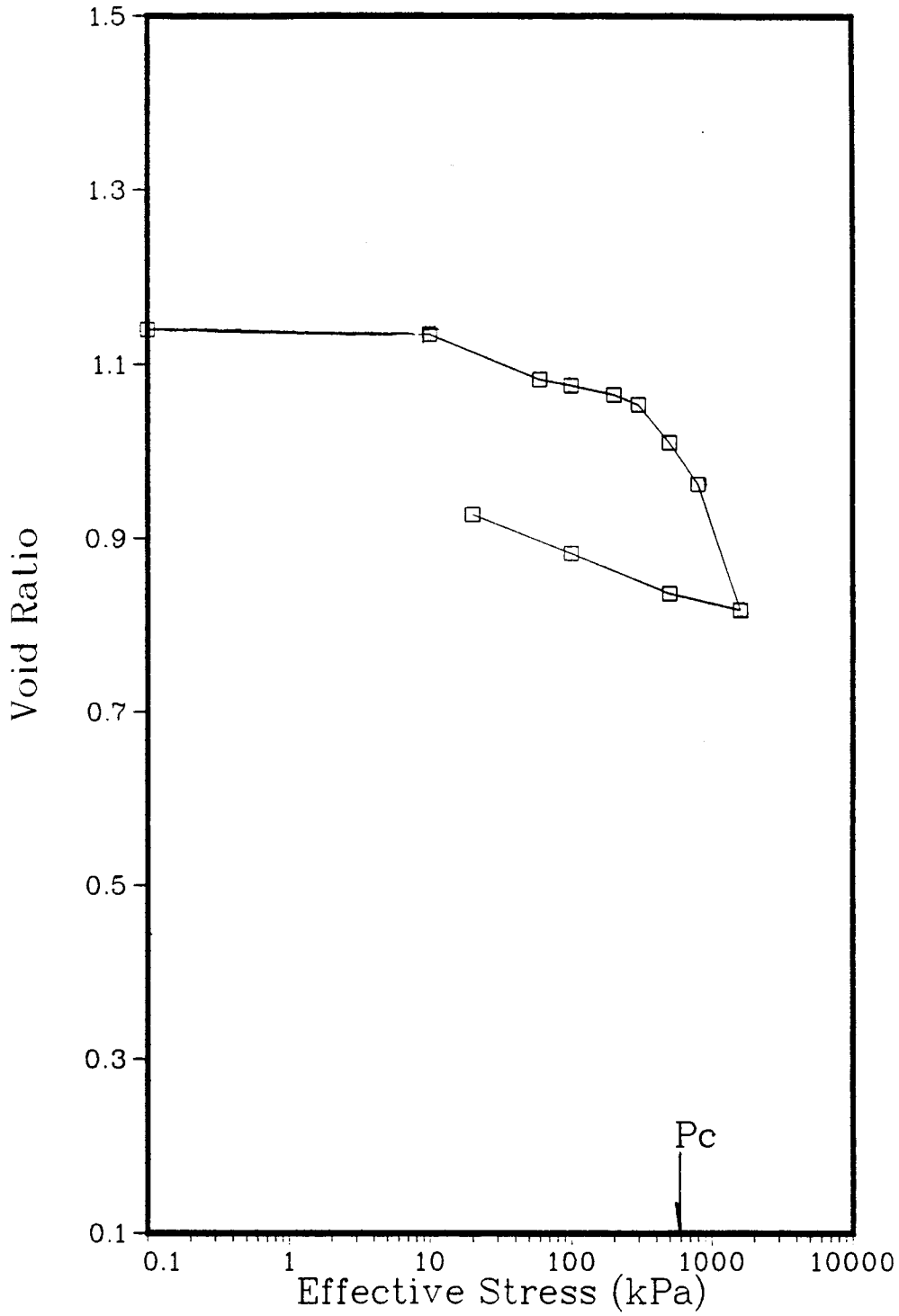

Figure 5.7: Consolidation of Horizontally Laminated Block Specimen #2

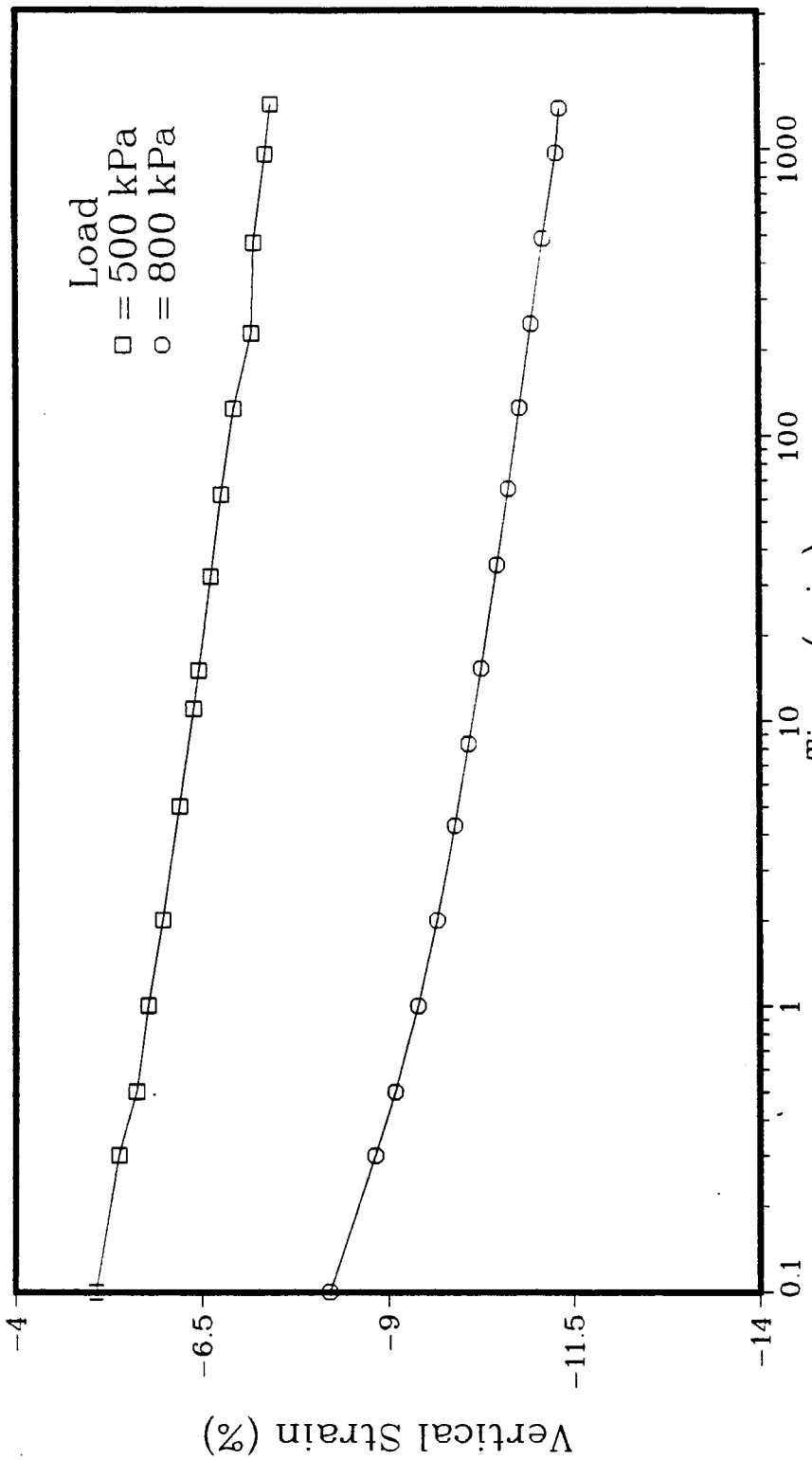

Figure 5.8: Consolidation of Vertically Laminated Block Specimen #1

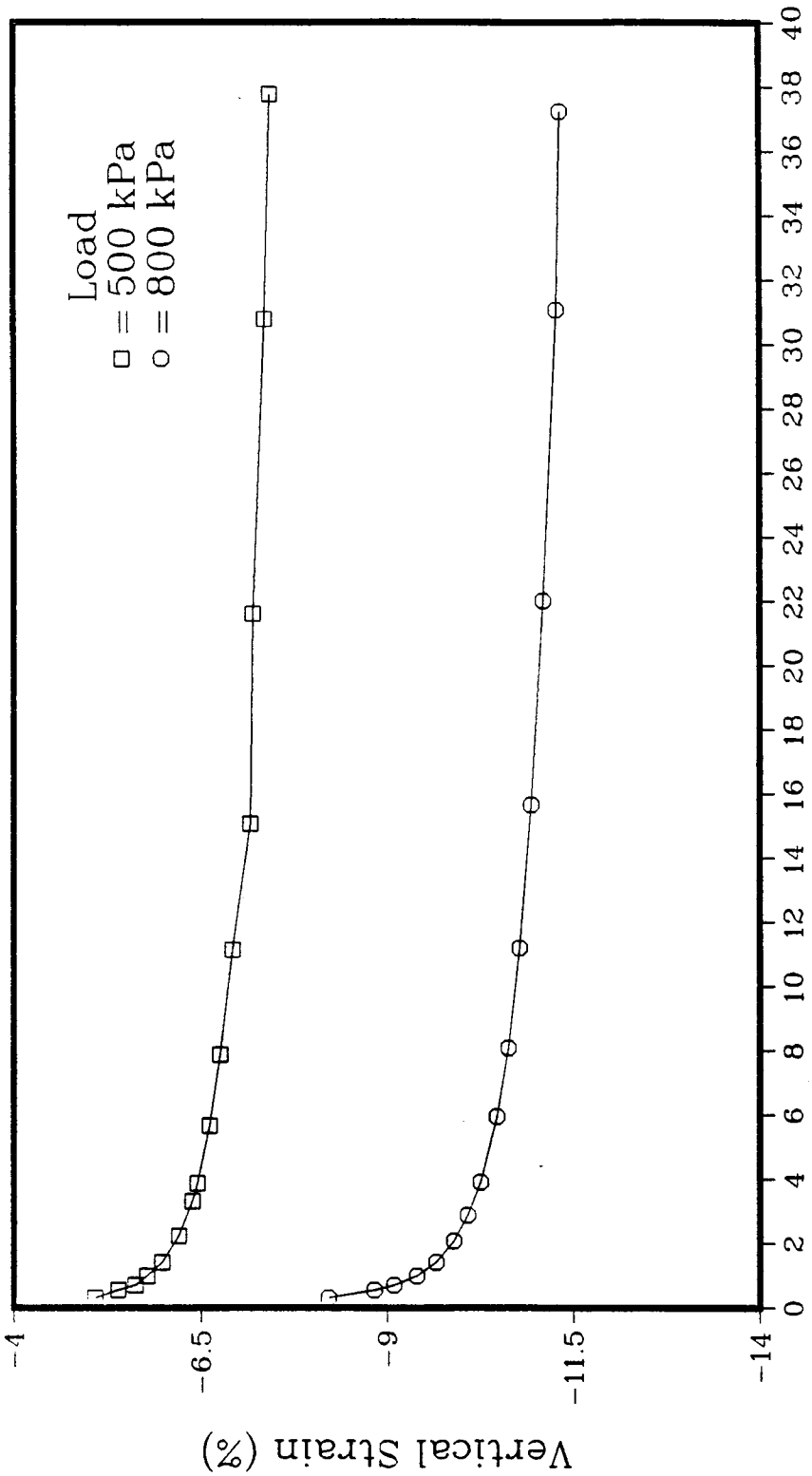

Figure 5.9: Consolidation of Vertically Laminated Block Specimen #1

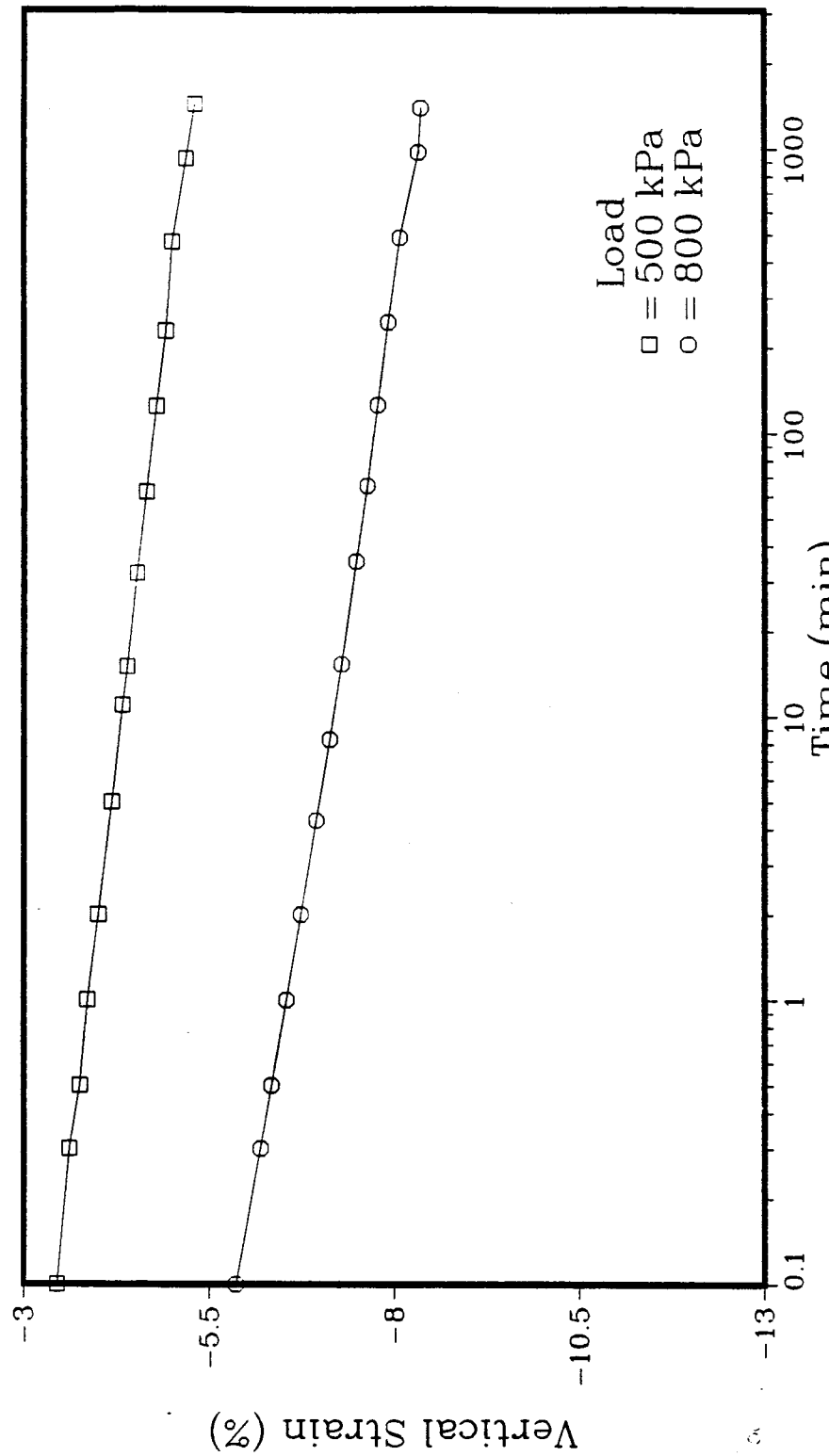

Figure 5.10: Consolidation of Vertically Laminated Block Specimen #2

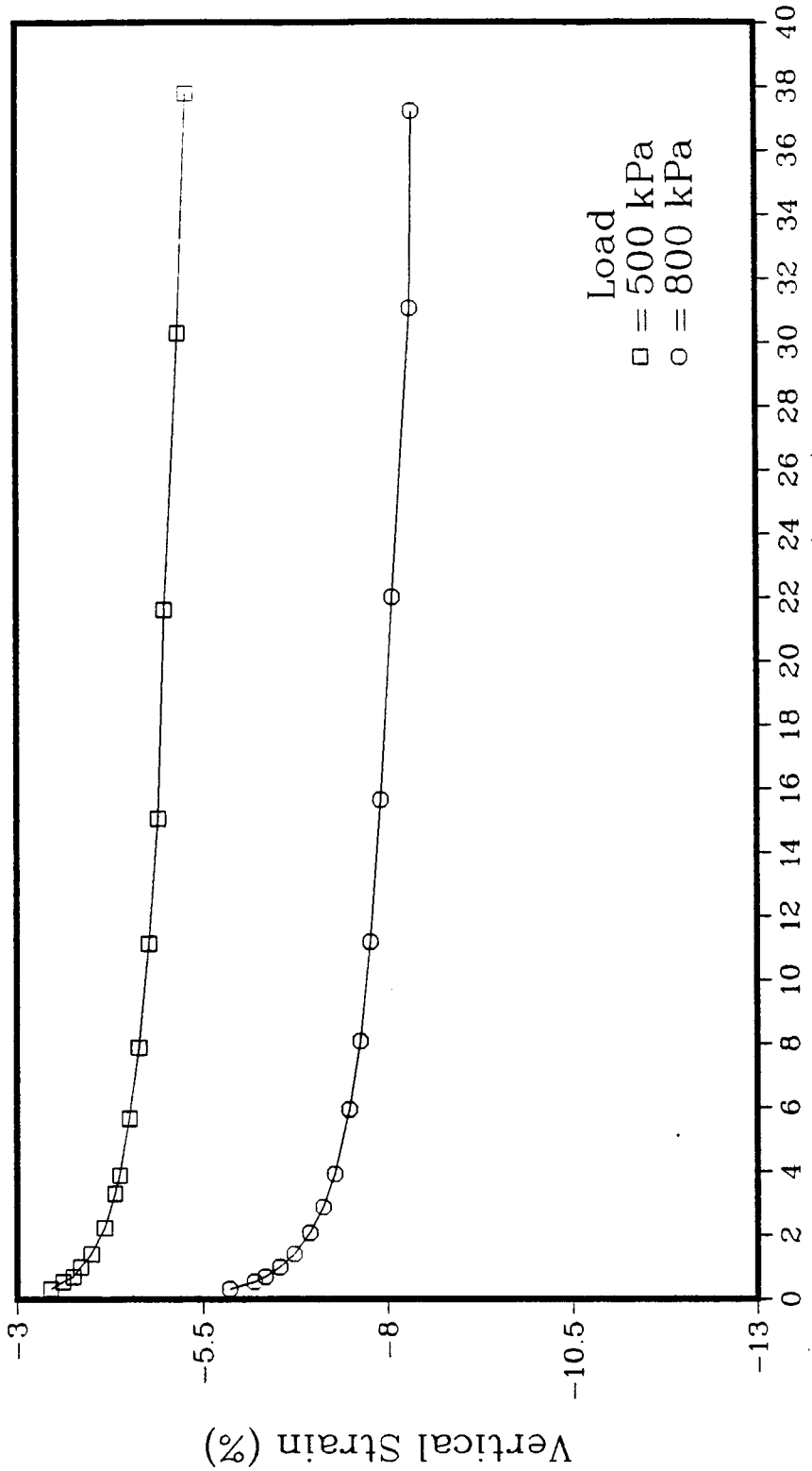

Figure 5.11: Consolidation of Vertically Laminated Block Specimen #2

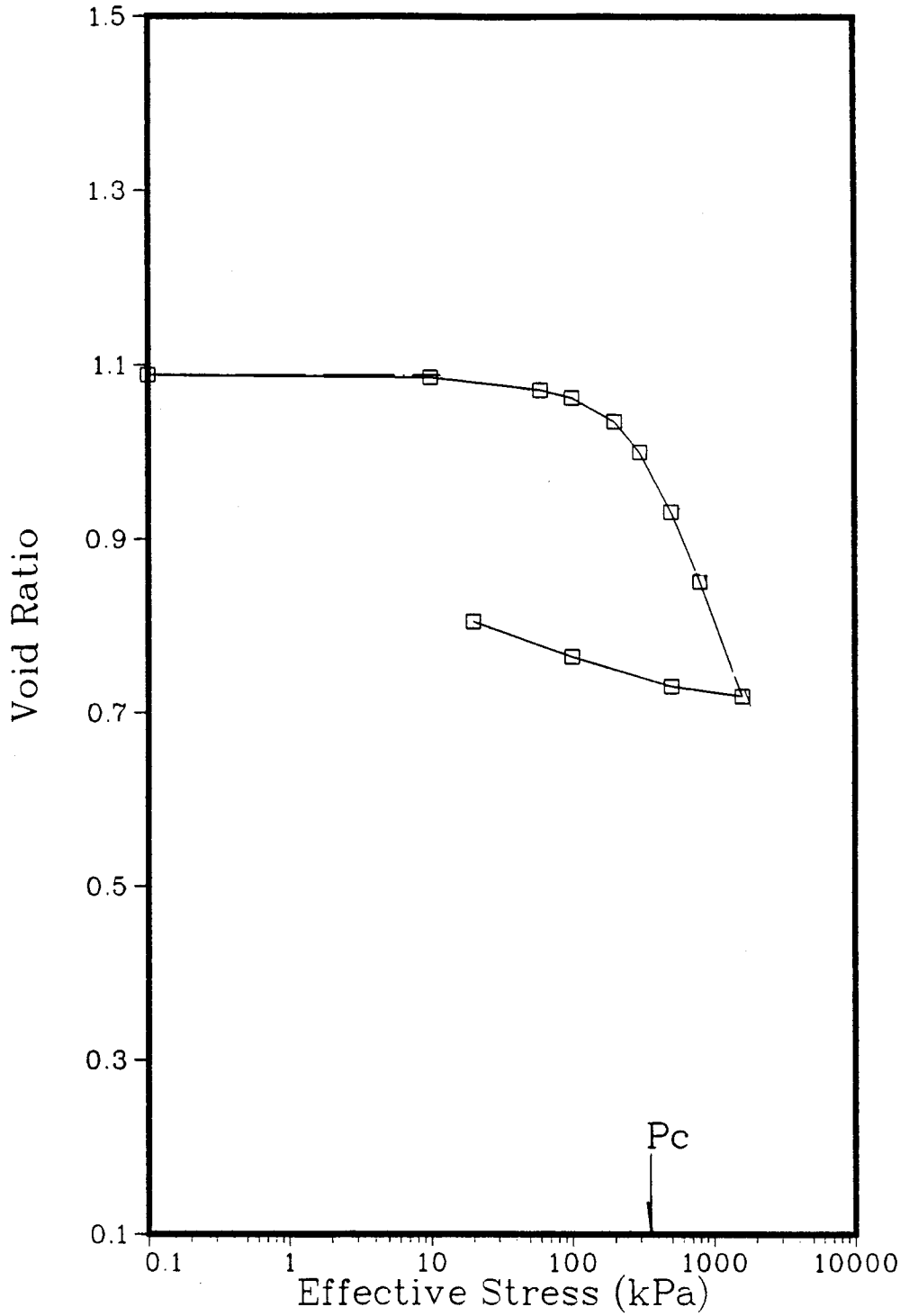

Figure 5.12: Consolidation of Vertically Laminated Block Specimen #1

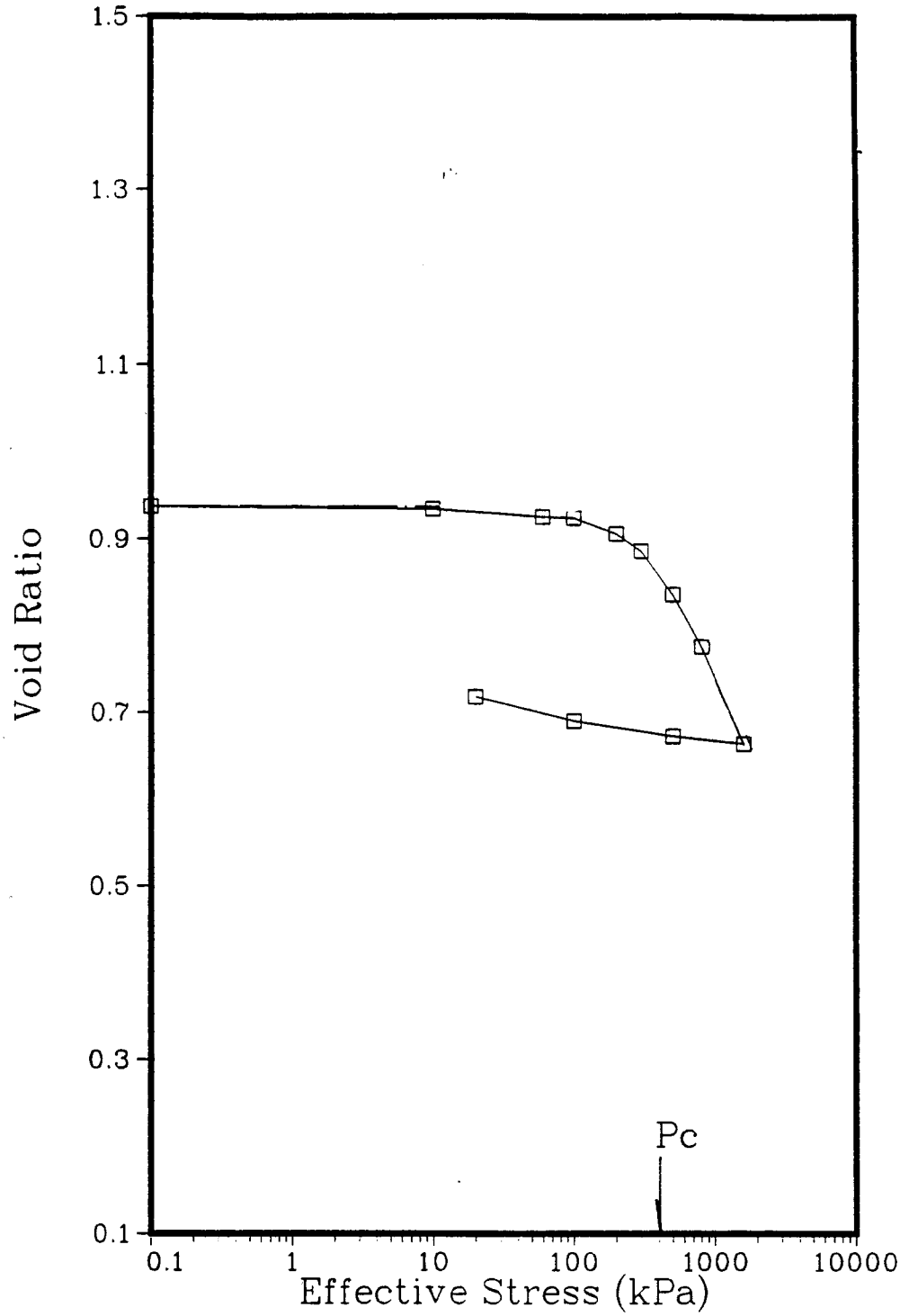

Figure 5.13: Consolidation of Vertically Laminated Block Specimen #2

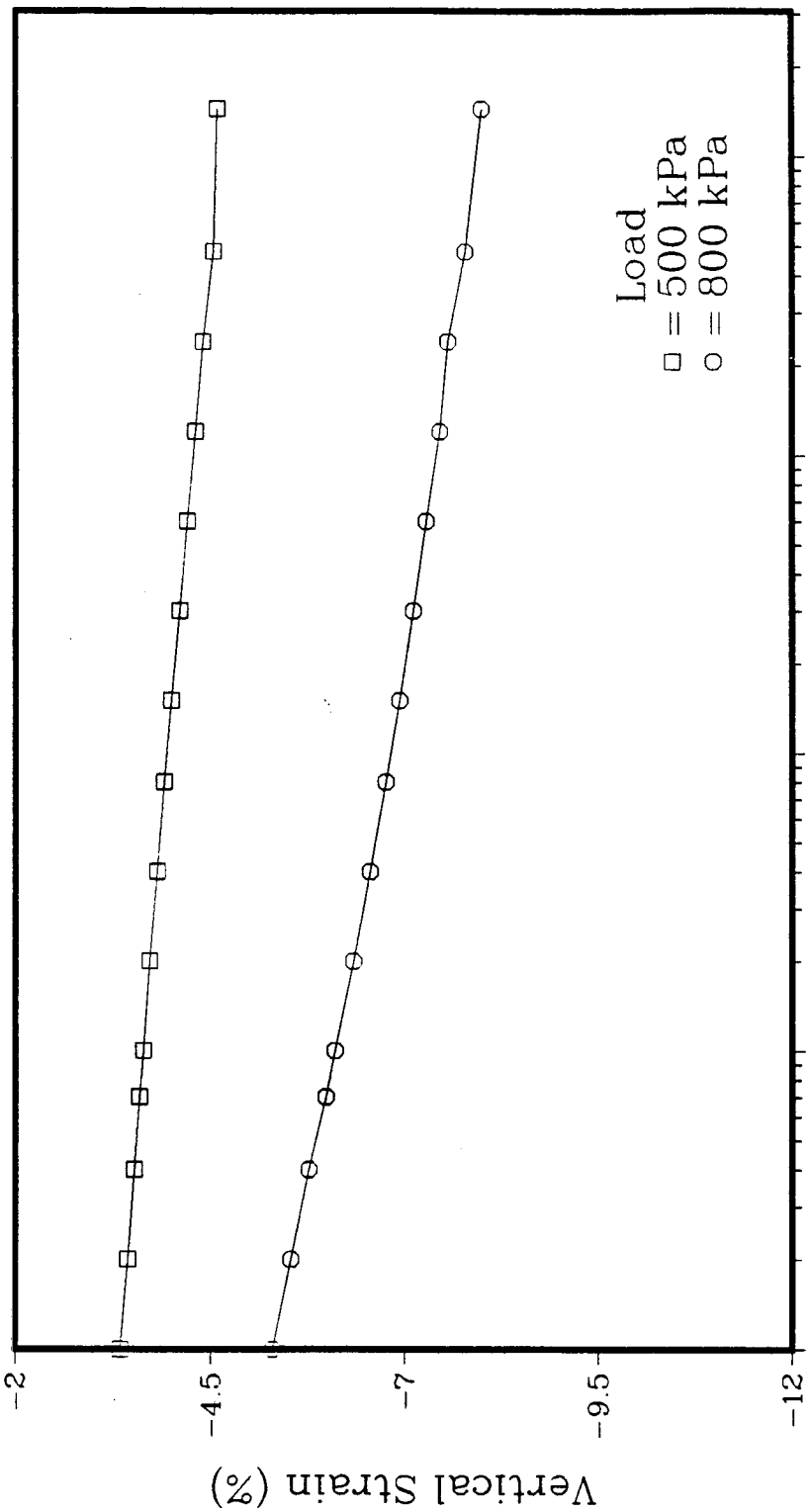

Figure 5.14: Consolidation of Shelby Tube Specimen #1

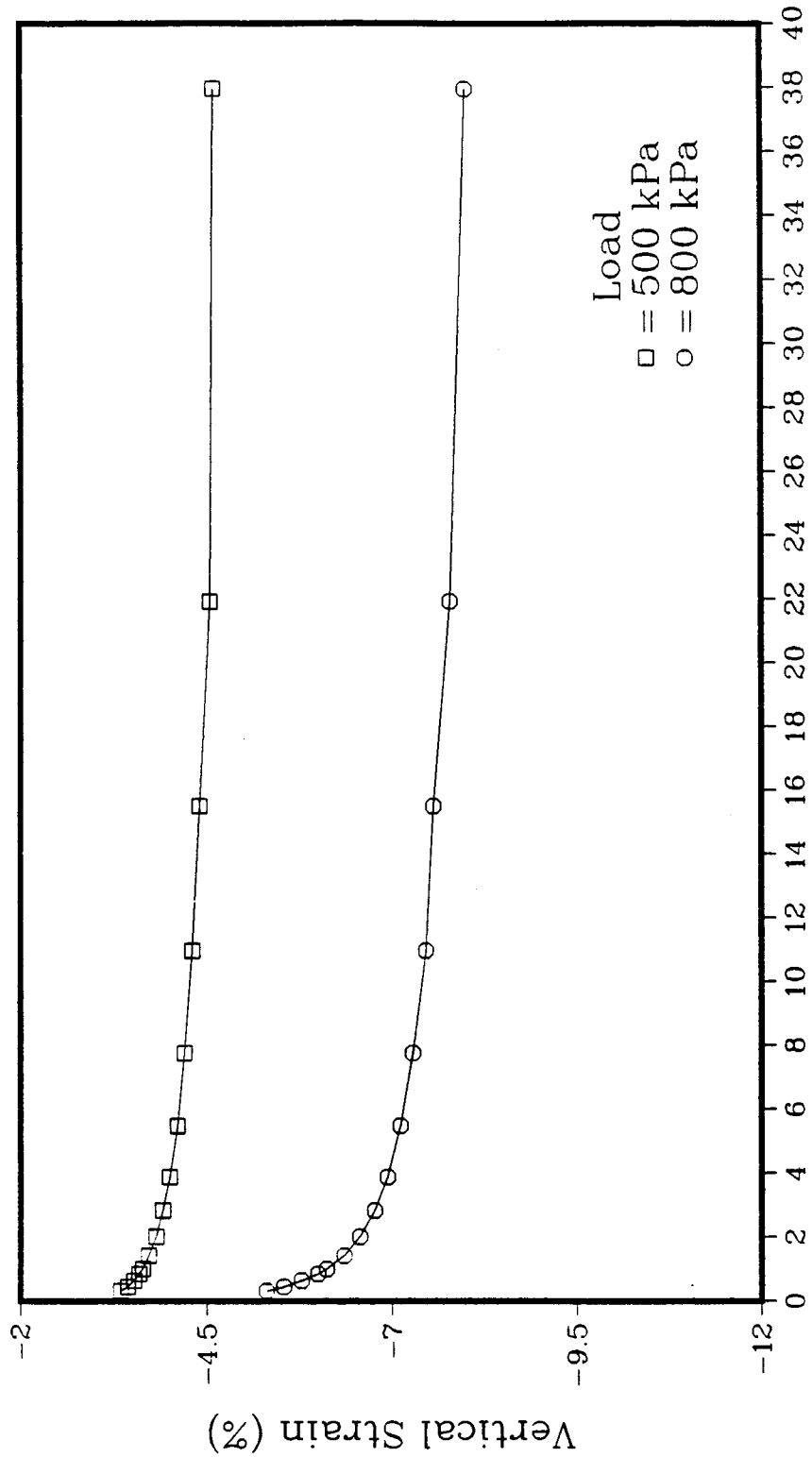

Figure 5.15: Consolidation of Shelby Tube Specimen #1

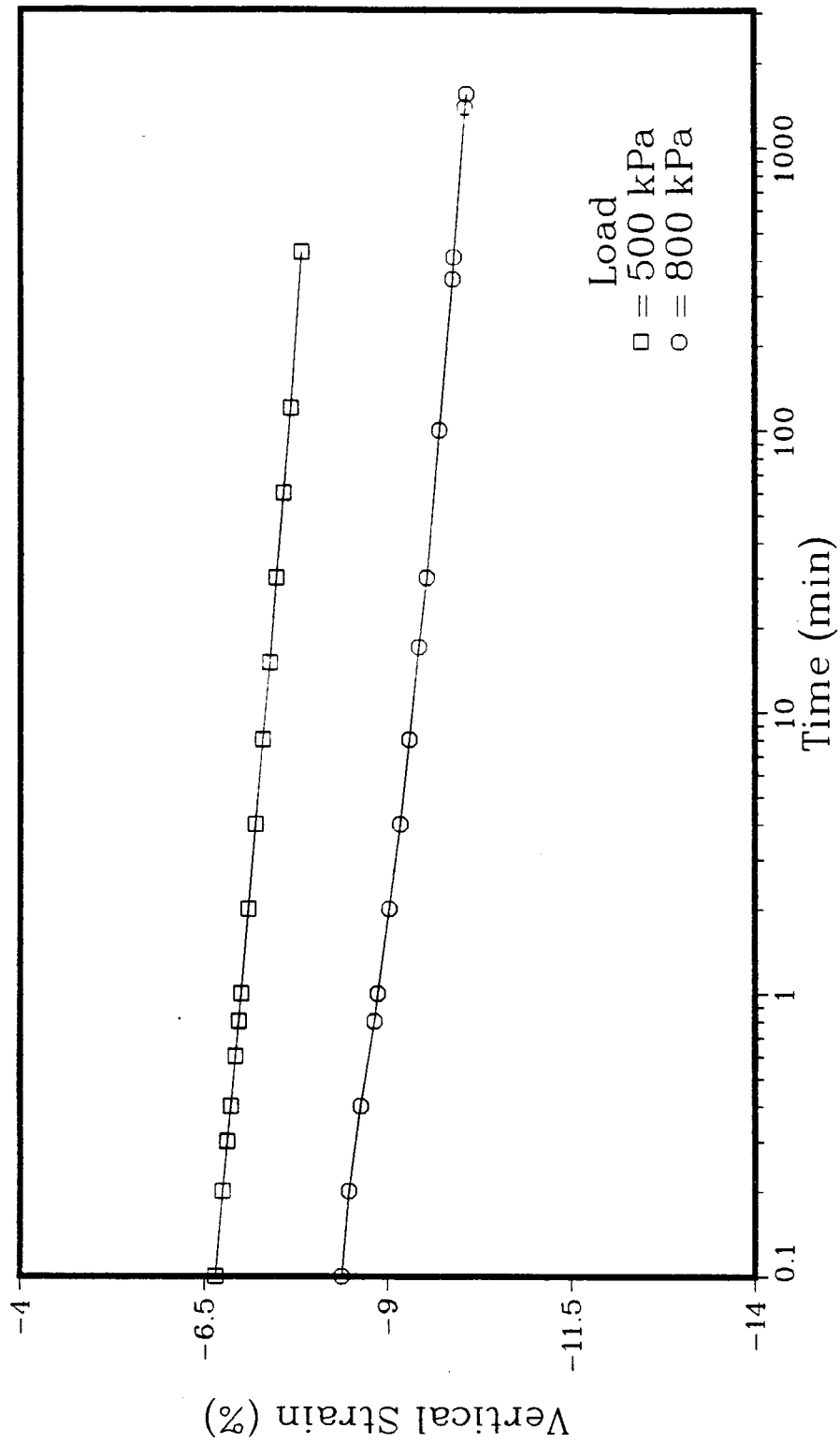

Figure 5.16: Consolidation of Shelby Tube Specimen #2

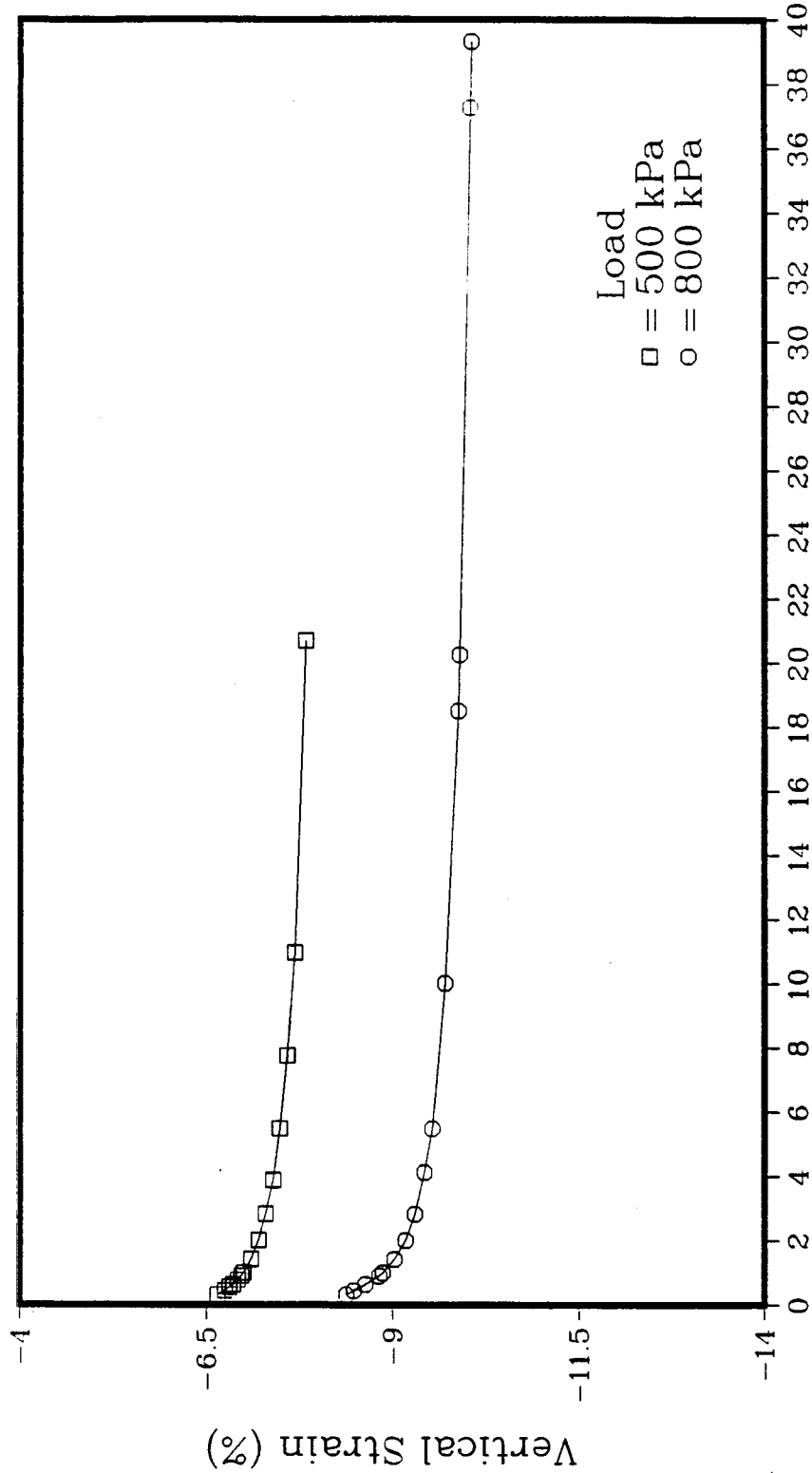

Figure 5.17: Consolidation of Shelby Tube Specimen #2

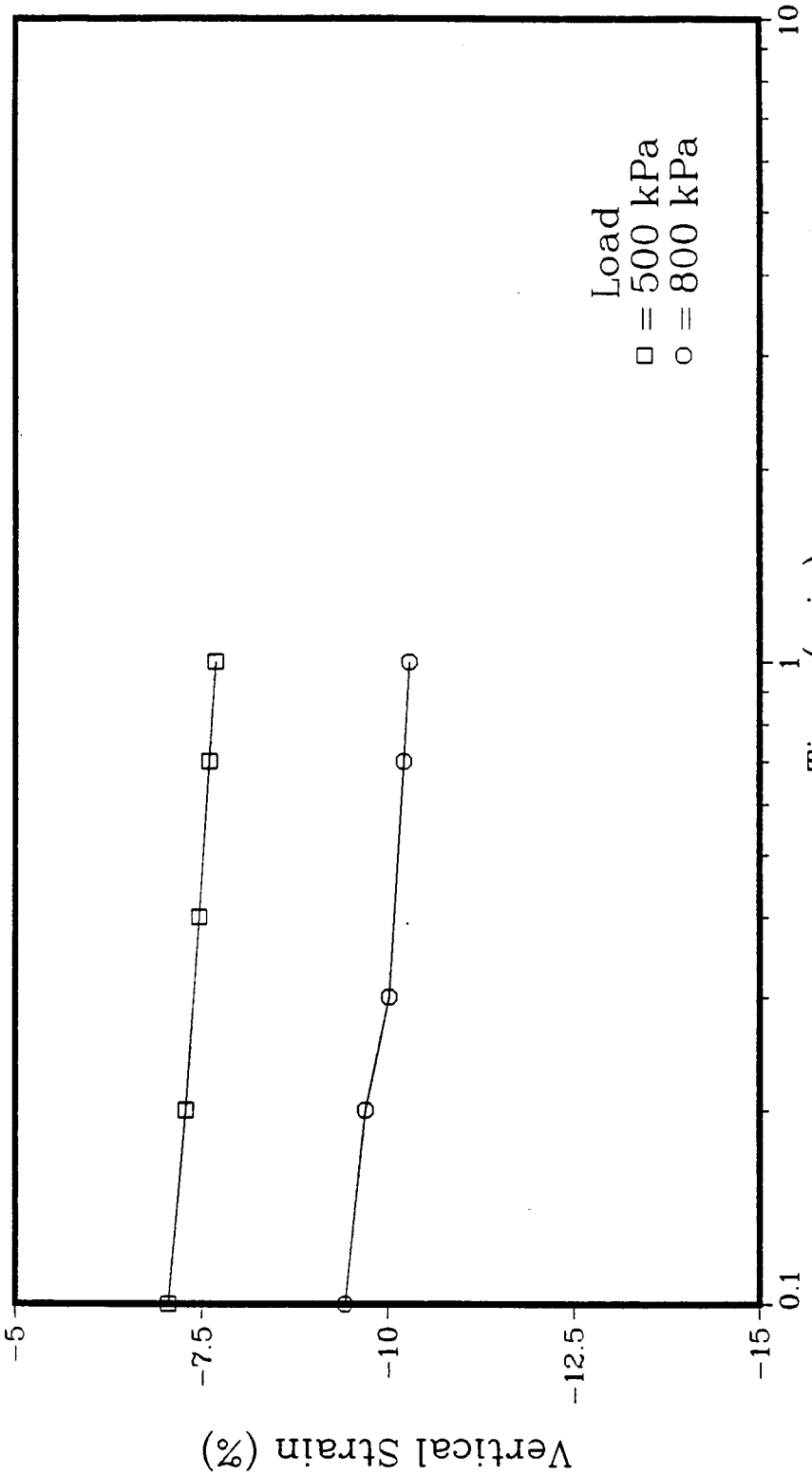

Figure 5.18: Primary Consolidation of Shelby Tube Specimen #3

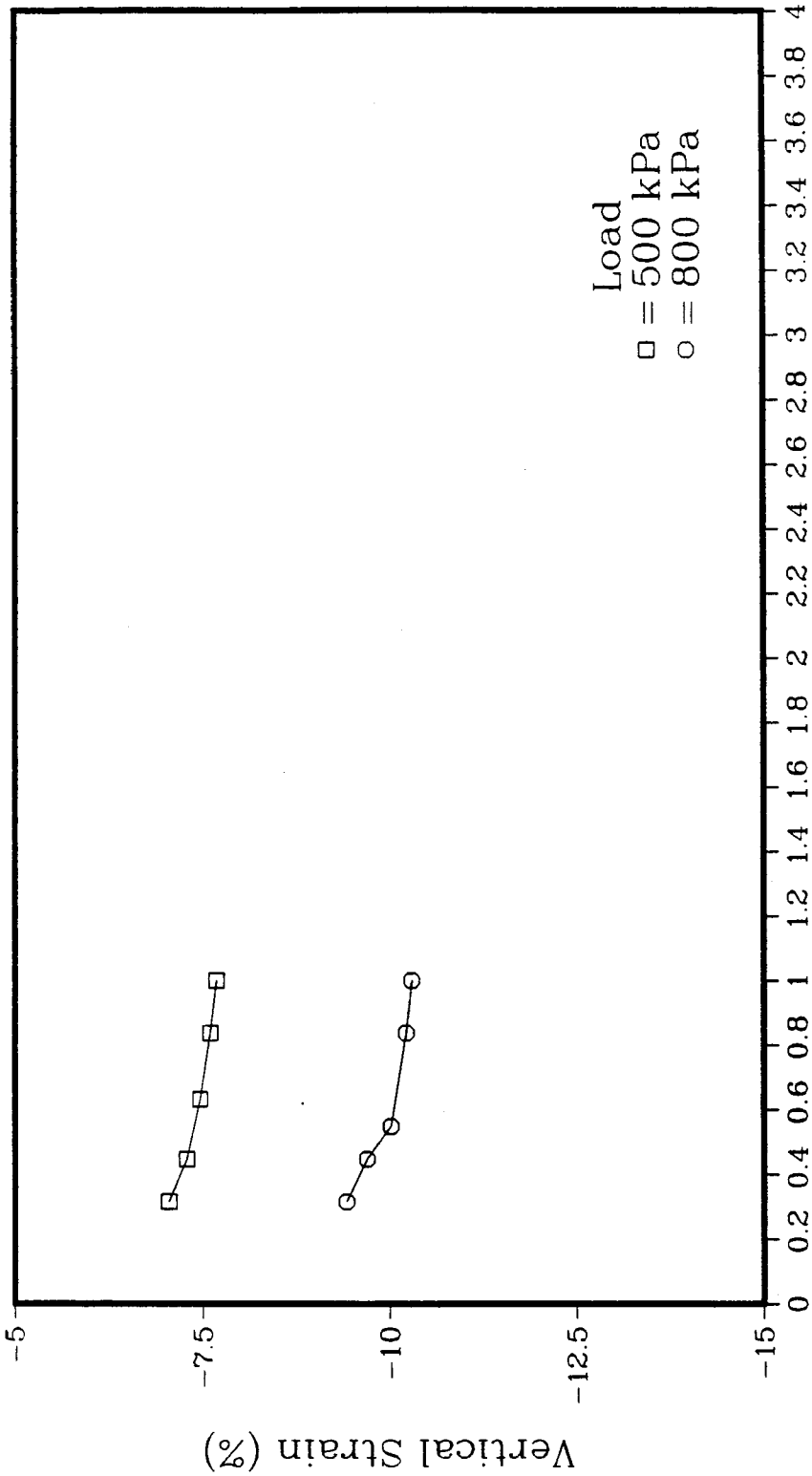

Figure 5.19: Primary Consolidation of Shelby Tube Specimen #3

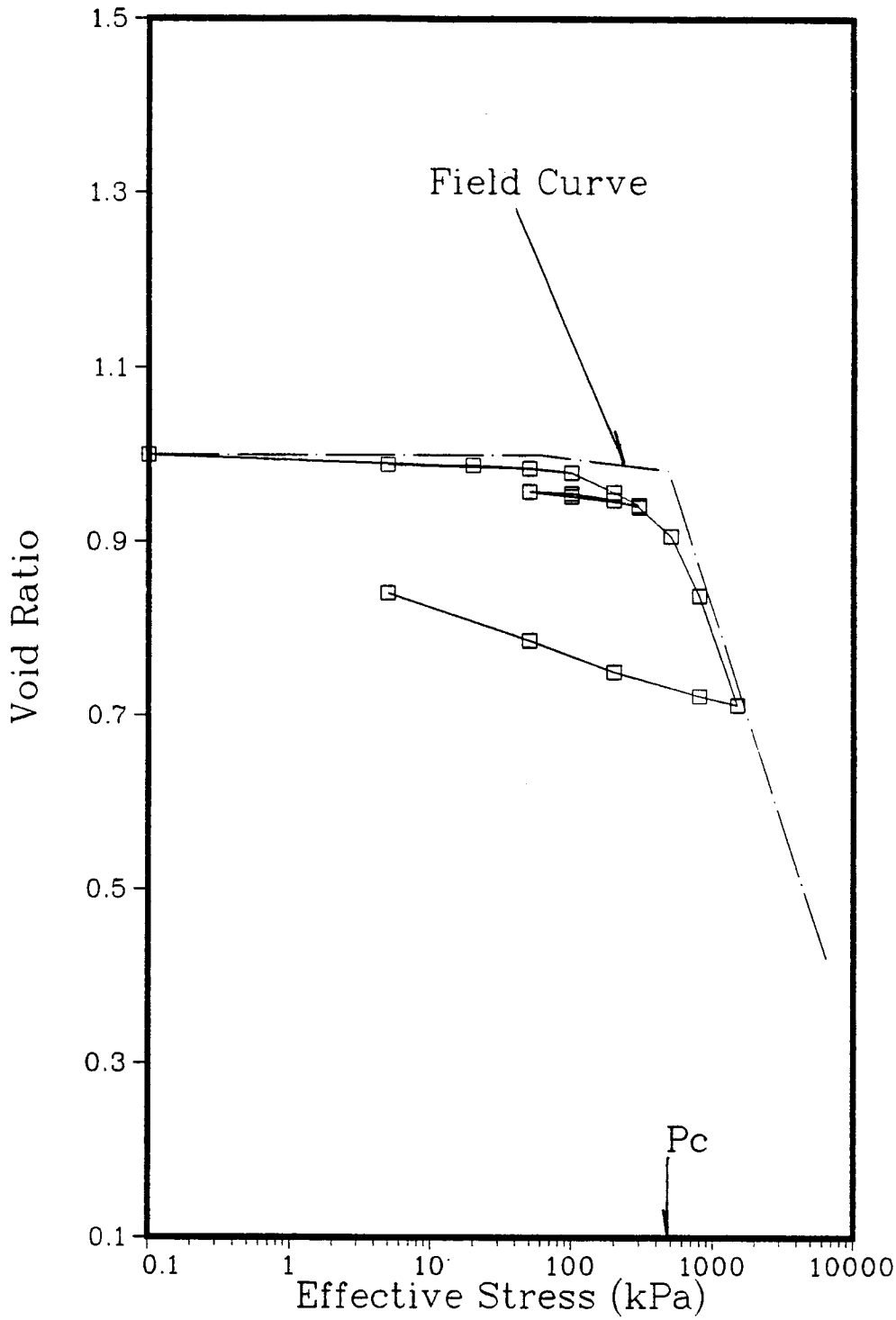

Figure 5.20: Consolidation of Shelby Tube Specimen #1

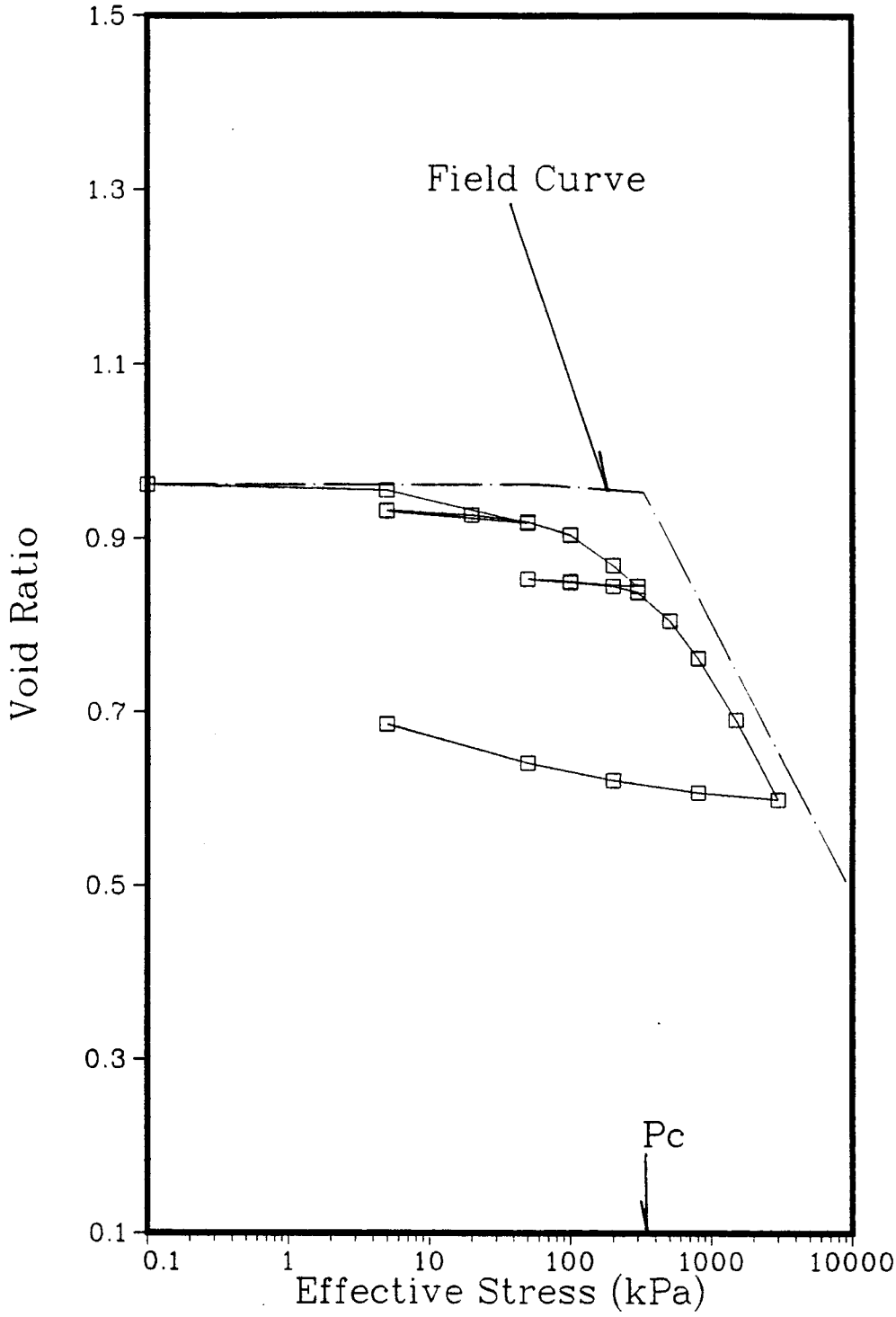

Figure 5.21: Consolidation of Shelby Tube Specimen #2

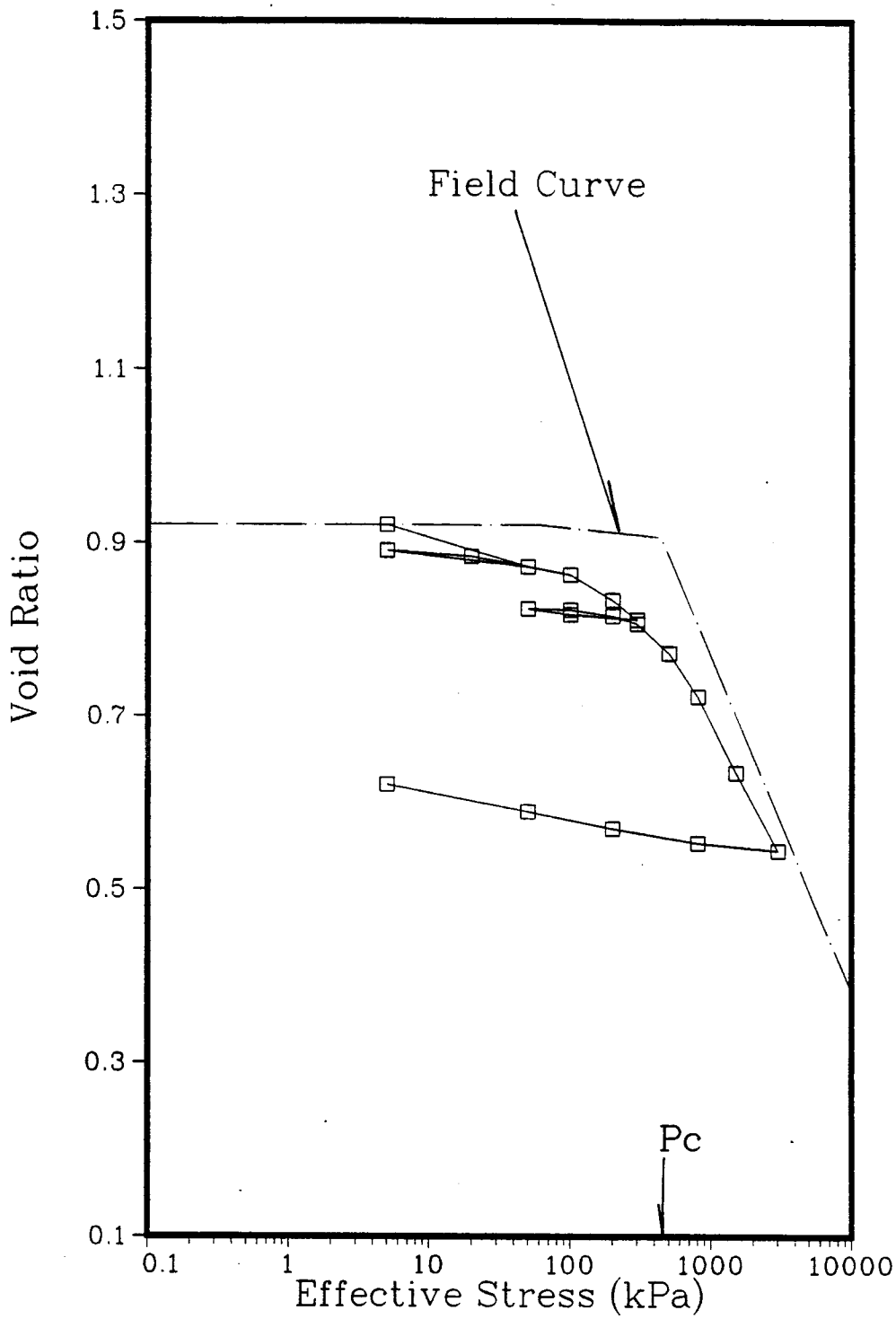

Figure 5.22: Consolidation of Shelby Tube Specimen #3

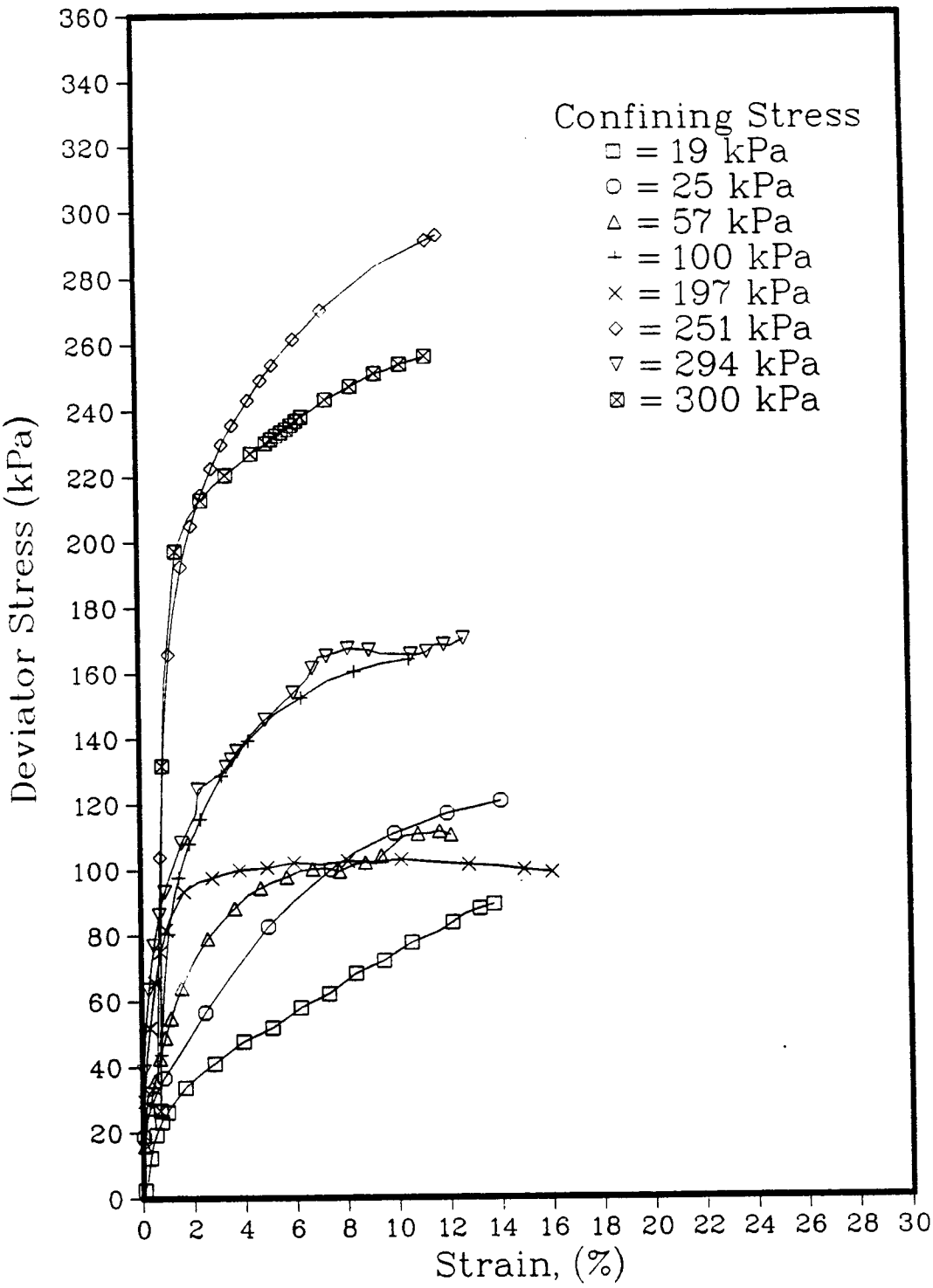

Figure 5.23: CU Triaxial Tests on Foundation Tube Specimens

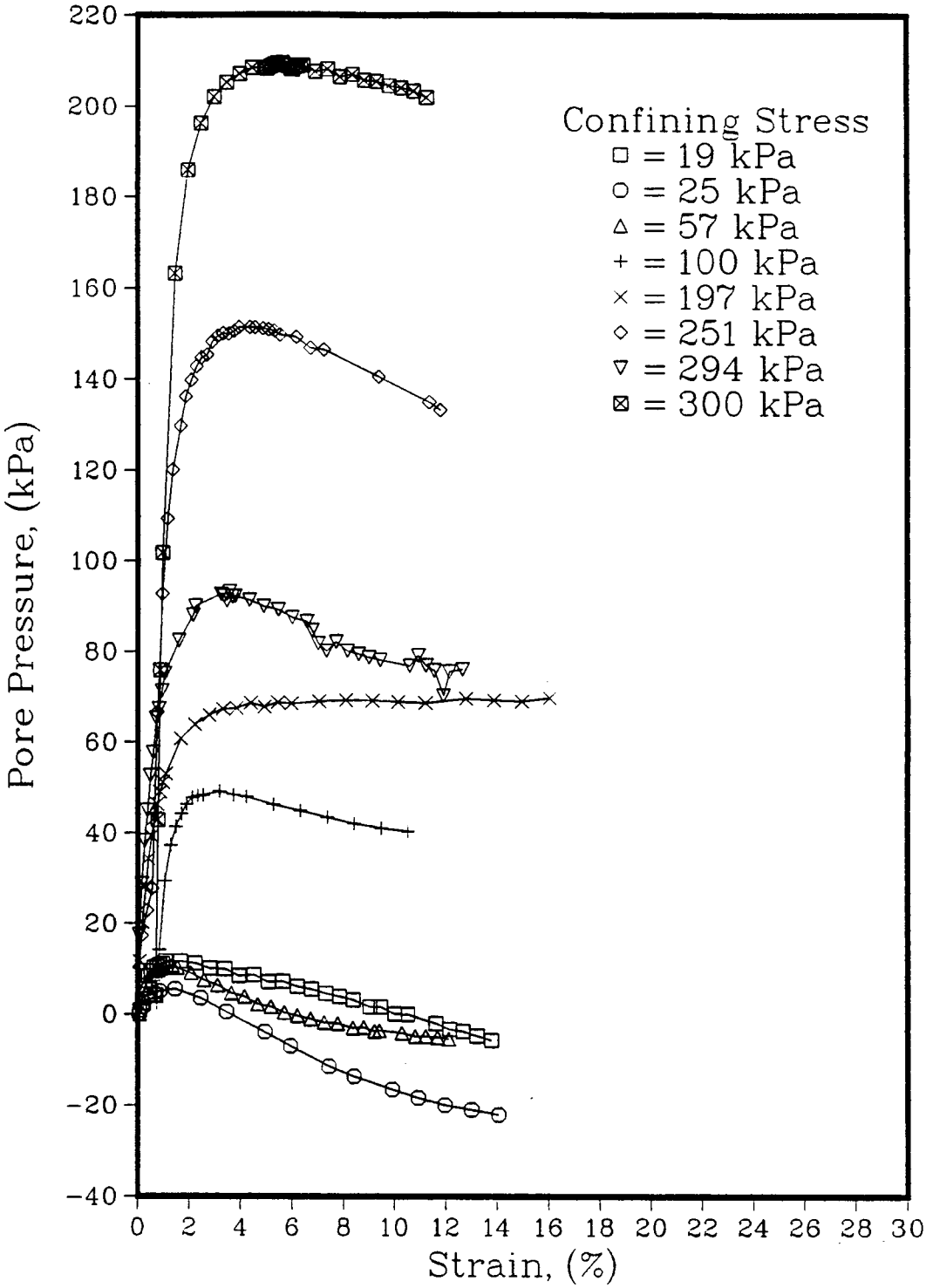

Figure 5.24: CU Traixial Tests on Foundation Tube Specimens

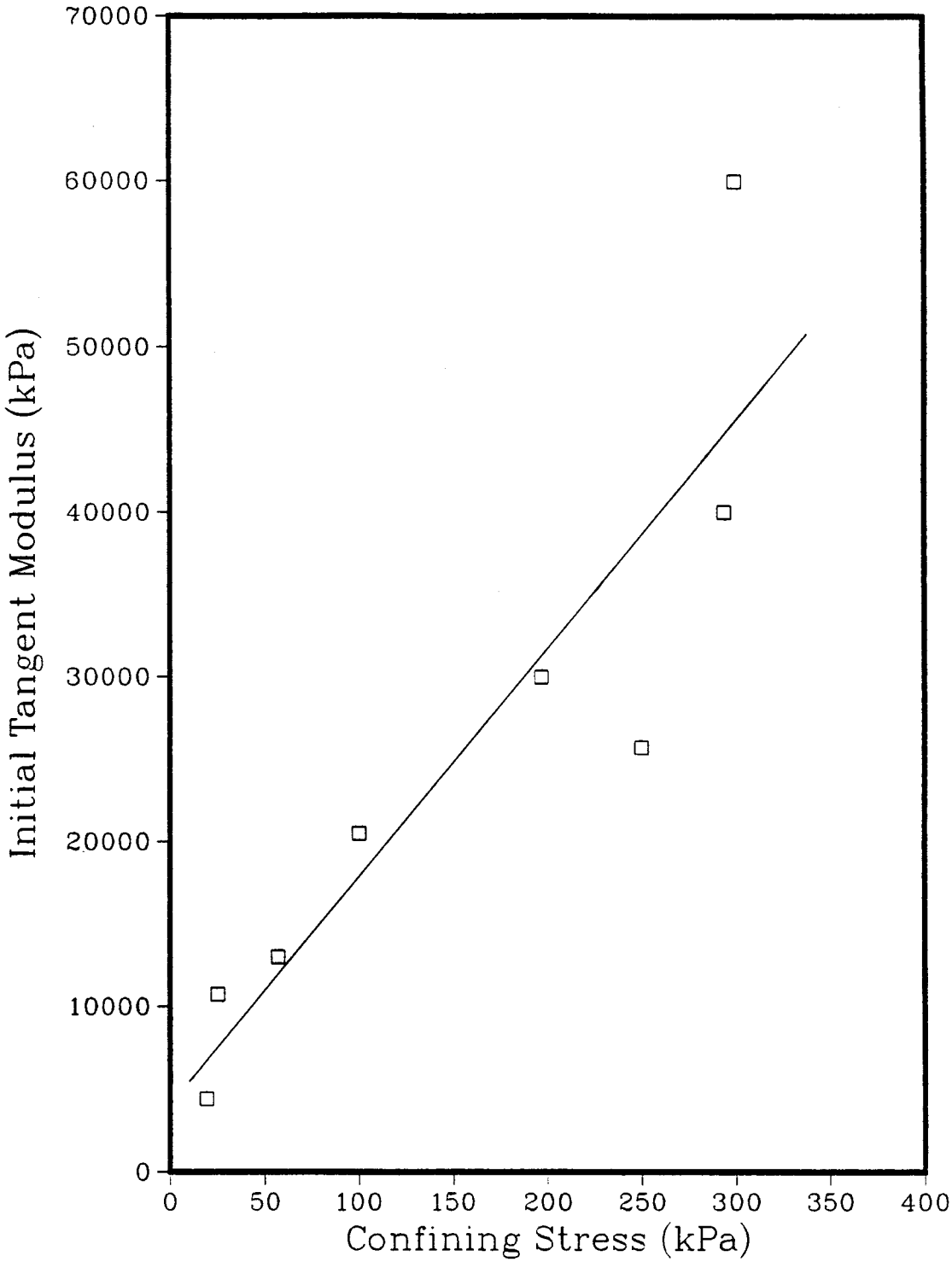

Figure 5.25: Variation of E Obtained from CU Triaxial Tests on Tube Specimens

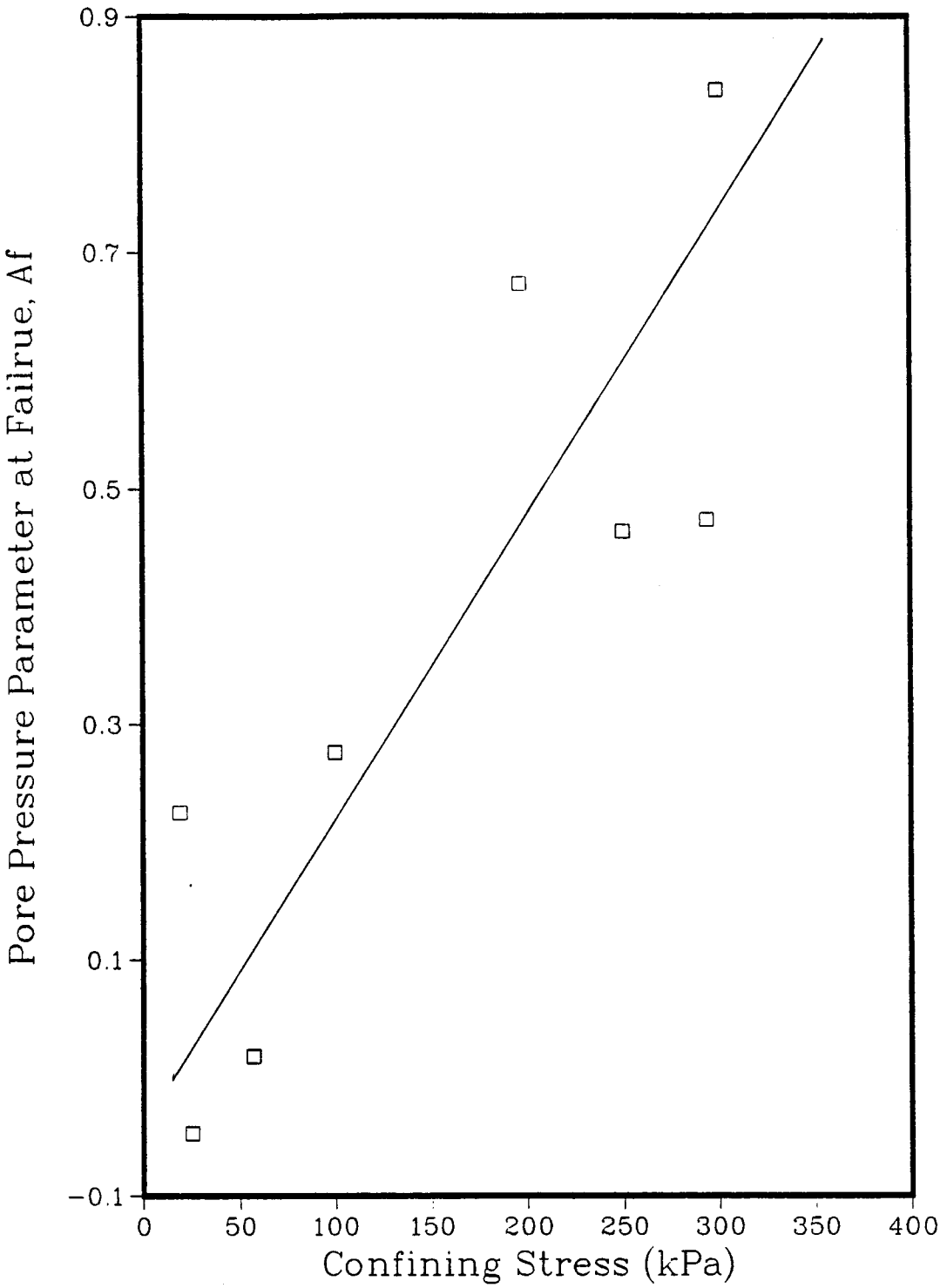

Figure 5.26: Variation of Af Obtained from CU Triaxial Tests on Tube Specimens

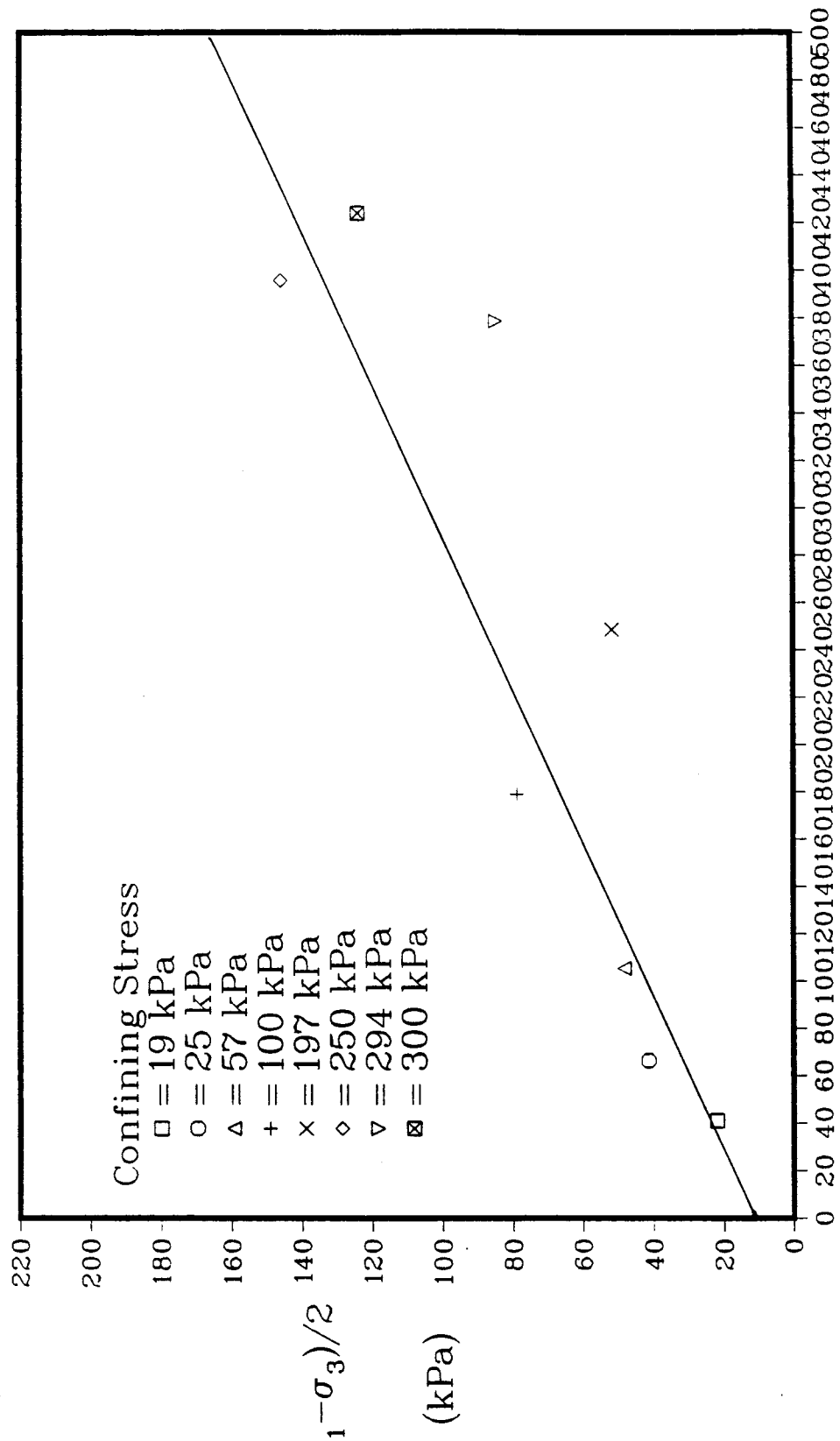

Figure 5.27: Total Stress P–Q Plot for Foundation Tube Specimens

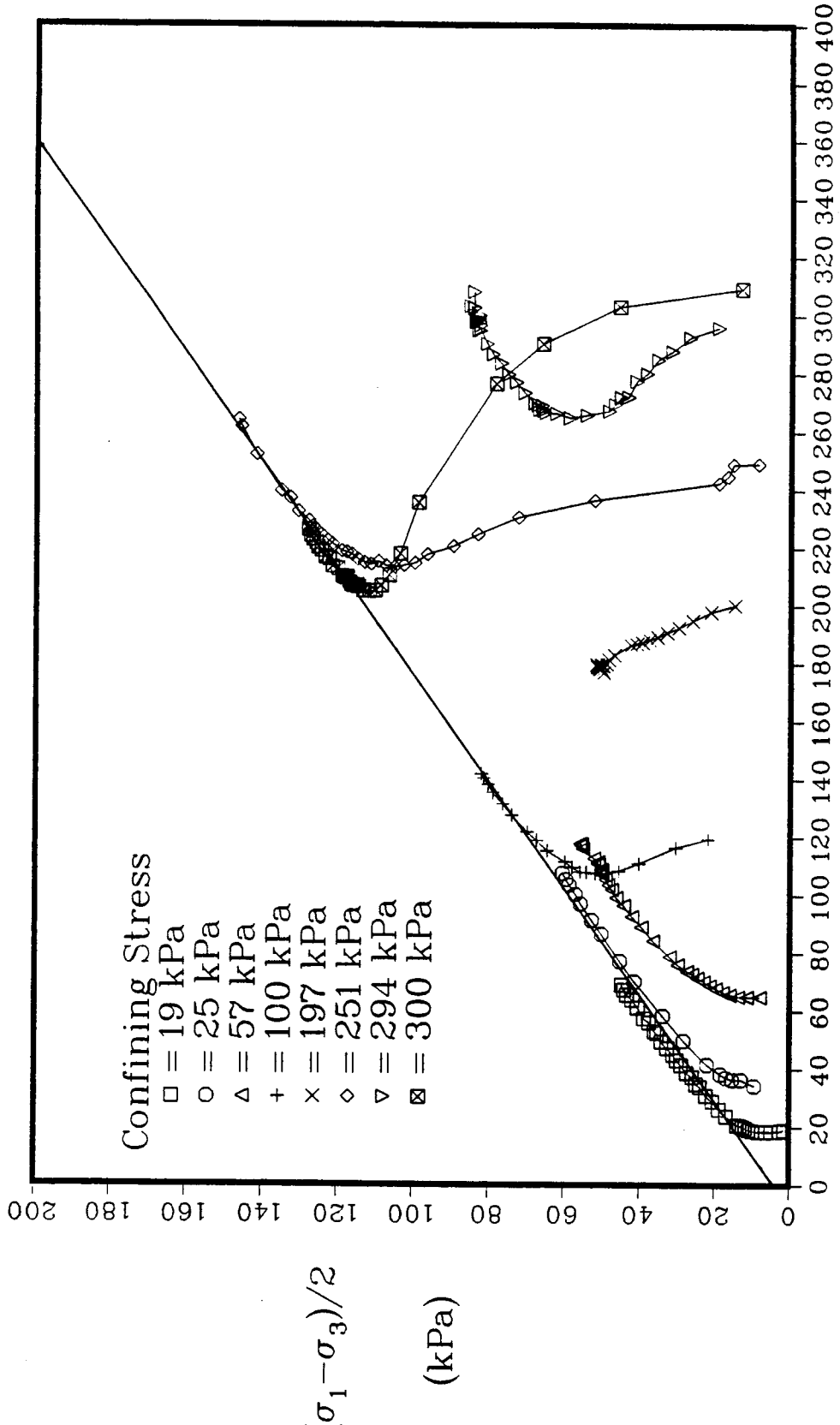

Figure 5.28: Effective Stress P–Q plot for Foundation Tube Specimens

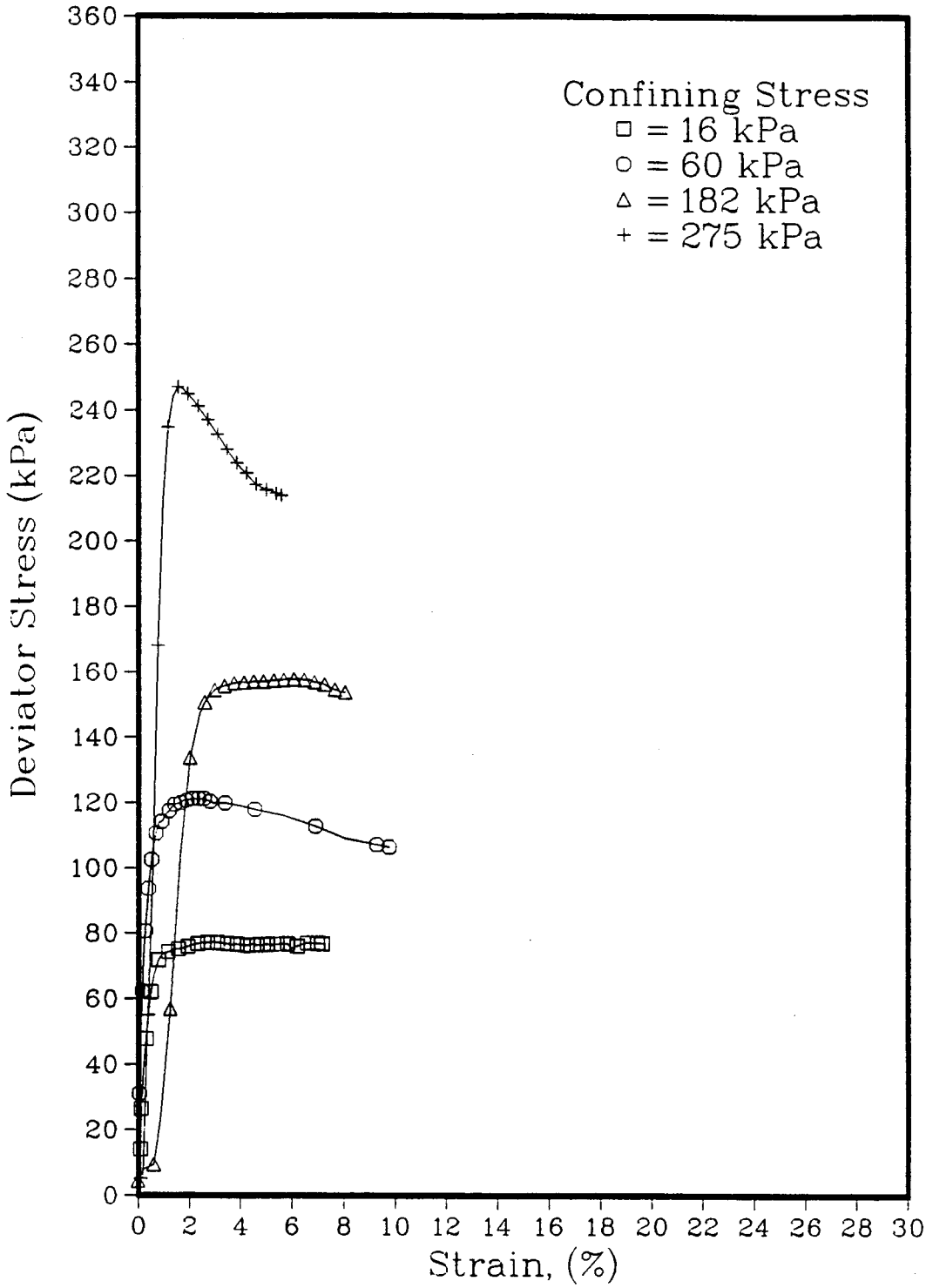

Figure 5.29: CU Triaxial Tests on Foundation Block Specimens

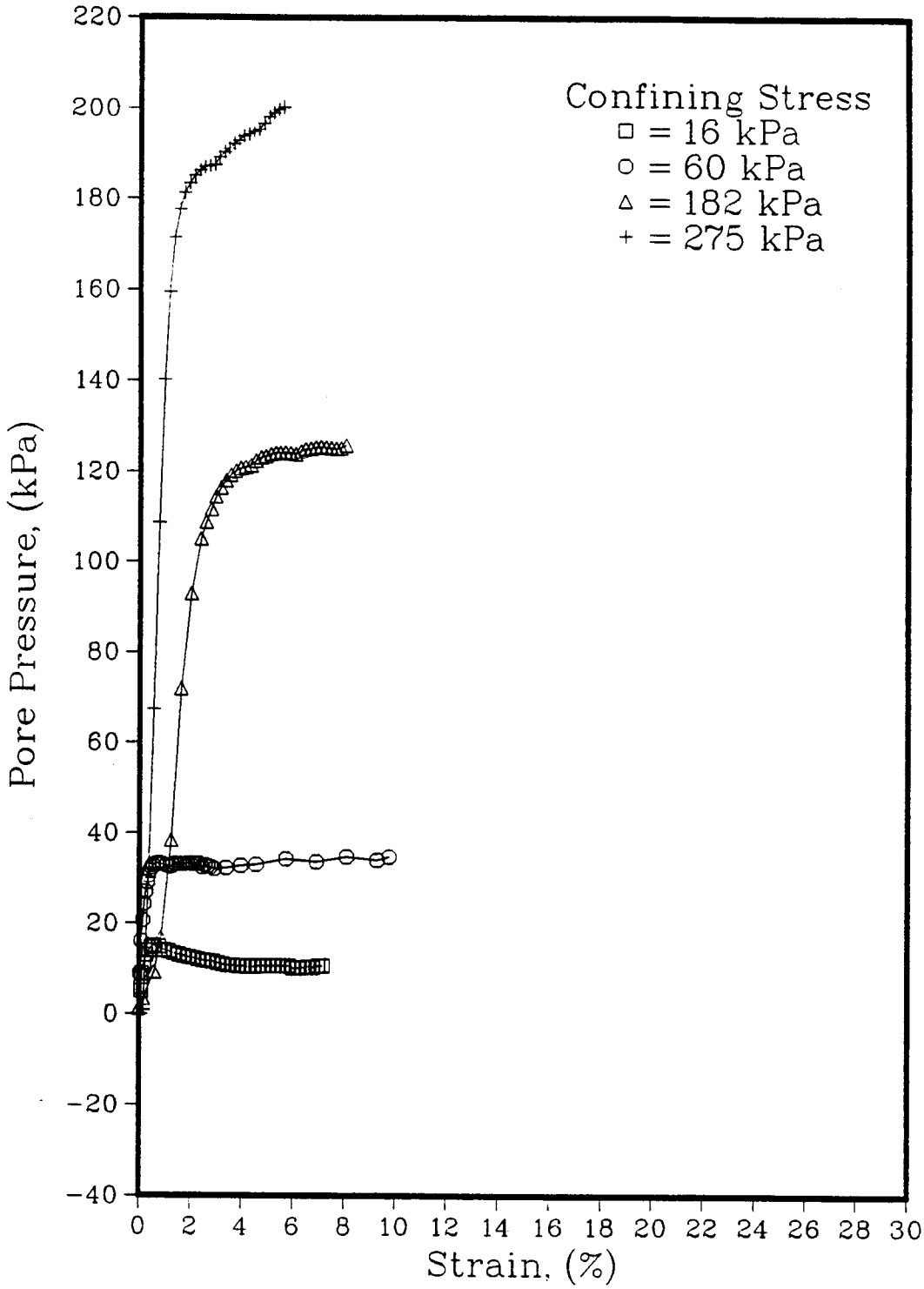

Figure 5.30: CU Traixial Tests on Foundation Block Specimens

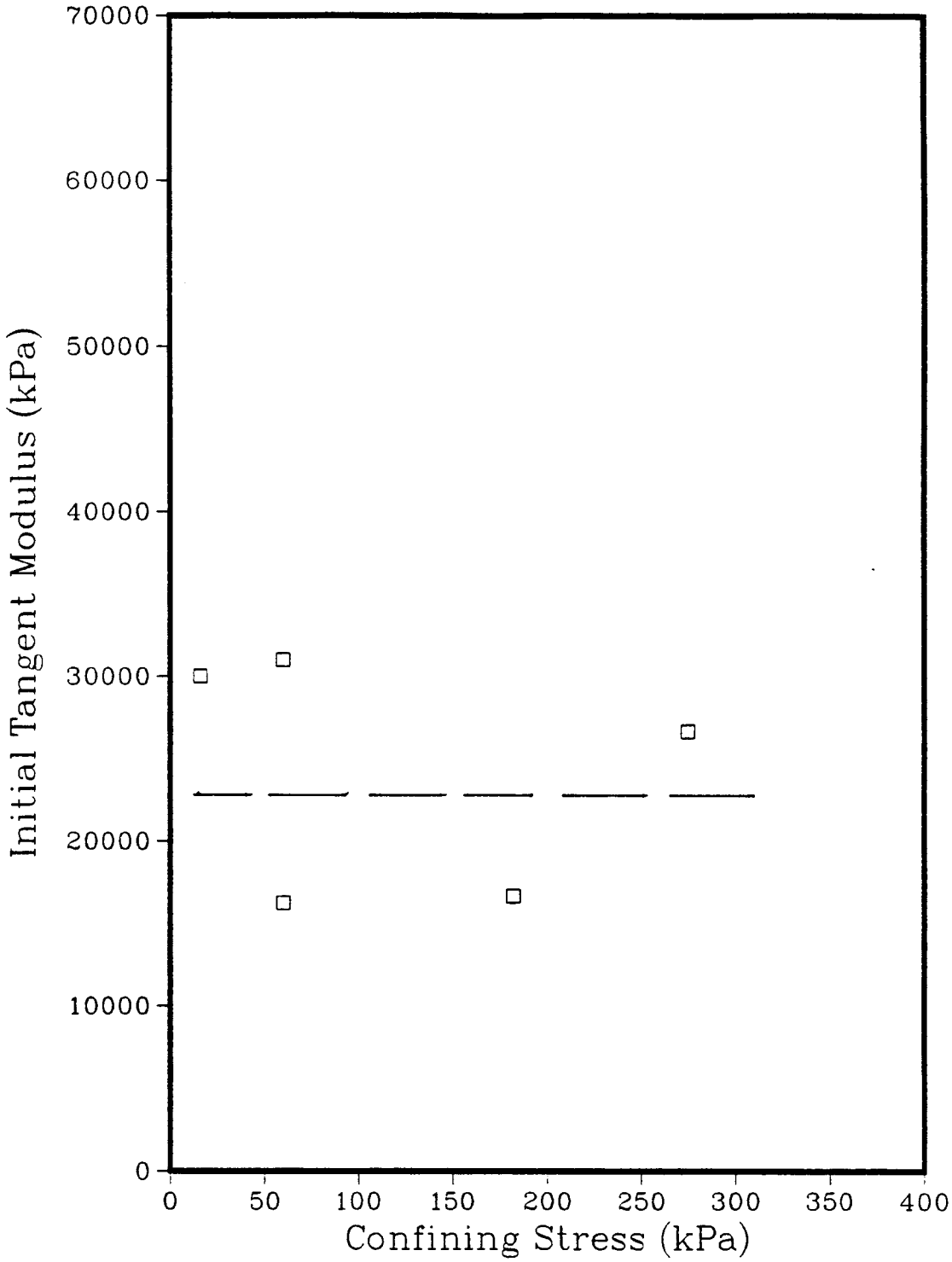

Figure 5.31: Variation of E Obtained from CU Triaxial Tests on Block Specimens

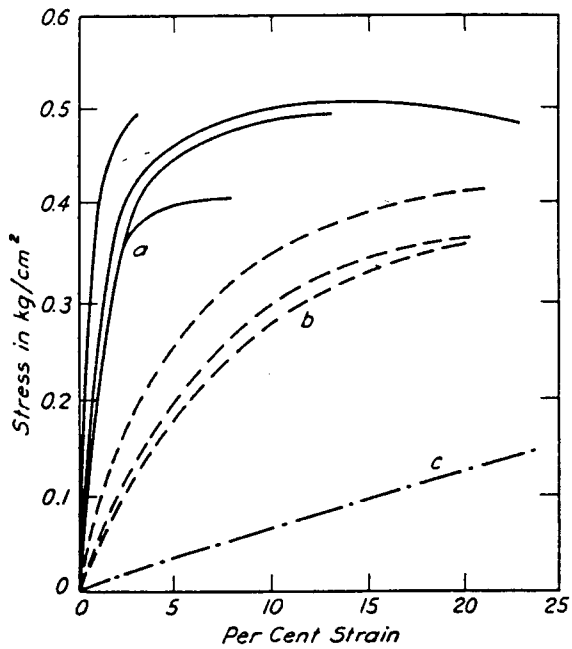

Figure 5.32: Stress-Strain Curves Obtained from Unconfined Compression Tests on Different Specimens of Chicago Clay.
(a) Undisturbed samples
(b) Tube samples of same clay.
(c) Remouled samples (Modified from Peck, 1940)

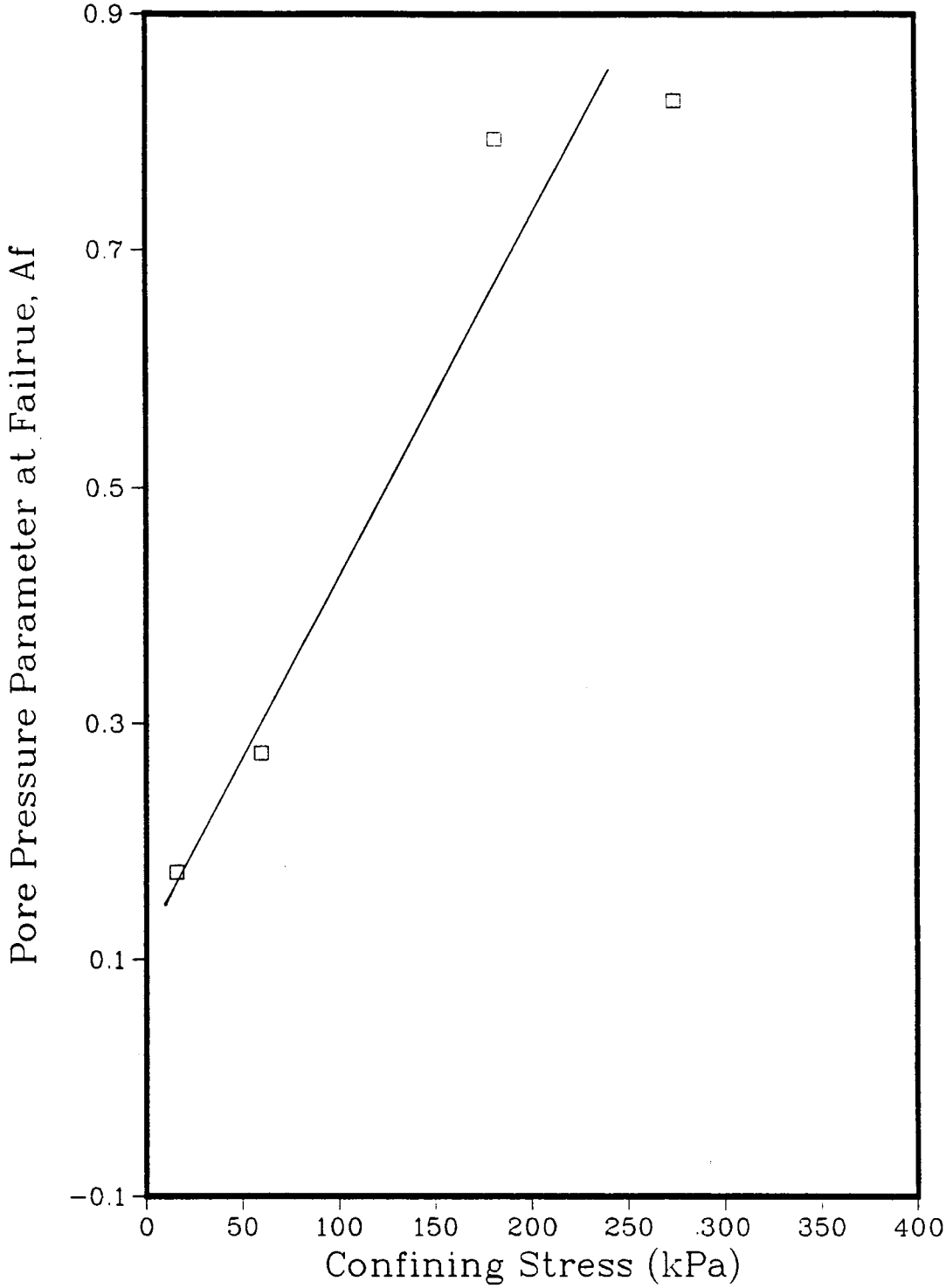

Figure 5.33: Variation of Af Obtained from CU Triaxial Tests on Block Specimens

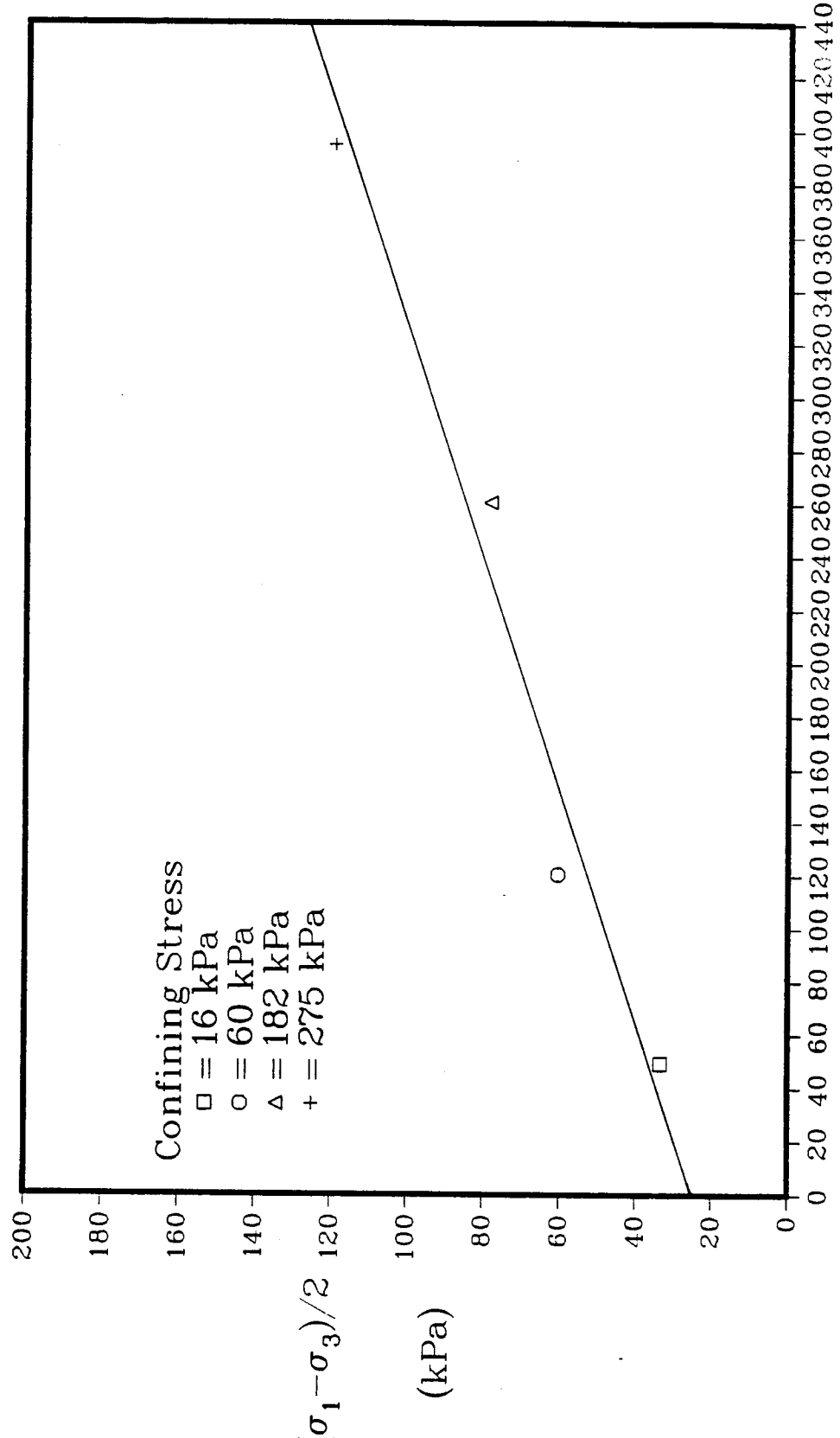

Figure 5.34: Total Stress P–Q Plot for Foundation Block Specimens

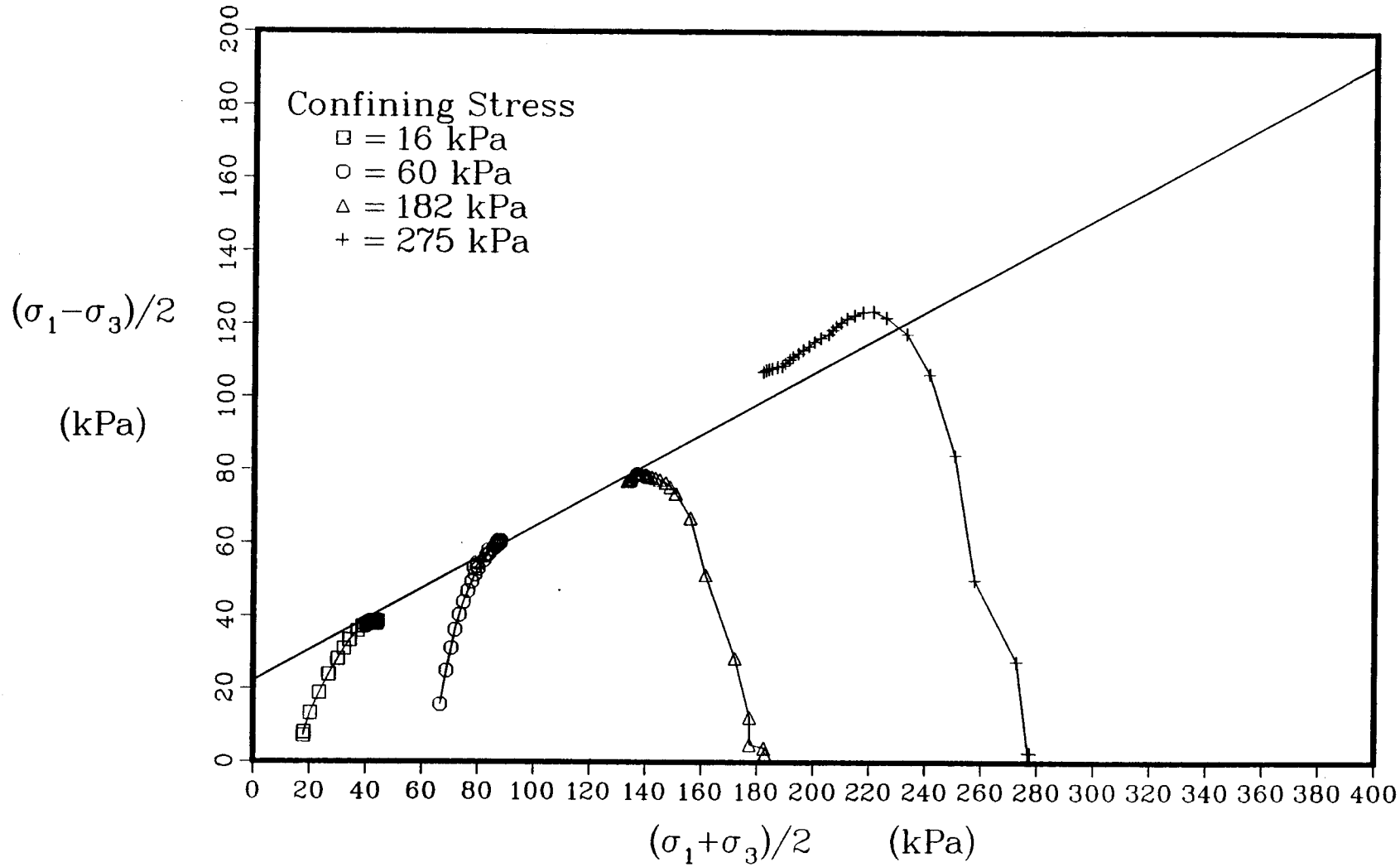

Figure 5.35: Effective Stress P--Q plot for Foundation Block Specimens

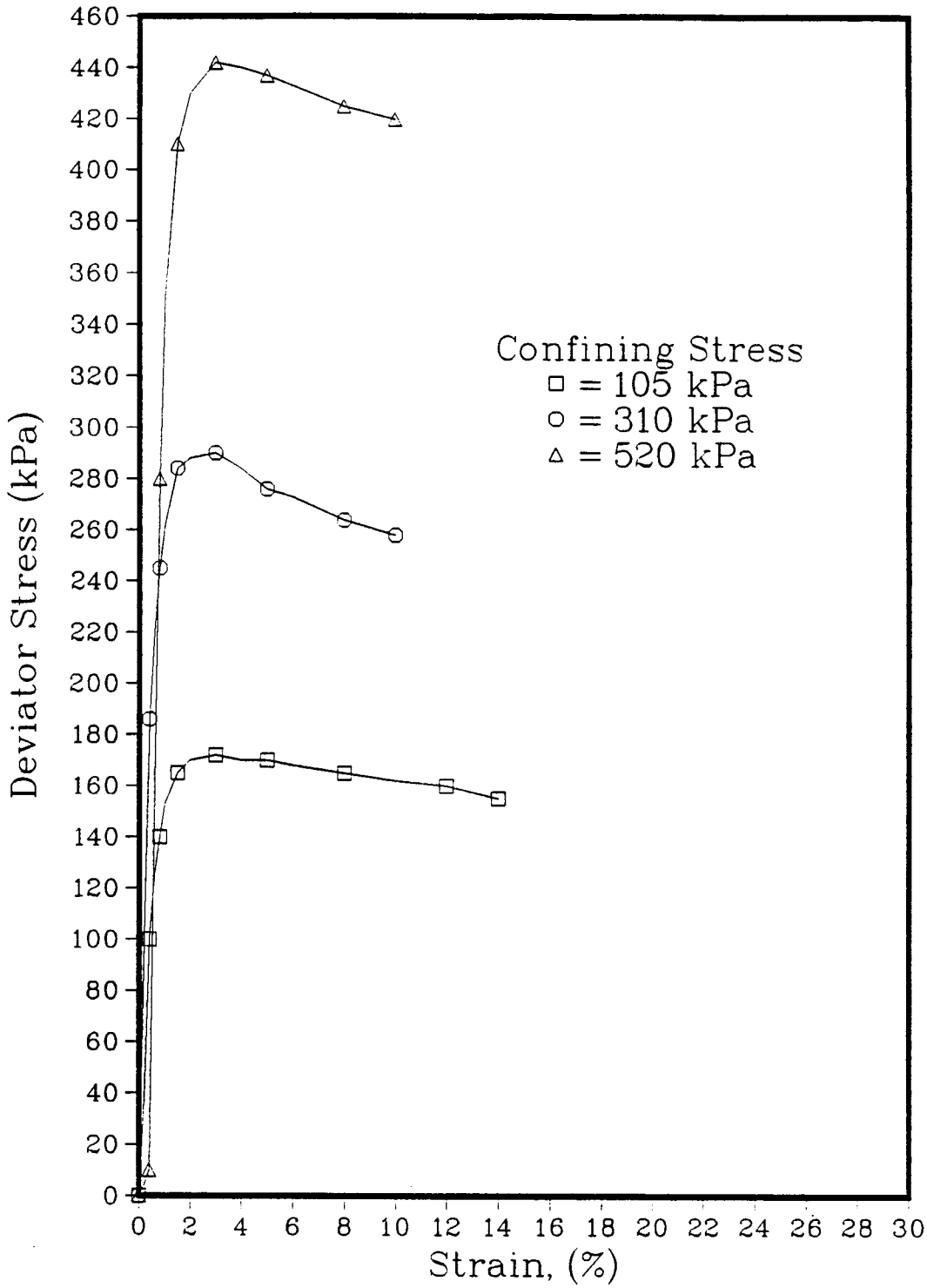

Figure 5.36: CU Triaxial Tests on Foundation Tube Specimens from BH 28

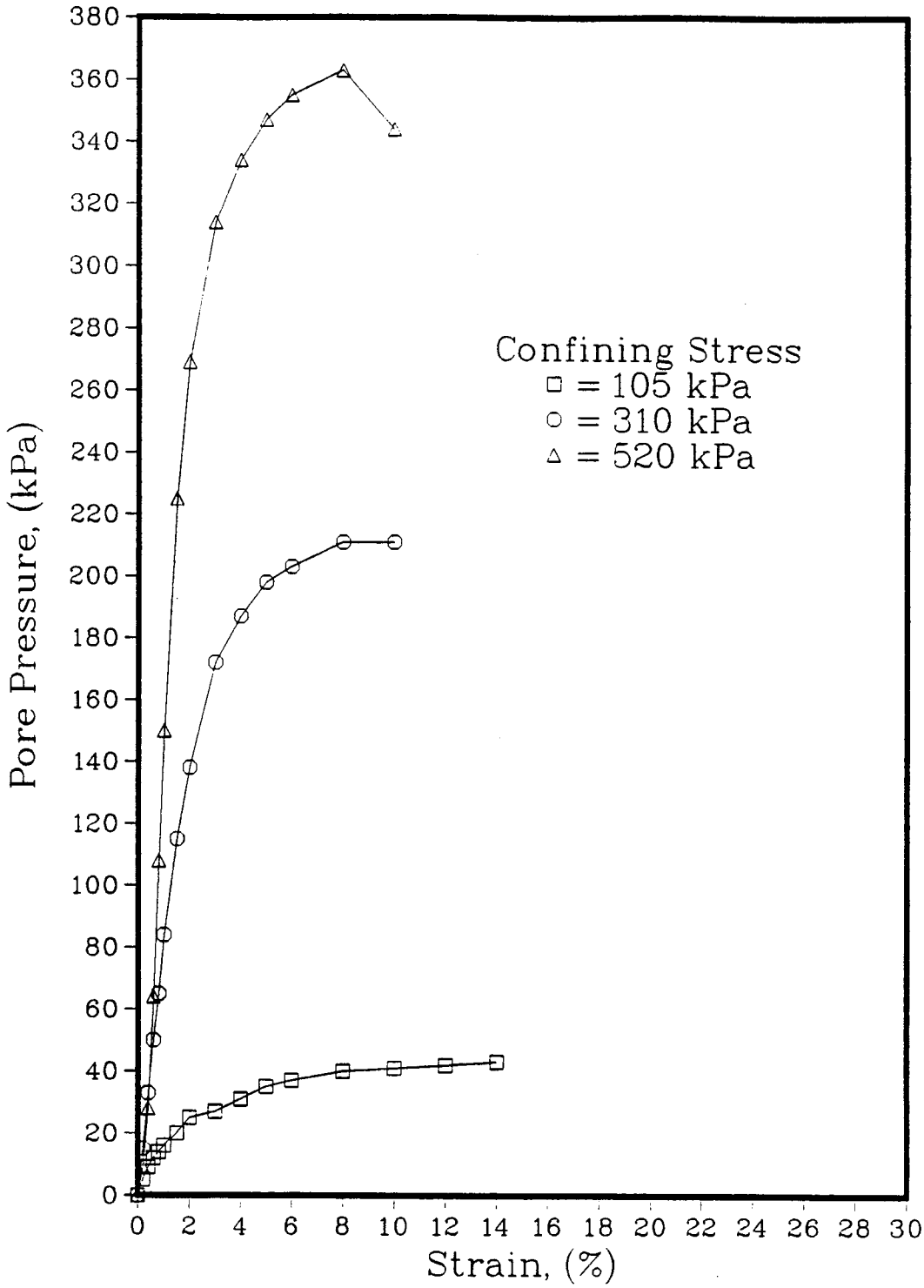

Figure 5.37: CU Traixial Tests on Foundation Tube Specimens from BH 28

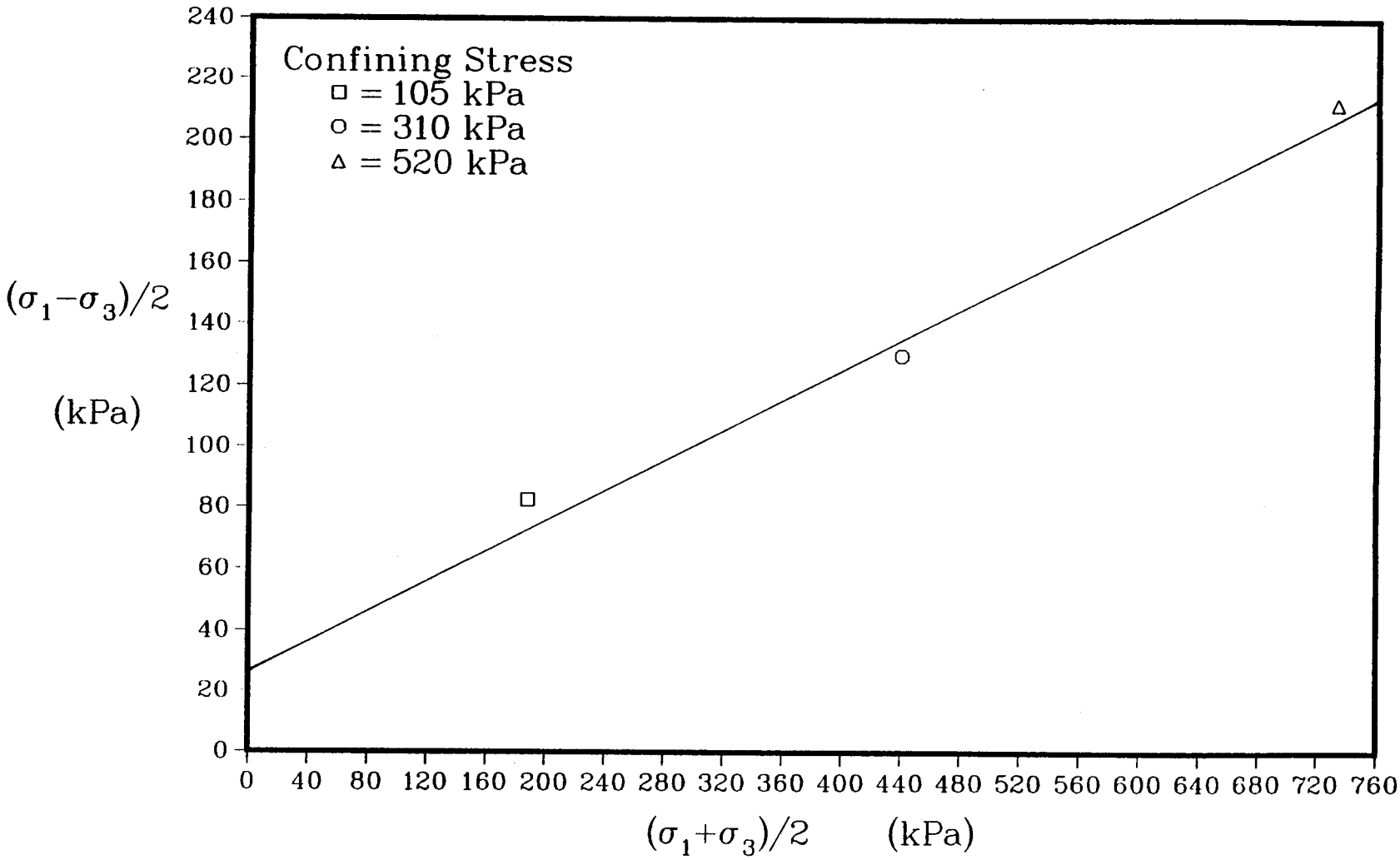

Figure 5.38: Total Stress P–Q Plot for Foundation Tube Specimens Obtained from BH 28

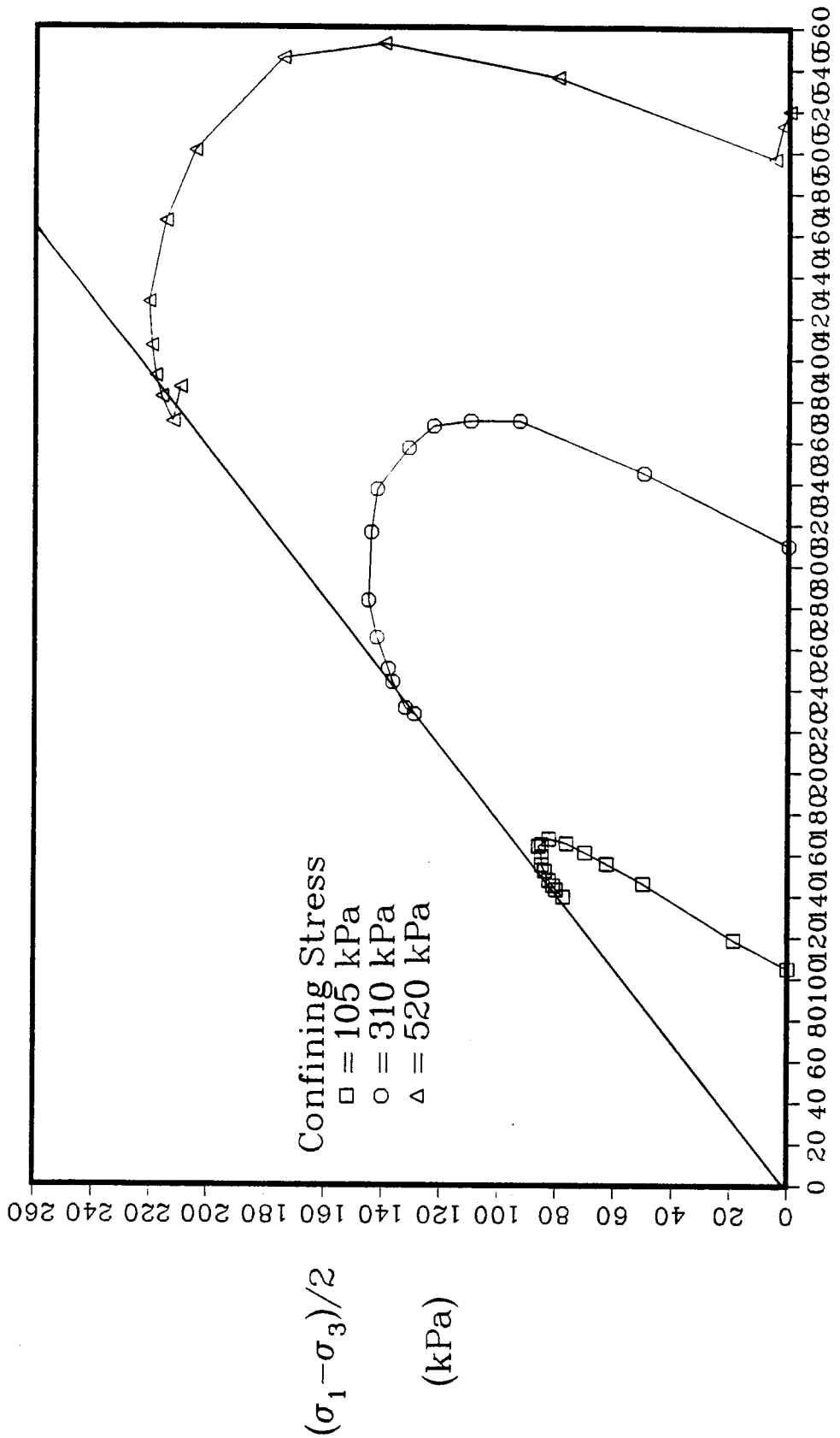

Figure 5.39: Effective Stress P–Q plot for Foundation Tube Specimens from BH 28

6. STABILITY AND DEFORMATION ANALYSES OF THE EMBANKMENT

6.1 Introduction

Geogrid manufacturers suggest that geogrids should not be subject to strains of greater than 5%. Beyond this level of strain, only small increases in stress lead to either a tensile failure or, in some cases, accelerated creep of the grid material. Ideally, in order to gain the most amount of information, the test fill should be designed such that strain levels of just under 5% occur within the reinforced slopes. However, a complete shear failure of the embankment must be avoided so that measurement of the deformations occurring within the soil and the geogrids may be carried out over a period of several years.

To determine the maximum height to which the embankment may be constructed, without inducing a shear failure, the short and long term factors of safety were calculated for 8, 10 and 12 m high slopes using a limit equilibrium analysis. Bishop's Method of Slices was chosen to evaluate the factors of safety since this method has proven to be an accurate limit equilibrium method for predicting the stability of such slopes. The soil properties selected for the short term and long term analyses will be discussed followed by a presentation of the analytical results.

To estimate the deformations which may ultimately be developed in the soil due to drained shearing a finite element analysis was conducted using a program called SAGE

(Stress Analysis in Geotechnical Engineering), developed by Chan (1988). The analysis was performed using the consolidated drained stress-strain and volume change-strain curves obtained for the fill soil and the consolidated undrained stress-strain curves obtained for the foundation soil from laboratory tests. The selection of soil properties used in the finite element model will be discussed. The results from the analysis will be presented for fill heights of 6, 8, 10 and 12 m in the form of the horizontal strain distributions acting at the elevations of the geogrids in the adjacent slopes. The horizontal strains acting in the soil at these elevations may be compared to the strains measured in the geogrids once the embankment has been constructed to its full height.

6.2 Stability Analysis

The Bishop Method of Slices uses overall moment equilibrium around the center of an assumed slip circle and vertical equilibrium of slices of soil bounded by the slip circle to establish an equation for the factor of safety of a slope. This equation may be written as:

$$F=(1/\sum w*\sin\alpha)*\sum (c'b+(w-\mu b)\tan\phi)/M\alpha \quad [6.1]$$

where $M\alpha=\cos\alpha+\sin\alpha*\tan\phi'/F$

Figure 6.1 shows the forces acting on a typical slice.

Although this method does not satisfy horizontal force equilibrium, it has been found to be an accurate method of analysis for homogeneous slopes (Duncan and Wright, 1980) such as the test fill.

6.2.1 Short Term Stability

The short term stability analysis was conducted assuming that up to 6 m of fill would be placed quickly, during the third construction season, on the existing, consolidated 6 m embankment. To simulate these conditions the pore pressure ratios, r_u, used in the analyses were increased from the base of the fill slope to its crest as shown in Table 6.1b and Figure 6.2. r_u is equal to the pore pressure divided by the total overburden stress. That is,

$$r_u = \frac{\gamma_w * H_{water}}{\gamma_t * H_{soil}} \qquad [6.2]$$

where H_{water} = the head of water at the point at which r_u is being calculated

The particular r_u values were chosen to reflect the pore pressure response measured with pneumatic piezometers during placement of the first 6 m of fill soil. The r_u values calculated from field measurements are given in Table 6.1a.

Piezometers were installed in the embankment, as shown in Figure 6.3, on either side of an assumed slip circle and at various points along the centerline of the fill.

Immediately after the embankment was constructed to a height of 3m, the piezometers at location 2 yielded an average r_u value of 0.92 and the piezometers at location 3 yielded an average r_u value of 0.41. Similar observations were recorded from these piezometers for a fill height of up to 6 m. It was therefore assumed that the embankment pore pressures would respond in a similar manner to the rapid placement of an additional 6 m of soil during the following construction season.

Pore pressures equal to 92% of the increase in total stress due to the addition of 6 m of soil were calculated for the zones located to the left of the slip circle in Figure 6.3 and pore pressures equal to 41% of the increase in overburden stress were calculated for the regions to the right of the slip circle. r_u values were calculated for each 2 m of soil up to an embankment height of 6 m and for the entire uppermost 6 m of soil. The average of the r_u values calculated to the right and left of the assumed slip circle was then taken for each of the four embankment sections. These averages, given in Table 6.1, were used as the high values for the limit equilibrium analyses. The high r_u values were each reduced by 0.1 to obtain the low values used in the analyses.

6.2.1.1 Fill and Foundation Soil Properties

The short term analysis was conducted in terms of effective stress such that pore pressures could be considered. The consolidated undrained triaxial tests

conducted on the silt and clay fill soils yielded an effective stress friction angle of 27° to 30°. The more conservative effective stress friction angle of 27° was used for calculation of the short term factors of safety as the fill height was increased from 8 to 12 m. Table 6.2 shows the design effective stress cohesive strengths determined from the consolidated undrained tests conducted on the various fill soils. As shown in Chapters 2 and 4, the cohesive strength intercept of the effective stress failure envelope increases with an increase in the compacted dry density. The dry densities of the silt specimens correspond more closely with the average dry density of the field-compacted specimens (Table 6.2). Therefore, an effective stress cohesive strength of 20 kPa was used for the stability calculations for fill heights of 8 to 12 m. Additional cases were also run for the 12 m height to establish the variation in the factor of safety with changes in the shear strength parameters.

Table 6.3 shows the design strengths determined from the consolidated undrained triaxial tests conducted on foundation soil specimens. A significant difference exists between the parameters established for the shelby tube and the block sample specimens. As stated in Chapter 5 the tube specimens were significantly disturbed. Hence, the parameters determined for the block sample specimens were considered to be more valid.

The effective stress friction angle of 24° determined for the block sample specimens was used along with an effective stress cohesive strength of 20 kPa, to calculate the short term factors of safety for fill heights of 8, 10, and 12 m. The cohesive strength chosen is slightly less than that determined for the block samples specimens in order to take into consideration the low values determined for the tube soil specimens. Additional analyses were also conducted considering a possible range of shear strength parameters to determine the sensitivity of the short term factor of safety to these changes.

6.2.1.2 Discussion of the Results

Figure 6.2 shows the critical slip circle established for a fill height of 12 m, using the maximum r_u values. The short term factors of safety calculated for fill heights of 8, 10 and 12 m and for various shear strength parameters are given in Table 6.4. A factor of safety of greater than 1.0 was determined for a fill height of up to 10 m when high r_u values were used. Similar calculations, using the lower r_u values, showed that failure is pending at a fill height of 12 m. Consequently, it will be necessary to monitor closely the deformations taking place within the embankment with vertical slope indicators and horizontal magnetic extensometers as the fill height is raised above 10 m. If significant movements begin to take place,

construction may have to be terminated until the excess pore pressures have dissipated sufficiently.

The analyses conducted for variations in the shear strength parameters showed that the factor of safety is most sensitive to changes in the cohesive strength, while variations in the friction angle have little affect. Since the critical failure circle always passed through the fill soil, varying the shear strength parameters of the foundation soil had no influence on the factor of safety.

6.2.2 Long Term Stability

The long term analysis was conducted assuming that the excess pore pressures in both the fill and foundation soils will have dissipated to zero. The long term factors of safety were calculated for fill heights of 8, 10 and 12 m using two different values of cohesive strength for the fill soil and for a 12 m height considering variations in the shear strength of both the fill and foundation soils. This was done to examine the sensitivity of the long term factors of safety to a reduction in the effective stress cohesive strength.

6.2.2.1 Fill and Foundation Soil Properties

The long term factors of safety were analysed using effective stress parameters for the fill and foundation soils and r_u values equal to 0.01. The consolidated drained tests conducted on the fill soil yielded an

effective frictional strength of 27° and an effective cohesive strength of 22 kPa. One set of analyses was conducted, for fill heights of 8, 10 and 12 m, using these parameters and one set was performed using the same friction angle but, a lower cohesive strength of 15 kPa. Variations in the shear strength parameters of both the fill and foundation soils were also considered for a fill height of 12 m to examine the sensitivity of the long term factor of safety to these changes.

Drained triaxial tests were not conducted on the foundation soil. However, as discussed in Chapter 2, Bjerrum and Simons (1960) show that the effective stress cohesive and frictional strength parameters determined from consolidated drained and consolidated undrained triaxial tests are the same for most clays. Therefore, the shear strength parameters of 24° and 20 kPa, determined for the foundation soil using undrained tests, were considered valid for the long term analysis.

6.2.2.2 Discussion of the Results

The long term factors of safety calculated for fill heights of 8, 10, and 12 m and for various shear strength parameters are shown in Table 6.4. The critical slip circle established for the long term analysis for a fill height of 12 m and an effective stress cohesive strength of 20 kPa for the fill soil is shown in Figure 6.2. As was the result for the short term calculations, the critical slip circle passes through the toe of the

slope. Therefore, changes in the shear strength parameters of the foundation soil had no influence on the factor of safety. Table 6.4 shows that the long term factor of safety is greater than 1.0 even for a fill height of 12 m and an effective cohesive strength of only 10 kPa for the fill soil.

6.2.3 Conclusions from the Limit Equilibrium Analysis

Comparison of the long and short term factors of safety shows that the conditions immediately after construction, before the excess pore pressures have had a chance to dissipate, are the most critical. Hence, provided that the pore pressures are monitored during the placement of the last few metres of soil and that critically high excess pore pressures are allowed to dissipate, both the short and long term stability of the embankment should be adequate. The lower factors of safety calculated for the short term analysis show that the shear stresses in the embankment, and therefore the rate of shear strains which take place, will be greatest immediately after construction.

Both the short and long term factors of safety are very sensitive to the effective stress cohesive strength selected for the fill soil. This parameter is difficult to establish in cases where test data shows any degree of scatter. Hence, for a case such as this, where the stability of the slope is highly dependent upon a parameter which is difficult to establish, the factor of safety of the slope cannot be

determined with confidence.

6.3 Deformation Analysis with Finite Elements

A finite element analysis was conducted in order to predict the horizontal strains which may occur in the unreinforced slope of the test fill. The study was intended to model the long term conditions of the embankment. Hence, it was assumed that the excess pore pressures would have dissipated completely.

6.3.1 Mesh Design

The section of the test fill modelled with finite elements is shown in Figure 6.4. The embankment is 12 m high with a slope angle of 45° and consists of compacted silty clay. In agreement with the borehole information obtained from the site, the foundation soil is divided into two layers. The upper 6 m consisits of a compacted silty clay, of medium consistency, beneath which lies 12 m of a very stiff to hard till.

The boundaries of the mesh were chosen far enough away from the slope face such that they would not influence the deformations occurring in that region. Nodes along the left and right-hand boundaries are free to move vertically but cannot move horizontally, while nodes along the lower boundary of the foundation are free to move horizontally but not vertically. All other nodes may displace either horizontally or vertically. The mesh consists of 166

isoparametric foundation elements and 147 isoparametric embankment elements, defined by a total of 934 nodes.

6.3.2 Analysis Procedure

The analysis was divided into 7 load steps. The stresses in the foundation soil were initialized by "turning on gravity" in the first step. The strains and displacements were reset to zero after this step. Construction of the embankment then proceeded by incremental loading, with successive 2 m lifts, up to a height of 12 m. This allowed for adjustment of the elastic modulus in the fill soil according to the changing levels of stress.

6.3.2.1 Foundation Soil Models

Construction of the test fill was assumed to proceed slowly, thereby allowing the pore pressures in the foundation soil to dissipate under each new lift of compacted fill. Consolidated drained triaxial tests conducted by increasing the vertical stress by increments of $\Delta\sigma_1$ and increasing σ_3 by increments equal to $\Delta\sigma_1 * K_o$, would correctly model the stress path undergone by the foundation soil in the field. However, time constraints did not allow for elaborate testing of this nature. As an expedient although approximate alternative, the behaviour of the clayey silt foundation soil was modelled based on the stress-strain curves obtained from the consolidated undrained triaxial tests conducted on the undisturbed block sample and tube

sample specimens.

Table 6.6 gives the initial tangent modulii and the peak strengths obtained from the tests. A modulus of 35000 kPa was chosen for the finite element analysis. This number is slightly higher than the values obtained from the triaxial tests. However, it was felt that the sampling process disturbed the foundation soil samples sufficiently to reduce the stiffness of the soil from that which exists in the field. The shapes of the consolidated undrained stress-strain curves could best be represented by an Elastic-Perfectly Plastic Tresca model. The model is defined by an elastic modulus, a Poisson's ratio, a peak yield stress and a residual yield stress. The parameters selected from the laboratory data for Tresca model 1 are given in Table 6.6 and the resulting model stress-strain curve is shown in Figure 6.5.

Triaxial tests were not conducted on the stiff, clay till foundation soil. However, based on the relative stiffnesses of the till unit and the clayey silt foundation soils, as portrayed by their relative N values (Figure 3.3), a similar Tresca model was established for the till. According to the data obtained from CD triaxial tests conducted by Medeiros and Eisenstien (1983), typical elastic modulii values for Edmonton till range between 105,000 kPa for a confining stress of 298 kPa and 144,000 kPa for a confining stress

of 329 kPa. The till unit in the Edmonton and Devon areas was laid down by the same advance of ice (Bayrock and Hughes, 1962). A modulus of 100000 kPa was chosen for the clay till foundation soil model. The parameters used for the second Tresca model are given in Table 6.6 and the model stress-strain curve is shown in Figure 6.5.

Measurements taken during construction of the Light Rail Transit (LRT) System in Edmonton have shown that the in situ coefficient of earth pressure at rest, K_o, of the till unit located directly below the clayey silt deposit, is between 0.7 and 0.8. The rust stained fissures evident in the clayey silt block sample, removed from the test fill site, indicate that the horizontal in situ stresses have been reduced, perhaps due to downcutting of the North Saskatchewan River in the near by valley. Hence, K_o is probably less than 0.8 at the test fill site.

K_o may be calculated for normally consolidated soil based on its effective stress friction angle and an effective stress cohesive strength of 0 kPa (Brooker and Ireland, 1965) using the following empirical relation:

$$K_o=(1-SIN\phi') \qquad [6.3]$$

The effective friction angle of 24° established for the

clayey silt foundation soil yields a K_o of 0.593. However, as noted in Chapter 3, the clayey silt glaciolacustrine deposit may be overconsolidated due to the migration of large sand dunes throughout the Devon Area. A hysteresis effect occurs when a soil is unloaded, or becomes overconsolidated, causing an increase in K_o (Holtz and Kovacs, 1981). If K_o is taken as 0.7, the average of the values obtained from pressuremeter measurements in the Edmonton till and the empirically derived number, a Poisson's ratio of about 0.4 may be calculated from Equation 6.4.

$$\upsilon = K_o/(1+K_o) \qquad [6.4]$$

For a lack of more accurate information, a Poisson's ratio of 0.40 was used for both the clayey silt and clay till foundation soils.

Two types of foundation soil models are given in Table 6.6: a linear elastic model and a tresca model. Linear elastic models, without yield points, were first used for the foundation soils to set up the initial stress field by "turning on gravity". The strains and displacements were then both reset to zero. Before placement of the first embankment lift, the Tresca models were implemented in the foundation soils. The Tresca models remained in place to represent the

foundation soil behaviour as the fill was built up to its final height of 12 m.

6.3.2.2 Fill Soil Models

A hyperbolic elastic model was used to represent the stress-strain curves established from the consolidated drained triaxial tests conducted on the laboratory-compacted silty clay fill soil. It should be pointed out that the stress path followed during a triaxial test does not follow that which would be followed by the embankment fill soil. If construction of the test fill proceeds slowly, the fill soil would undergo a series of undrained step loads after each of which the excess pore pressures would be allowed to dissipate. However, there was insufficient time to conduct triaxial tests which would model the field conditions. Furthermore, it was not known exactly at what rate construction of the embankment would proceed. Hence, as an approximation, the stress-strain curves obtained from conventional consolidated drained triaxial tests were used for the finite element analysis.

The hyperbolic stress-strain model incorporates an instantaneous elastic modulus and a Poisson's ratio which vary with confining stress. The procedures outlined by Duncan *et al.* (1980) were followed to extract the material parameters required for the hyperbolic model from laboratory data. The model parameters are given in Table 6.5 and the idealized

hyperbolic stress-strain curves are shown in Figure 6.6. The volume change curves obtained from the drained triaxial tests during shearing were expressed in terms of an equation, given in Duncan *et al.* (1980), which relates the bulk modulus of the soil to the confining stress. The contribution of volume change, induced by shear stresses, to the horizontal and vertical strains in the fill soil, therefore, has been included in the analysis. However, the volume strains due to consolidation of the embankment have not been considered.

Since the hyperbolic model is confining stress dependent, a certain amount of stress must exist in a lift of fill soil before the elastic and bulk modulii can be calculated. Hence, a layer of fill soil was first introduced using a linear elastic model to initialize the stresses. Then, as the second lift of soil was placed using a linear elastic model, the model representing the first lift was changed from linear to hyperbolic. Once the hyperbolic model had been implemented in a particular lift of soil, it was left in place during subsequent loading by additional lifts of fill soil. This process was carried out, successively, for each 2 m layer of fill up to an embankment height of 12 m.

Eisenstein and Law (1979) have shown that during construction of a dam, the principal effective stress

ratio, K, is approximately constant for most regions within the dam. They concluded that K varied between 0.41 at mid-height, half-way between the centerline and the slope face, and 0.53 at the base of the dam along its centerline. Consequently, a Poisson's ratio of 0.30 calculated from an average K of 0.47, was chosen for the initial linear elastic model used to represent the fill soil. The second and third linear elastic models given in Table 6.5 were used to aleviate problems arising due to the development of tensile stresses in the embankment. These forces arise due to the fact that the nodes along the centerline of the embankment are fixed with respect to movement in the horizontal direction. As a lift of soil tries to deform laterally, movement is restrained along the centerline boundary causing small tensile stresses to be generated. The hyperbolic model used in this analysis cannot handle tensile stresses. Therefore, tensioned hyperbolic elements had to be replaced with linear elastic elements.

6.3.3 Analytical Results

The information obtained from the finite element analysis will be presented in terms of horizontal and vertical strains since it is primarily these parameters which must be considered when assessing the performance of the test fill.

6.3.3.1 Horizontal Strains

The horizontal strain contours determined for a fill height of 12 m are shown in Figure 6.7. Similar plots for fill heights of 6, 8 and 10 m are given in Appendix B. A maximum horizontal extension strain of 2%, shown as contour 1, occurs at an elevation of between 5 and 6 m in the 12 m high slope. Compressive strains are shown along the slope face which penetrate as much as 2 m into the slope along the lower half of the embankment. As a new lift of soil is added to the embankment, it tries to deform laterally but is restrained along its lower boundary by the underlying soil which is stiffer due to a higher σ_3. This restraint causes compressive strains to be generated in the uppermost layer of soil. These compressive strains may be due to the finite element modelling technique and may not occur in the field.

The distribution of horizontal strains occurring within the embankment as the fill height is increased are shown in Figures 6.8, 6.9 and 6.10 at elevations of 1, 3 and 5 m, respectively. Geogrids are being installed at these elevations in three quadrants of the test fill. The largest horizontal strain of 2% occurs at an elevation of 5 m, appoximately 7 m into the slope face. Although the soil being used to build the test embankment is quite deformable, the horizontal strains predicted with finite elements are small. The

incremental increase in horizontal strain as the fill height increases is also greatest in this region. Figure 6.8 shows that the horizontal strains at the 1 m elevation increase by only about 0.6% as the fill height is increased from 6 m to 12 m. This is most probably due to the restraint offered by the stiffer foundation soil at the base of the embankment.

Figures 6.9 and 6.10 show that at elevations of 3 and 5 m horizontal strains of between 0.5% and 1.0% exist at a distance of 13 m into the slope face. The geogrids installed at elevations of 3 and 5 m in the three reinforced quadrants of the test fill are 13 m long. Hence, the plots show that the grids are not anchored in a zone of negligible horizontal soil strain. They therefore will not be completely effective in reducing the lateral deformation of the embankment. For example, at an elevation of 5 m, Figure 6.10 shows that a horizontal strain of 1.2% exists 12 m into the slope face. The average horizontal strain occuring between 12 and 13 m into the slope face is 1.1%. Hence, over a distance of 1 m this represents a movement of 11 cm. However, although the geogrids may not be long enough to resist horizontal strains completely, they are sufficiently long to prevent a pullout failure. The geogrids were designed to extend at least 4 m beyond the critical failure circle determined from limit equilibrium analyses. Chalaturnyk (1988) presents a

discussion of pullout failures and of the influence of geogrids on the location of failure surfaces within embankments.

6.3.3.2 Vertical Strain

The contours of vertical strain determined from the finite element analysis for a fill height of 12 m are shown in Figure 6.11. The vertical strain contours for embankment heights of 6, 8 and 10 m are given in Appendix B. The maximum vertical strain of 4.5% occurs in the 12 m fill at an elevation of between 2 and 5 m under the crest of the slope. This is shown by contour 21. Relatively small vertical shear strains occur in the stronger foundation soil. The distribution of vertical strain acting along a vertical line drawn from the crest of the 12 m slope, 6 m into the foundation soil is shown in Figure 6.12. A vertical magnetic extensometer is located along the position of this line in each quadrant of the test fill.

The numerically predicted vertical strains represent the strains caused by shear stresses and do not include vertical strains due to consolidation of the fill or foundation soil. The consolidation strains which take place in the embankment could be calculated from the volume change measurements taken during the consolidation phase of the consolidated undrained triaxial tests conducted on the fill soil. However, since the change in sample height was not recorded

during the triaxial tests, it would not be possible to determine the horizontal and vertical components of the volume strain in order to add them to components of shear strain calculated from the finite element analysis. Settlement of the foundation soil due to primary consolidation was calculated to be 3.4 cm in Chapter 5, based on the data obtained from the oedometer tests conducted on Shelby tube samples.

6.3.3.3 Comparison of the Limit Equilibrium and Finite Element Analyses

As a check for agreement of the two methods, it is possible to compare the maximum principal strains predicted to occur within the test embankment using finite element analyses with those estimated based on the results obtained from limit equilibrium analyses. Figure 6.13 shows the maximum principal strains occuring within the embankment determined from the finite element analysis. A maximum strain of 5% is found 6 m into the slope at an elevation of 4 m. The confining stress at this point is equal to:

$$k_o * \sigma_1 = 0.67 * 6m * 20kN/m^3 \qquad [6.5]$$
$$= 80 \text{ kPa}$$

The long term factor of safety calculated for the 12 m high slope and a cohesive strength of 20 kPa is 1.36. On

the consolidated drained hyperbolic stress-strain curve for a confining stress of 80 kPa, a factor of safety of 1.36 represents a deviator stress of about 200 kPa and a corresponding strain of 5%. Therefore, both the long term limit equilibrium and finite element analyses predict similar deformations in the unreinforced slope of the test fill due to the long term shear stresses.

6.4 Summary of Analytical Results

It was concluded in Section 6.2.3 that the conditions immediately after construction of the test fill are the most critical in terms of a shear failure of the unreinforced slope. Table 6.4 shows that at this stage the short term limit equilibrium analyses predicted a factor of safety of less than unity. It was also pointed out that since the predicted factor of safety is highly dependent upon the cohesive strength chosen for the fill soil, the margin of safety cannot be predicted with a great deal of confidence. Hence, the excess pore pressures which develop in the embankment during placement of the last few meter of soil should be monitored closely such that if critically high pressures develop, construction may be stopped to allow for dissipation of these pressures.

The finite element analysis predicted a maximum horizontal extension strain of 2% at an elevation of 5 m, about 7 m into the slope face, for an embankment height of 12 m. Although laboratory tests suggested that the soil

being used to construct the test fill is quite deformable, this represents a small strain.

Figures 6.9 and 6.10 show that the geogrids are not anchored in a zone of negligible horizontal soil strain. Therefore, they may not be completely effective in reducing the lateral deformation of the embankment. However, the geogrids were designed to extend 4 m beyond the critical failure circle determined by limit equilibrium analyses, thus they are sufficiently long to prevent a pullout failure.

The maximum vertical strain predicted with the finite element analysis is 4.5%, as shown in Figure 6.11. This occurs in the 12 m high embankment, at an elevation of between 2 and 5 m, under the crest of the slope. This numerically predicted vertical strain represents the strain caused by shear stresses only and does not include the vertical strain caused by consolidation of the fill or foundation soil.

Table 6.1: Pore Pressure Ratios Used for Short Ter m Stability Analyses

Soil Region	Fill Height=8 m		Fill Height=10 m		Fill Height=12 m	
	r u max	ru min	r u max	ru min	r u max	ru min
I	0.66	0.56	0.66	0.56	0.66	0.56
II	0.44	0.34	0.54	0.44	0.56	0.46
III	0.27	0.17	0.35	0.25	0.39	0.29
IV	0.13	0.03	0.21	0.11	0.18	0.08
V	0.10	0.01	0.10	0.01	0.10	0.01

Table 6.2: Effective stress Cohesive Strengths of Fill Soil Compacted at Different Densities

Specimens	C′ (kPa)	Pd (g/cm3)
Clay	8	1.589
Silt	20	1.703
Sandy Clay	24	1.790
Tube Samples	-	1.700

Table 6.3: Summary of CU Test Results for Foundation Soil

Specimens	C′ (kPa)	ϕ' (degrees)
Block Sample	23	24
Tube Samples	6	33
Tube Samples (AB.T)	0	31

Table 6.4: Factors of Safety Calculated using Bishop's Modified Method of Slices

Test Fill Height (m)	Short Term Analysis		Long Term Analysis	
	High ru C'_{fill} = 20 kPa	Low ru C'_{fill} = 20 kPa	ru = 0.0 C'_{fill} = 15 kPa	ru = 0.0 C'_{fill} = 20 kPa
** 8m	1.57	1.69	1.61	1.86
** 10m	1.15	1.26	1.39	1.59
** 12m	0.87	0.98	1.20	1.36
case 1 * 12m	0.53	0.65	1.14	-
case 2 * 12m	0.53	0.65	1.14	-
case 3 * 12m	1.01	1.13	1.44	-

** base case: fill - ϕ = 27 c' = 20kPa; fnd - ϕ =24 c'=20 kPa

* case 1: fill - ϕ = 30 c'=10kPa ; fnd - ϕ =33 c'=6 kPa

* case 2: fill - ϕ = 30 c'=10kPa ; fnd - ϕ =24 c'=20kPa

* case 3: fill - ϕ = 26 c'=25kPa ; fnd - ϕ =33 c'=6 kPa

Table 6.5: Fill Soil Model Parameters

Model Type	γ	E	υ	σ_P	σ_R	K	Ku	n	Rf	C'	ϕ'	Kb	m
Linear Elastic 1	20	2700	0.30	–	–	–	–	–	–	–	–	–	–
Linear Elastic 2	20	3300	0.30	–	–	–	–	–	–	–	–	–	–
Linear Elastic 3	20	2067	0.40	–	–	–	–	–	–	–	–	–	–
Hyperbolic	20	–	–	–	–	59.5	119	0.28	0.86	20	28	50.0	0.28

Table 6.6: Foundation Soil Model Parameters

Model Type	γ	E	υ	σ_P	σ_R	K	Ku	n	Rf	C'	ϕ'	Kb	m
Linear Elastic 4	20	35000	0.40	–	–	–	–	–	–	–	–	–	–
Linear Elastic 5	20	100000	0.40	–	–	–	–	–	–	–	–	–	–
Tresca 1	20	35000	0.40	180	180	–	–	–	–	–	–	–	–
Tresca 2	20	100000	0.40	300	300	–	–	–	–	–	–	–	–

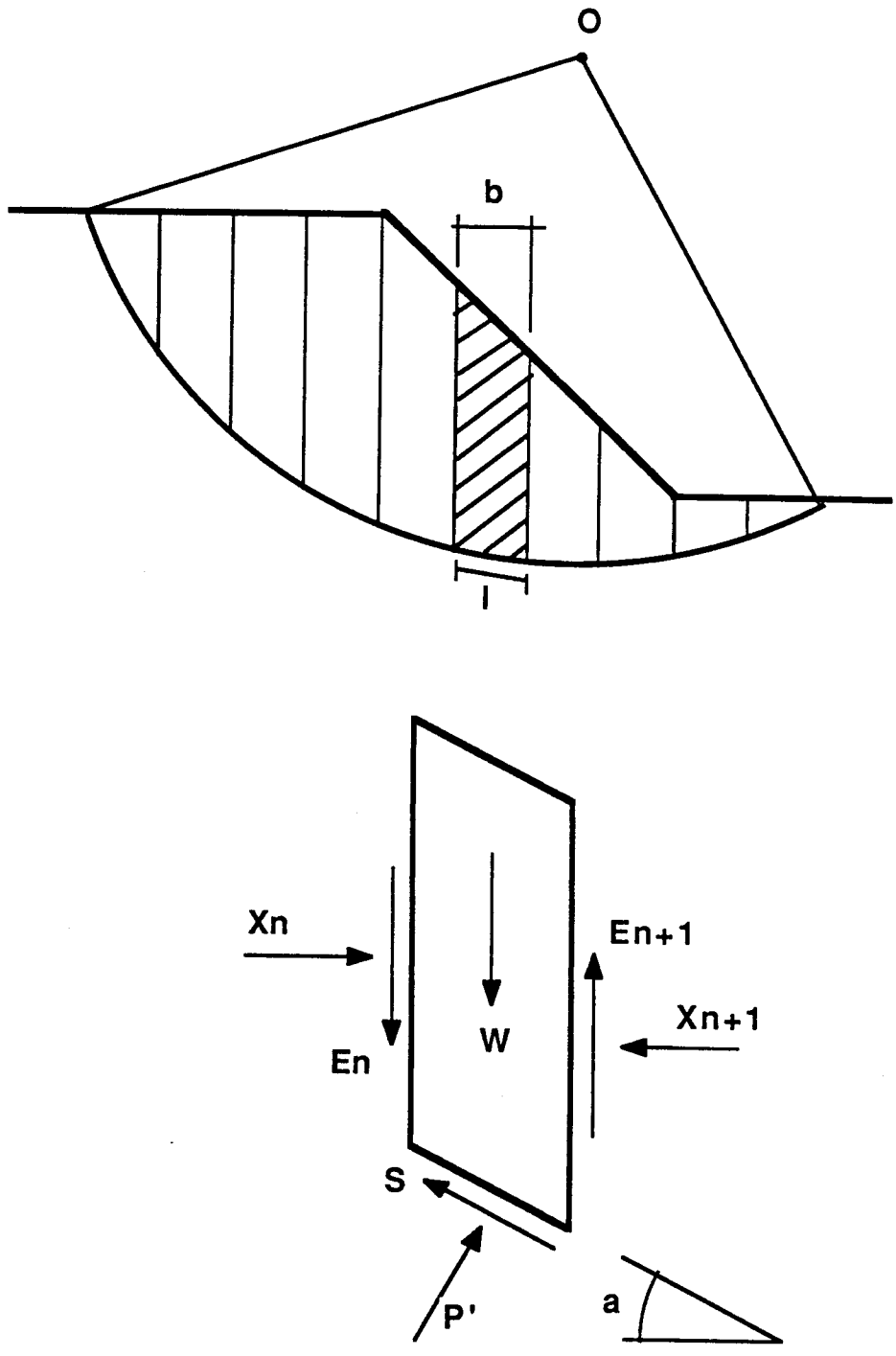

Figure 6.1: Forces on a Typical Slice

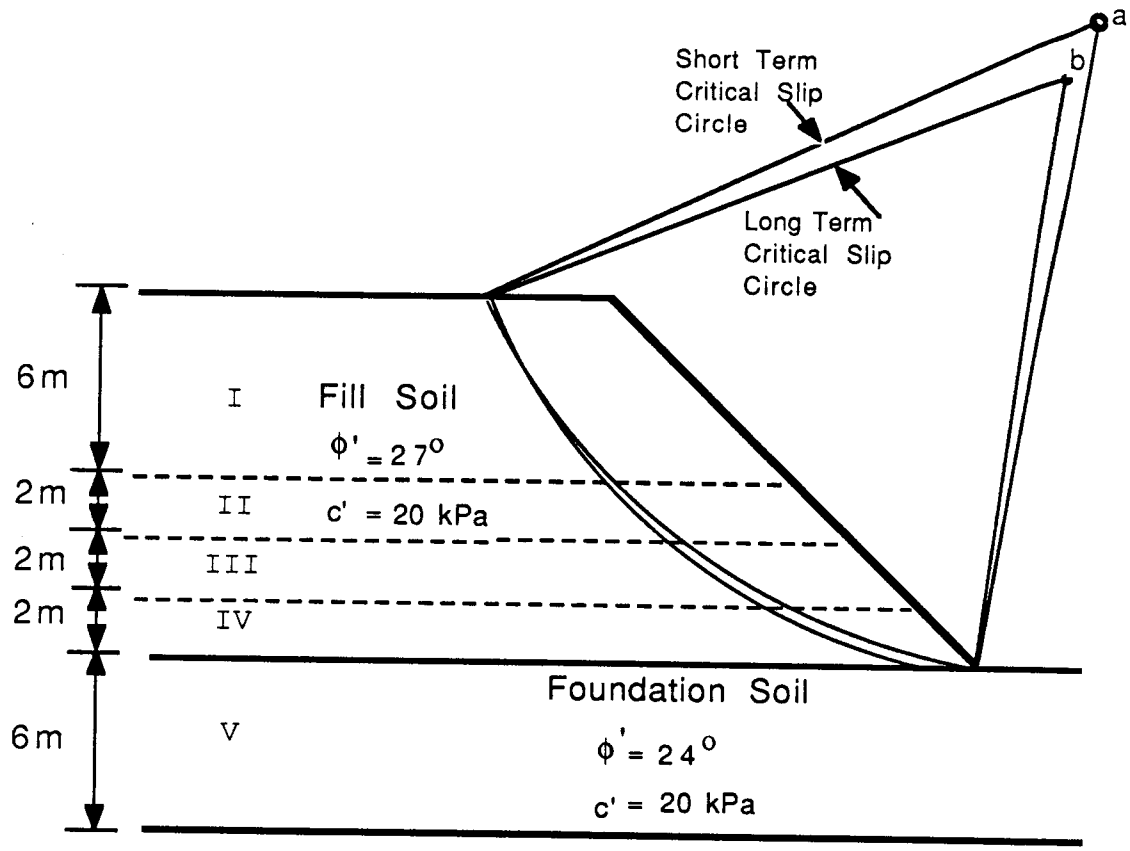

Figure 6.2: Critical Slip Circles Established for Short and Long Term Stability Analyses

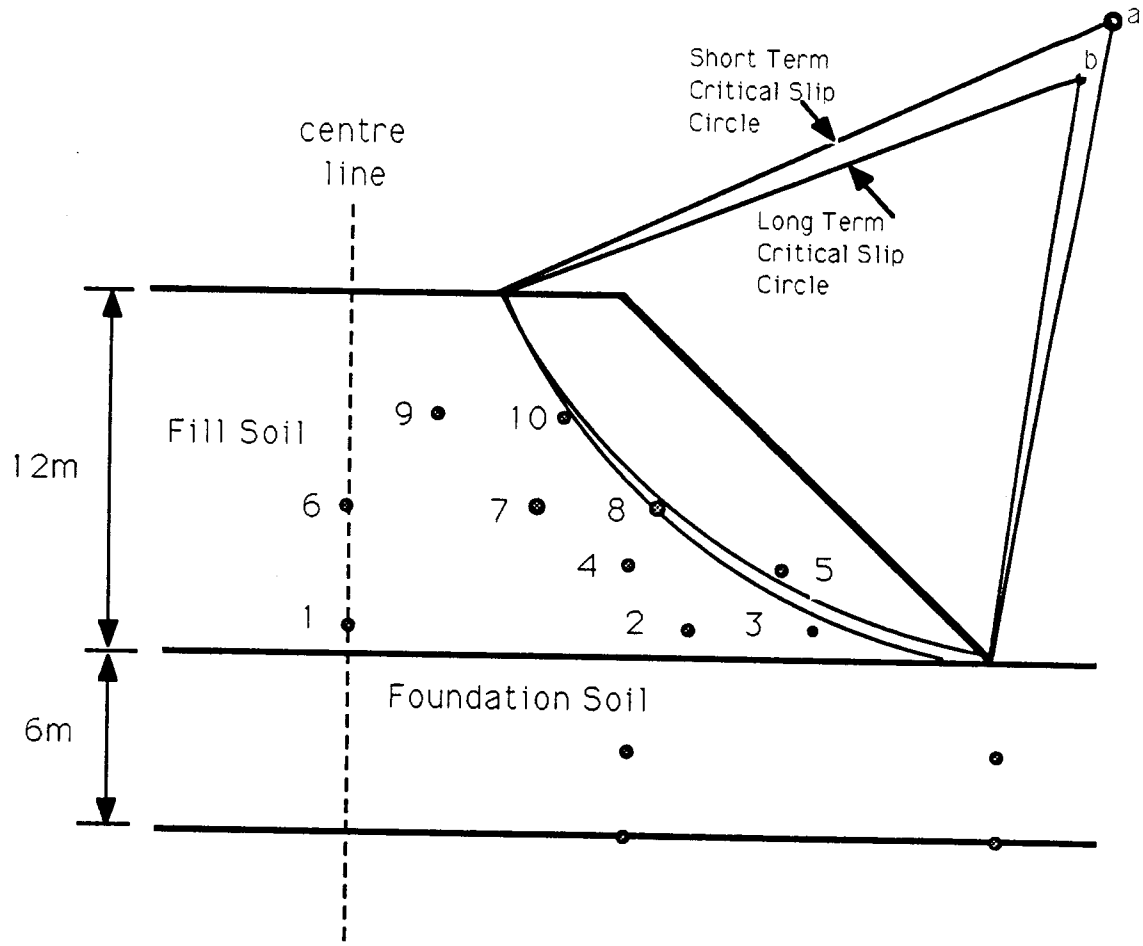

Figure 6.3: Location of Pneumatic Piezometers Installed in Test Fill

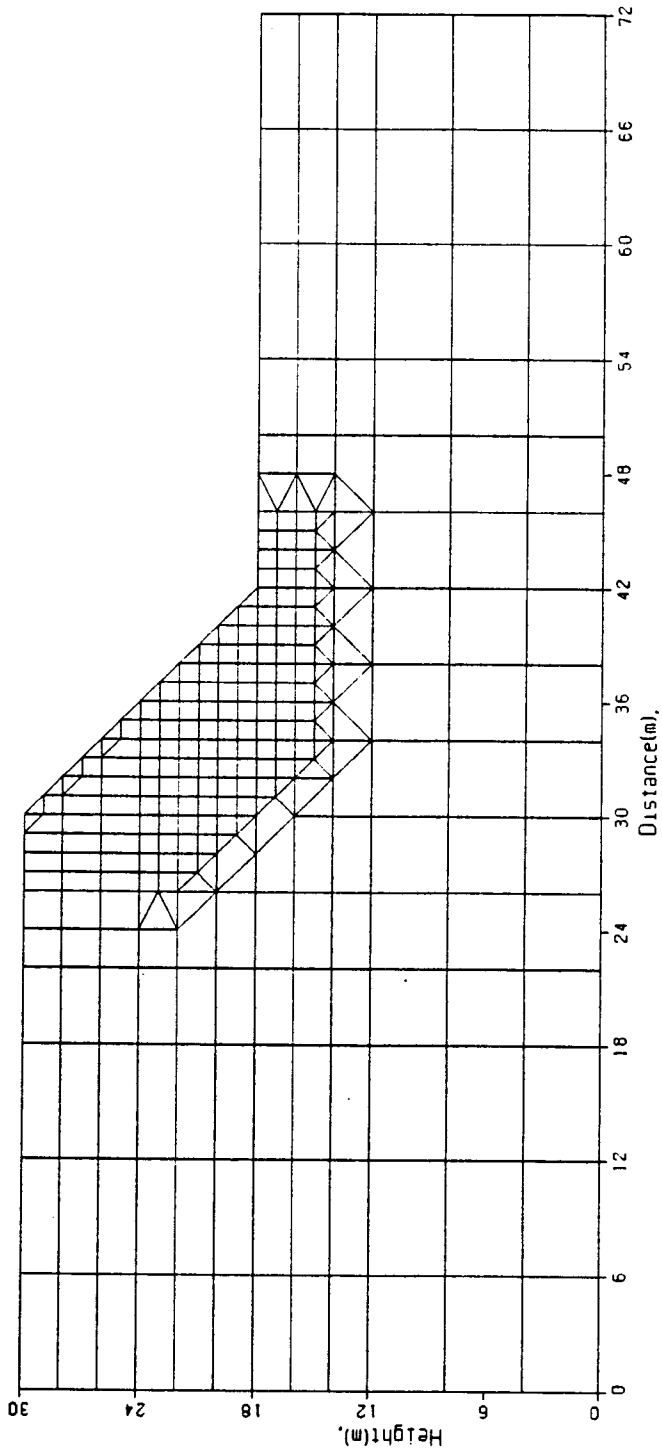

Figure 6.4: Mesh for Finite Element Analysis.

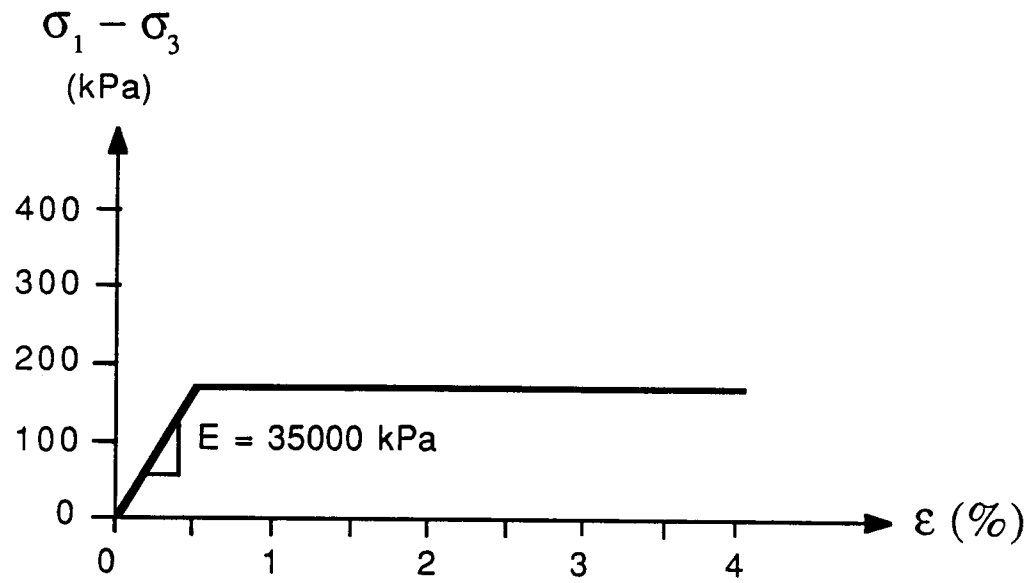

(a) Clayey Silt Foundation Soiil

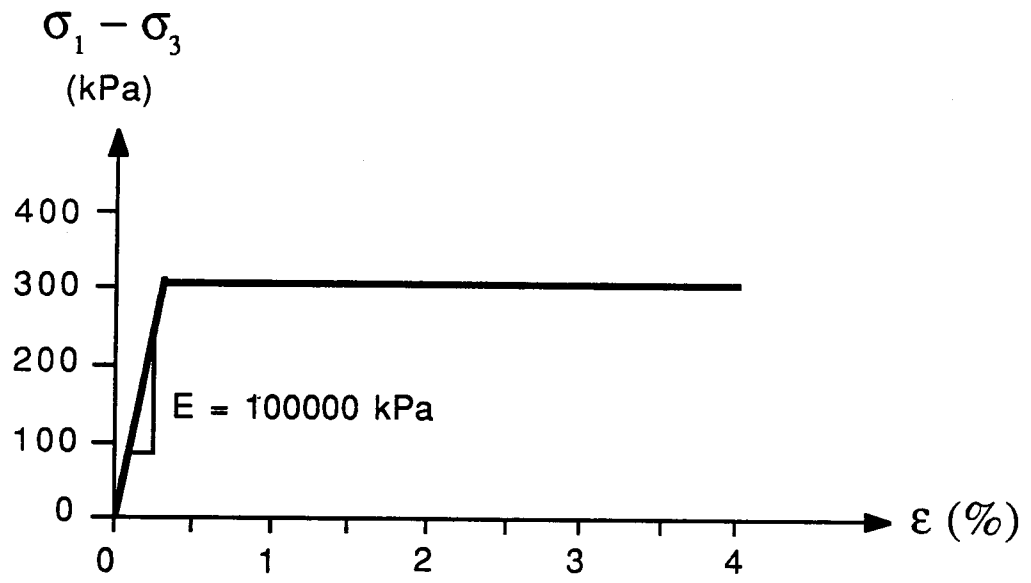

(b) Clay Till Foundation Soil

Figure 6.5 : Stress-Strain Curves for Foundation Tresca Models

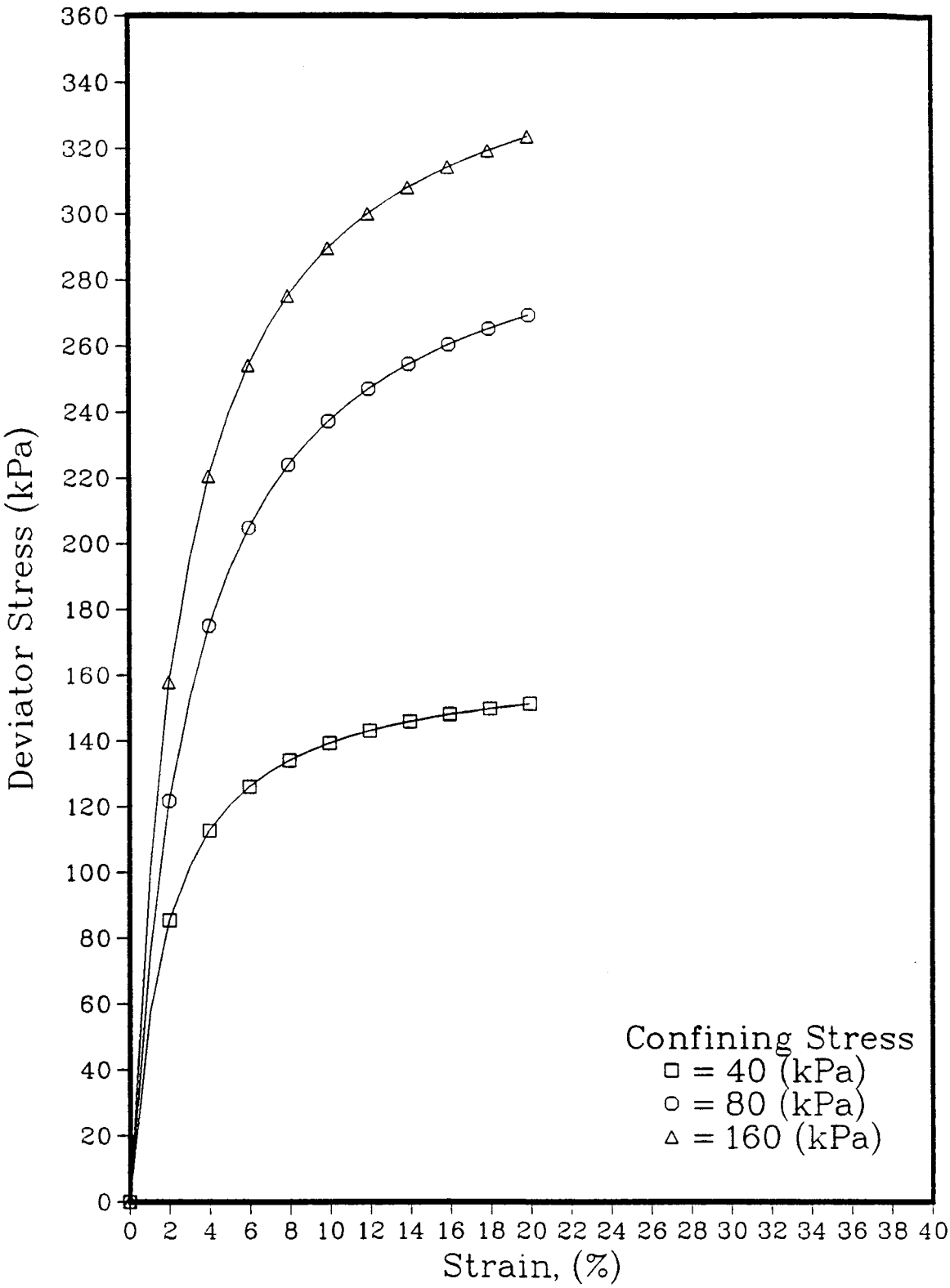

Figure 6.6: Hyperbolic Stress–Strain Models for CD Triaxial Test Data

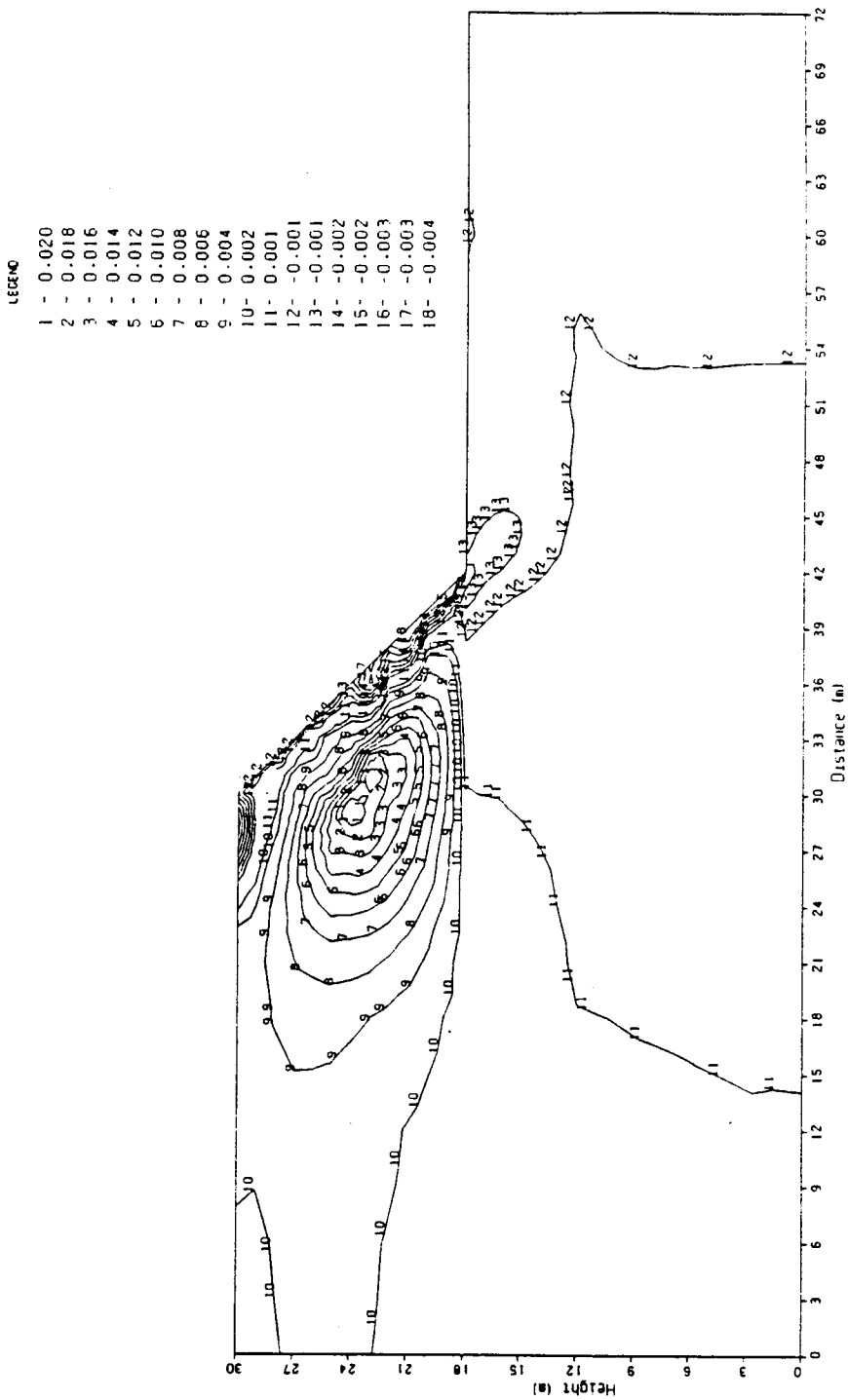

Figure 6.7: Horizontal Strains in Unreinforced Fill Slope: Ht=12m

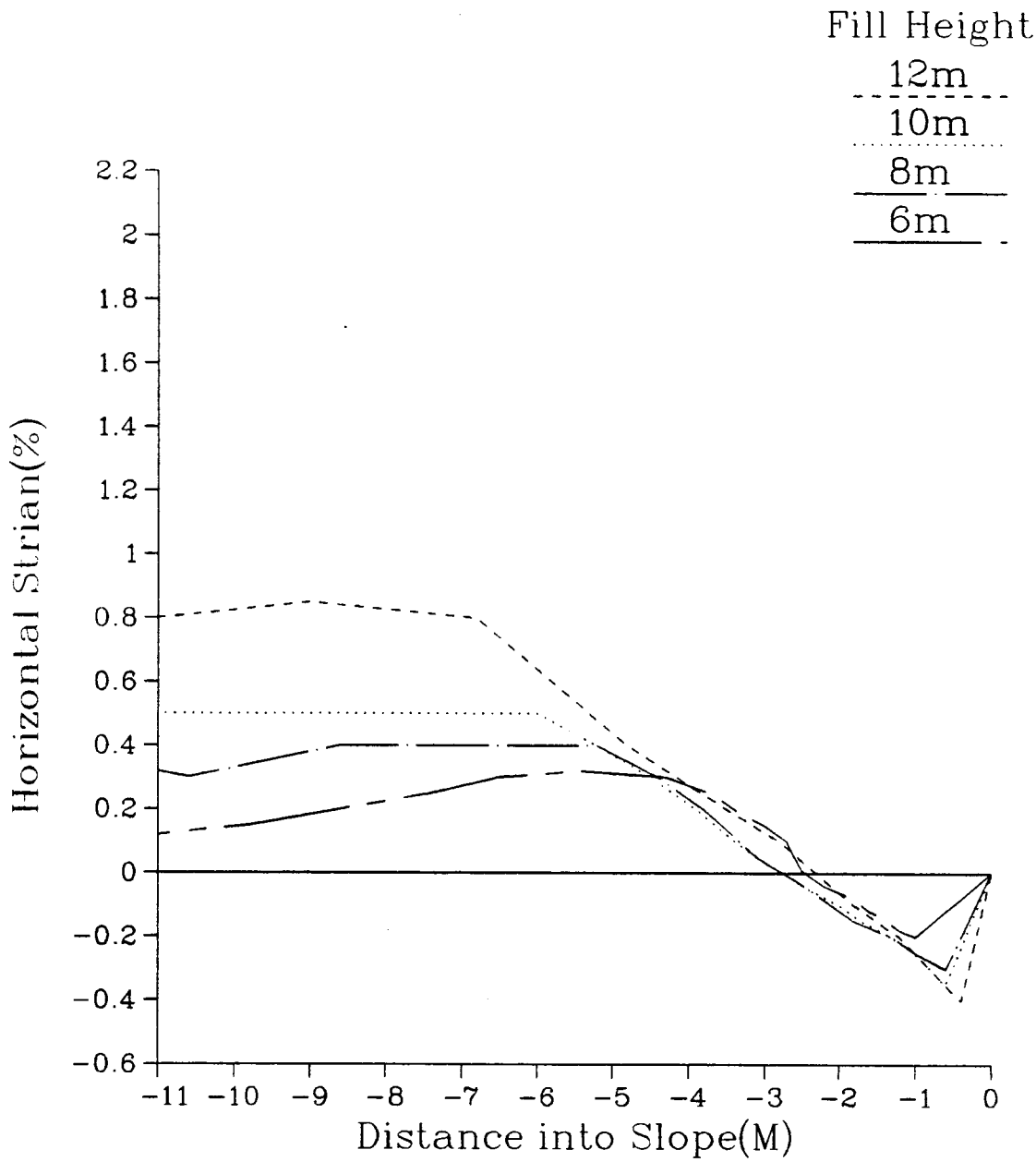

Figure 6.8: Horizontal Strains in Embankment at 1m Elevation

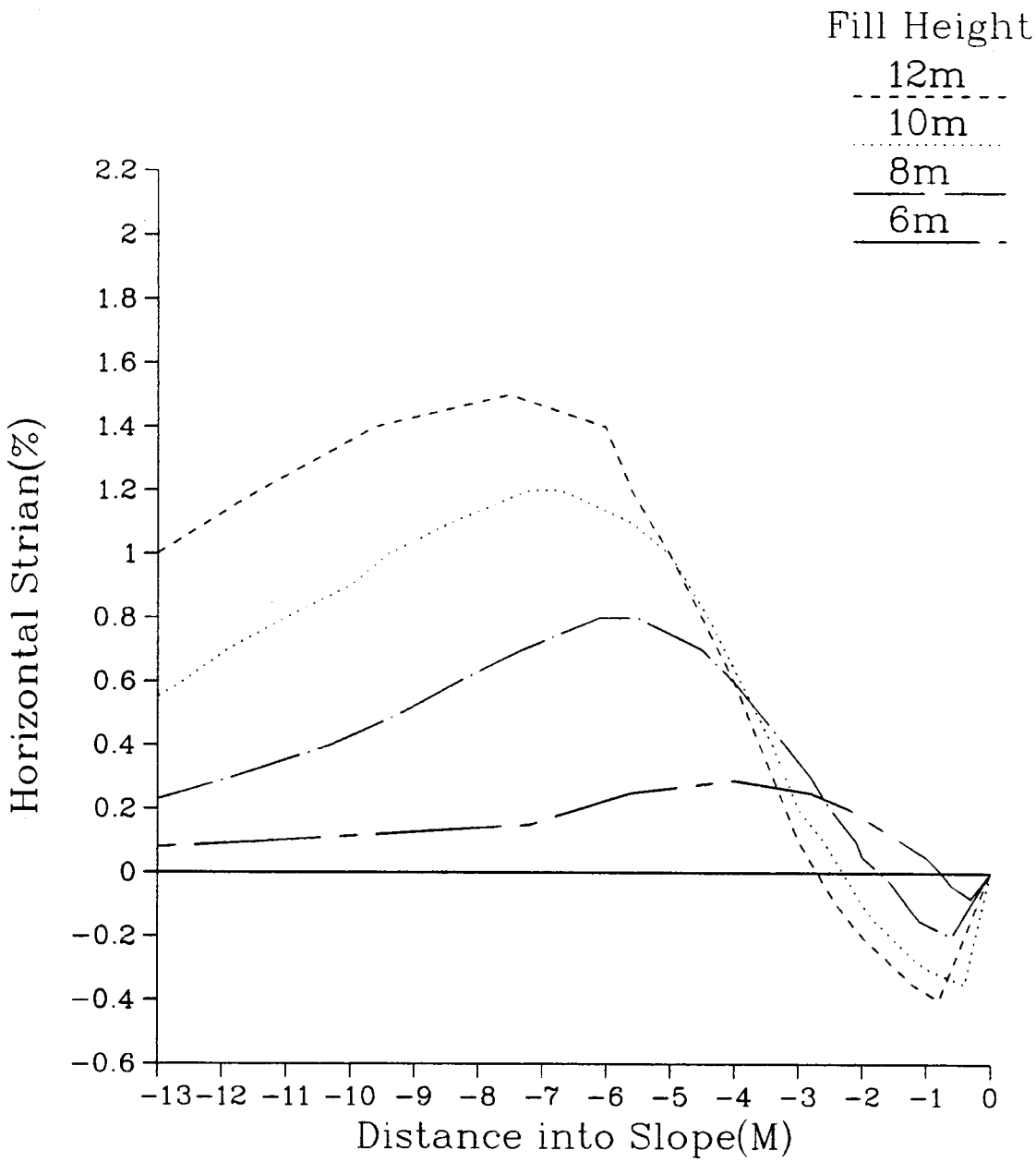

Figure 6.9: Horizontal Strians in Embankment at 3m Elevation

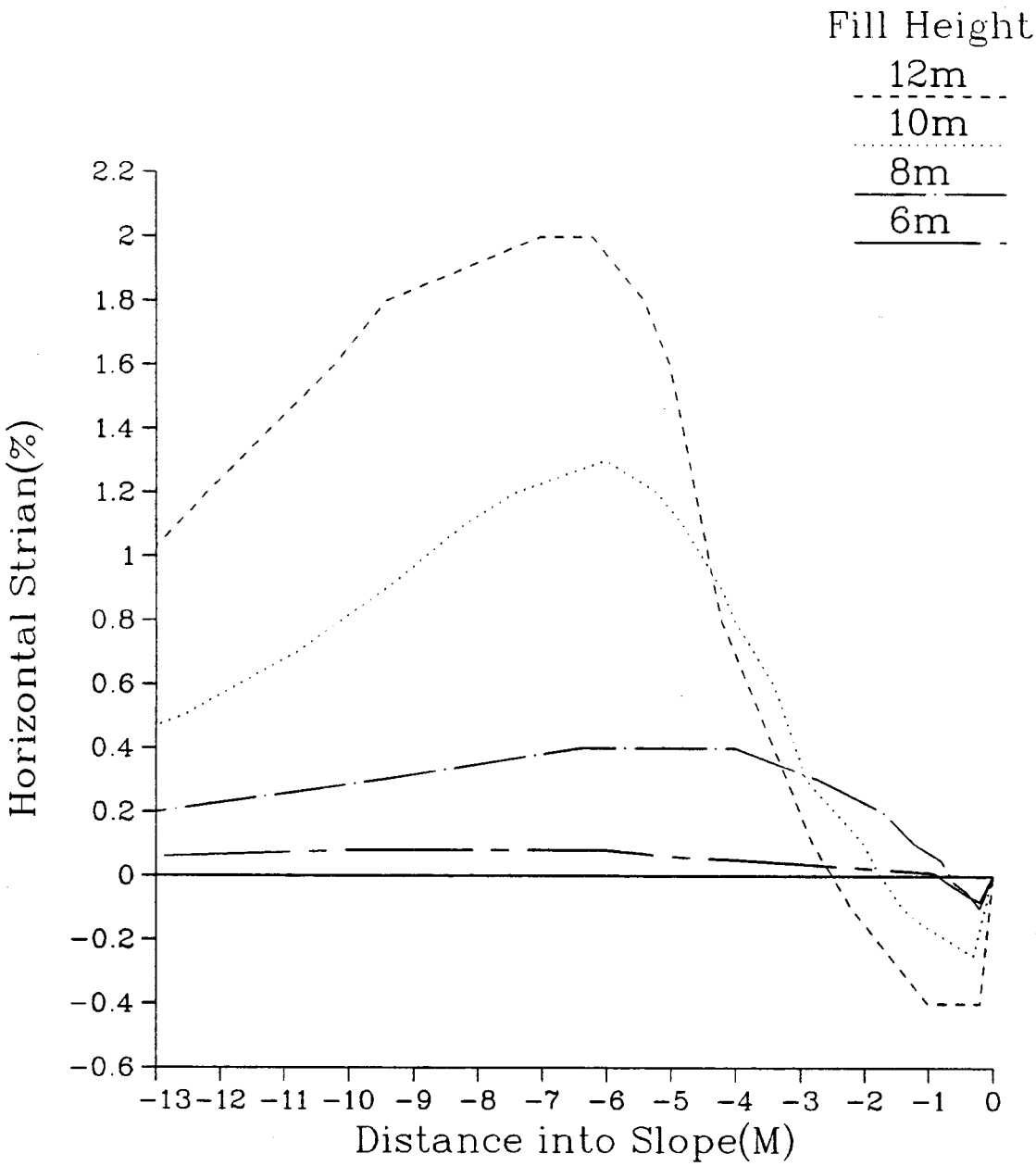

Figure 6.10: Horizontal Strians in Embankment at 5m Elevation

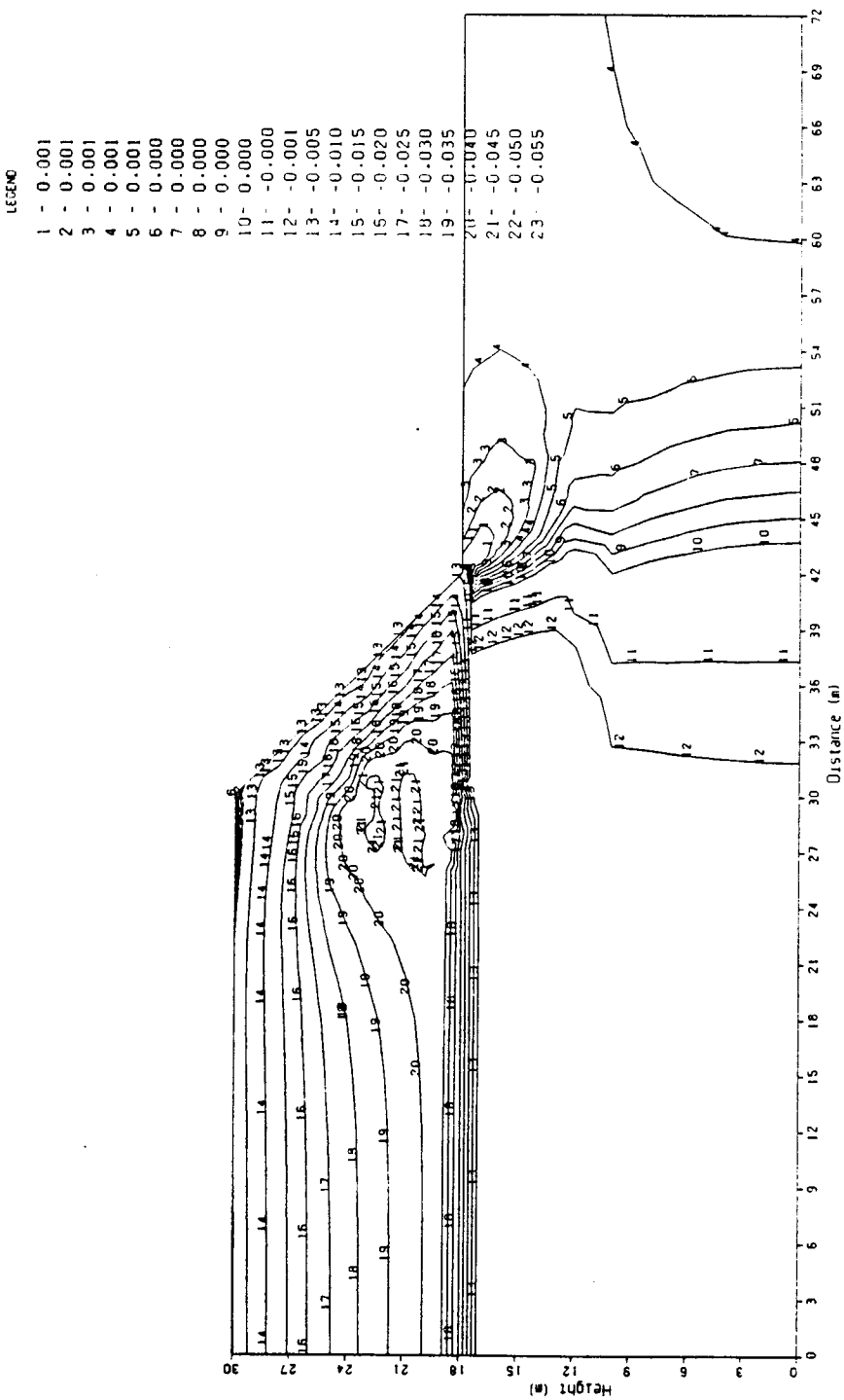

Figure 6.11: Vertical Strains in Unreinforced Fill Slope: Ht=12m

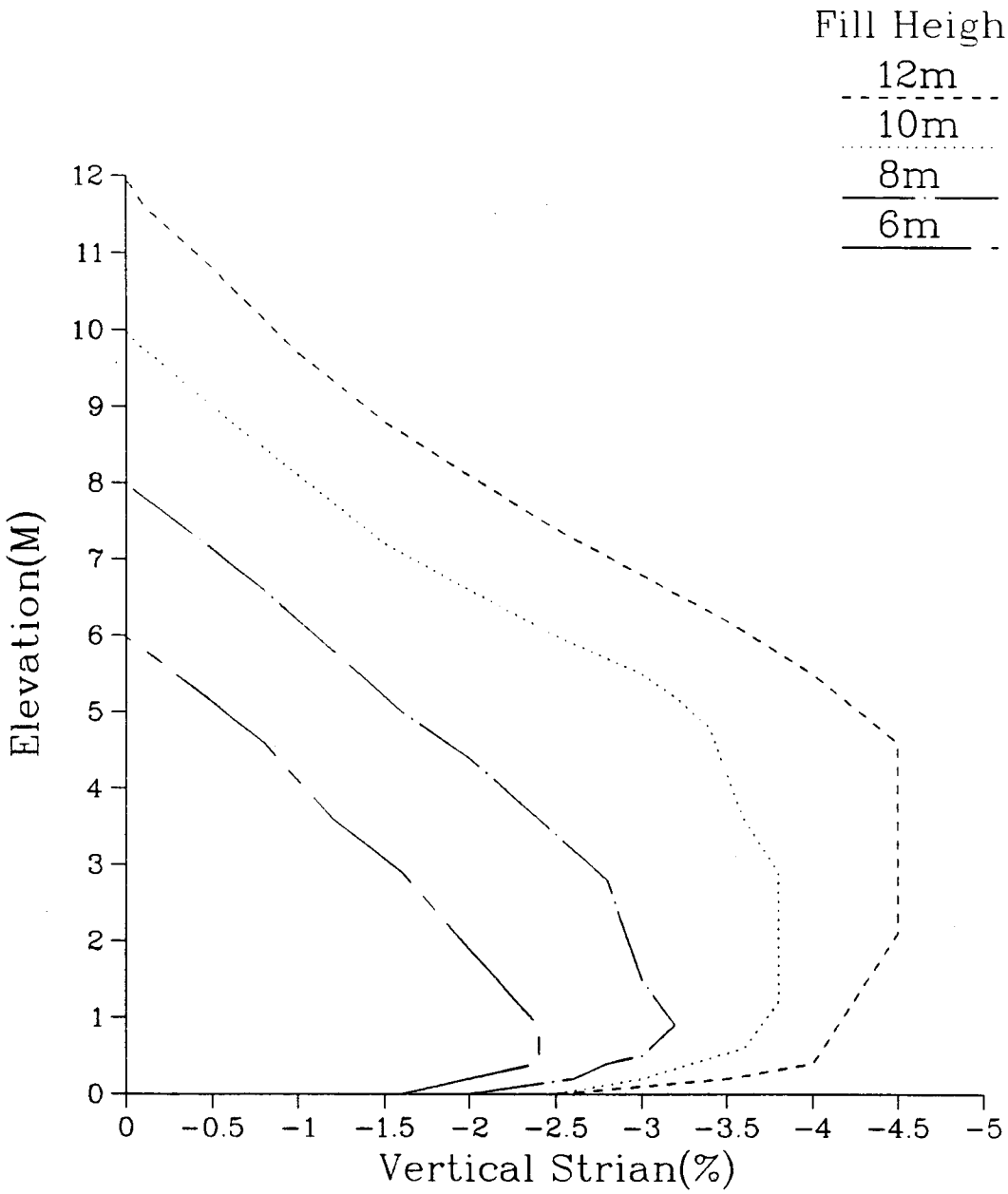

Figure 6.12: Vertical Strains in Embankment Acting Beneath the Crest of the 12 m Slope

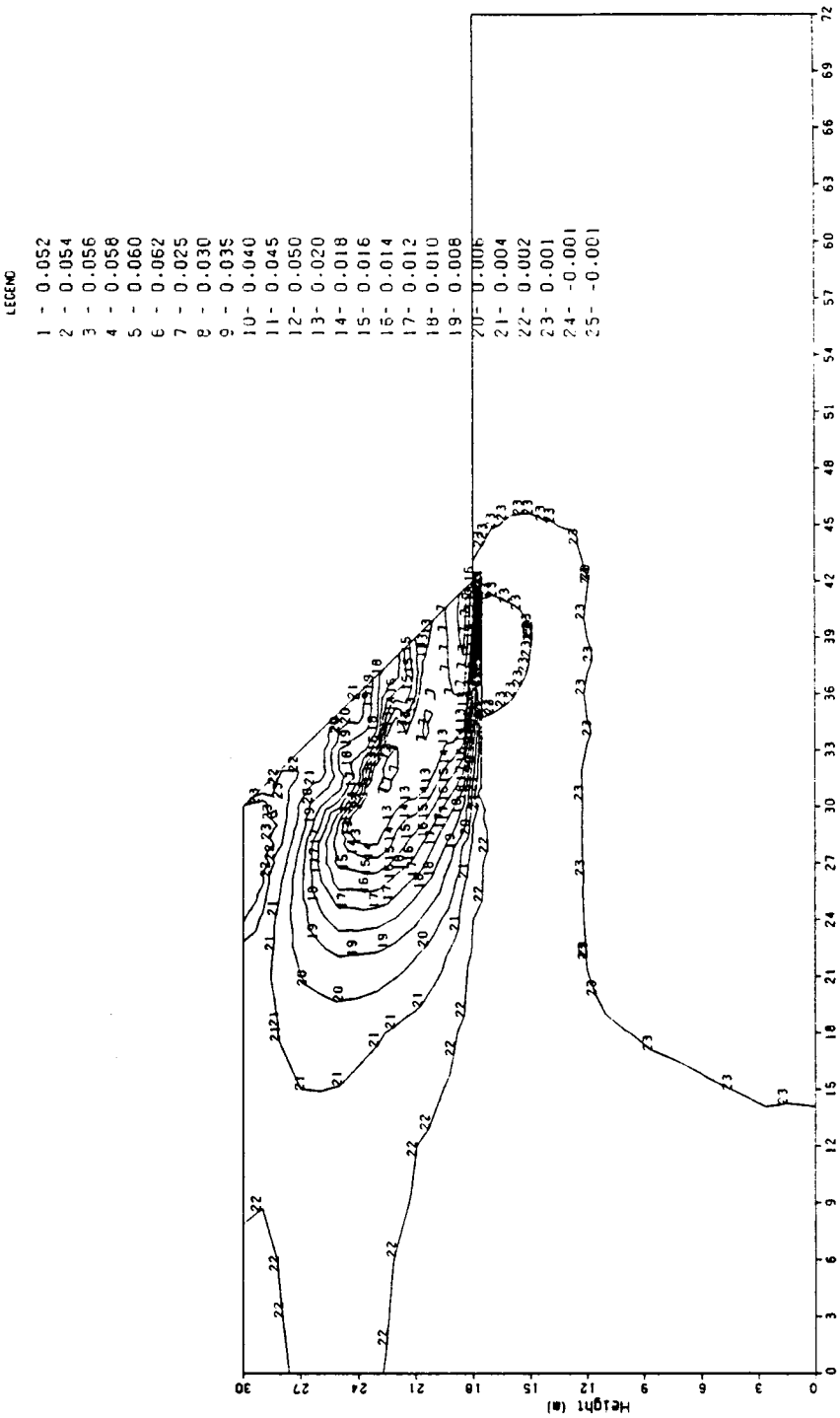

Figure 6.13: Maximum Principal Strains in Unreinforced Fill Slope: Ht=12m

7. CONCLUSIONS AND RECOMMENDATIONS FOR FURTHER RESEARCH

It is required that the test embankment be built such that it will deform substantially in order that the soil/geogrid stress transfers which take place can be monitored. Furthermore, the embankment slopes must be of homogeneous shear strength to allow for comparison between each of the geogrid reinforced slopes and the unreinforced slope. Therefore, it was necessary to fully define the stress-strain properties of the various fill soils available to construct the embankment. It was also necessary to assess the stress-strain properties of the foundation soil such that stability and deformational analyses of the unreinforced control slope could be conducted.

The stress-strain properties of both the fill and foundation soils determined through laboratory testing will be summarized below and recommedations will be made as to construction procedures for the test embankment. The factors of safety against slope instability and the predicted deformational behaviour determined using the soil parameters established in the laboratory will then be reviewed. Finally, recommendations for further research will be presented.

7.1 Summary of the Strength, Stress-Strain and Pore Pressure Properties of the Fill Soils

1.

The Atterberg limits, activities and grain size

distributions of the clay and silt fill soils are similar. However, their compaction curves differ significantly. The same compaction effort applied to silt and clay soil at the same water content results in denser silt specimens.

2. The unconsolidated undrained strengths of the silt and clay specimens, compacted at 3% wet of their respective optimum water contents are the same. Thus to take into account variations in the silt content of the fill soil being used to build the embankment, compaction specifications had to be established based on a homogeneous undrained shear strength rather than on a constant dry density and water content.
3. The stress-strain behaviour of the silt and clay fill soils, exhibited during the unconsolidated undrained triaxial tests, differ considerably at strains of between 2 and 10%. For a constant strain, higher stresses exist in the clay soil.
4. The unconsolidated undrained triaxial tests conducted by Alberta Transportation and Utilities on sandy clay fill compacted to the maximum dry standard compaction density at the optimum water content show a greater cohesive strength but no change in the frictional strength.
5. The consolidated undrained effective stress strength parameters obtained for the silt and clay fill soils are similar. However, the stress-strain behaviour of the soils differ in the same manner that was exhibited

during the unconsolidated undrained triaxial tests.

6. Positive pore pressures were developed in the silt and clay specimens during consolidated undrained triaxial tests. The A_f parameters measured during the tests increased with confining stress up to a maximum of only 0.5 under a confining stress of 175 kPa. Therefore, pore pressures developed due to shear stresses in the test embankment should not be significantly high.
7. In agreement with the pore pressure behaviour observed during consolidated undrained triaxial tests, the volume changes measured during consolidated drained shearing of the clay fill soil were small. The largest volume change recorded was a contraction of 1.1%.

7.2 Construction Specifications for the Test Embankment

If the clay fill soil is compacted at a 2 to 3% higher water content than the silt fill soil, then a homogeneous undrained shear strength will be achieved. The complete compaction specifications include a water content of between 22 and 24% at a corresponding dry density of between 1.66 and 1.59 g/cm^3 for the clay fill soil and a water content of between 20 and 22% at a corresponding density of between 1.71 and 1.66 g/cm^3 for the silt fill soil. Close control of the type of fill soil being placed in the field and the corresponding compaction requirements specified for each type of soil must be exercised if homogeniety with respect to shear strength within the embankment is to be maintained.

It should be emphasized that although the undrained shear strengths of the two fill soils are the same, the stress-strain behaviour differs significantly at strains of between 2 and 10%. Silt specimens show approximately twice as much strain as the clay specimens at the same stress level. Consequently, the strains which are induced in a layer of geogrid in the test embankment will depend upon the type of fill soil in which the geogrids have been installed.

7.3 Summary of the Strength, Stress-Strain and Pore Pressure Properties of the Foundation Soil

1. The results obtained from oedometer tests conducted on the foundation soil showed that the preconsolidation stress is approximately 400, which is more than the increase in stress the foundation soil will be subject to due to the weight of the test fill. Therefore, settlement of the foundation soil due to the weight of the overlying test fill is not expected to be large. Settlement, due to primary consolidation under a 12 m high embankment was calculated to be only 3.4 cm based on the coefficient of recompression calculated for the Shelby tube foundation soil samples.
2. The pore pressures developed during consolidated undrained triaxial tests conducted on block samples and Shelby tube specimens of foundation soil were similar to

those developed in the fill soil specimens. The maximum A_f paramter calculated for the foundation soil specimens under a confining stress of 300 kPa was 0.84.

3. The average horizontal and vertical coefficients of permeability calculated for the foundation soil under normal loads of 500 and 800 kPa were 5.3x10-7 cm/s and 1.3x10-7 cm/s, respectively. The permeability of the soil would probably be higher under lower normal stresses, however, due to the shapes of the consolidation curves, the permeabilities could not be calculated for normal stresses equal to those that would be applied by the test embankment. The time required for the foundation soil to complete 90% of the primary consolidation in the field, if the test fill were built to a height of 12 m quickly, was calculated to be only 21 days.

7.4 Summary of the Limit Equilibrium Anayses Conducted on the Unreinforced Slope of the Test Embankment

To ensure that the test fill deforms as much as possible without undergoing a shear failure, the geometry of the embankment and the soil properties should be such that the minimum factor of safety of the unreinforced slope is 1.0. The short term factor of safety calculated for the unreinforced slope of the test fill, considering high pore pressures, is 1.15 for a 10 m high embankment and 0.87 for a 12 m high embankment. The long term factor of safety

calculated, assuming that the excess pore pressures have dissipated to zero, is 1.36 for a 12 m high slope. Therefore, the limit equilibrium analyses show that the above objective has been met.

7.5 Summary of the Finite Element Analysis Conducted on the Unreinforced Slope of the Test Embankment

The finite element analysis shows that the maximum horizontal strain which occurs in the embankment is only 2%. This strain occurs within a region located about 7 m into the slope face at an elevation of approximately 5 m. The load that would be induced in a typical geogrid with a secant modulus of 950 kN/m at a strain of 2% would be 19 kN/m. This load is significantly less than the working tensile strength specified by many geogrid manufacturers.

7.6 Recommedations for Further Research

During construction of the test embankment and once it has been constructed to the full height of 12 m, the actual deformations and pore pressures occurring within the embankment should be monitored. The deformations occuring within the unreinforced slope of the embankment may be compared with those predicted in this study.

An attempt should be made to model the behaviour of the reinforced slopes of the test embankment using a finite element program which incorporates layers of geogrid into the analysis. Chalaturnyk (1988) has modified the finite

element program SAGE, developed at the University of Alberta (Chan, 1986), to include two dimensional, plane strain reinforcement elements. Interface elements which allow for relative displacements to occur between the soil and reinforcement have also been developed by Chalaturnyk. This computer program could be used to model the deformations and stress transfers which take place within the reinforced slopes of the test embankment. The finite element program may be calibrated with the strain measurements taken along the actual geogrids and within the fill soil composing the embankment. This may be the key to understanding the mechanisms by which geogrids act to reinforce a mass of soil.

REFERENCES

American Society for Testing and Materials (ASTM) Standards, 1986. Annual Book of ASTM Standards, Vol. xx.

Bayrock, L.A., and Hughes, G.M., 1962. Surficial Geology of the Edmonton District, Alberta. Alberta Research Council, Geology Division, PREL Report 62-6.

Bishop, A.W., 1955. The Use of the Slip Circle in the Stability Analysis of Slopes. Géotechnique, Vol. 7, No. 1, pp. 7-17.

Bishop, A.W., and Henkle, D.J., 1962. The Measurement of Soil Properties in the Triaxial Test. William Clowes and Sons Limited, London, Reccles and Clochester, pp. 106-119.

Bjerrum, L., and Simons, N.E., 1960. Comparison of Shear Strength Characteristics of Normally Consolidated Clays. Research Conference on Shear Strength of Cohesive Soils, ASCE, Boulder Colorado, pp. 711-726.

Bobey, L.W.M., 1988. Soil-Geogrid Interfacial Shear Strength. M.Sc. Thesis, Department of Civil Engineering, University of Alberta, pp. 1-176.

Brooker, E.W., and Ireland, H.O., 1965. Earth Pressures at Rest Related to Stress History. Canadian Geotechnical Journal, Vol. 2, No. 1, pp. 1-15.

Carlson, V.A., 1967. Bedrock Topography and Surficial Aquifers of the Edmonton District, Alberta. Alberta Research Council, Report 66-3, pp. 1-21.

Casagrande, A., 1936. Determination of the Pre-consolidation Load and its Practical Significance. Discussion D-34, Proceedings of the First International Conference on Soil Mechanics and Foundation Engineering, Cambridge, Massachusetts, Vol. 3, pp.60-64.

Casagrande, A., 1938. Notes on Soil Mechanics - First Semester. Harvard University (unpublished), pp. 1-129.

Casagrande, A., 1948. Classification and Identification of Soils. Transactions, ASCE, Vol. 113, pp. 901-930.

Casagrande, A., and Hirschfeld, R.C., 1960. First Progress Report on Investigation of Stress-Deformation and Strength Characteristics of Compacted Clays. Pierce Hall, Harvard University, Cambridge, Massachusetts, May, 1960.

Casagrande, A., and Hirschfeld, R.C., 1962. Second Progress Report on Investigation of Stress-Deformation and Strength Characteristics of Compacted Clays. Pierce Hall, Harvard University, Cambridge, Massachusetts, April, 1962.

Chalaturnyk, R., 1988. The Behaviour of a Reinforced Soil Slope. M.Sc. Thesis, Department of Civil Engineering, University of Alberta, pp. 1-320.

Chan, D., 1986. Finite Element Analysis of Strain Softening Material. Ph.D. Thesis, Department of Civil Engineering, University of Alberta, pp. 1-345.

Duncan, J.M., and Wright, S.G., 1980. The Accuracy of Equilibrium Methods of Slope Stability Analysis. Engineering Geology, Elsevier Scientific Publishing Co., Amsterdam, Vol. 16, pp. 5-17.

Eisenstien, Z., and Law, S.T.C., 1979. The Role of Constitutive Laws in Analysis of Embankments. Third International Conference on Numerical Methods in Geomechanics, Aachen, April, 1979, pp. 2-6. CHECK!

Gabert, Gordon, M., 1968. The Geology and Hydrogeology of the Surficial Deposits in the Devon Area, Alberta. University of Alberta, Department of Geology, B.Sc. Thesis.

Hirschfeld, R.C., 1959. The Relationship Between Shear Strength and Effective Stress. First Pan-American Conference on Soil Mechanics and Foundation Engineering, Mexico, September, 1959.

Holtz, W.G., and Ellis, W., 1963. Comparison of the Shear Strengths of Laboratory and Field-Compacted Soils. ASTM Symposium on Laboratory Shear Testing of Soils, STP No. 361, vii, pp. 1-505.

Holtz, R.D., and Kovacs, W.D., 1981. An Introduction to Geotechnical Engineering. Prentice-Hall Inc., Englewood Cliffs, N.J. pp. 1-733.

Lambe, T.W., 1958. The Engineering Behaviour of Compacted Clay. ASCE Proceedings, Paper 1655, May, 1958. JSMFD Vol. 84, No. SM2, pp. 1655-1 to 1655-35.

Lambe, T.W., 1958. The Structure of Compacted Clay. ASCE Proceedings, Paper 1654, May 1958. JSMFD, Vol. 84, No. SM2, pp. 1654-1 to 1654-34. No. SM2,

Leonards, G.A., 1976. Estimating Consolidation Settlements of Shallow Foundations on Overconsolidated Clays. Special Report 163, Transportation Research Board, pp.

13-16.

Lovell, C.W., and Johnson, J.M., 1981. Shearing Behaviour of Compacted Clays After Saturation. Laboratory Shear Strength of Soil. SPT 740, ASTM Symposium, June 25, 1980, pp. 277-293.

Ower, J.R., 1958. The Edmonton Formation. Edmonton Geological Society, Quart., Vol. 2, No. 1, pp. 3-11.

Peck, R.B., 1940. Sampling Methods and Laboratory Tests for Chicago Subway Soils. Proceedings, Purdue Conference on Soil Mechanics, pp. 140-150.

Peck, R.B., 1960. Failure Hypotheses for Soils. Discussion, Proceedings of the Research Conference on the Shear Strength of Cohesive Soils. ASCE, Boulder, Colorado, pp. 987-989.

Peck, R.B., Hanson, Walter, E., Thornburn, Thomas, H., 1974. Foundation Engineering, Second Edition, John Wiley and Sons, Inc., New York, p.114.

Rivard, P.J., and Goodwin, T.E., 1978. Geotechnical Characteristics of Compacted Clays for Earth Embankments in the Prairie Provinces. Canadian Geotechnical Journal, Vol. 15, 1978, pp. 391-401.

Seed, H.B., and Chan, C.K., 1959. Structure and Strength Characteristics of Compacted Clays. ASCE Proceedings, Paper 2216, October, 1959.

Seed, H.B., and Chan, C.K., 1959. Undrained Strength of Compacted Clays After Soaking. ASCE Proceedings, Paper 2293, December, 1959.

Seed, H.B., Mitchell, J.K.m, and Chan, C.K., 1960. The Strength of Compacted Cohesive Soils. ASCE Research Conference on Shear Strength of Cohesive Soils. University of Colorado, Boulder, Colorado, June 1960.

Skempton, A.W., 1954. The Pore Pressure Coefficients A and B. Géotechnique, Vol. 4, No. 4, p. 143.

Taylor, D.W., 1948. Fundamentals of Soil Mechanics. John Wiley and Sons, Inc., New York, pp. 1-700.

Terzaghi, K., 1943. Theoretical Soil Mechanics. John Wiley and Sons, pp. 265-296.

U.S. Army Engineer Waterways Experiment Station, 1960. The Unified Soil Classification System. Technical Memorandum No. 3-357, Appendix A, Characteristics of Soil Groups Pertaining to Embankments and Foundations, 1953;

Appendix B, Characteristics of Soil Groups Pertaining to Roads and Airfields, 1957.

Vaughan, P.R., 1978. Factors Controlling the Stability of Clay Fills in Britain. Clay Fills: Proceedings of the conference held at the Institution of Civil Engineers, November, 14 and 15, 1978.

APPENDIX A: ADDITIONAL CONSOLIDATION DATA FOR FOUNDATION SOIL

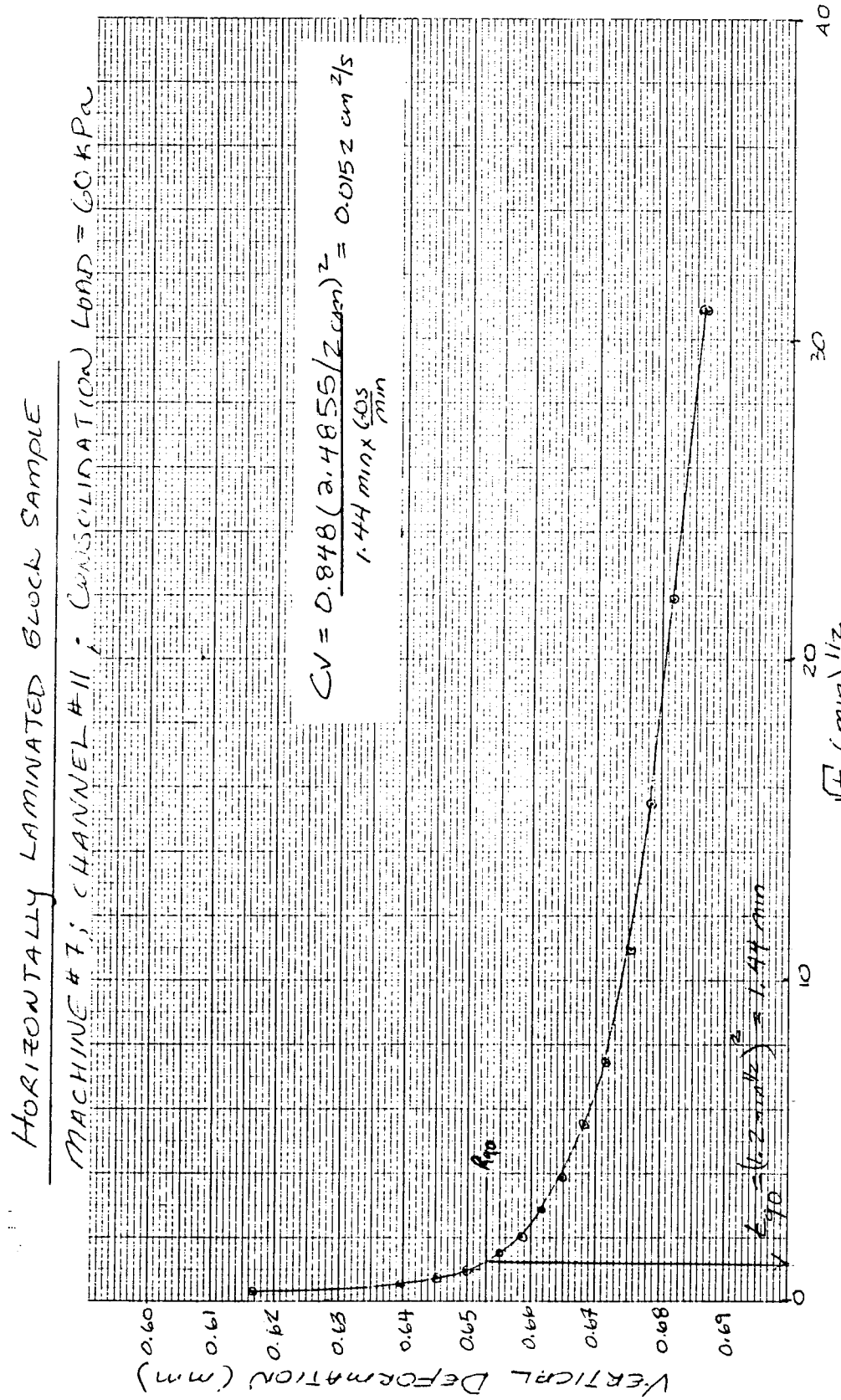

Figure A1: Horizontally Laminated Block Sample #1; Consolidation Load = 60 kPa

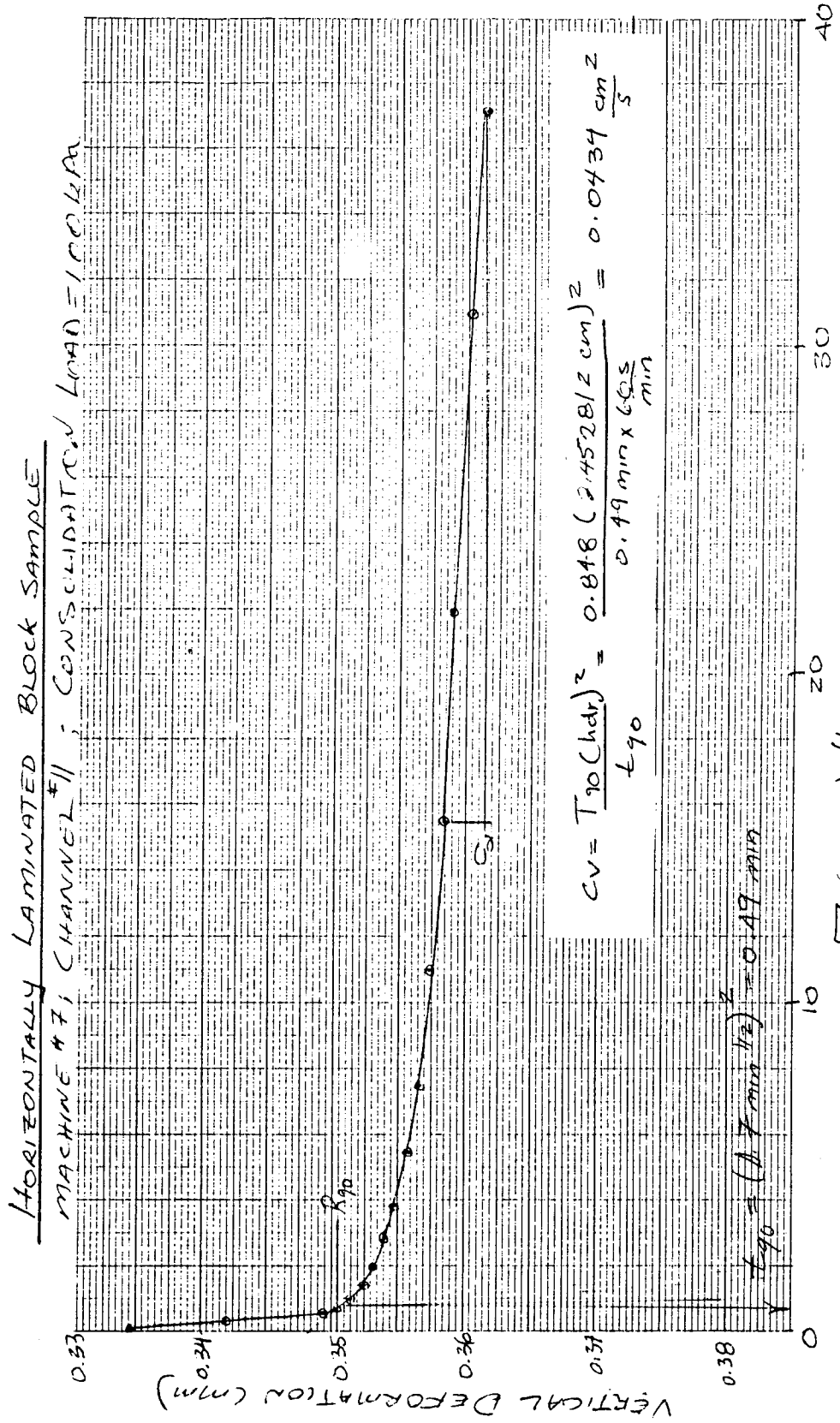

Figure A2: Horizontally Laminated Block Sample #1; Consolidation Load = 100 kPa

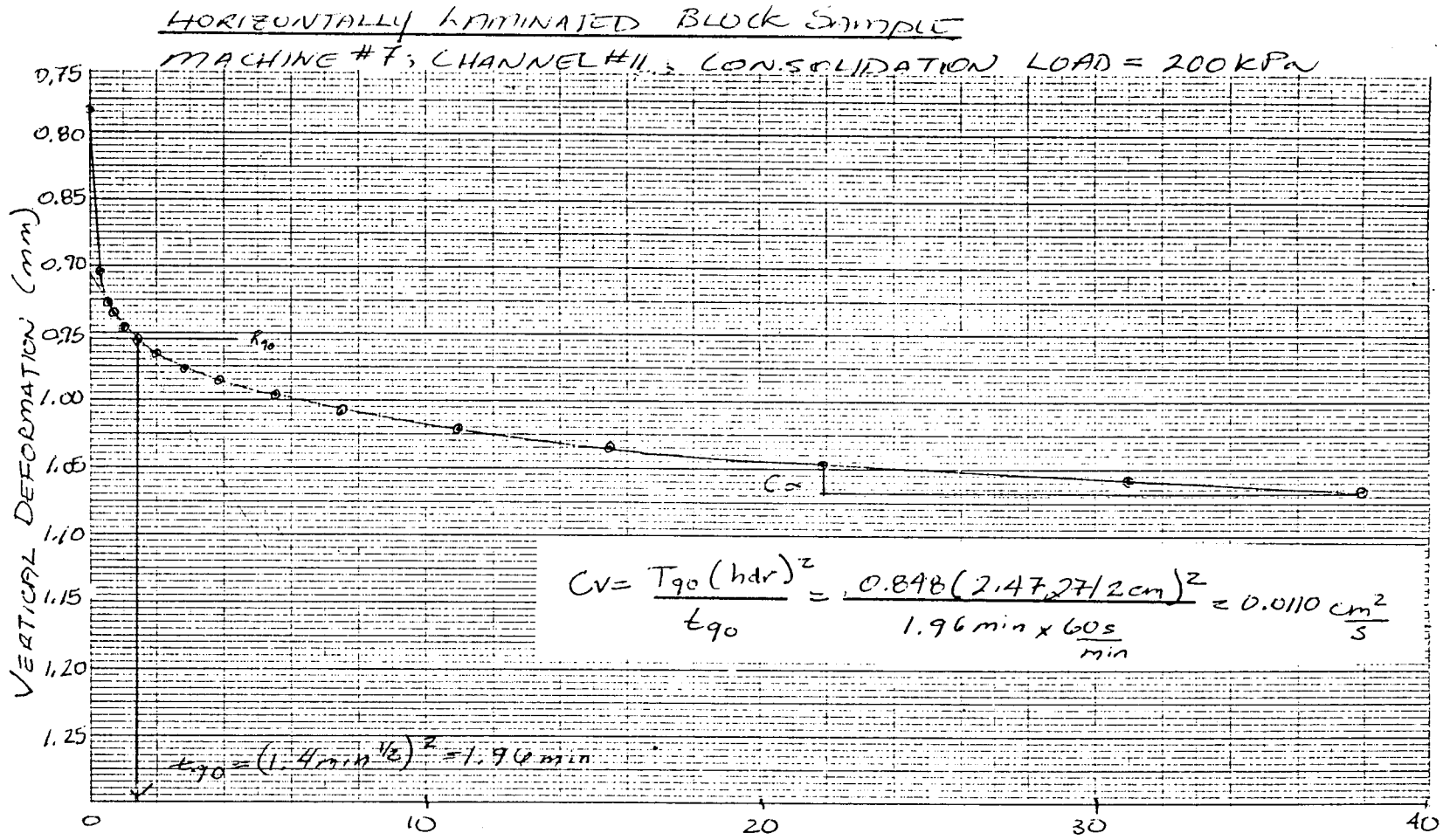

Figure A3: Horizontally Laminated Block Sample #1; Consolidation Load = 200 kPa

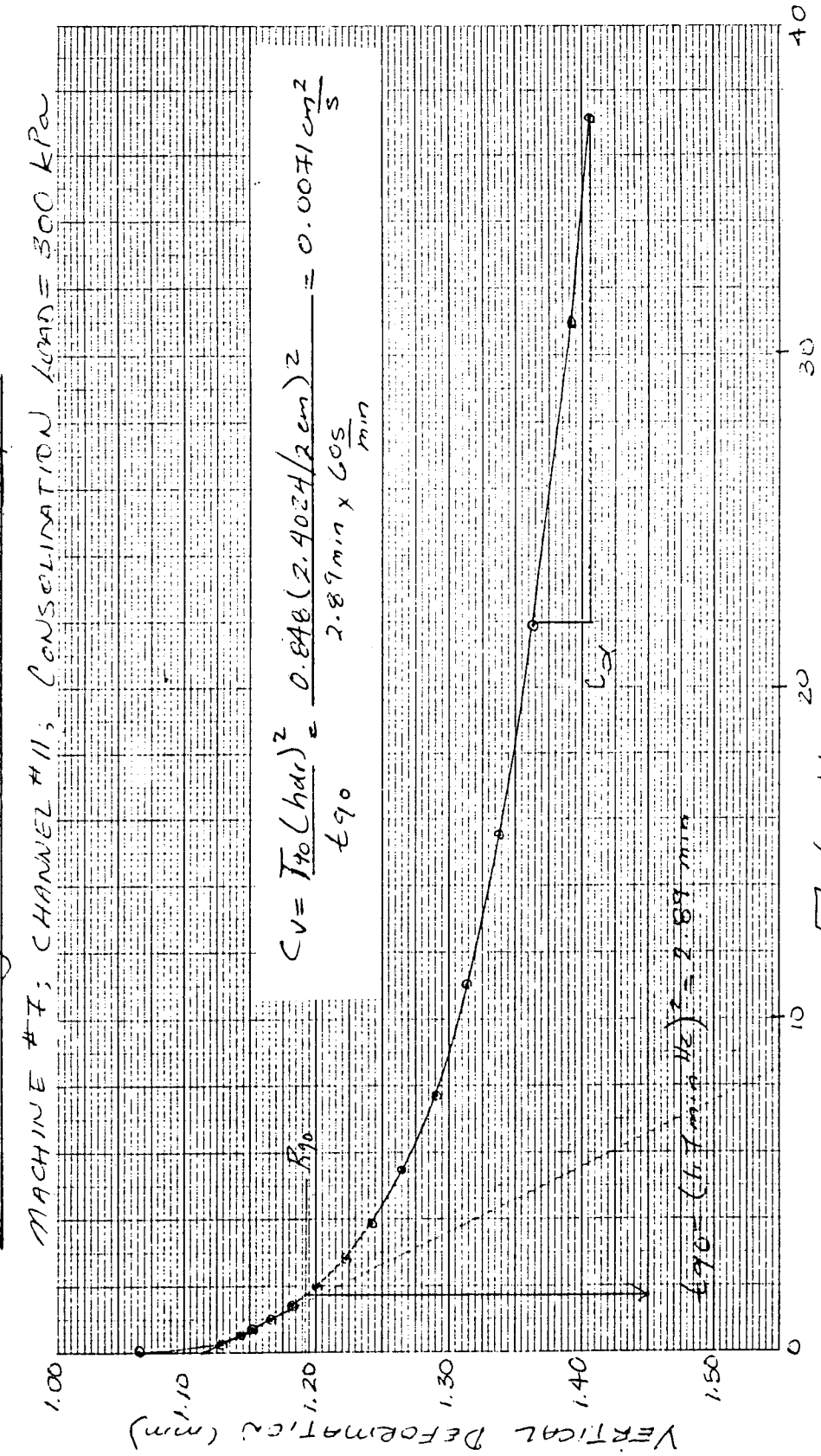

Figure A4: Horizontally Laminated Block Sample #1; Consolidation Load = 300 kPa

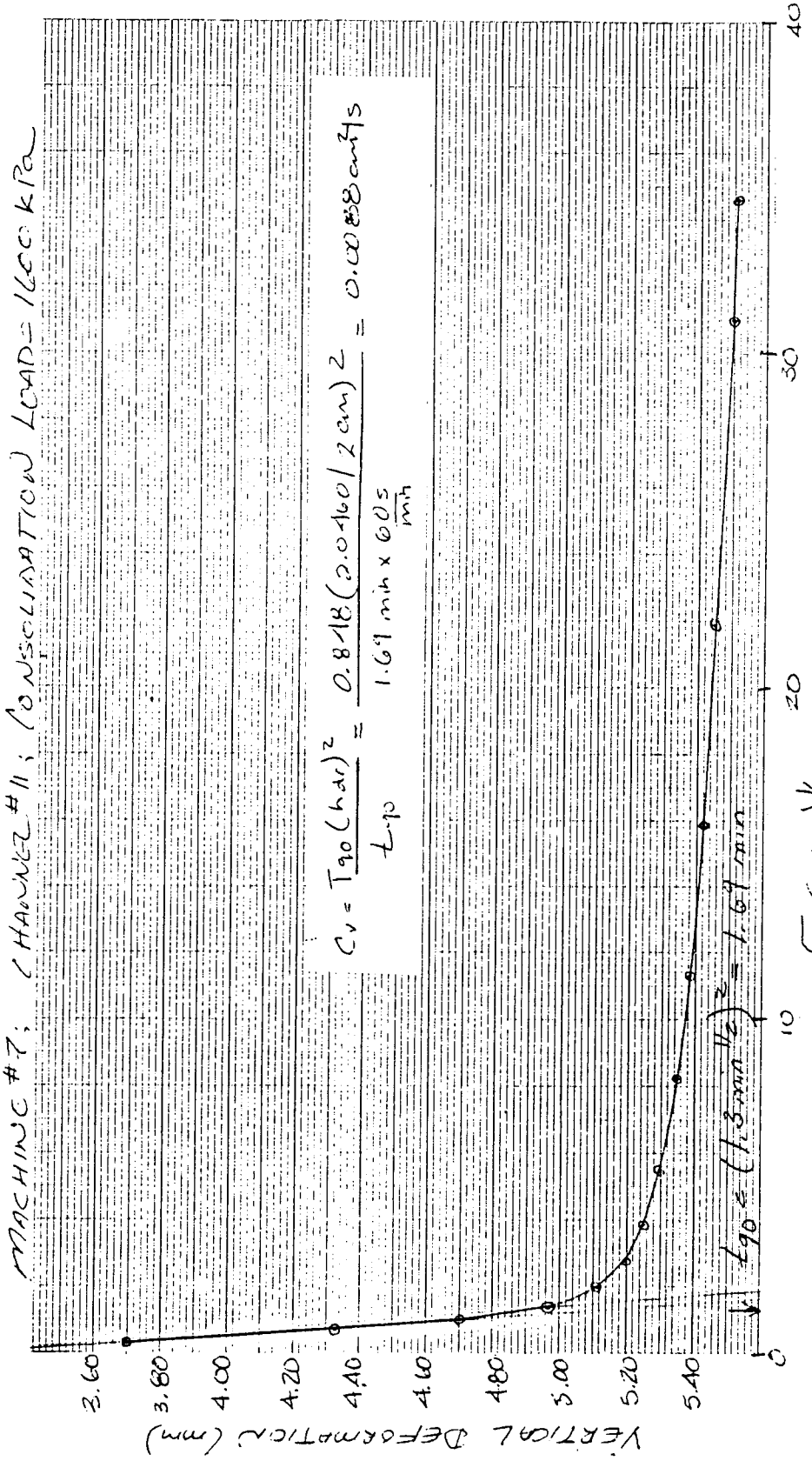

Figure A5: Horizontally Laminated Block Sample #1; Consolidation Load = 1600 kPa

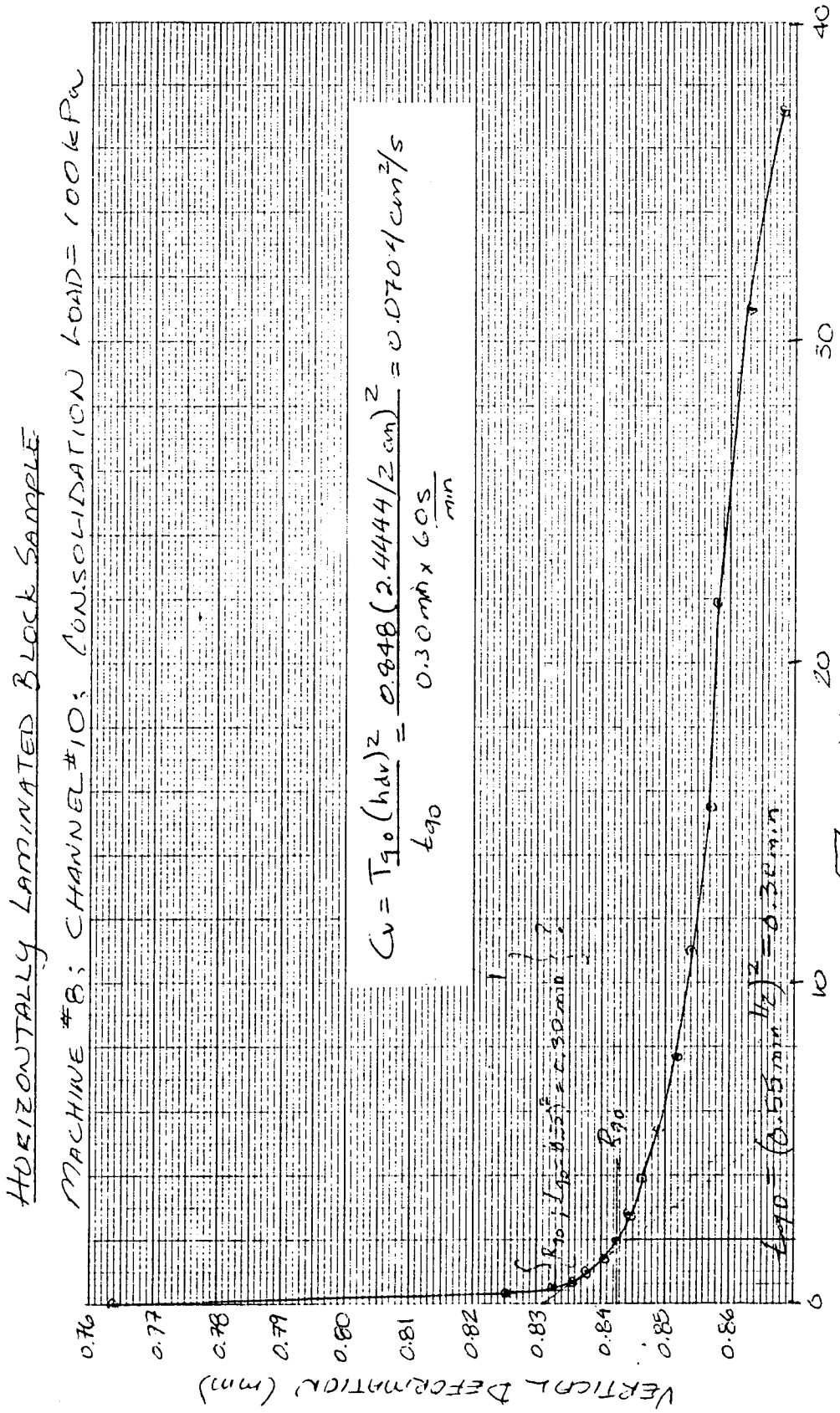

Figure A6: Horizontally Laminated Block Sample #2; Consolidation Load = 100 kPa

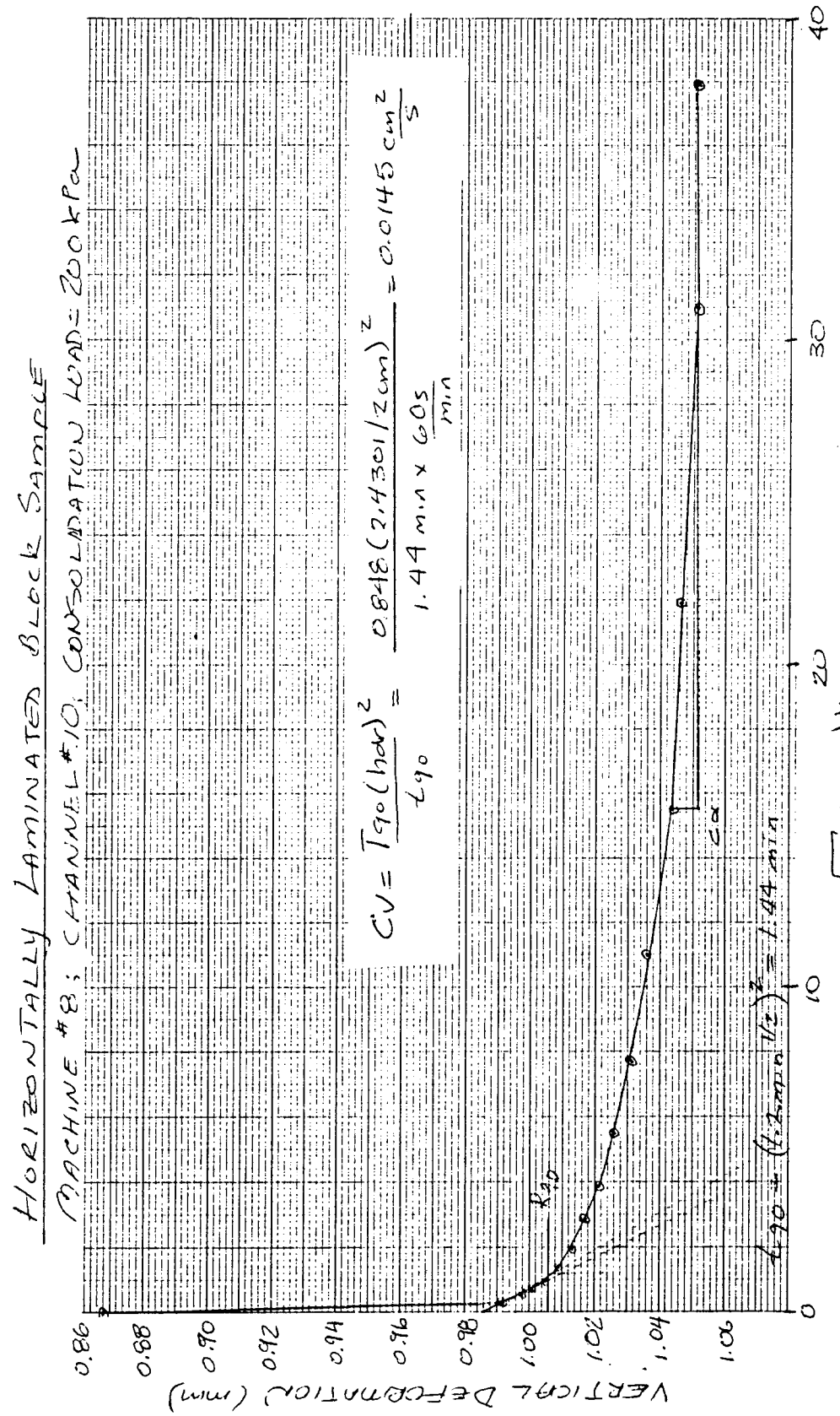

Figure A7: Horizontally Laminated Block Sample #2; Consolidation Load = 200 kPa

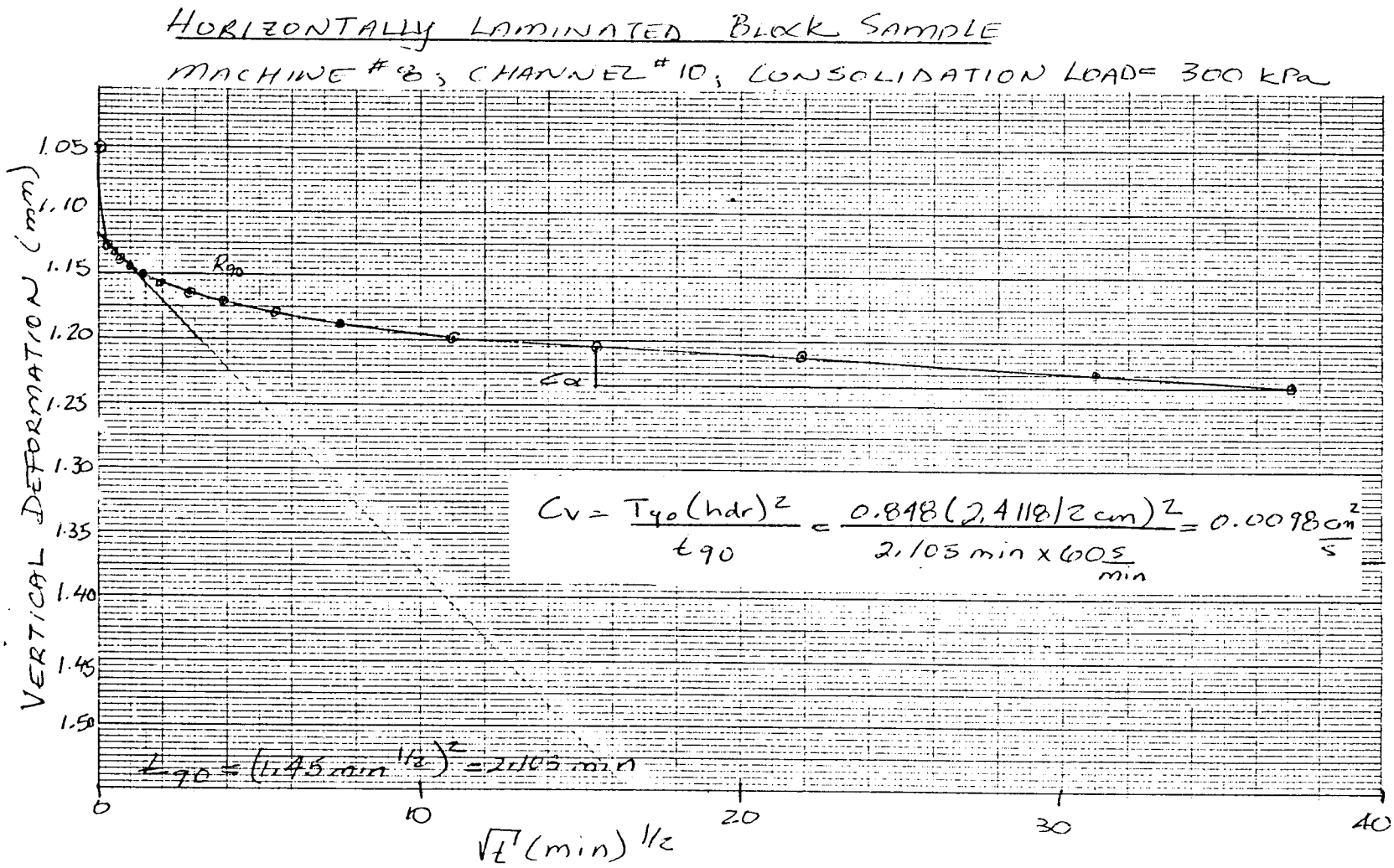

Figure A8: Horizontally Laminated Block Sample #2; Consolidation Load = 300 kPa

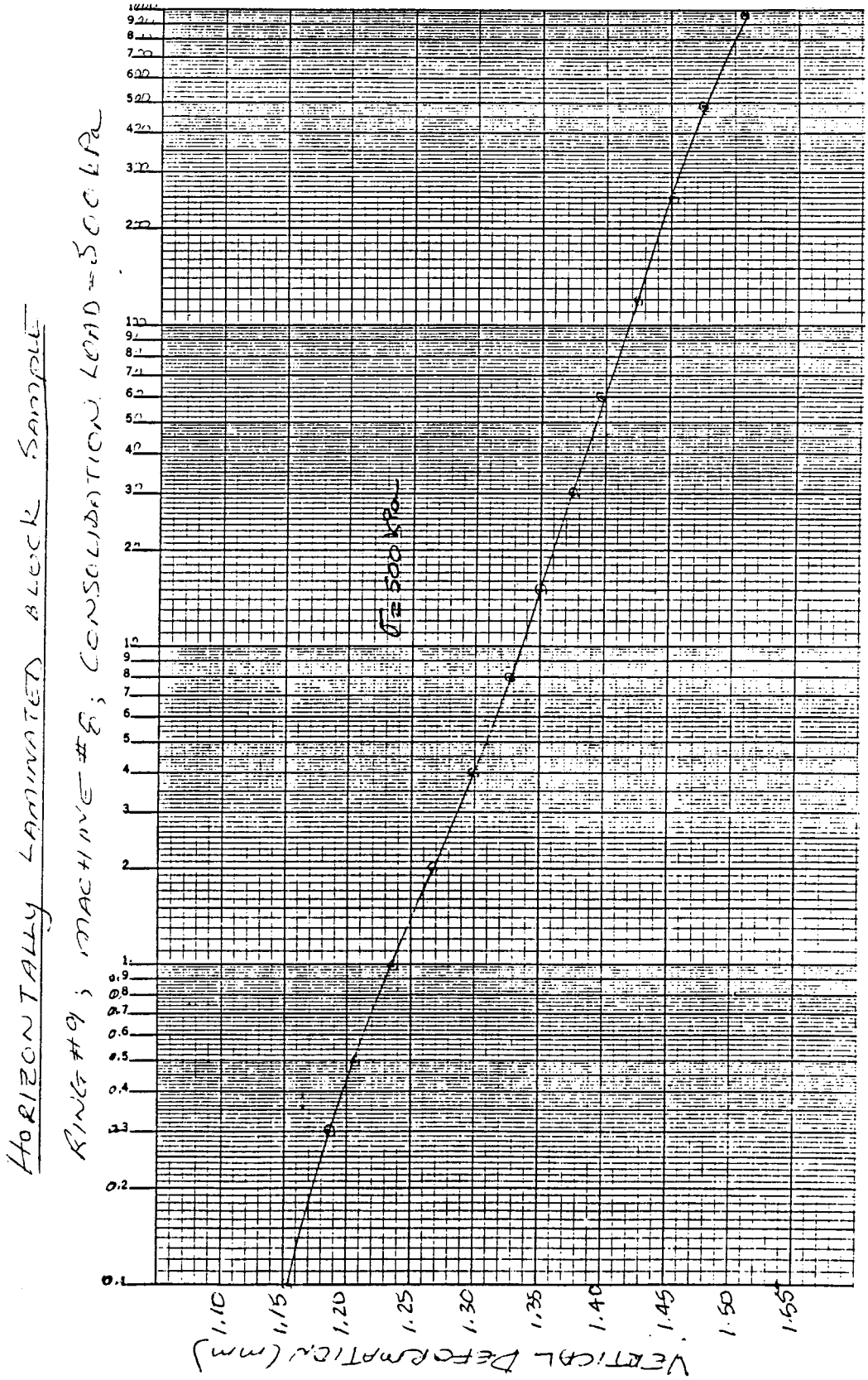

Figure A9: Horizontally Laminated Block Sample #2; Consolication Load = 500 kPa; Log-Time Plot

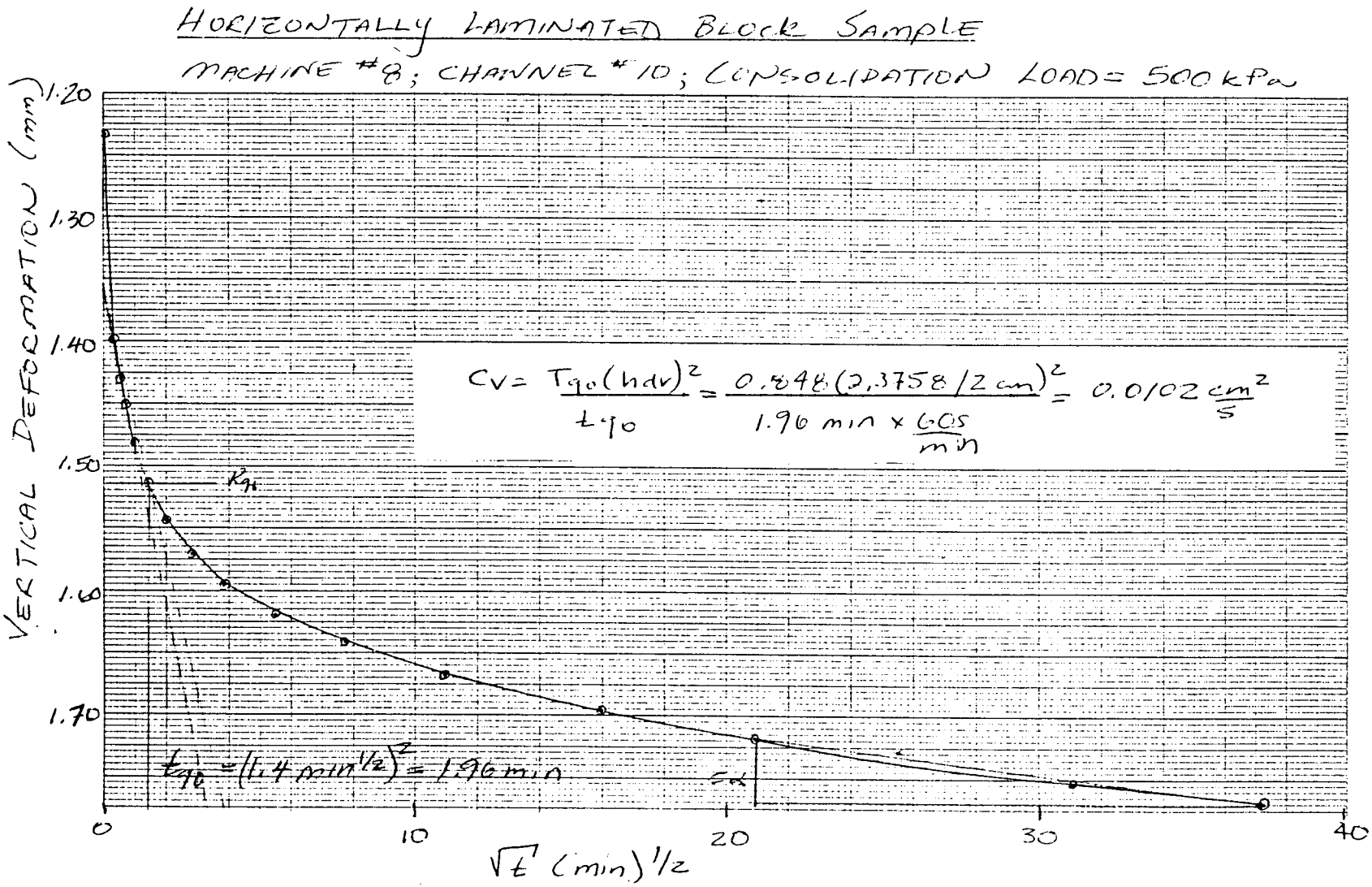

Figure A10: Horizontally Laminated Block Sample #2; Consolidation Load = 500 kPa; Square-root-Time Plot

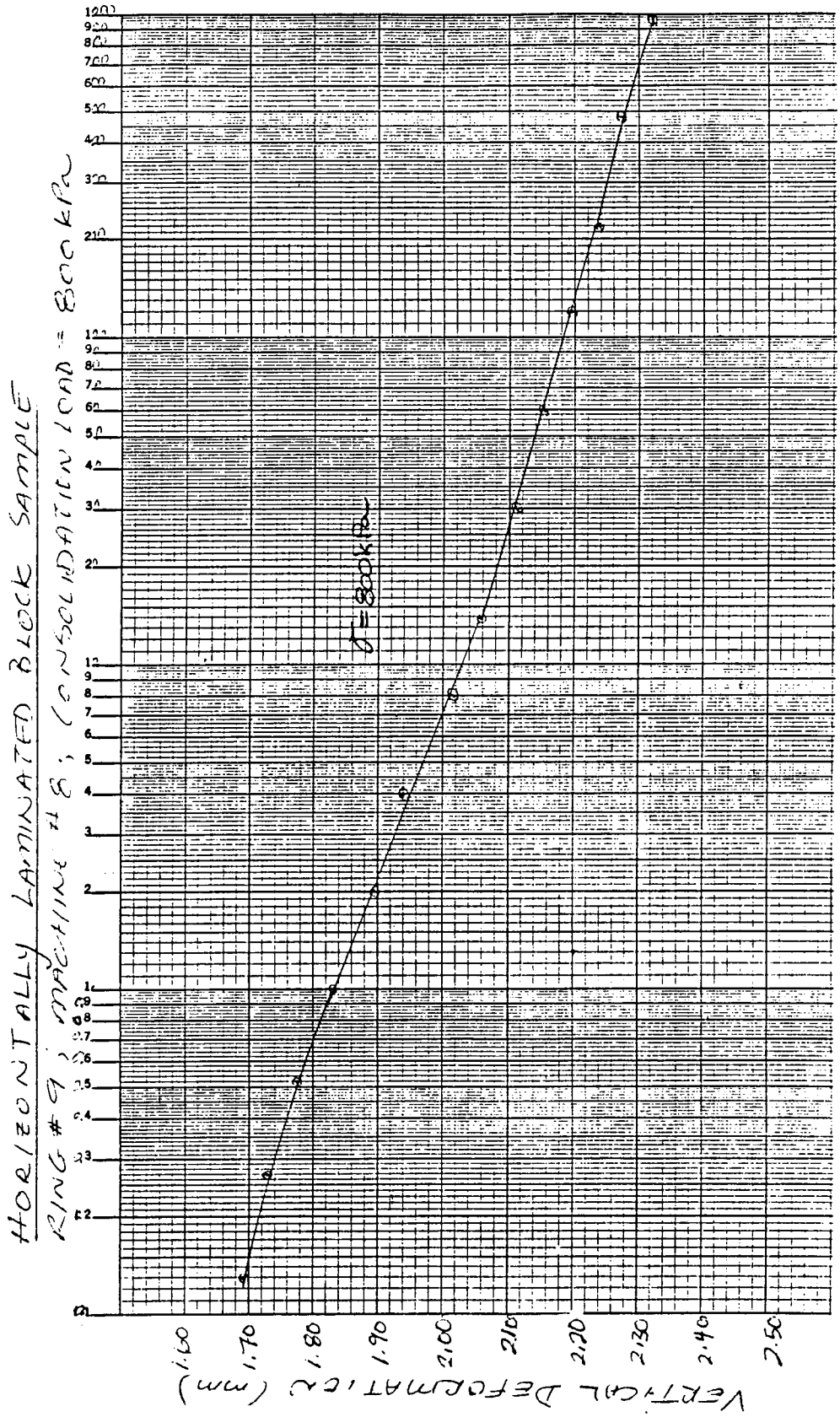

Figure A11: Horizontally Laminated Block Sample #2; Consolidation Load = 800 kPa; Log-Time Plot

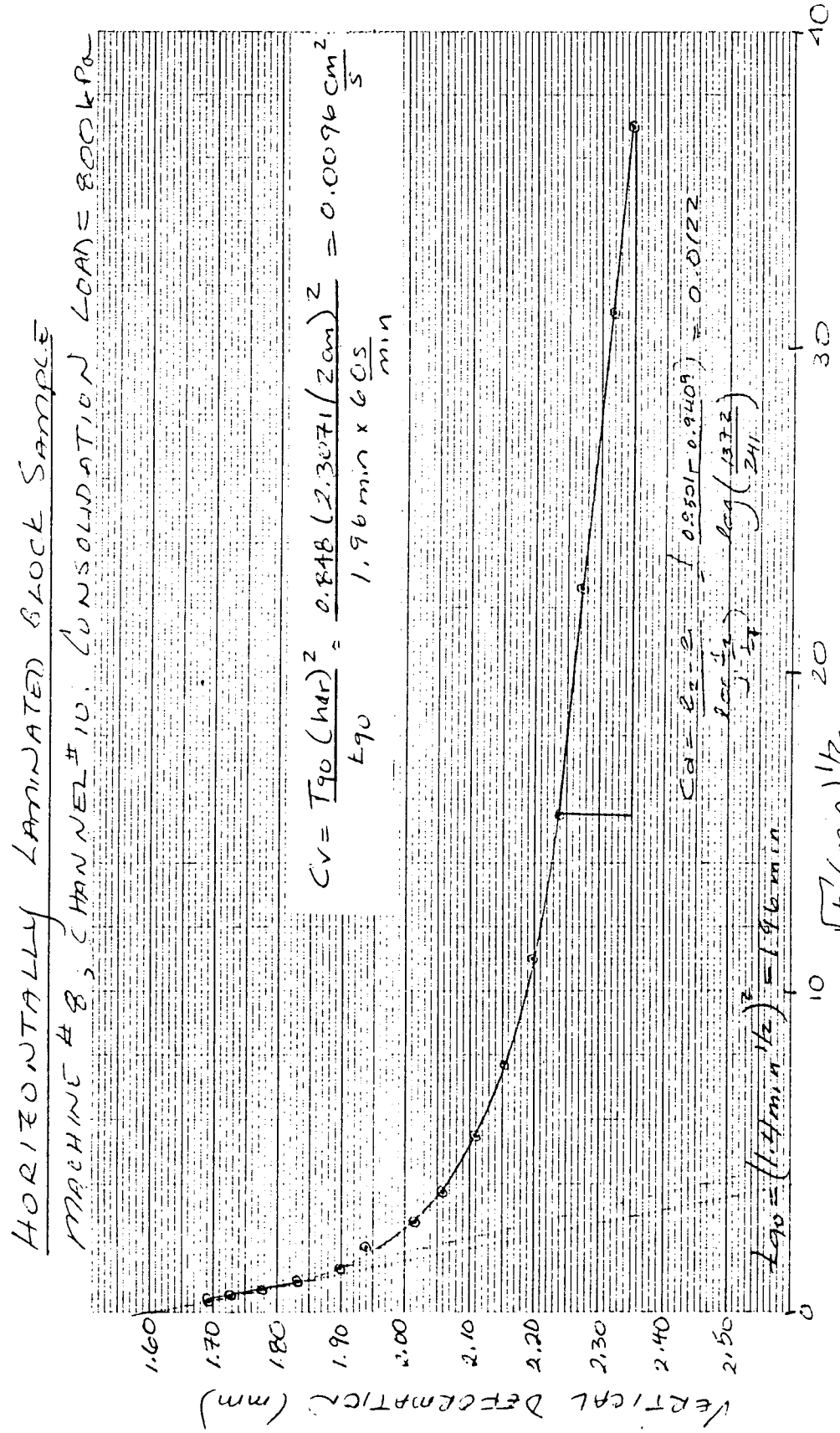

Figure A12: Horizontally Laminated Block Sample #2; Consolidation Load = 800 kPa; Square-root-Time Plot

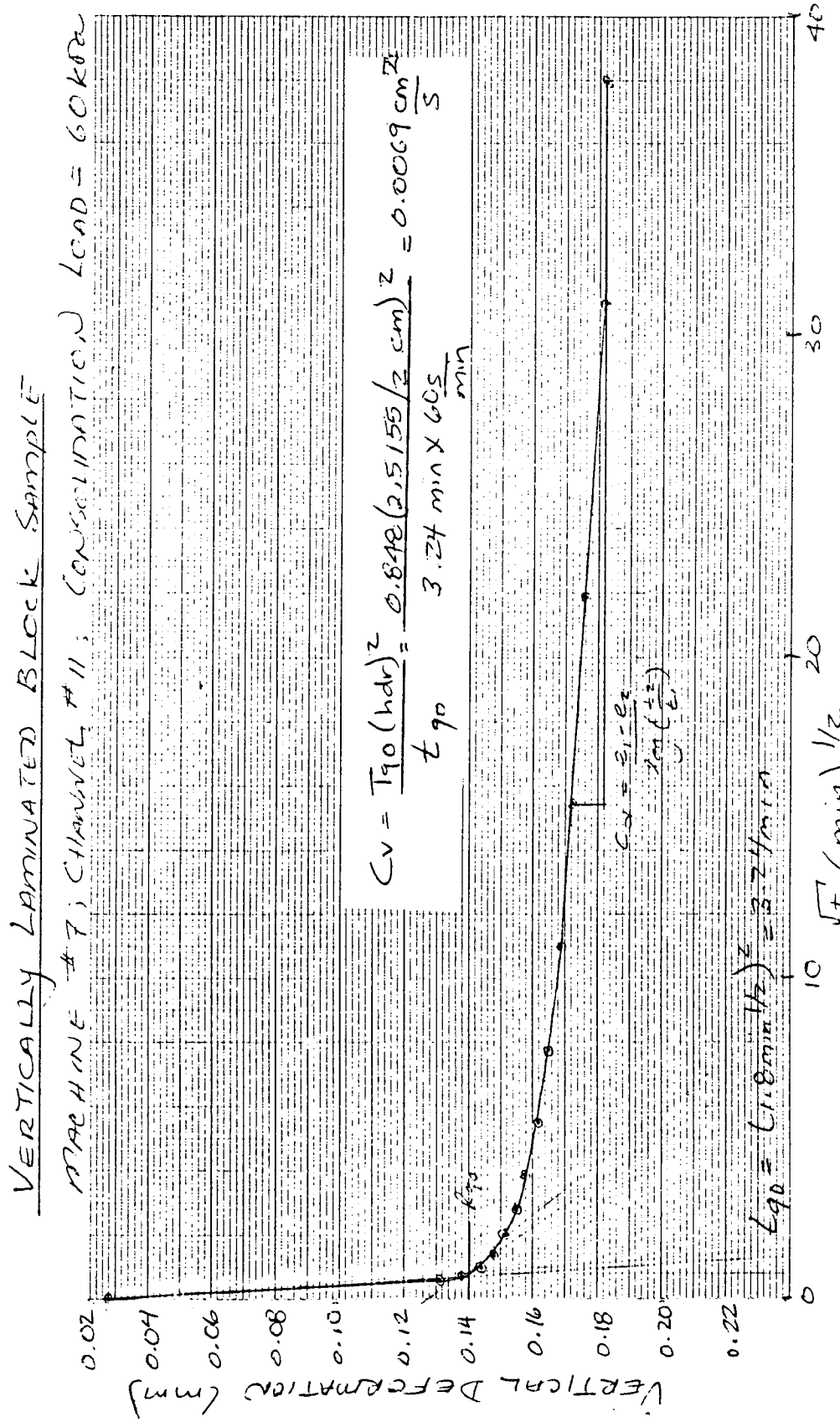

Figure A13: Vertically Laminated Block Sample #1; Consolidation Load = 60 kPa

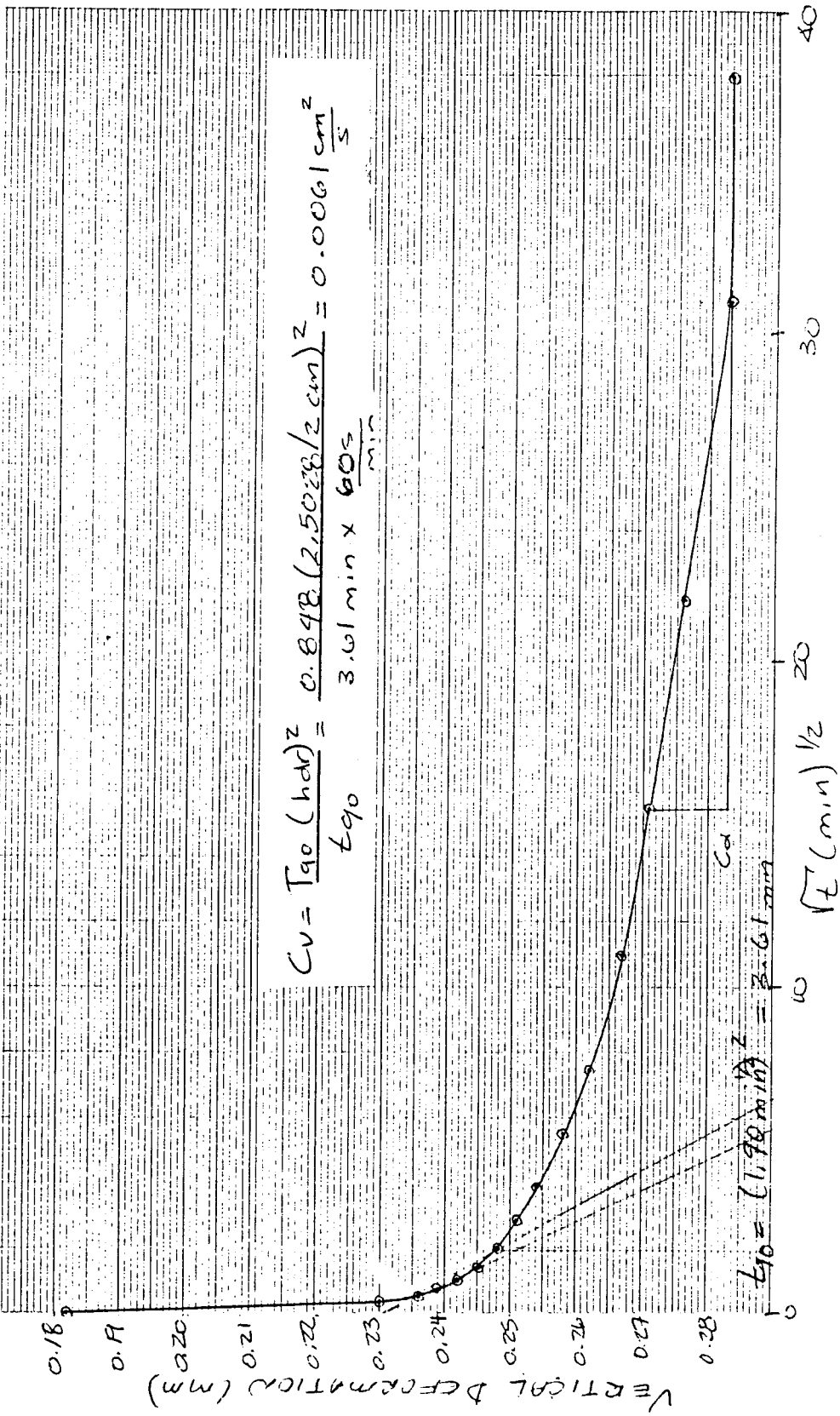

Figure A14: Vertically Laminated Block Sample #1; Consolidation Load = 100 kPa

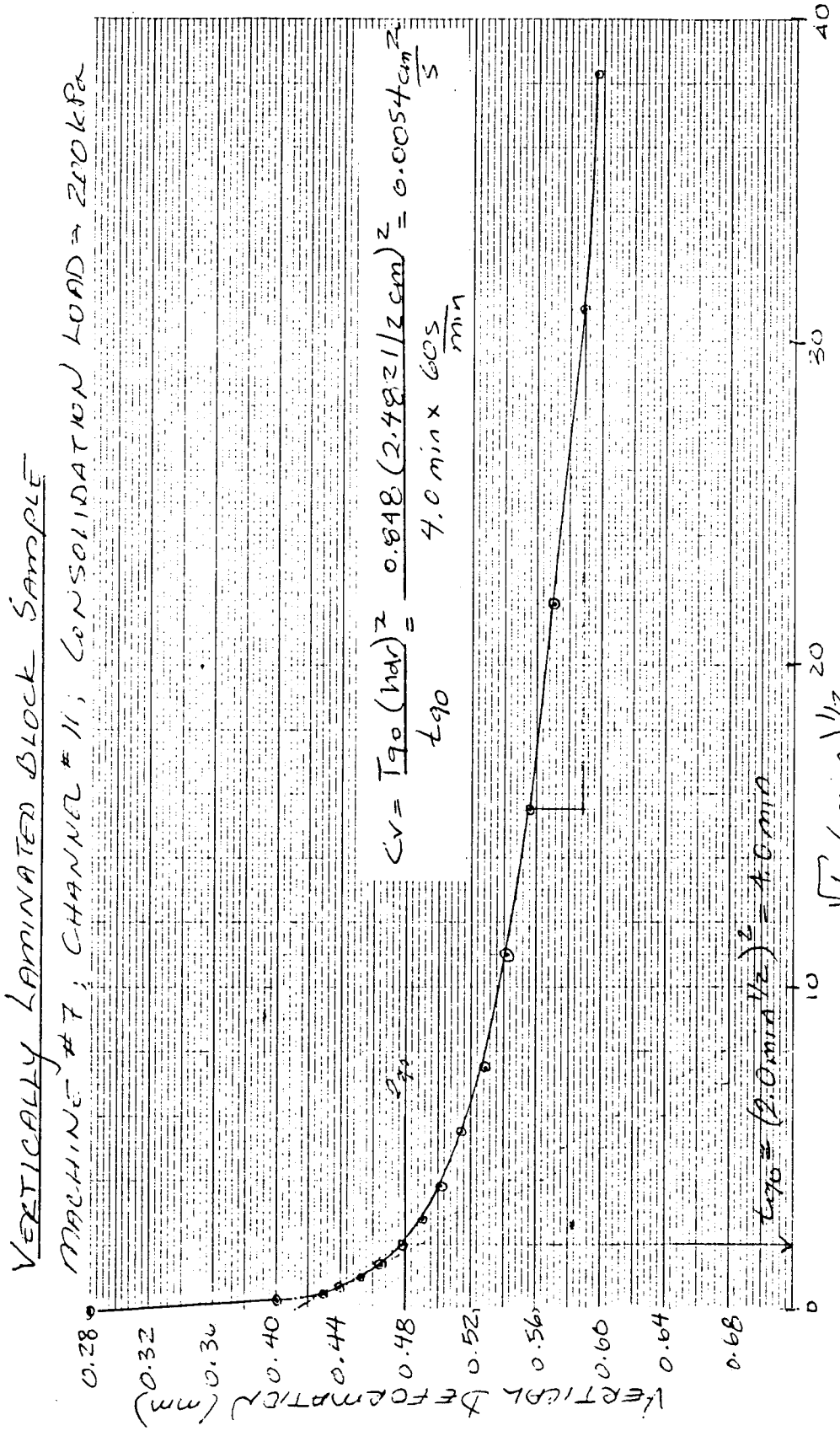

Figure A15: Vertically Laminated Block Sample #1; Consolidation Load = 200 kPa

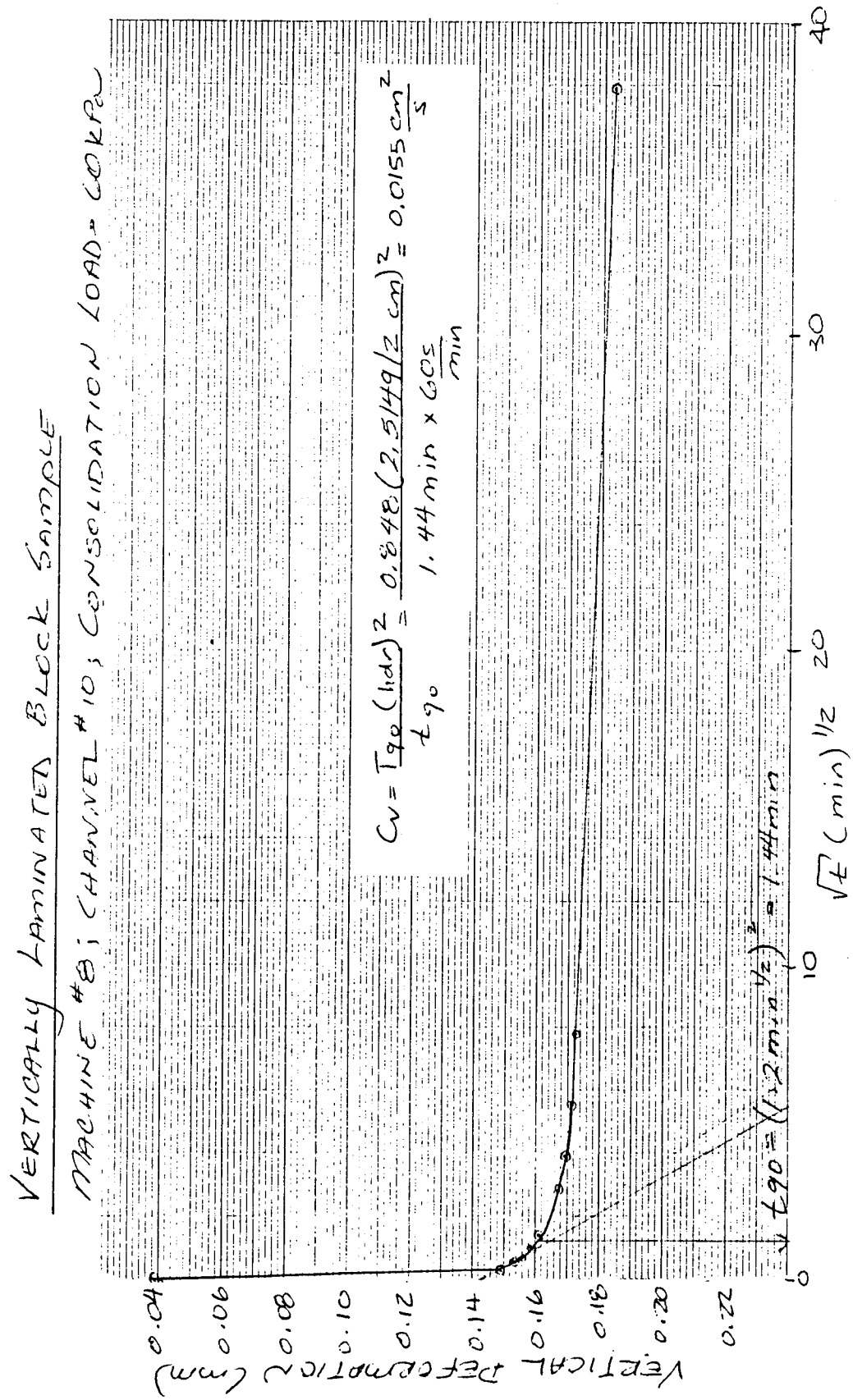

Figure A16: Vertically Laminated Block Sample #2; Consolidation Load = 60 kPa

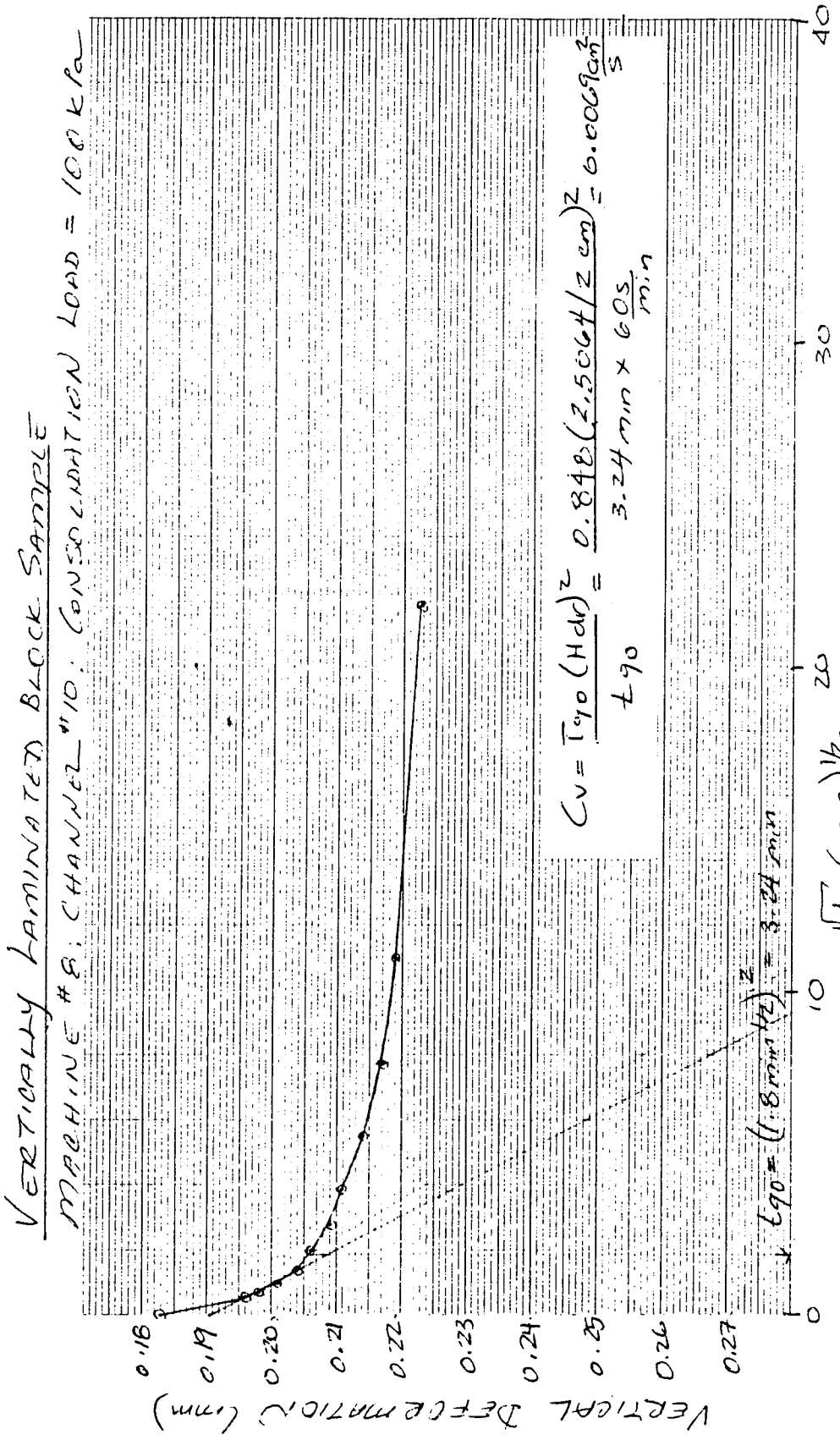

Figure A17: Vertically Laminated Block Sample #2; Consolidation Load = 100 kPa

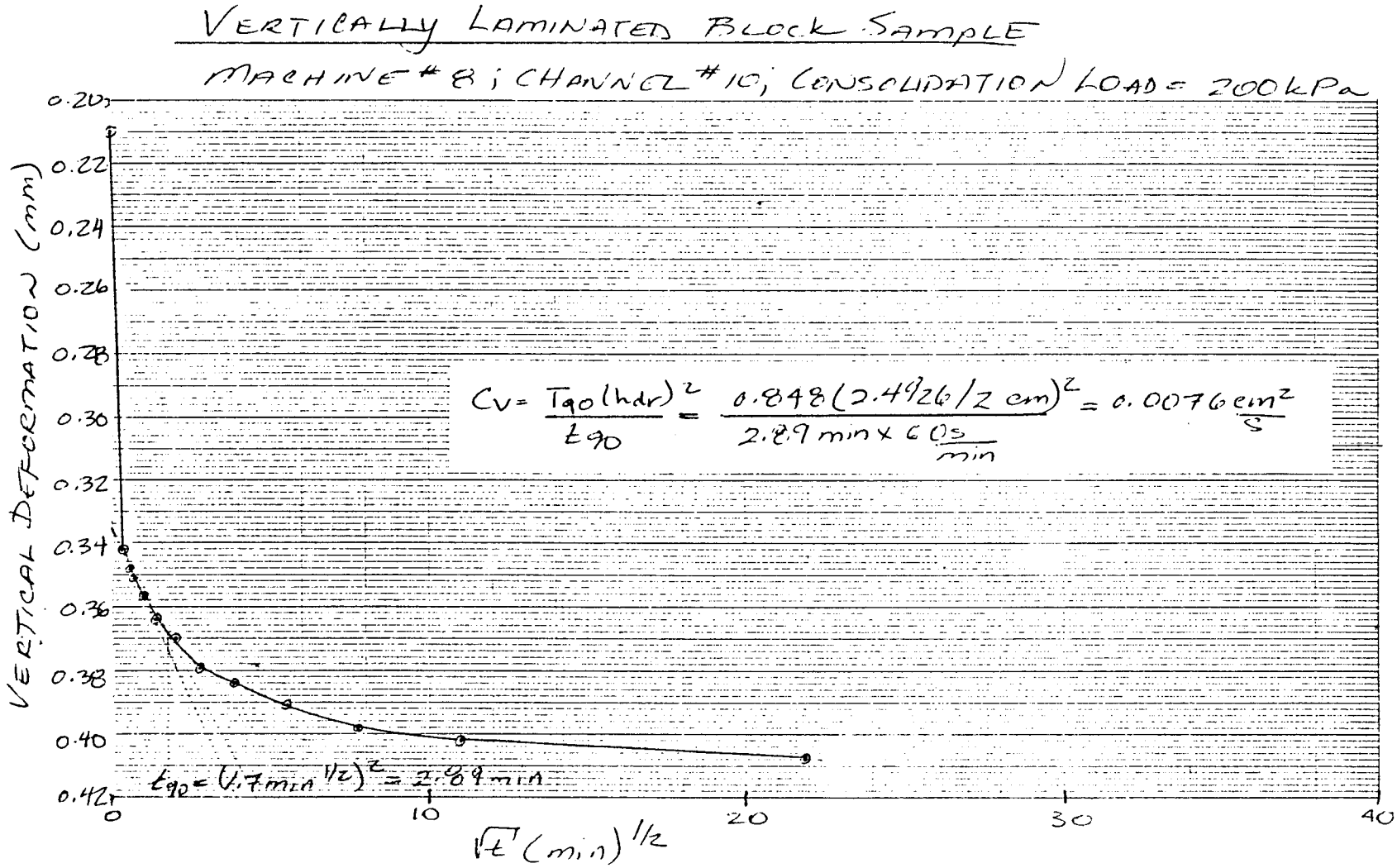

Figure A18: Vertically Laminated Block Sample #2; Consolidation Load = 200 kPa

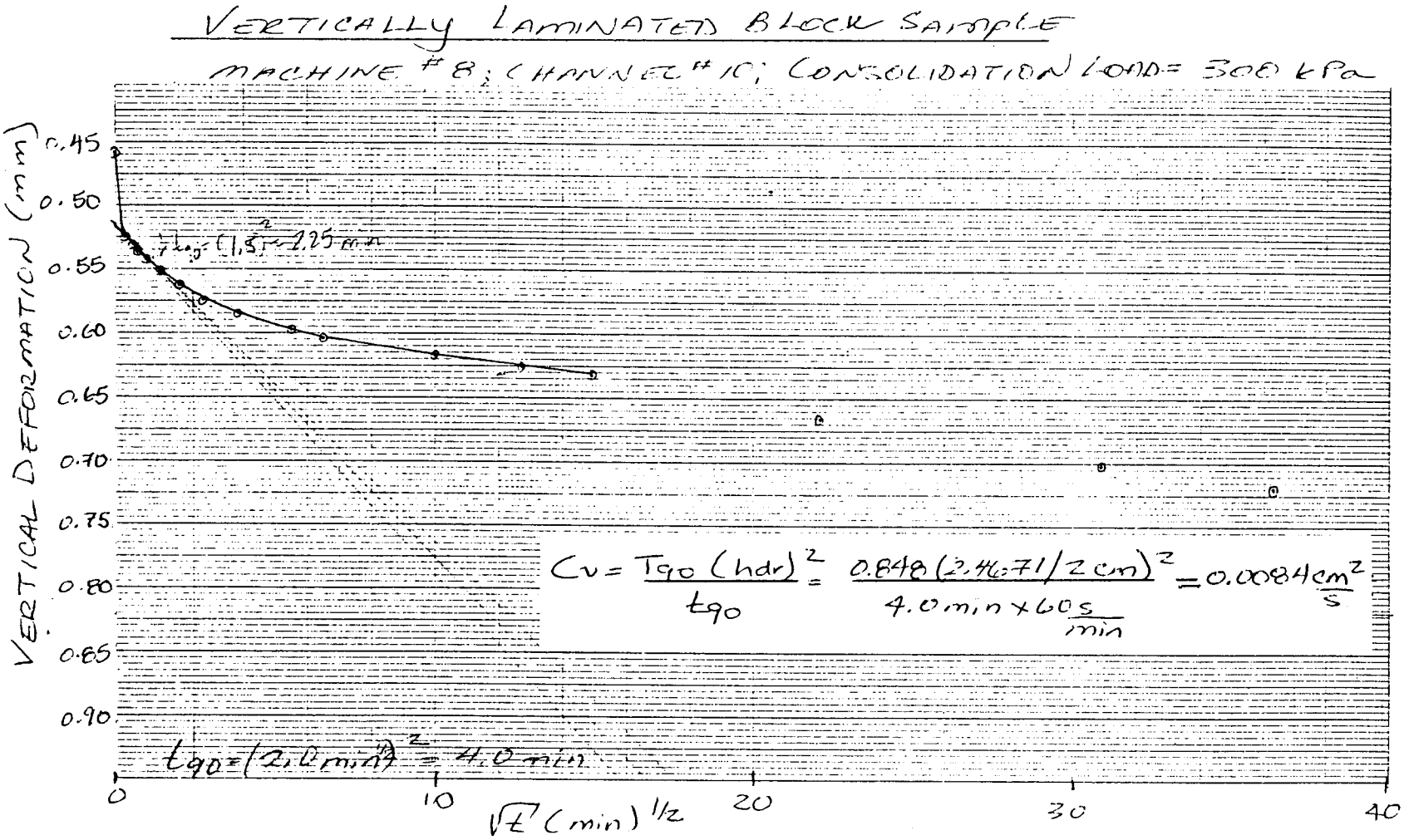

Figure A19: Vertically Laminated Block Sample; Consolidation Load = 300 kPa

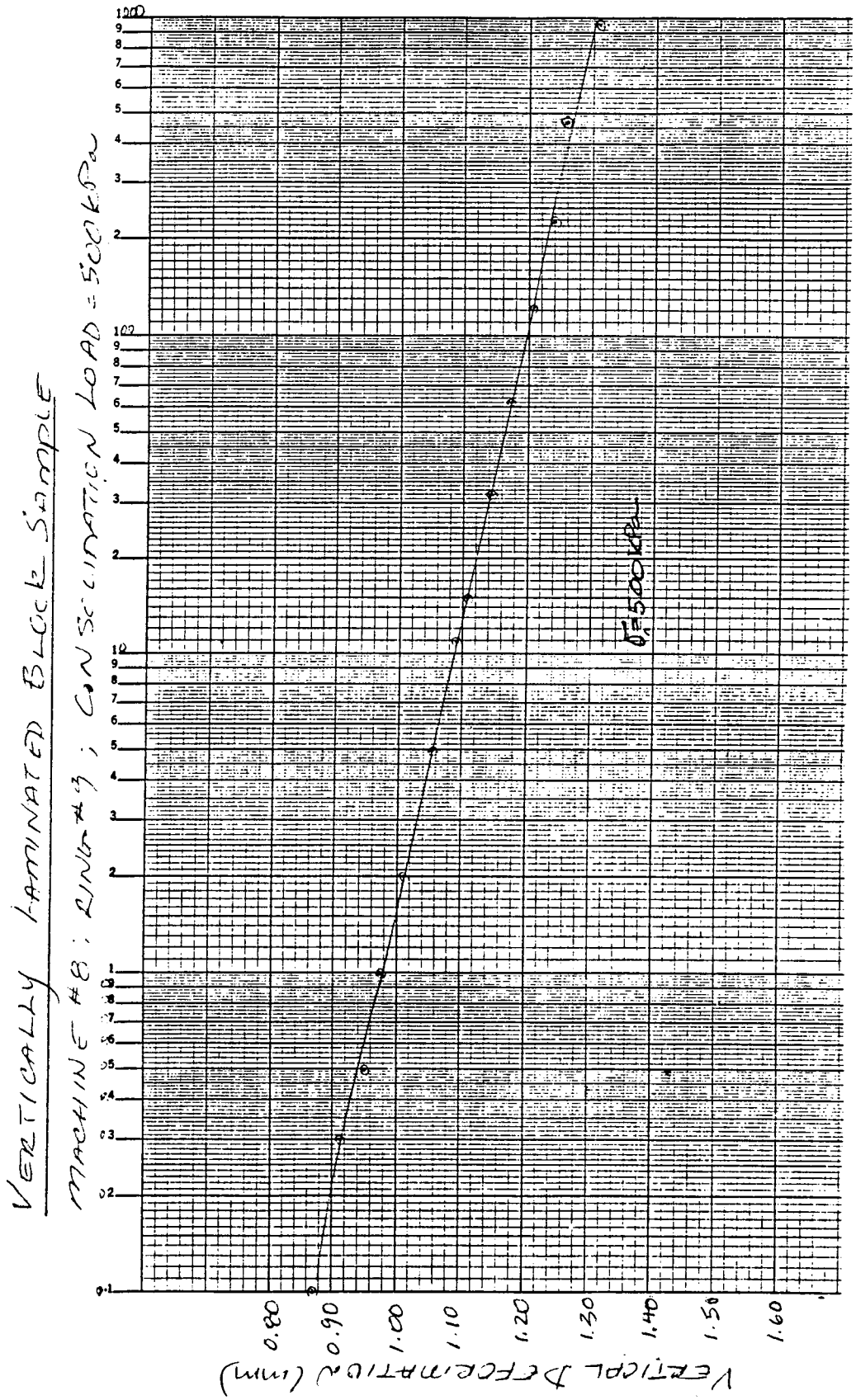

Figure A20: Vertically Laminated Block Sample #2; Consolidation Load = 500 kPa; Log-Time Plot

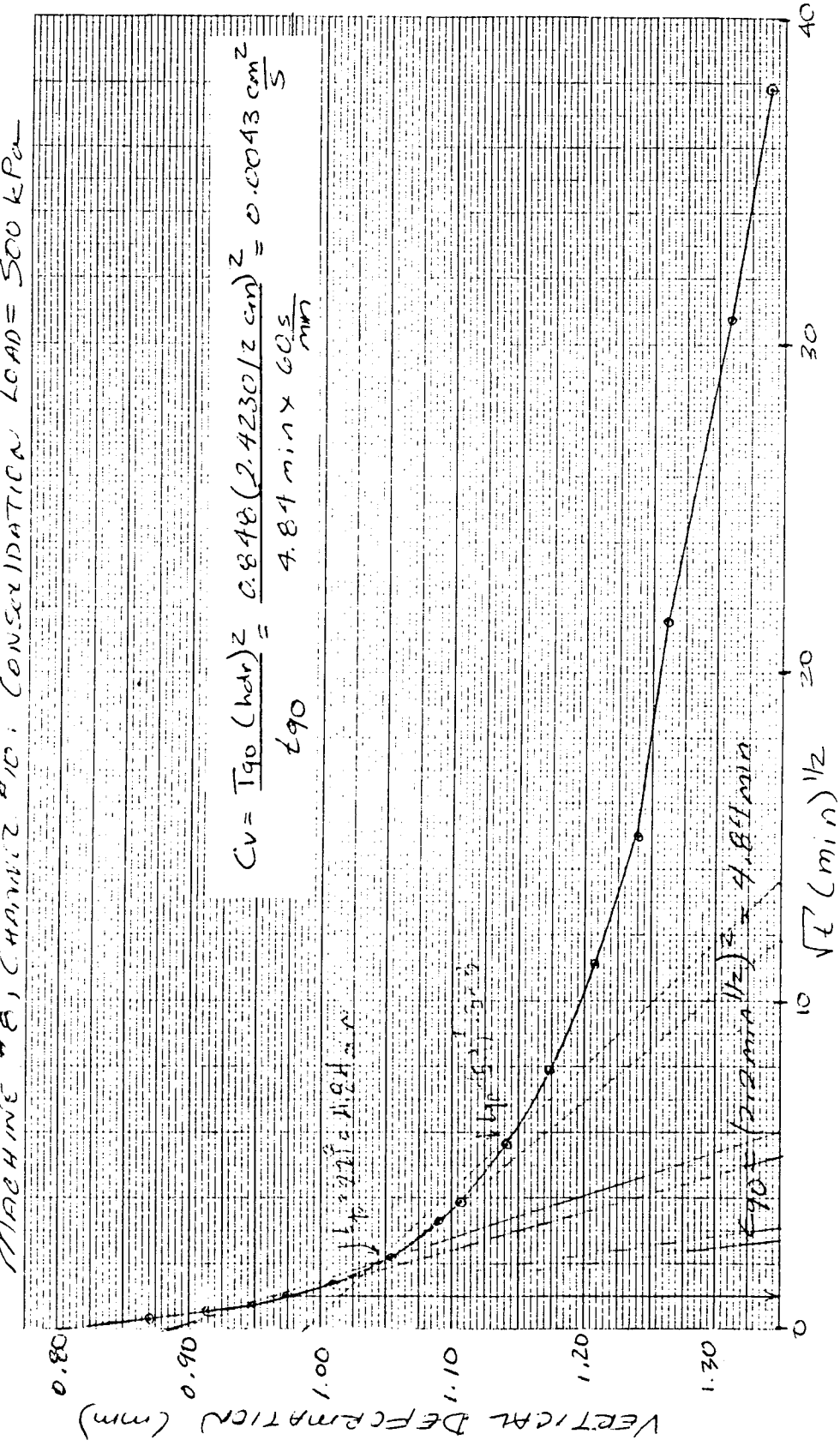

Figure A21: Vertically Laminated Block Sample #2; Consolidation Load = 500 kPa; Square-root-Time Plot

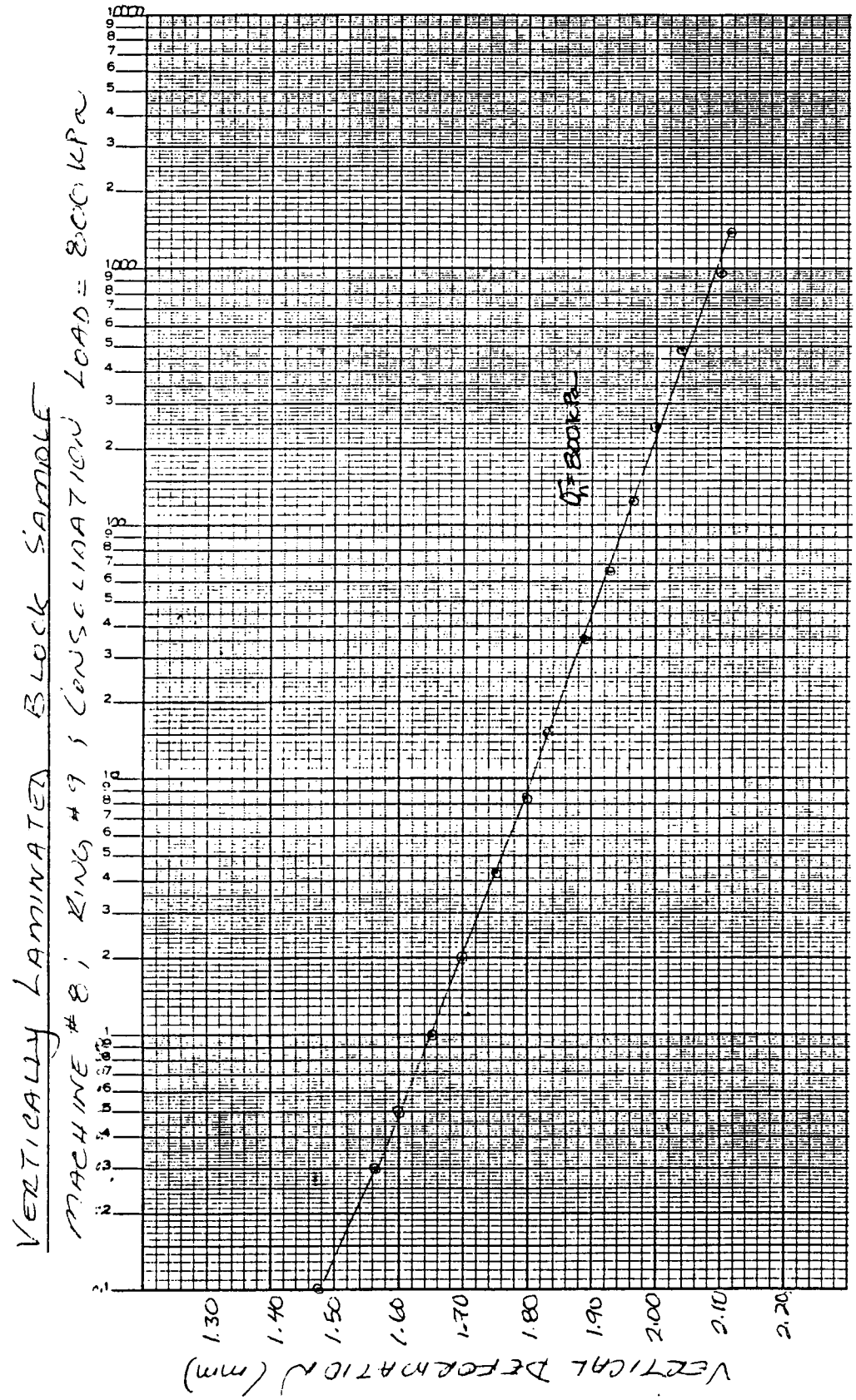

Figure A22: Vertically Laminated Block Sample #2; Consolidation Load = 800 kPa; Log-Time Plot

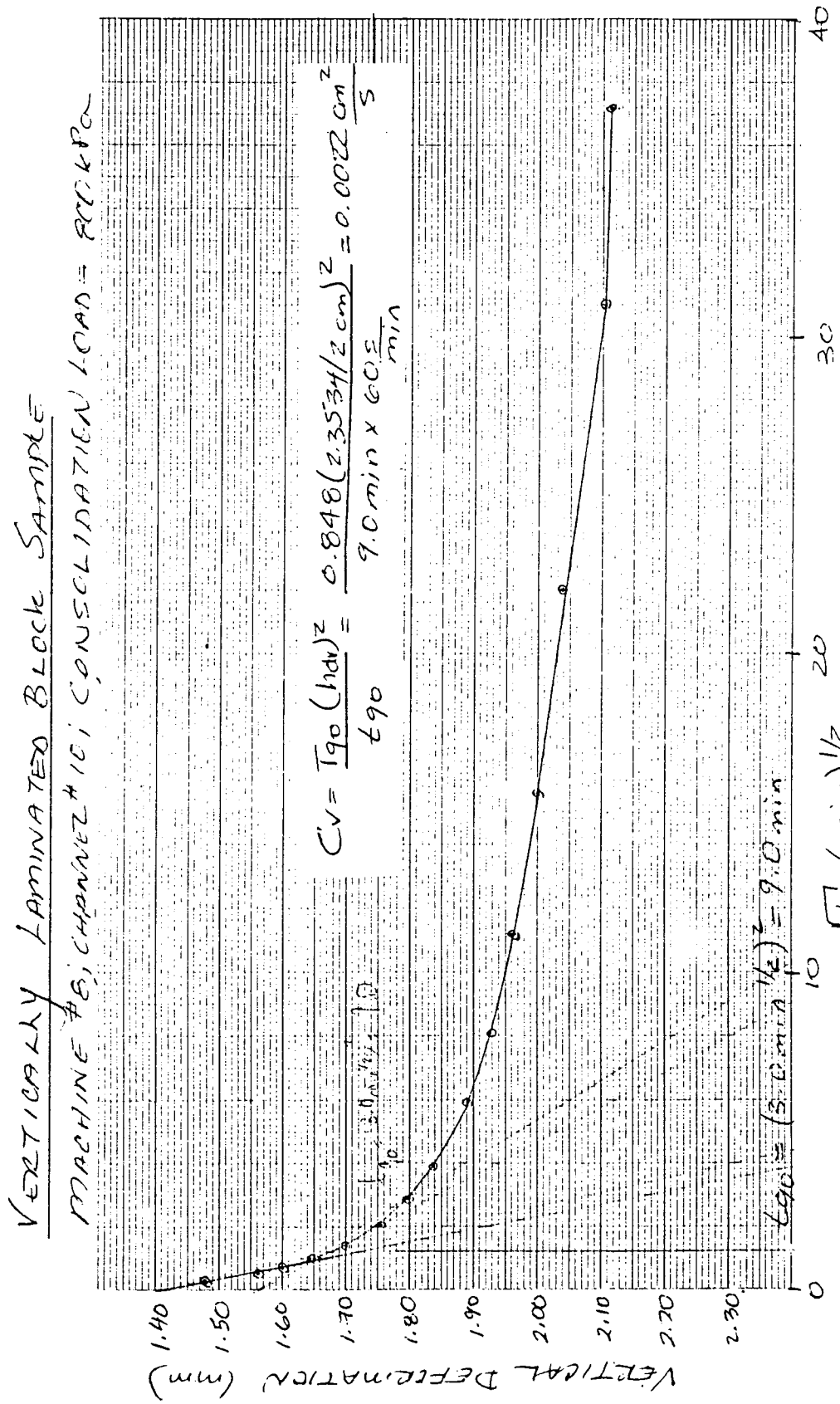

Figure A23: Vertically Laminated Block Sample #2; Consolidation Load = 800 kPa; Square-root-Time Plot

APPENDIX B: FINITE ELEMENT OUTPUT

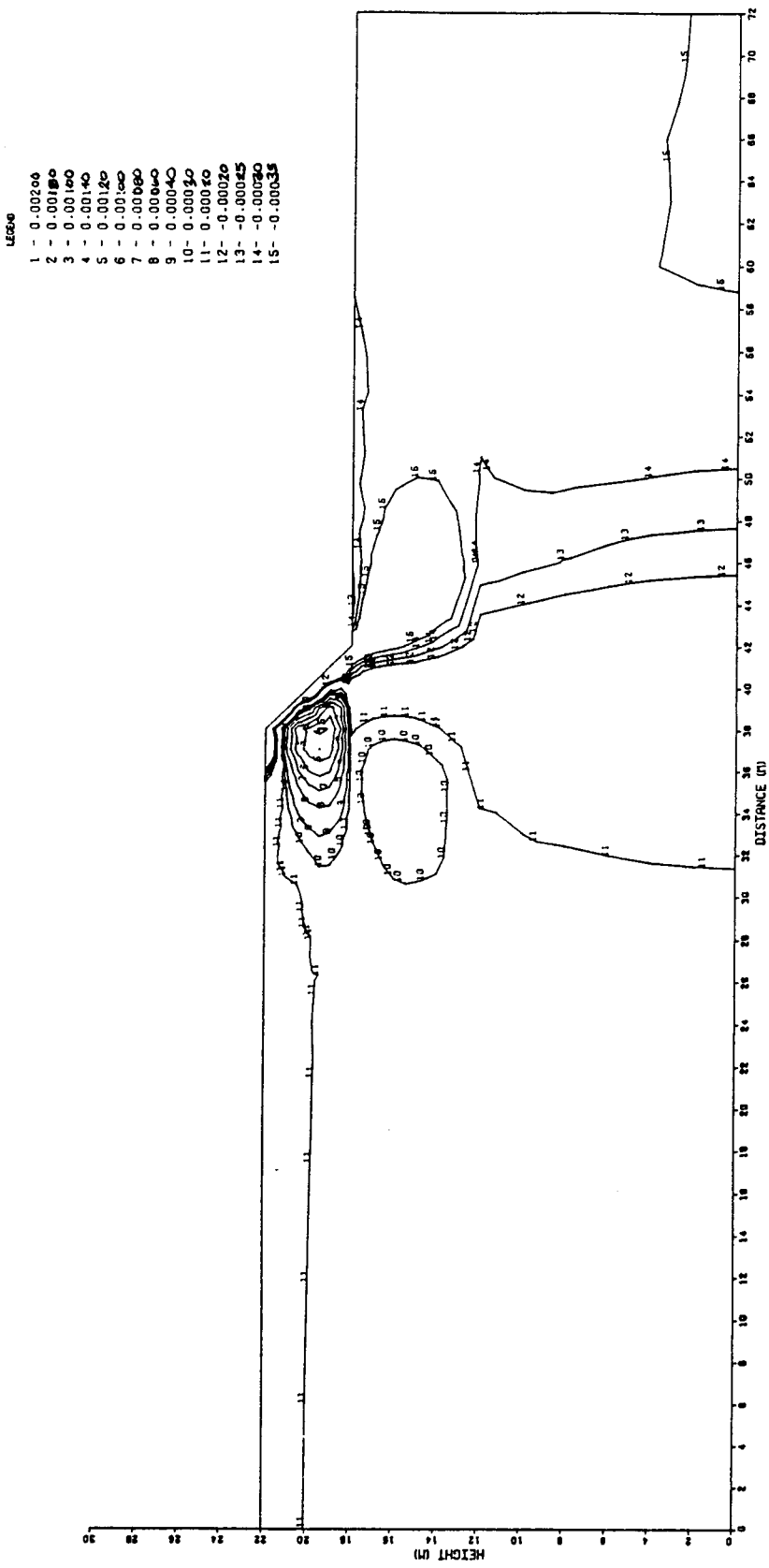

Figure B.1 Horizontal Strains in Unreinforced Fill Slope: Height = 4 m

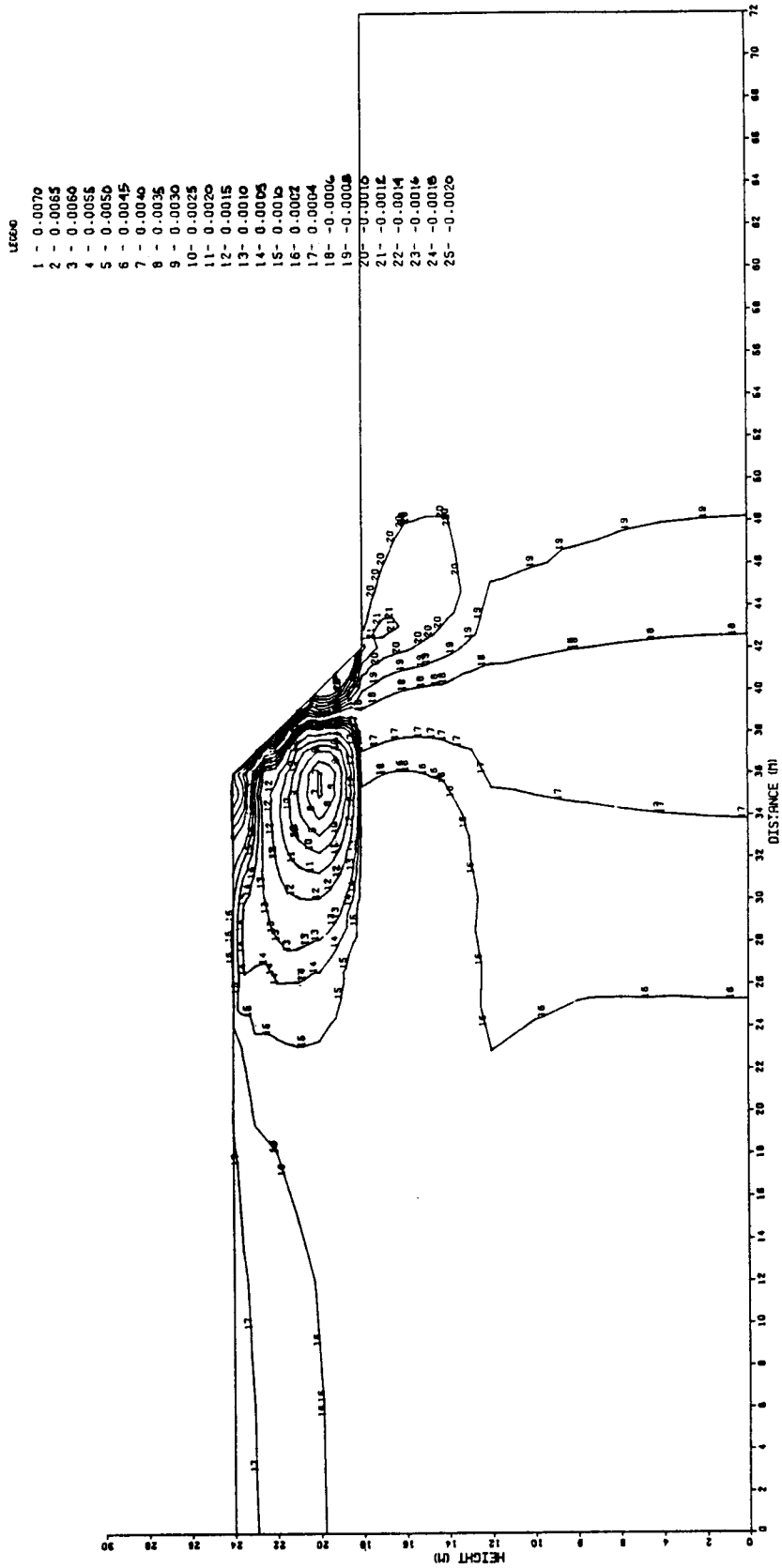

Figure B.2 Horizontal Strains in Unreinforced Fill Slope: Height = 6 m

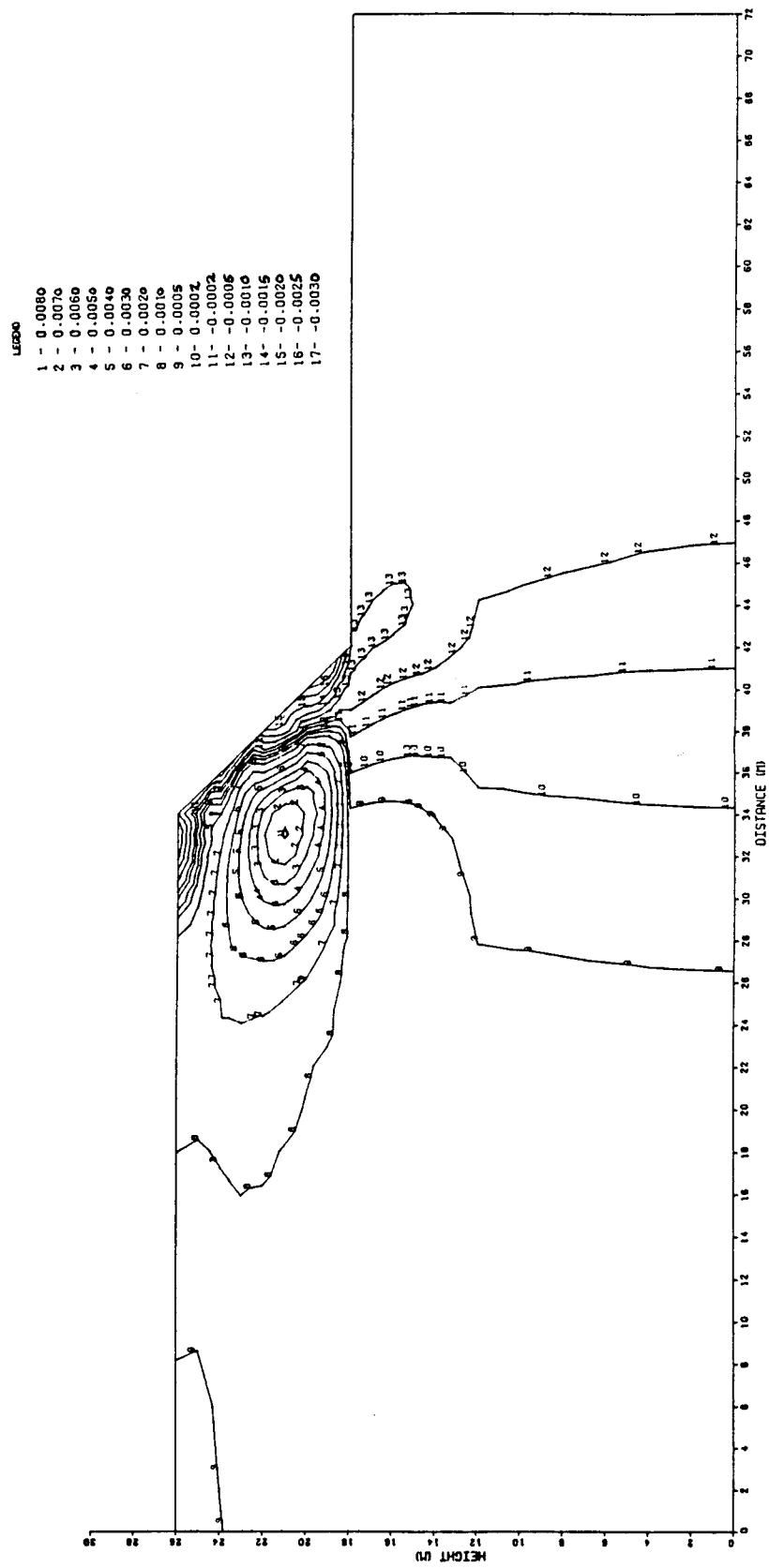

Figure B.3 Horizontal Strains in Unreinforced Fill Slope: Height = 8 m

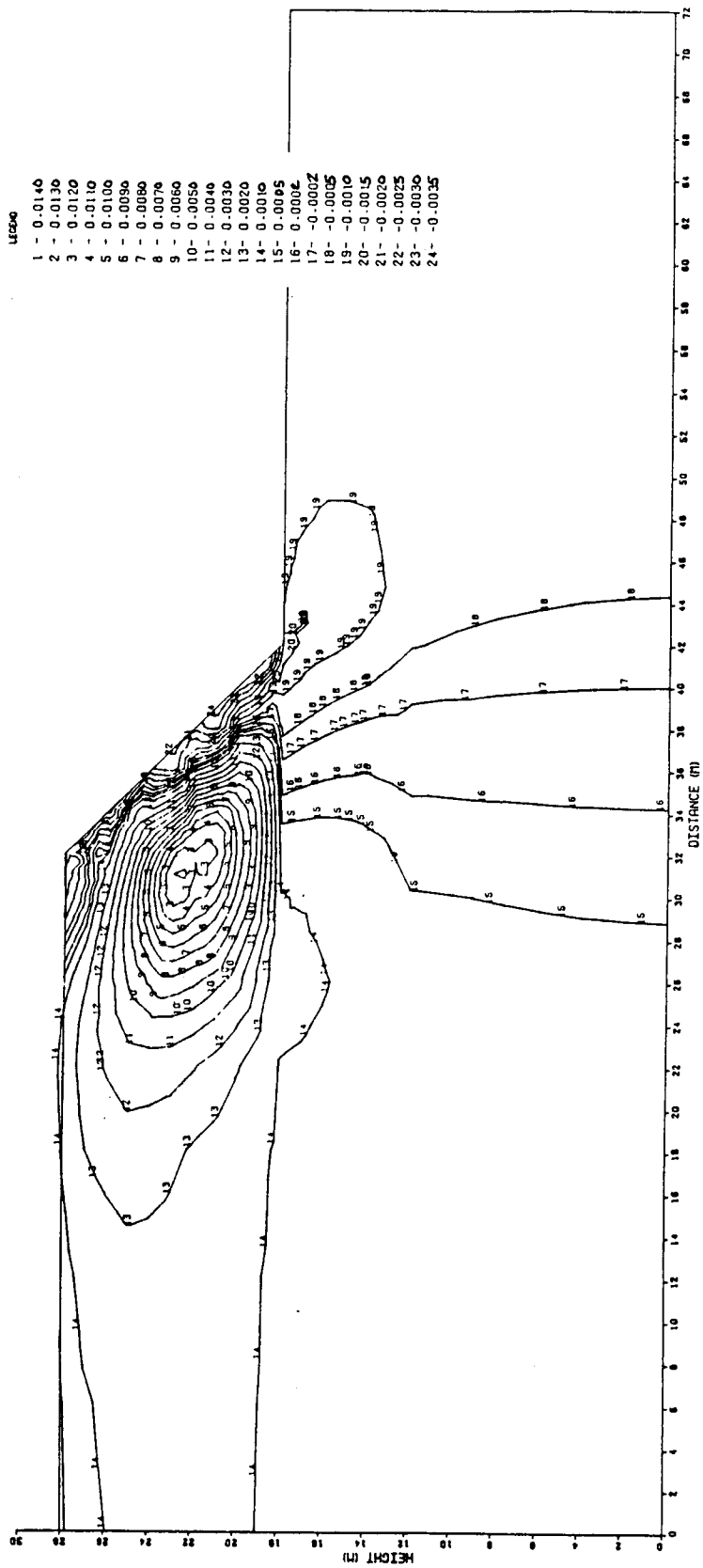

Figure B.4 Horizontal Strains in Unreinforced Fill Slope: Height = 10 m

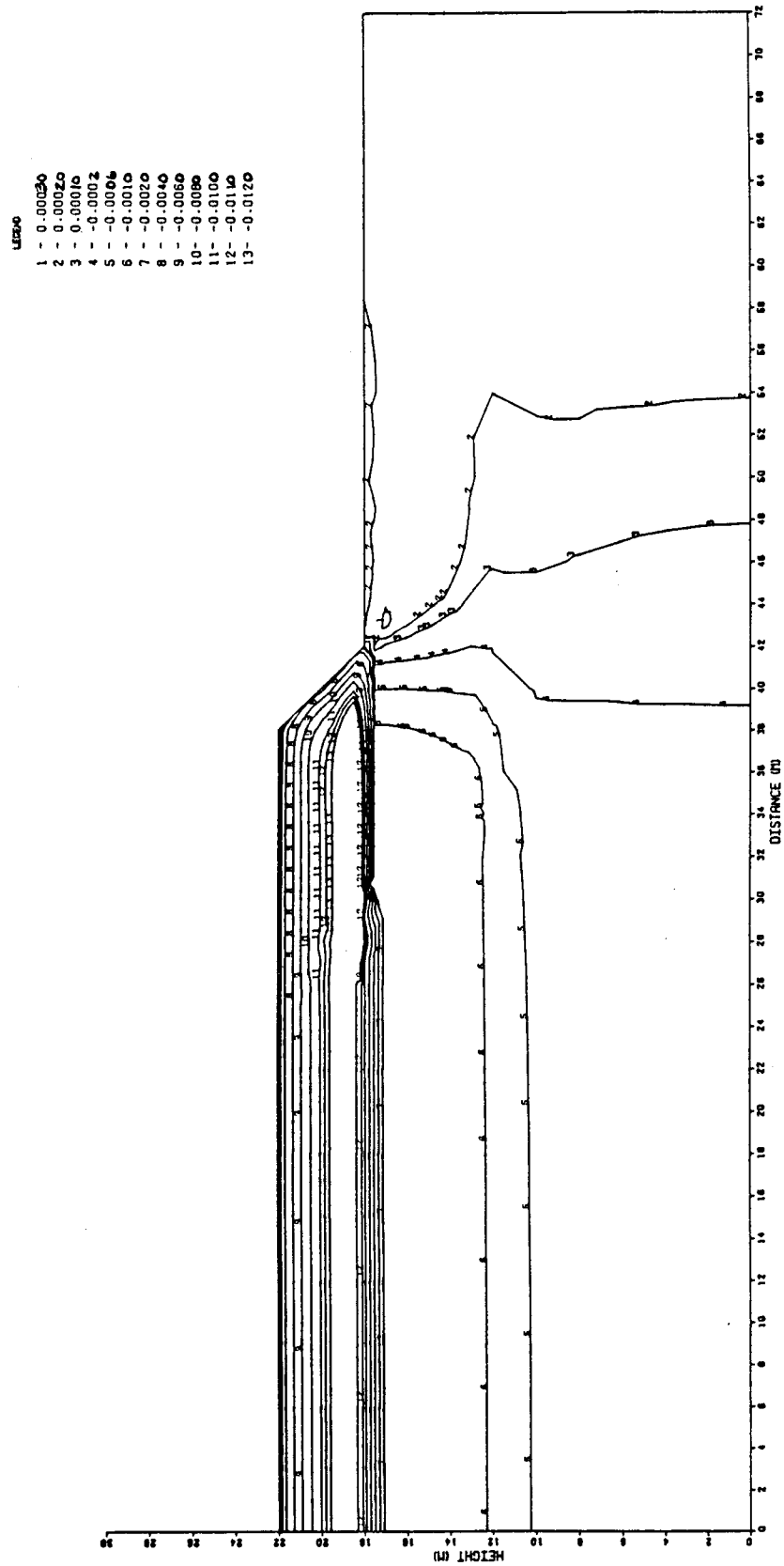

Figure B.5 Vertical Strains in Unreinforced Fill Slope: Height = 4 m

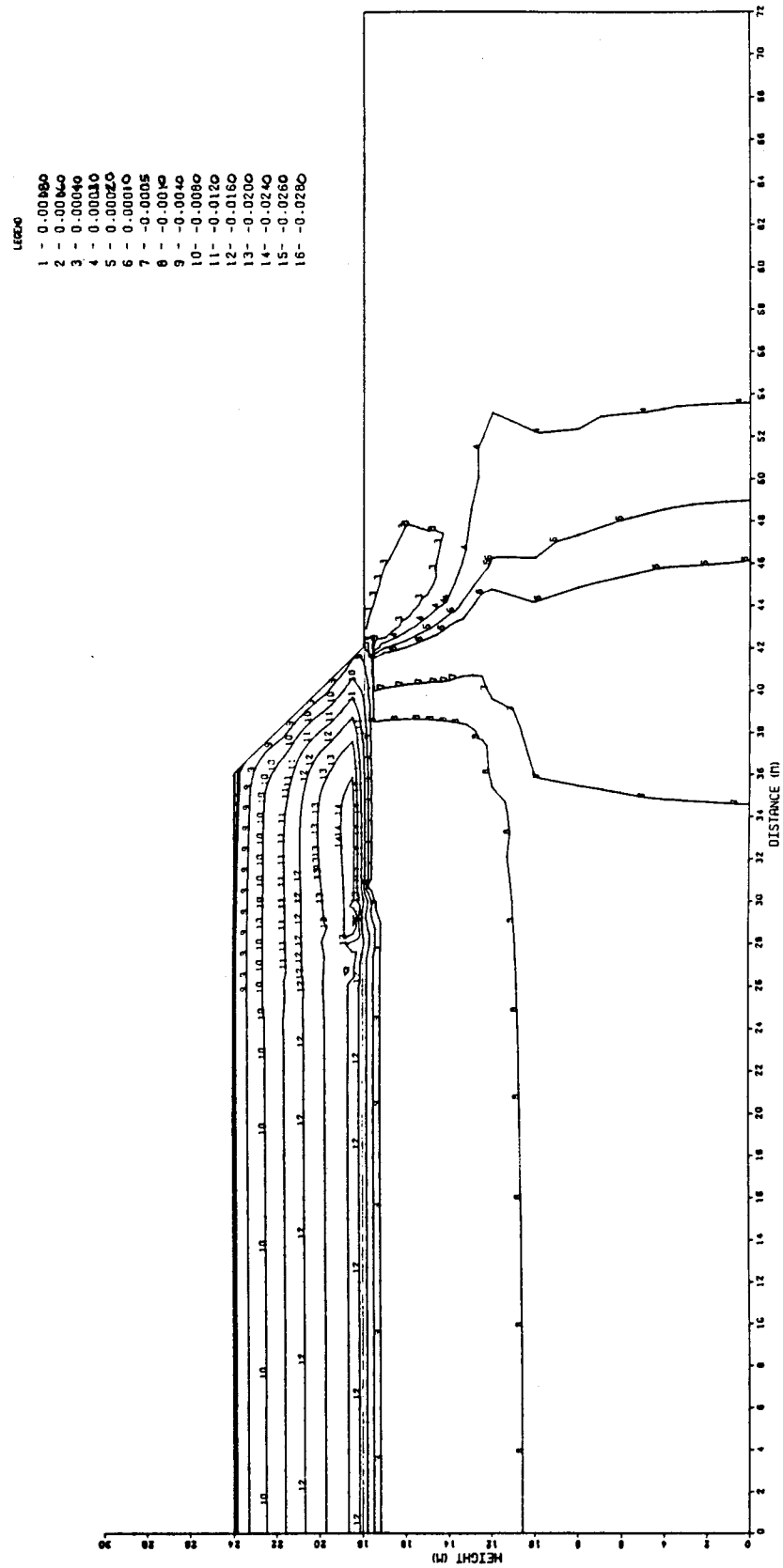

Figure B.6 Vertical Strains in Unreinforced Fill Slope: Height = 6 m

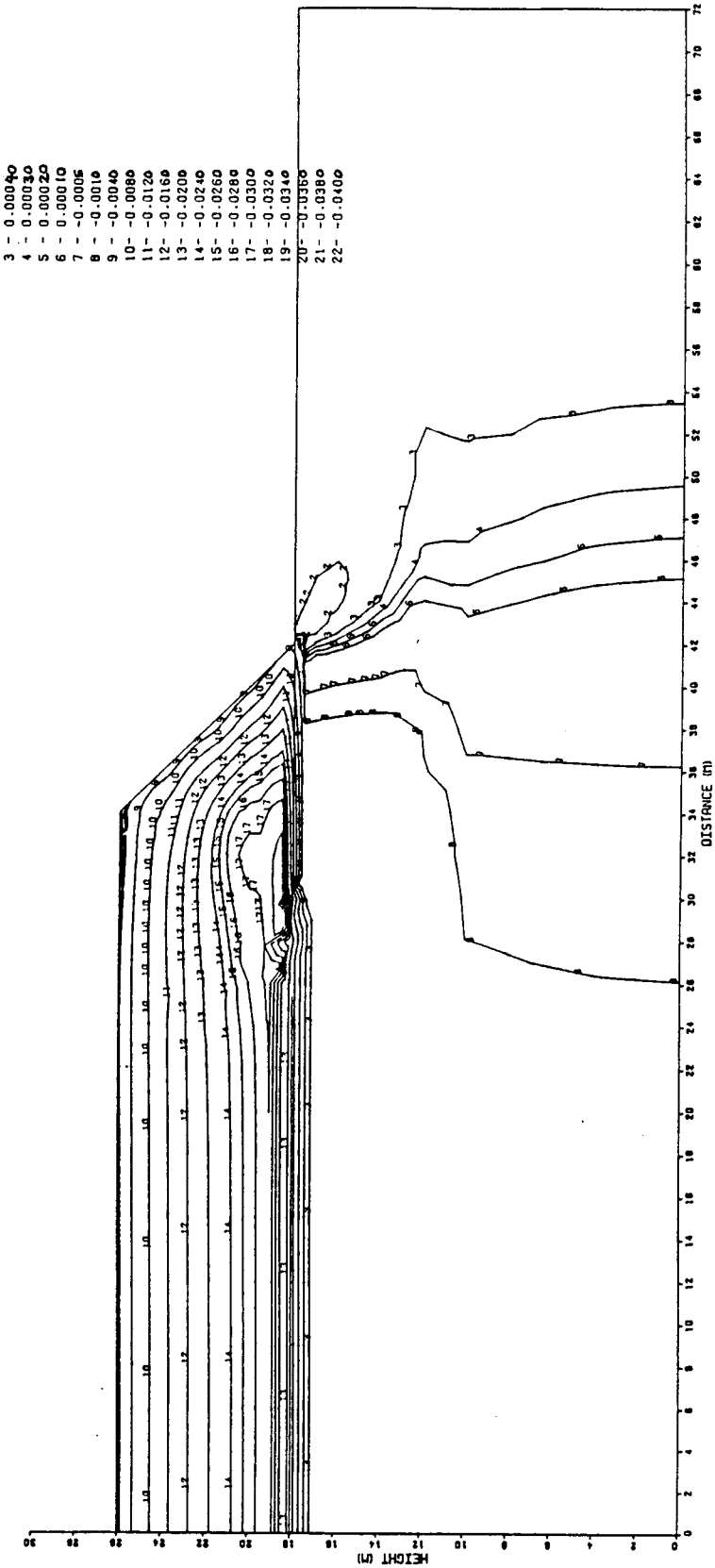

Figure B.7 Vertical Strains in Unreinforced Fill Slope: Height = 8 m

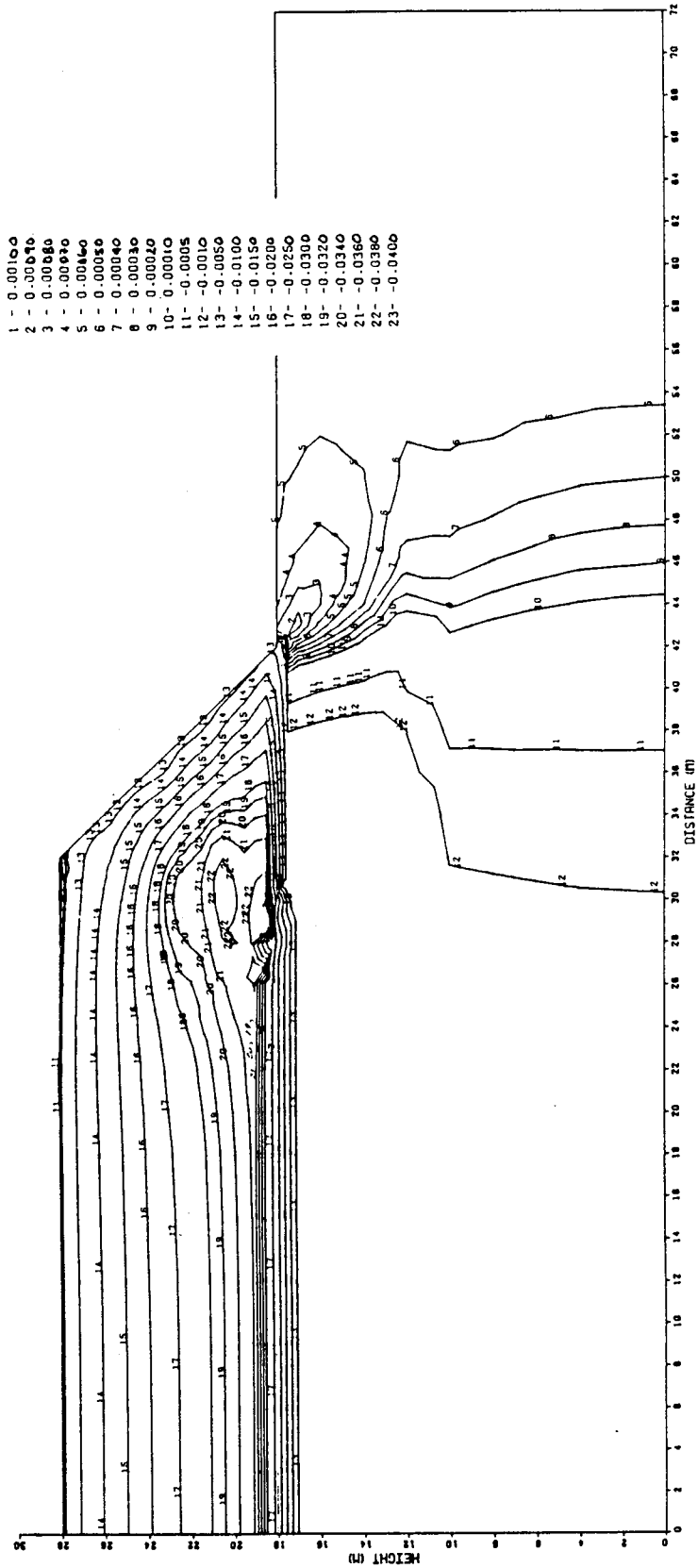

Figure B.8 Vertical Strains in Unreinforced Fill Slope: Height = 10 m

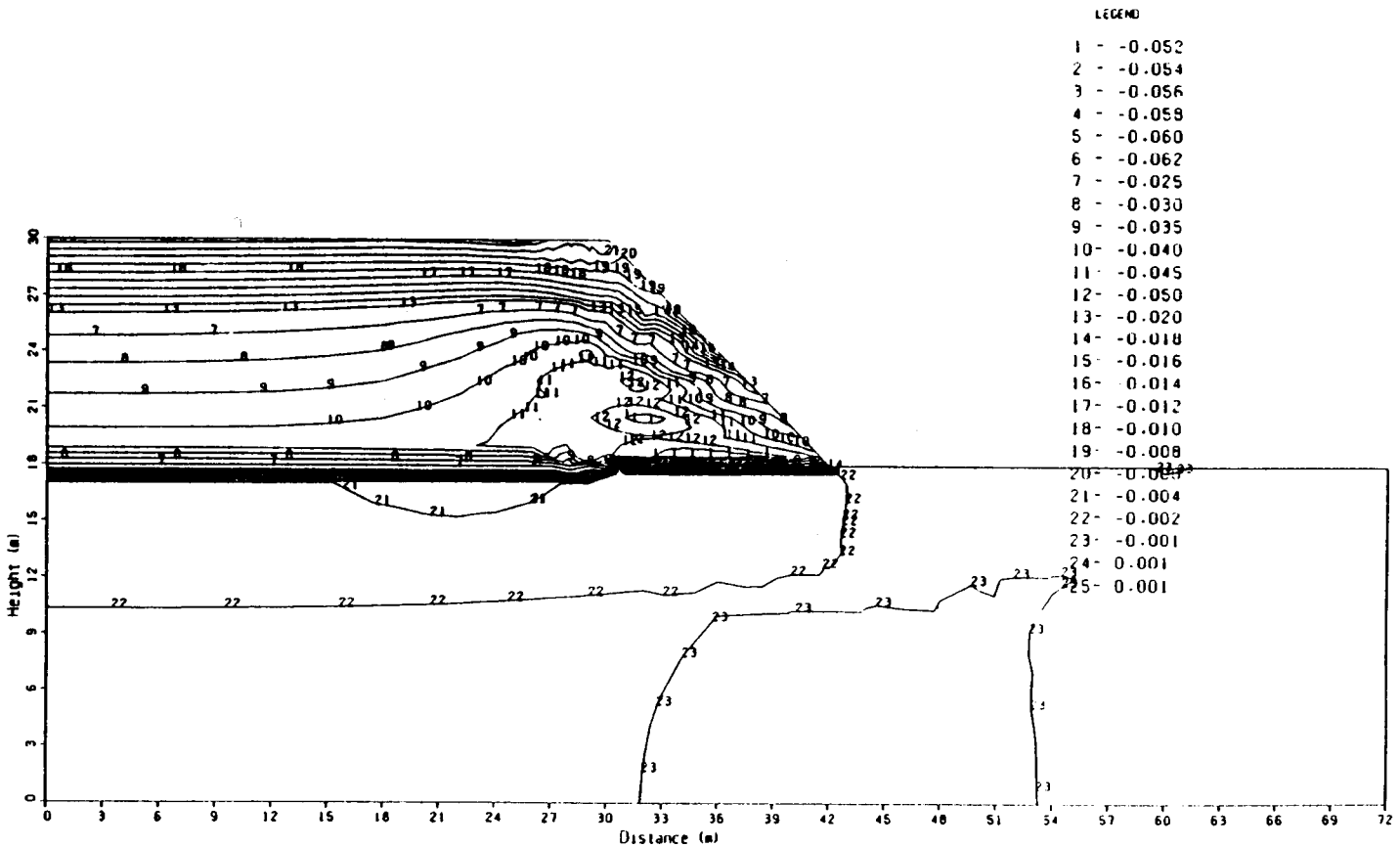

Figure B.9 Minimum Principal Strains in Unreinforced Fill Slope: Height = 12 m